Semiquantitative bond models from quantum chemical topology

Rubén Laplaza

Semiquantitative bond models from quantum chemical topology

THESIS

submitted the 8^{th} July 2020

for the obtention of

Diplôme National de Doctorat

Título de Doctor por la Universidad de Zaragoza

by

Rubén Laplaza

Jury members:

Jury :	Prof. Ángel Martín Pendás
	Prof. Clémence Corminboeuf
	Dr. Mónica Calatayud
	Prof. Pedro Merino
Reviewers :	Prof. Christopher Morell
	Prof. Frank de Proft
Supervisors:	Dr. Julia Contreras-García
	Dr. Victor Polo

Laboratoire de Chimie Théorique – UMR 7616
Departamento de Química Física de la Universidad de Zaragoza

A Rubén y Gloria,
de cuya infinita paciencia y amor
sin duda nacen, hoy y siempre,
todas mis virtudes.

Acknowledgements

One should always be grateful, if I may, for this present we are bequeathed by many. Thus, however difficult, I will try to spare a word as well: for all who were, for all who are, for those to come.

I thank my supervisors, Julia Contreras-García and Victoriano Polo, first and foremost for their kindness; only then for their sincere support, which has brought me this opportunity. I thank them as well for their sincere company at all times, from the darkest hours to the brightest laughter. Last but not least, I thank them both for their scientific advise. I could not have had better examples on how to stay strong yet human in the pursuit of knowledge.

Over these years I have enjoyed the company of many wonderful people in science (generally over a cup of coffee) who deserve a spot here. In the Laboratoire de Chimie Théorique, where I have developed most of my work, the list would be endless: Daniele, Felipe, Felix, Maya, Jeremy, toute la jeunesse, mais aussi Patrick, Mónica, Peter, Andreas, Emmanuel... enfin, toute l'expérience, ce que n'est pas peu. Francesca deserves a brighter spotlight because she has been bearing with me for the longest, and that, as anyone knows, is not an easy thing to do. Grazie! A part of me will forever remain in the dreamy city of lights of these years.

In Universidad de Zaragoza I would like to thank Julen in particular, for his guidance and friendship, but also the young generations (Asier, Héctor, Sergio) who have always been as friendly as they come, Alberto, Jefferson and other *chemical* company. Further thanks are due to the faculty that has contributed to my education over the years, with particular emphasis on Prof. Milagros Medina and Dr. Asunción Gallardo for their trust and dedication over the years.

My most sincere thanks to Prof. Paul W. Ayers for accommodating and mentoring me in his group during three sunny summer months in Hamilton, and to Dr. Carlos Cárdenas for doing so in Santiago. Best wishes and dearest thanks to all the fellow students I met over these two periods of time: Trini, Thomas, Xiao, Kumru, Gallo, Mella, Mar and so many more. Analogously, cheers to Tatiana, Eline, Derrick, Dave, David, Bruno, Erna, Maxime, Merche and the other visiting or temporary coffee-drinkers and collaborators. In spite of my strong preference for café au lait and my never ending verbosity, hopefully I will have been somewhat of a positive influence for everyone involved.

As far as the scientific community goes, I would like to finish by thanking the reviewers and jury of this thesis, all of whom I deeply admire, for dedicating their precious time to improve and polish this manuscript and my research as a whole.

Por supuesto, también hay agradecimientos para todos aquellos que me han acompañado durante este tiempo prácticamente *a pesar* de lo pesado que soy con la ciencia. E intensito, como estas líneas constatan. Mis niños (temporales y atemporales: Josemi, Funes, Marín, Estér, Eva, Érika y tantos más), mi queridísima Sara y mis chicas sonrientes (Ana, Raquel, Julia), mis muchachos Dani y Gonza, mi compañero de desayunos Moldavo, el triplete de íñigo, Darío y Eva, mis Paulas y Manu y Julia y nuestra enorme familia en común, mis Conchis invencibles y compañía (Elisa, Carla, Alba, Olga, Alberto, Herena), Pablo (peibol) y Julio (julius), Aroita e Inech, todos los seres del mal y asiduos del Sputnik, hijos e hijas del rock and roll, familiares (abuelitas, tíos y tías, primos)... y tantísimos otros más. De un modo u otro, esta tésis no se habría concretado sin todos vosotros. Así que gracias, gracias, gracias mil veces (y perdón otras mil a los irremediables olvidados).

En fin, siempre me he dicho que lo que sea que soy se lo debo a todo aquel que jamás haya compartido conmigo su alegría. Quizás sea el momento de agradecer, también, a todo aquel que me haya enseñado algo alguna vez, a todos los profesores que me han aportado algo a lo largo de los años.

A fin de cuentas, si de profesores se trata, he sido muy afortunado: he tenido a la mejor profesora en casa desde el principio. Todo lo demás es necesario, pero ella es imprescindible, y ni todas las páginas del mundo albergarían todo lo que le debo a mi madre, fuerza de la naturaleza que la ciencia aún no puede comprender: gracias, Gloria.

R. Laplaza Solanas Paris, 30^{th} June 2020

Contents

List of abbreviations

AIM : *Atoms In Molecules.*
AO : *Atomic Orbital.*

BCM : *Bond Charge Model.*
BCP : *Bond Critical Point.*
BDE : *Bond Dissociation Energy.*
BE : *Bond Energy.*
BLA : *Bond Length Alternation.*
BOVB : *Breathing Orbital Valence Bond.*
BSSE : *Basis Set Superposition Error.*

CAS : *Complete Active Space.*
CAS : *Restricted Active Space.*
CBS : *Complete Basis Set.*
CC : *Coupled Cluster.*
CCP : *Cage Critical Point.*
CCSD : *Coupled Cluster with Single and Double excitations.*
CCSD(T) : *Coupled Cluster with Single, Double and perturbative Triple excitations.*
CGTO : *Contracted Gaussian Type Orbitals.*
CI : *Configuration Interaction.*
CIS : *Configuration Interaction with Single excitations.*
CISD : *Configuration Interaction with Single and Double excitations.*
CMO : *Canonical Molecular Orbital.*
CP : *Critical Point.*
CSF : *Configuration State Function.*

DFA : *Density Functional Approximation.*
DFT : *Density Functional Theory.*
DH : *Double Hybrid.*
DIIS : *Direct Inversion of the Iterative Subspace.*

EA : *Electron Affinity.*
ELF : *Electron Localization Function.*

FCI : *Full Configuration Interaction.*
FMT : *Folk Molecular Theory.*

GAP : *Gross Atomic Population.*
GGA : *Generalized Gradient Approximation.*
GOP : *Gross Orbital Population.*
GTO : *Gaussian Type Orbitals.*

HEG : *Homogeneous Electron Gas.*
HF : *Hartree-Fock.*
HFT : *Hartree-Fock Theory.*
HOMO : *Highest energy Occupied Molecular Orbital.*

IBE : *Intrinsic Bond Energy.*
IP : *Ionization Potential.*
IQA : *Interacting Quantum Atoms.*

KS : *Kohn-Sham.*
KS-DFT : *Kohn-Sham Density Functional Theory.*

LCAO : *Linear Combination of Atomic Orbitals.*
LDA : *Local Density Approximation.*
LOL : *Localized Orbital Locator.*
LUMO : *Lowest energy Unoccupied Molecular Orbital.*

MCSCF : *Multi Configurational Self-Consistent Field.*
MO : *Molecular Orbital.*
MOM : *Maximum Overlap Method.*
MOT : *Molecular Orbital Theory.*
MP2 : *Møller-Plesset 2nd order perturbation theory.*

NCP : *Nuclear Critical Point.*
NO : *Natural Orbital.*

PES : *Potential Energy Surface.*

QCT : *Quantum Chemical Topology.*

RCP : *Ring Critical Point.*
RE : *Reorganization Energy.*
RHF : *Restricted Hartree-Fock.*
ROHF : *Restricted Open Hartree-Fock.*
RSH : *Range-Separated Hybrid.*

SC : *Spin Contamination.*

List of abbreviations

SCF : *Self-Consistent Field.*
SIE : *Self-Interaction Error.*
STO : *Slater Type Orbitals.*

UHF : *Unrestricted Hartree-Fock.*

VB : *Valence Bond.*
VBSCF : *Valence Bond Self-Consistent Field.*
VBT : *Valence Bond Theory.*
VSEPR : *Valence Shell Electron Pair Repulsion.*

Résumé

Résumé en Français.

Mots-clés: liaison chimique, théorie de la fonctionnelle de la densité, chimie quantique

Introduction

Cette thèse s'inscrit dans un domaine relativement nouveau de la chimie : la chimie quantique, développée à partir de la mécanique quantique dans la seconde moitié du XXe siècle. La chimie quantique combine la chimie avec les méthodes de la mécanique quantique, ce qui permet de décrire in silico des systèmes chimiques avec une grande précision.

Cela nécessite un traitement quantique des électrons, qui ne ressemblent rien au monde macroscopique que nous connaissons. Cependant, les équations de la mécanique quantique n'ont pas de solutions exactes pour les systèmes polyélectroniques. Par conséquent, divers modèles simplifiés comprenant des approximations mathématiques sont couramment utilisés. N'ayant aucune expérience empirique de la dynamique électronique, les modèles approximatifs de la chimie quantique sont souvent utilisés comme fondements ontologiques. Par exemple, le concept "orbital moléculaire", qui est pratiquement indispensable en chimie, n'est pas défini dans la théorie exacte.

En même temps, la chimie traditionnelle hérite d'un certain nombre de modèles et de concepts dérivés, résultat d'une longue tradition scientifique. Certains de ces concepts, tels que "électronégativité" ou la "liaison covalente", sont fondamentaux pour comprendre la chimie. Ces types de concepts ne sont pas définis d'un point de vue quantique, et la grande majorité d'entre eux ne sont pas rigoureusement définis dans aucune théorie approximative. Cela est problématique car les modèles que nous utilisons pour comprendre la réalité orchestrent également notre raisonnement : ils nous permettent de faire des prévisions, d'imaginer de nouvelles espèces chimiques et d'interpréter les phénomènes observés empiriquement. Comme les modèles basés sur la mécanique quantique et les modèles basés sur des concepts historiques ne sont pas réductibles ontologiquement, nous utilisons souvent des concepts issus de différents modèles

L'utilité d'un modèle est double. Tout d'abord, lors du processus de construction, il nécessite un effort d'abstraction et de mathématisation. Ensuite, dans son application, il nous aide à comprendre les interactions entre différents facteurs, y compris les causes et les effets. En raison de sa grande utilité, la construction et l'application de modèles est une partie fondamentale de tout domaine scientifique. Cependant, en chimie, nous trouvons parfois des modèles et des concepts très différents qui conduisent à des arguments opposés sur la façon de comprendre les processus chimiques.

Cette thèse se concentre sur le développement d'un modèle de liaison chimique basé sur des composants subatomiques. Contrairement à la plupart des modèles contemporains, qui se concentrent sur l'idée de l'atome, ce modèle se concentre sur le concept de liaison chimique : il définit la liaison chimique comme une entité authentique et localisée qui interagit avec des pseudo-atomes. Cela nous permet de penser au-delà des atomes et présente donc un potentiel d'innovation. Pour comprendre ses vertus et

ses défauts, il est nécessaire de comprendre les différents modèles conceptuels qui existent actuellement, et où ils échouent. Il est également nécessaire de comprendre les problèmes liés au paramétrage et les fondements des principales méthodes de la chimie théorique.

Par conséquent, dans cette thèse, le Chapitre 1 est consacré aux concepts qui appartiennent à la soi-disant intuition chimique. Ensuite, dans le Chapitre 2, les bases de la chimie quantique sont expliquées en détail d'un point de vue mathématique et formel. Par la suite, deux Chapitres, 3 et 4, sont consacrés aux cadres interprétatifs utilisant respectivement les orbitales et les champs scalaires dérivés de la fonction d'onde. Une fois ces bases établies, le modèle en question est développé et appliqué dans le Chapitre 5, qui est appelé "ELF-BCM". Dans le Chapitre 6, certaines questions concernant la relation entre les propriétés d'une liaison chimique et sa description computationnelle sont abordées en relation avec le modèle précédent.

Interprétation chimique

L'interprétation chimique fait référence à la manière dont nous devons expliquer et rationaliser les observations chimiques empiriques, soit in vitro ou in silico. En chimie, nous essayons généralement de comprendre des processus complexes, tels que les transformations chimiques, dans des termes qui nous permettent de faire des prédictions. La théorie interprétative historique utilisée en chimie trouve son origine moderne dans la révolution chimique des 17ème et 18ème siècles, dont le représentant plus important est Lavoisier. À ce stade, la chimie se distancie de la philosophie naturelle et acquiert sa propre entité. Nous appellerons cet ensemble de connaissances, qui a eu des contributions importantes au 20ème siècle, la "Folk Molecular Theory" (FMT).

Les trois principaux piliers de la FMT sont la structure chimique, les propriétés chimiques et les interactions, dans lesquelles nous incluons la formation et la rupture des liaisons chimiques. On suppose couramment qu'une fois la structure de la matière est déterminée, des propriétés émergent d'une combinaison de cette structure et des propriétés fondamentales des éléments. Il est donc important de comprendre les propriétés que nous associons aux atomes et aux éléments, ce que nous entendons par structure chimique, et comment ces concepts sont liés à la mécanique quantique.

En chimie quantique, et en mécanique quantique en général, chaque système est représenté par une fonction d'onde définie dans un espace de Hilbert. Les propriétés du système résultent de l'application d'un opérateur (dans les espaces Hilbert finis, cet opérateur est linéaire et hermitique) à cette fonction d'onde. Par conséquent, aucun objet qui ne peut être représenté comme un opérateur n'est défini.

Cela implique que l'épistémologie de la chimie est coincée entre deux limites fonctionnelles : l'épistémologie quantique dans le contexte subatomique, et l'expérience empirique au monde macroscopique, qui est rarement compréhensible en termes de molécules et d'atomes.

Le concept le plus fondamental dans l'histoire de la chimie est celui de l'élément chimique. Nous définissons l'élément comme une "espèce" d'atome, tous les atomes ayant le même numéro atomique. La prise en compte de ces espèces provient de l'identification d'élémentaux particuliers, et était à l'origine associée à leur numéro de masse, puisque le tableau périodique de Mendeley date de 1869 et la notion de numéro atomique de 1913. En général, nous classons les atomes en fonction de la position de leurs éléments correspondants dans le tableau périodique, et nous associons des propriétés qui suivent généralement une périodicité aux différents éléments. Quelques

exemples sont l'électronégativité, dont il existe de nombreuses échelles empiriques en termes atomiques (un exemple est l'échelle de Pauling, définie dans l'équation 1.1, et le rayon atomique. Cependant, en termes quantiques, un atome est un système idéal, et les atomes n'existent pas en tant que partie d'une molécule parce que l'opérateur de position ne commute pas avec l'hamiltonien du système. De ce fait, les électrons sont intrinsèquement délocalisés.

Dans la FMT, la structure chimique est comprise comme un ensemble d'atomes ayant diverses propriétés qui interagissent par des liaisons chimiques, qui sont généralement compréhensibles en termes de différence de valence ou d'électronégativité. La molécule est représentée par des symboles atomiques et des symboles liés aux électrons de valence (liaisons, paires libres). Il est possible de généraliser ces structures en utilisant des formes résonantes, dont la contribution est proportionnelle à leur stabilité relative. La stabilité relative est évaluée à l'aide des mêmes critères basés sur la valence et l'électronégativité. L'arrangement géométrique est souvent prévisible en se basant sur la théorie de la répulsion des paires d'électrons de valence (VSEPR) qui repose sur ces idées. En bref, on entend par structure chimique les propriétés des atomes constitutifs, qui cherchent à avoir des couches de valence complètes et/ou à satisfaire la VSEPR.

Cependant, pour interpréter les interactions chimiques, nous n'utilisons pas seulement les propriétés atomiques. Les groupes fonctionnels sont également fréquemment inclus. Certains groupes d'atomes ont des propriétés spécifiques qui sont transférables d'un environnement chimique à un autre, comme l'effet inductif ou certains types de liaisons chimiques.

Liaison chimique

La liaison chimique est l'interaction chimique prédominante : des forces qui agissent sur les atomes (ou groupes d'atomes) et les maintiennent ensemble en agrégats relativement stables. Nous ne pouvons pas définir la liaison chimique de cette manière si nous n'acceptons pas les concepts d'atome et de groupe fonctionnel ci-dessus. En chimie, nous classons généralement les liaisons chimiques en plusieurs types ayant des propriétés différentes. Le type de liaison est déterminé par les propriétés des atomes liés.

La liaison covalente est celle qui repose sur le partage des électrons, et l'exemple paradigmatique est celui des molécules diatomiques homonucléaires, puisque la force nette entre les deux atomes est nulle à moins qu'il n'y ait une accumulation de densité d'électrons dans l'axe internucléaire.

Les liaisons ioniques, au contraire, naissent lorsque cette accumulation est minimale et ce qui se produit est, fondamentalement, le transfert d'un électron d'un atome à l'autre et l'interaction électrostatique qui s'ensuit entre les deux atomes. Il n'existe pas de cas parfait de liaison ionique, mais les sels binaires composés d'atomes alcalins et d'halogènes en sont un bon exemple.

Le troisième type principal est celui des liaisons métalliques, qui résultent du partage délocalisé d'électrons entre plusieurs atomes. En plus de ces grands types, il existe également plusieurs catégories moins établies mais utilisées, comme les liaisons haptiques, datives ou hydrogène. En général, les types de liaisons chimiques ne sont pas des catégories définies de manière positive, mais elles sont suffisamment conventionnelles pour être utiles.

Fondations de la chimie quantique

La fonction d'onde d'un système non relativiste obéit à l'équation de Schrödinger dépendant du temps (Equation 2.1). En évitant la dépendance temporelle, nous pouvons nous concentrer sur les états stationnaires, régis par l'équation de Schrödinger indépendante du temps (Equation 2.6). Si nous acceptons que les noyaux atomiques sont des charges ponctuelles qui restent approximativement statiques par rapport aux électrons (approximation de Born-Oppenheimer), nous pouvons résoudre la structure électronique pour n'importe quelle configuration nucléaire. Nous appelons surface d'énergie potentielle (PES) l'hypersurface donnée par l'énergie en fonction des coordonnées des noyaux d'un système.

Cependant, cette équation n'est généralement pas soluble pour les systèmes à plus d'un électron. Les solutions analytiques fermées de l'équation mono-électronique sont appelées orbites. Dans les systèmes polyélectroniques, nous construisons généralement une fonction d'onde approximative comme un produit antisymétrique des orbitales (atomiques). La façon la plus courante de construire une fonction d'onde avec ces caractéristiques est le dénommé déterminant de Slater (Equation 2.22).

La minimisation variationnelle de l'énergie d'une fonction d'onde à un seul déterminant définit la méthode dite de Hartree-Fock (HF). Ce processus est réalisé de manière itérative jusqu'à ce que l'on parvienne à une cohérence d'ensemble. Dans la méthode HF, les électrons n'interagissent pas explicitement entre eux, mais chaque électron interagit électrostatiquement avec la moyenne de tous les autres électrons par l'intermédiaire de l'intégrale biélectronique de Coulomb. De plus, l'intégrale biélectronique d'échange annule exactement la contribution du même électron dans ce champ moyen. Le problème de minimisation est résolu par calcul en utilisant une base finie, généralement composée d'orbitales atomiques. Le plus souvent en chimie, les orbitales atomiques sont exprimées comme des combinaisons linéaires d'orbitales de type gaussien (GTO).

Grâce au théorème variationnel, nous savons qu'en utilisant l'hamiltonien précis, la fonction d'onde exacte produit l'énergie minimale. Pour une base finie donnée, l'énergie la plus basse est obtenue en utilisant la méthode FCI (Full Configuration Interaction). Le coût de calcul de cette méthode augmente considérablement avec le nombre d'électrons dans le système. La différence d'énergie entre l'énergie HF et l'énergie FCI est appelée énergie de corrélation. L'absence de corrélation est le principal problème de la méthode HF. On subdivise généralement l'énergie de corrélation en deux parties : une partie forte, due au caractère monodéterminé, qui est meilleure en ajoutant d'autres déterminants à la fonction d'onde (comme la combinaison linéaire, par exemple) ; et une autre partie, typiquement appelée faible, qui est plutôt due à l'utilisation du champ moyen. Différentes méthodes incluent, explicitement ou implicitement, certaines quantités de corrélation électronique. En général, les méthodes sans corrélation électronique ne sont pas assez précises pour être utilisées en chimie, mais le coût des méthodes corrélées augmente de façon exponentielle.

Théorie de la fonctionnelle de la densité

La théorie de la fonctionnelle de la densité (DFT) est basée sur les théorèmes de Hohemberg et Kohn, qui affirment que l'énergie est une fonction univoque de la densité électronique $\rho(\mathbf{r})$. La forme de cette fonctionnalité est inconnue, aussi utilise-t-on généralement le schéma de Kohn et Sham, ce qui donne naissance à ce que l'on appelle le KS-DFT. Le schéma KS-DFT est analogue à celui de Hartree-Fock et utilise les

déterminants de Slater et les bases finies. Ce schéma suppose que les orbitales de ce déterminant correspondent à la fonction d'onde d'un système fictif qui a la même densité électronique que le système réel. Cela permet de calculer l'interaction moyenne de champ et l'énergie cinétique en utilisant ces orbitales : la différence entre ces termes et les énergies réelles (respectivement coulombienne électron-électron et cinétique) est supposée être faible, et est appelée énergie d'échange-corrélation. Seulemenet cette petite partie $E_{xc}[\rho]$ de la fonction exacte est inconnue.

Au cours des dernières décennies, de nombreuses approches de la densité fonctionnelle exacte (DFA) ont été proposées. Les approches les plus simples sont basées sur le modèle du gaz électronique homogène, et sont appelées approches locales (LDA). Des approximations plus sophistiquées incorporent des gradients de densité (GGA), des densités d'énergie cinétique (meta-GGA), ou une certaine quantité d'échange exact analogue à la théorie HF. Ces dernières approches sont souvent qualifiées d'hybrides, et beaucoup d'entre elles donnent des résultats très précis. Un exemple de LDA est le DFA SVWN3; PBE est un GGA et B3LYP est une DFA hybride. Les différents DFA contiennent différents ingrédients et une quantité variable de paramètres empiriques, de quelques uns (par exemple B3LYP) à des dizaines (par exemple M062X).

Malgré l'énorme diversité des approches, la plupart d'entre elles comportent des erreurs communes. La plus importante d'entre elles est l'erreur d'auto-interaction (SIE). Le SIE est dû au fait que chaque électron, formellement, interagit avec lui-même, puisqu'il n'y a pas d'annulation exacte entre le champ moyen et le terme d'échange dans le KS-DFT. Les autres erreurs identifiées sont l'absence de discontinuité dans la courbe énergie/nombre de particules, et la mauvaise description des effets à longue distance (due à l'absence de faible corrélation). La dernière erreur prise en compte est l'erreur dite de densité, qui fait référence à l'erreur due au fait que le potentiel d'échange-corrélation conduit le système à une densité électronique erronée, plutôt qu'à l'adéquation de l'approximation à la fonctionnelle d'échange-corrélation.

Interprétation fondé sur orbitales

Les orbites atomiques sont les solutions d'un système mono-électronique. Il semble naturel d'utiliser les orbitales atomiques pour construire des fonctions d'ondes approximatives, en combinant les orbitales atomiques des atomes constitutifs pour former de nouvelles orbitales. Comme les orbitales atomiques ont des énergies et des formes spécifiques pour chaque type d'atome, le but est de rationaliser la structure électronique d'un système en fonction de sa composition atomique.

Théorie de l'orbitale moléculaire

La théorie de l'orbitale moléculaire (MOT) admet que la fonction d'onde d'un système polyatomique peut être décrite à l'aide des orbitales moléculaires (MO), qui sont dérivées de l'interaction des différentes orbitales atomiques. L'interaction de deux orbitales atomiques conduit à la formation d'un MO de plus faible énergie (liante) et d'un MO de plus forte énergie (antiliante). Cela permet de prédire les propriétés moléculaires, y compris les énergies relatives, en fonction des atomes ou groupes d'atomes constitutifs, de leurs orbitales et de leur recouvrement.

Dans ce contexte, certains concepts fondamentaux sont définis, tels que l'hybridation, et l'importance interprétative des orbitales frontières (HOMO et LUMO) est mise en évidence. Il est également possible de définir des charges atomiques à l'aide de schémas de localisation orbitale. Les succès de la MOT sont nombreux. Cependant, les MO ne sont

pas observables : il ne s'agit que de fonctions mono-électroniques et ne sont pas définies, à moins que l'hamiltonien exact (bielectronique) soit simplifié en un hamiltonien effectif d'un corps. De plus, les MO ne sont pas des solutions uniques, et il est possible de trouver des ensembles infinis de MO qui reproduisent l'énergie variationnelle totale. Les limites des MO se manifestent par des prédictions erronées, telles que la non-stabilité du dimère He_2.

Théorie de la liaison de valence moderne

L'alternative la plus importante à la MOT est la théorie des liaisons de valence (VBT). Le VBT est basé sur des orbitales atomiques, qu'il combine linéairement pour former des orbitales de liaison de valence. La fonction d'onde totale est un produit antisymétrique de ces orbites, qui ne sont généralement pas orthogonales. La construction des orbitales se fait en termes chimiques, en considérant les structures covalentes (dans lesquelles les électrons impliqués dans la liaison de deux atomes ont des spins appariés) et ioniques (dans lesquelles les électrons impliqués dans la liaison occupent les orbitales atomiques d'un seul atome). Il s'agit donc d'une théorie atomique. La génération des structures pertinentes est dimensionnée de manière factorielle, elle doit donc généralement être tronquée en tenant compte des règles standard de stabilité des formes résonantes. Les fonctions d'onde résultantes, minimisées de façon variable, sont meilleures que celles de la méthode HF (pour la même base finie) car elles contiennent plus d'un déterminant.

Cependant, ils ne saisissent pas la corrélation électronique complète et sont nettement plus difficiles à calculer en raison du manque d'orthogonalité. Les orbitales utilisées ont une interprétation chimique claire, et leur contribution à la fonction d'onde, par le biais du coefficient respectif dans la combinaison linéaire, correspond à la notion de structure chimique en termes de formes résonantes avec différentes "probabilités". En tout cas, les orbitales restent indéfinies dans la théorie exacte, et celles-ci sont relativement variables selon la construction des orbitales atomiques.

Topologique chimique quantique

Au lieu d'utiliser les orbitales pour l'interprétation chimique, il est possible de se concentrer sur la densité des électrons, qui, dans la DFT, détermine l'énergie. La densité d'électrons est un champ scalaire défini dans l'espace tridimensionnel, de sorte que la dimensionnalité de l'objet d'étude est considérablement réduite par rapport à la fonction d'onde pleine. Ce type de champ scalaire peut être étudié de manière très pratique en utilisant la théorie de Morse, qui se concentre sur les points critiques et leurs variétés associées. Dans un sens plus large, ce type d'outil mathématique appartient au domaine de la topologie.

Le champ scalaire par excellence est la densité électronique elle-même, $\rho(\mathbf{r})$. L'étude de ce phénomène avec des outils topologiques est généralement appelée théorie quantique des atomes dans les molécules (AIM). Il n'y a que quatre types de points critiques différents dans la densité d'électrons, qui sont associés aux positions nucléaires (NCP), aux liaisons chimiques (BCP), aux anneaux (RCP) et aux boîtes (CCP). Le gradient de densité électronique divise l'espace de manière exhaustive en variétés stables associées aux NCPs, qui peuvent être interprétées comme des atomes. Nous appelons couramment ces sous-espaces des "bassins" atomiques ou des atomes topologiques. Si l'action d'un opérateur linéaire peut être exprimée en termes de densité d'électrons, nous pouvons intégrer cette fonction dans un bassin atomique pour obtenir des véritables propriétés atomiques, telles que les charges atomiques.

De même, nous pouvons analyser d'autres champs scalaires, tels que la fonction de localisation électronique (ELF). L'ELF est basée sur la relation entre différentes densités d'énergie cinétique. Généralement, elle est exprimée en termes de $\eta_{ELF}(\mathbf{r})$ (Equation 4.47) qui est une fonction contrainte entre 0 et 1. Sous forme simplifiée, $\eta_{ELF}(\mathbf{r})$ approche 1 dans les régions où les électrons sont appariés ou bien localisés, et 0 dans les régions où les électrons sont non appariés ou très pauvrement localisés. Le gradient de la ELF divise également l'espace de manière exhaustive, ce qui donne lien à des bassins qui s'associent aux noyaux (bassins nucléaires) et des bassins qui s'associent aux électrons de valence (liaisons et paires libres). Les bassins nucléaires contiennent les positions nucléaires du système et sont petits et forment des couches pratiquement sphériques. Les bassins de valence sont classés en fonction du nombre de bassins nucléaires adjacents, et diffèrent grandement par leur forme et leur volume. En règle générale, un bassin associé à une liaison sera adjacent à deux bassins nucléaires, et par conséquent nous l'appelons une bassin dysynaptique.

La méthode des atomes quantiques interactifs (IQA) peut être utilisée à partir de n'importe quelle partition exhaustive de l'espace. Dans cette méthode, des matrices de densité réduite de premier et de second ordre sont partitionnées, ce qui permet de répartir l'énergie totale exactement en fonction des différents bassins d'espace. En effet, l'hamiltonien exact ne dépend que de deux particules. Cette méthode fournit des énergies quantitatives avec une interprétation directe, mais génère une grande quantité de termes qui doivent être regroupés. En outre, elle exige l'intégration numérique de plusieurs termes. Cela est coûteux en termes de calcul et dangereux pour l'interprétation. Des petites erreurs en termes opposés de grande ampleur produisent des erreurs qualitatives importantes. En outre, le cloisonnement conditionne l'interprétation des différents termes. En raison de ces limitations, cette méthode n'est pas très répandue dans la communauté.

Résultats

Un modèle de charge de liaison moderne

Il est possible de décrire la courbe du potentiel énergétique d'une molécule diatomique homonucléaire en utilisant un potentiel Morse. Toutefois, il est également possible de construire un potentiel de la forme $W(R) = W_0 + W_1/R + W_2/R^2$ où R est la distance internucléaire. Pour le même nombre de paramètres empiriques, ce modèle est capable de s'adapter à des résultats empiriques similaires. Selon le théorème du viriel moléculaire, nous pouvons supposer que le terme W_1/R provient de l'énergie potentielle, et le terme W_2/R^2 de l'énergie cinétique. En considérant cela, nous pouvons construire un modèle de charge de liaison, que nous pouvons décrire en considérant que la liaison chimique est comme une particule chargée négativement confinée entre deux atomes chargés positivement de façon distincte. Les deux atomes interagissent de façon coulombienne, c'est-à-dire, à raison de $1/R$. La particule de liaison a une charge nette négative q, et interagit coulombiquement avec les deux atomes, donc proportionnellement à q/R. De plus, le lien possède sa propre énergie cinétique, qui dépend de l'espace dans lequel il est confiné. Dans une molécule diatomique, le volume accessible est proportionnel à R, comme une particule dans une boîte de potentiel monodimensionnelle. Par conséquent, nous pouvons supposer que le terme cinétique s'échelonne comme $\propto 1/\nu R^2$, soit ν la fraction accessible de l'espace.

Cela nous permet d'interpréter de manière qualitative l'origine des différents termes

de la première expression. Parr et ses co-auteurs ont utilisé des expressions analytiques pour dériver W_1/R et W_2/R^2 et ont utilisé le modèle résultant pour ajuster différentes propriétés expérimentales. Il est remarquable que, connaissant l'expression analytique de $W(R)$, il soit possible d'obtenir la distance d'équilibre internucléaire R_{eq} ; la constante de force k_e, avec laquelle la fréquence harmonique peut être calculée, et l'énergie de dissociation. Cependant, comme il n'existe pas de moyen empirique de quantifier la valeur de q, il est difficile de paramétrer le modèle de manière cohérente. Pour les systèmes simples, il est possible d'obtenir des valeurs absurdes des deux paramètres considérés, q et ν.

Toutefois, le modèle présente des propriétés particulièrement intéressantes. Pour commencer, il considére explicitement la liaison chimique et ses propriétés. En d'autres termes, il déconnecte les électrons de valence de leurs atomes respectifs. En ce sens, il est plus souple pour intégrer des corrections. Par exemple, une liaison sous contrainte (par exemple dans le cyclopropane) peut être représentée par une charge de liaison déviée de l'axe internucléaire. Il permet également de faire varier l'ordre de la liaison formelle de façon continue, en transférant la charge des atomes à la liaison et vice-versa. Un champ de force atomique nécessite des potentiels différents pour des ordres de liaison différents.

Le modèle de charge de liaison – fonction de localisation électronique

Si le calcul de q est possible, plusieurs des problèmes du modèle original sont résolus. D'une part, il est possible de s'assurer que q reste rationnel. D'autre part, il est possible d'intégrer la migration de la densité électronique, en comprenant la variation dq/dR. De manière pratique, q et ν peuvent être définis à partir de la topologie ELF. q est simplement l'intégrale de $\rho(\mathbf{r})$ dans le bassin correspondant a la liaison considerée, et ν peut être obtenu en soustrayant le rayon des bassins nucléaires à la distance internucléaire. Cela implique que les atomes sont clairement identifiés avec les bassins nucléaires donnés par l'ELF. Nous appellerons ces pseudo-atomes nucléaires simplement des noyaux, en nous rappelant qu'ils comprennent les électrons les plus proches et pas simplement le noyau atomique ponctuel.

Comme q est le terme fondamental du modèle, nous pouvons proposer une expression de la forme $W = D + V + T + XC$, où D est l'énergie du système avec $R \to \infty$; V est l'énergie potentielle, qui comprend des termes noyau-noyau proportionnels à $1/R$ et des termes noyau-liaison proportionnels à q/R. T est un terme cinétique, pour lequel nous proposons une forme proportionnelle à $q^{5/3}/R^2$ basée sur une approximation locale. XC reprend les effets de corrélation et d'échange liés à $E_{xc}[\rho]$. Nous supposons que ce terme est petit et négligeable car les bassins ELF minimisent la répulsion de Pauli les uns pour les autres.

Pour valider le modèle, des calculs ont été effectués en utilisant la méthode ELF–IQA. En assimilant les termes de notre modèle à des termes rigoureux issus de la décomposition IQA, il est possible de tester empiriquement les principales hypothèses du modèle et l'insignifiance relative de XC. En utilisant les données d'un certain nombre de molécules simples, nous avons confirmé que les principales hypothèses du modèle sont remplies pour les liaisons covalentes et aussi les partiellement ioniques. Les liaisons ioniques presque parfaites ne sont pas compatibles, car l'ELF n'est pas capable d'assigner un bassin à la liaison, et les liaisons métalliques (par exemple Li_2) ne sont pas bien décrites. Cette dernière problématique est cohérente puisque la liaison métallique ne ressemble pas à la représentation initiale. Le caractère métallique d'une liaison peut être mesuré quantitativement en utilisant l'Équation 5.28, basée sur

l'homogénéité de la densité électronique dans le BCP associé.

Nous pouvons donc conclure que le modèle est adapté pour décrire des liaisons chimiques covalents très variées de façon robuste.

Application sur la liaison C-C

À titre d'exemple d'application, le modèle que nous avons développé peut être utilisé pour prédire l'énergie de liaison intrinsèque des liens C−C. L'énergie de liaison intrinsèque est l'énergie d'une liaison in-situ, et donc une propriété d'équilibre d'un système chimique qui ne correspond pas à l'énergie de dissociation.

Pour cela, il est nécessaire d'affiner le terme d'énergie cinétique proposé ci-dessus, puisqu'il était basé sur une densité électronique homogène. Nous incluons un facteur de blindage pour décrire correctement l'énergie cinétique dans une échelle de R supérieure. Comme données de référence, nous avons calculé q, R_{eq} et l'énergie de liaison intrinsèque pour 13 liens caractéristiques: C−C C_3H_6, H_3C-CH_3, C_6H_6, $H_3C_4-C_4H_3$, $H_2C=CH_2$, HC≡C−C≡CH, HC≡CH et C_2 pour échantillonner différents ordres de liens, et les conformations *gauche-* et *trans-* du 1,2-Difluoroéthane, ainsi que les isomères 1,2-Difluoroéthène *cis-* et *trans-* et le Tétrafluoroéthène pour montrer l'effet des différents substituants. Cette base de données est destinée à minimiser les effets de réarrangement et les interactions entre les fragments autrement que par la liaison C−C en question.

En utilisant un modèle analytique à trois paramètres, il est possible d'ajuster cette base de données avec un coefficient de détermination $r^2 = 0.992$ (au niveau ωB97XD/def2-QZVP). D'autres niveaux de théorie conduisent à des valeurs similaires pour le même modèle. Si, au lieu de se limiter à un seul niveau de théorie, on prend comme données les résultats obtenus avec 61 méthodes différentes (59 DFA, HF et MP2), l'ajustement se détériore à $r^2 = 0.985$, ce qui est de toute façon assez bon. Cela implique que différentes méthodes établissent un rapport similaire entre les densités et les énergies des liaisons. La méthode la moins adaptée est la méthode HF, ce qui est cohérente car cette méthode ne décrit pas la corrélation de manière adéquate et repose sur des approches différentes au reste. L'erreur associée au modèle ajusté est similaire à l'erreur estimée pour les DFA contemporains, et donc le modèle est suffisamment robuste pour être utilisée de manière semi-quantitative. Deux exemples d'application sont donnés : l'énergie de la liaison C−C dans le cyclopentadiényle est réduite d'environ 14 kcal/mol lorsqu'elle fait partie d'une molécule de ferrocène. D'autre part, nous estimons que les liaisons du diamant sont similaires aux autres liaisons C−C simples, tandis que les liaisons du graphite sont plus faibles que celles du benzène.

Liens entre densités et énergies

L'importance des erreurs de densité est une question controversée dans la communauté des DFT. La plupart des DFAs modernes contiennent un certain nombre de paramètres empiriques. Ces paramètres sont généralement ajustés pour reproduire certaines énergies, absolues ou relatives. Certains auteurs suggèrent que cela peut conduire à ce que certains DFAs entraînent des densités électroniques erronées même si les énergies sont correctes. Cela implique que le système sera mal décrit en général. Cependant, la quantification des erreurs dans la densité électronique n'est pas triviale. L'évaluation de l'erreur de densité en termes d'énergie n'est pas univoque, car il existe au moins deux voies reliant l'évaluation d'un DFA dans sa densité autoconsistante et l'évaluation d'un autre DFA dans sa propre densité autoconsistante.

La plupart de la densité est concentrée autour des noyaux. En comparant la densité autoconsistante donnée par une méthode avec une densité de référence, on constate que la plupart des erreurs se concentrent également dans les régions nucléaires. Toutefois, en termes relatifs, cette erreur est minime (1-2%) alors que dans les régions de valence, où l'erreur est faible en termes absolus, elle peut être supérieure à 10% en termes relatifs.

De ce fait, il est déconseillé d'utiliser des descripteurs globaux de la qualité de la densité électronique, et il est recommandé d'opter pour des descripteurs locaux utilisant des outils topologiques. Par exemple, la population des bassins de liaison donnée par l'ELF est un indicateur intuitif. En outre, il peut être calculé entre différentes géométries, et comme nous avons vu précédemment son effet sur d'autres propriétés de liaison peut être interprété (R_{eq} et k_e par exemple). En général, la HF entraîne une densité de liaison excessive dans les systèmes covalents, qui à son tour entraîne des distances d'équilibre trop courtes et des fréquences harmoniques trop élevées. Cela est dû à l'absence de corrélation électronique. Les DFA locaux ont un comportement opposé en raison du SIE, et ont tendance à répartir la densité de manière homogène.

Les DFA hybrides utilisant une grande quantité d'échange exact ont un effet similaire à celui de la HF sur la densité, leur utilisation est donc déconseillée même si des énergies très précises peuvent être obtenues. Le SIE agit de manière similaire à la corrélation électronique dans les régions de liaison, provoquant une répulsion entre les électrons. L'incorporation de plus de propriétés, plutôt que seulement des énergies et des énergies relatives, est préconisée dans le paramétrage des nouveaux DFAs.

Paramètres de cellule unité

Dans les liaisons ioniques fortes, la HF conduit à des distances de liaison plus longues tandis que la DFA locale conduit à un raccourcissement fictif. C'est encore une fois dû au SIE. La HF préfère distinguer plus clairement les deux ions, tandis que dans la DFT on obtient des densités plus étalées.

Cette erreur est clairement évidente dans l'optimisation géométrique des systèmes ioniques périodiques. Les approches LDA conduisent à des paramètres cellulaires artificiellement petits, tandis que les HF conduisent à des paramètres cellulaires trop élevés. En général, ces deux limites font office de barres d'erreur par rapport à d'autres méthodes et des résultats expérimentaux. Dans ce cas, les résultats expérimentaux obtenus par diffraction des rayons X sont très précis et tombent dans le plupart de cas entre ces deux limites théoriques.

Conclusions

Cette thèse examine de manière critique les principaux cadres conceptuels et modèles interprétatifs de la chimie, en mettant l'accent sur l'omniprésence de la perspective atomistique.

Une révision du modèle de charge de liaison et la ELF a été proposé et développée. Elle a ensuite été validée empiriquement et ses limites ont été rationalisées en termes intuitifs. Un exemple concret dans lequel le nouveau modèle peut être utilisé est la liaison C−C, clairement covalente. Dans ce cas, les énergies de liaison intrinsèques ont été modélisées avec une précision semi-quantitative. Le modèle soulève des possibilités futures d'application dans de multiples domaines de la modélisation chimique.

Enfin, les problèmes associés à la quantification des erreurs de la densité électronique dues à ses caractéristiques locales sont abordés. De ce point de vue, il est cohérent d'utiliser des techniques locales pour étudier ce type d'erreur. Bien compris,

les différents modèles entraînent des conséquences cohérentes et introduisent des erreurs qualitatives dans la description du système. Les distances internucléaires associées aux liaisons covalentes et ioniques en sont un exemple.

Resumen

Resumen en Castellano.

Palabras clave: enlace químico, teoría del funcional de la densidad, química cuántica

Introducción

Esta tésis se enmarca dentro de un campo relativamente nuevo de la química: la química cuántica, desarrollada a partir de la mecánica cuántica de la segunda mitad del siglo XX. La química cuántica combina la química con los métodos de la mecánica cuántica, lo cual permite describir sistemas químicos in silico con gran precisión.

Esto requiere un tratamiento cuántico de los electrones, que no se asemejan en absoluto al mundo macroscópico que experimentamos los seres humanos. Sin embargo, las ecuaciones de la mecánica cuántica no tienen soluciones exactas para sistemas polielectrónicos. Consecuentemente, se utilizan rutinariamente distintos modelos simplificados que incluyen aproximaciones matemáticas. Al no tener experiencia empírica de la dinámica electrónica, a menudo los modelos aproximados de la química cuántica se utilizan como fundamentación ontológica. Por ejemplo, el concepto "orbital molecular", prácticamente imprescindible en química, no está definido en la teoría exacta.

Paralelamente, la química tradicional hereda una serie de modelos y conceptos derivados, fruto de una larga tradición científica. Algunos de estos conceptos, como "electronegatividad" o "enlace covalente" son fundamentales para comprender la química. Este tipo de conceptos no están definidos desde un punto de vista cuántico, y la inmensa mayoría no están definidos de forma rigurosa en ninguna teoría aproximada. Esto es problemático debido a que los modelos que utilizamos para entender la realidad orquestan también nuestro raciocinio: nos permiten hacer predicciones, imaginar nuevas especies químicas e interpretar fenómenos observados empíricamente. Dado que los modelos fundados en la mecánica cuántica y los modelos fundados en conceptos históricos no son ontologicamente reductibles, a menudo utilizamos conceptos provenientes de distintos modelos

La utilidad de un modelo es doble. Primero, durante el proceso de construcción, require un esfuerzo de abstracción y matematización. Después, en su aplicación, nos ayuda a comprender las interacciones entre distintos factores, incluyendo causas y efectos. Debido a su gran utilidad, la construcción y aplicación de modelos es parte fundamental de cualquier ámbito científico. Sin embargo, en química a veces encontramos modelos y conceptos muy distintos que llevan a argumentos opuestos sobre cómo entender los procesos químicos.

Este trabajo está centrado en la elaboración de un modelo de enlace químico basado en componentes subatómicos. A diferencia de la mayoría de los modelos contemporáneos, centrados en la idea de átomo, este modelo se centra en el concepto de enlace químico: define el enlace químico como una entidad genuina y localizada que interacciona con pseudoátomos. Esto permite pensar más allá de los átomos y por tanto tiene un potencial innovador. Para comprender sus virtudes y sus defectos, es necesario comprender los diferentes modelos conceptuales existentes actualmente, y en qué puntos fallan. También es necesario entender los problemas asociados a la parametrización y los fundamentos de los principales métodos de la química teórica.

En consecuencia, en esta tésis se dedica el Capítulo 1 a los conceptos que pertenecen a la llamada intuición química. Después, en el Capítulo 2 se explican con cierto detalle

los fundamentos de la química cuántica desde un punto de vista matemático y formal. Posteriormente, se dedican sendos capítulos, 3 y 4 a los marcos interpretativos que utilizan orbitales y campos escalares derivados de la función de onda respectivamente. Una vez asentadas estas bases, en el Capítulo 5 se desarrolla y aplica el modelo en cuestión, que lleva por nombre "ELF-BCM". En el Capítulo 6 se tratan, en relación con el modelo anterior, algunas cuestiones concernientes a la relación entre las propiedades de un enlace químico y su descripción computacional.

Interpretación química

El concepto de interpretación química hace referencia a la manera que tenemos de explicar y racionalizar las observaciones química empíricas, in vitro o in silico. En química, generalmente, tratamos de entender procesos complejos, como transformaciones químicas, en terminos que permitan realizar predicciones. La teoría interpretativa histórica que se utiliza en química tiene su origen moderno en la revolución química de los siglos 17 y 18, cuyo máximo representante es Lavoisier. En este punto la química se distancia de la filosofía natural y adquiere entidad propia. Llamaremos a este corpus de conocimiento, que tuvo importantes contribuciones en el siglo XX, la "Folk Molecular Theory" (FMT, teoría molecular tradicional).

Los tres principales pilares de la FMT son la estructura química, las propiedades químicas y las interacciones, en las que incluímos la formación y ruptura de enlaces químicos. Se asume rutinariamente que, una vez determinada la estructura de la materia, las propiedades emergen de una combinación de dicha estructura y las propiedades fundamentales de los elementos. Por tanto, es importante entender qué propiedades asociamos a los átomos y a los elementos, qué entendemos como estructura química y cómo se relacionan estos conceptos con la mecánica cuántica.

En química cuántica, y en mecánica cuántica en general, todo sistema es representado por una función de onda definida en un espacio de Hilbert. Las propiedades del sistema resultan de la aplicación de un operator (en espacios de Hilbert finitos, dicho operador es lineal y hermítico) a dicha función de onda. Por ende, ninguna propiedad que no pueda ser representada como operador está definida.

Esto implica que la epistemología propia de la química queda atrapada entre dos límites funcionales: la epistemología cuántica en lo subatómico, y la experiencia empírica de lo macroscópico, que rara vez es conceptualizado en términos de moléculas y átomos.

Los conceptos más fundamentales en la historia de la química es el de elemento químico. Definimos elemento como *especie* de átomo, todos los átomos con el mismo número atómico. La consideración de estas especies proviene de la identificación de particular elementales, y originalmente se asociaba a su número másico, ya que la tabla periódica de Mendeley data de 1869 y la noción de número atómico de 1913. Generalmente, clasificamos los átomos según la posición de sus elementos correspondientes en la tabla periódica, y asociamos propiedades a los distintos elementos. Algunos ejemplos son la electronegatividad, de la que existen muchas escalas empíricas en términos atómicos (un ejemplo es la escala de Pauling, definida en la Ecuación 1.1), y el radio atómico. Sin embargo, en términos cuánticos un átomo es un sistema ideal, y los átomos no existen formando parte de una molécula porque el operador posición no conmuta con el hamiltoniano del sistema.

En la FMT, la estructura química se comprende como un conjunto de átomos con propiedades diversas que interaccionan por medio de enlaces químicos, que son generalmente entendibles en términos de valencia o de diferencia de electronegatividad. La molécula se representa con símbolos atómicos y símbolos relacionados con los

electrones de valencia (enlaces, pares libres). Es posible generalizar estas estructuras usando formas resonantes, cuya contribución es proporcionalidad a su estabilidad relativa. La estabilidad relativa se evalua usando los mismos criterios basados en la valencia y la electronegatividad. La disposición geométrica es predecible a menudo en base a la teoría de repulsión de los pares de electrones de valencia (VSEPR por sus siglas en inglés) que se basa en estas ideas. En definitiva, la estructura química se entiende sujeta a las propiedades de los átomos constituyentes, que buscan tener capas de valencia llenas y/o satisfacer la VSEPR.

A la hora de interpretar las interacciones químicas, sin embargo, no sólo nos limitamos a usar propiedades atómicas. También se incluyen frecuentemente grupos funcionales. Algunos grupos de átomos tienen propiedades concretas transferibles de un entorno químico a otro, como el efecto inductivo o ciertos tipos de enlace químico.

Enlace químico

El enlace químico es la interacción química predominante: fuerzas que actúan en los átomos (o grupos de átomos) y los mantienen unidos en agregados relativament estables. No podemos definir el enlace químico así si no aceptamos los conceptos de átomo y grupo funcional anteriormente. Habitualmente, en química categorizamos el enlace químico en varios tipos con distintas propiedades. El tipo de enlace está determinado por las propiedades de los átomos enlazados.

El enlace covalente es aquel basado en la compartición de electrones, y el ejemplo paradigmático son las moléculas diatómicas homonucleares, ya que la fuerza neta entre ambos átomos es cero a menos que haya una acumulación de densidad electrónica en el eje internuclear.

Los enlaces iónicos, al contrario, surgen cuando esta acumulación es mínima y lo que tiene lugar es, fundamentalmente, la transferencia de un electron de un átomo a otro y la posterior interacción electrostática entre los dos átomos. No hay un caso perfecto de enlace iónico, pero las sales binarias compuestas de átomos alcalinos y halógenos son un buen ejemplo.

El tercer tipo principal son los enlaces metálicos, que surgen de la compartición de electrones de forma deslocalizada entre varios átomos. Además de estos tipos mayoritarios también hay varias categorías menos asentadas pero utilizadas, como los enlaces hápticos, dativos o de hidrógeno. En general, los tipos de enlace no son categorías definidas positivamente, pero si lo bastante convencionales como para ser útiles.

Fundamentos de la química cuántica

La función de onda de un sistema no-relativista obedece la ecuación de Schrödinger dependiente del tiempo (Ecuación 2.1). Obviando la dependencia del tiempo, podemos centrarnos en los estados estacionarios, gobernados por la ecuación de Schrödinger independiente del tiempo (Ecuación 2.6). Si aceptamos que los núcleos atómicos son cargas puntuales que permanecen aproximadamente estáticas respecto a los electrones (aproximación de Born-Oppenheimer), podemos resolver la estructura electrónica para cualquier configuración nuclear. Llamamos superficie de energía potencial (PES, por sus siglas en inglés) a la hipersuperficie dada por la energía en función de las coordenadas de los núcleos de un sistema.

De cualquier modo, esta ecuación no es generalmente resoluble para sistemas de más de un electrón. Las soluciones analíticas cerradas para la ecuación monoelectrónica se

denominan orbitales. En sistemas polielectrónicos solemos construir una función de onda aproximada como producto antisimetrizado de orbitales (atómicos). La forma más habitual de construir una función de onda con estas características es el llamado determinante de Slater (Ecuación 2.22).

La minimización variacional de la energía de una función de onda monodeterminantal define el llamado método de Hartree-Fock (HF). Este proceso se realiza de forma iterativa hasta lograr la autoconsistencia. En el método de HF los electrones no interactúan explícitamente unos con otros, sino que cada electrón interacciona electrostáticamente con el promedio del resto de electrones a través de la integral bielectrónica de Coulomb. Además, la integral de bielectrónica de intercambio cancela exactamente la contribución de un mismo electrón en este campo medio. Computacionalmente, el problema de minimización se resuelve utilizando una base finita, generalmente compuesta de orbitales atómicos. Muy habitualmente en química, los orbitales atómicos son expresados como combinaciones lineales de gausianas (Gaussian Type Orbitals, GTOs).

Por el teorema variacional sabemos que, usando el hamiltoniano preciso, la función de onda exacta produce la energía mínima. Para una base finita dada, la energía variacional más baja se obtiene utilizando el método FCI (Full Configuration Interaction). El coste computacional de este método aumenta drásticamente con el número de electrones del sistema. La diferencia de energía entre la energía HF y la energía FCI se denomina energía de correlación. La falta de correlación es el principal problema del método HF. Generalmente subdividimos la energía de correlación en dos partes: una fuerte, debida al carácter monodeterminantal, que mejora añadiendo otros determinantes a la función de onda (como combinación lineal, por ejemplo); y otra parte, típicamente llamada débil, que se debe al uso del campo medio. Distintos métodos incluyen, explícita o implícitamente, ciertas cantidades de correlación electrónica. En general, los métodos sin correlación electrónica no tienen precisión suficiente para ser utilizados en química, pero el coste de los métodos correlacionados escala exponencialmente.

Teoría del Funcional de la Densidad

La teoría del funcional de la densidad (DFT por sus siglas en inglés) se basa en los teoremas de Hohemberg y Kohn, que aseguran que la energía es un funcional unívoco de la densidad electrónica $\rho(\mathbf{r})$. Se desconoce la forma de este funcional, por lo que en general se emplea el esquema de Kohn y Sham, dando lugar a lo que se denomina KS-DFT. El esquema KS-DFT es análogo al de Hartree-Fock y usa determinantes de Slater y bases finitas. Este esquema asume que los orbitales en dicho determinante corresponden a la función de onda de un sistema ficticio que tiene la misma densidad electrónica que el sistema real. Esto permite calcular la interacción de campo medio y la energía cinética usando dichos orbitales: la diferencia entre estos términos y las verdaderas energías (coulombica electrón-electrón y cinética respectivamente) se presuponen pequeñas, y se denominan la energía de correlación-intercambio. Solo esa pequeña parte del funcional exacto, $E_{xc}[\rho]$, es desconocida.

A lo largo de las últimas décadas, se han propuesto multitud de aproximaciones al funcional de la densidad exacto (DFAs, por sus siglas en inglés). Las aproximaciones más simples se basan en el modelo del gas electrónico homogéneo, y se denominan aproximaciones locales (LDAs, por sus siglas en inglés). Aproximaciones más sofisticadas incorporan gradientes de la densidad (GGAs, por sus siglas en inglés), densidades de energía cinética (meta-GGAs) o cierta cantidad de intercambio exacto análogo al de la teoría de HF. Estas últimas aproximaciones se suelen denominar

híbridas, y muchas de ellas consiguen resultados muy precisos. Un ejemplo de LDA es la DFA SVWN3; PBE es una GGA y B3LYP es una aproximación híbrida. Distintas DFAs incorporan distintos ingredientes y una cantidad variable de parámetros empíricos, desde unos pocos (e.j. B3LYP) hasta decenas (e.j. M062X).

A pesar de la enorme diversidad de aproximaciones, la mayoría de las mismas incurre en algunos errores comunes. El más importante de los mismos es el error de auto-interaccion (SIE, por sus siglas en inglés). El SIE se debe a que cada electron, formalmente, interacciona consigo mismo, ya que no hay cancelación exacta entre el término de campo medio y el de intercambio en KS-DFT. Otros errores identificados son la falta de una discontinuidad en la curva de energía frente a número de partículas, y la mala descripción de los efectos de larga distancia (debido a la falta de correlación débil). El último error considerado es el llamado error de la densidad, que hace referencia al error debido a que el potencial de correlación-intercambio lleva el sistema a una densidad electrónica errónea, más que a la adecuación del funcional aproximado.

Interpretación basada en orbitales

Los orbitales atómicos son las soluciones de un sistema monoelectrónico. Parece natural usar los orbitales atómicos para construir funciones de onda aproximadas, combinando los orbitales atómicos de los átomos constituyentes para formar nuevos orbitales. Dado que los orbitales atómicos tienen energías y formas concretas para cada tipo de átomo, el objetivo es racionalizar la estructura electrónica de un sistema en base a su composición atómica.

Teoría de Orbitales Moleculares

La teoría de orbitales moleculares (MOT por sus siglas en inglés) acepta que la función de onda de un sistema poliatómico puede ser descrita usando orbitales moleculares (MOs por sus siglas en inglés), que se derivan de la interacción de los distintos orbitales atómicos. La interacción de dos orbitales atómicos lleva a la formación de un MO de energía menor (enlazante) y uno de energía mayor (antienlazante). Esto permite predecir propiedades moleculares, incluidas energías relativas, en base a los átomos o grupos de átomos constituyentes, sus orbitales y el solapamiento entre los mismos.

En este contexto se definen algunos conceptos fundamentales, como el de hibridación, y se destaca la importancia interpretativa de los orbitales frontera (HOMO y LUMO). También es posible definir cargas atómicas utilizando esquemas de localización de orbitales. Los éxitos de la MOT son numerosos. Sin embargo, los MOs no son observables: sólo son funciones de un único electrón y no están definidas a menos que el hamiltoniano exacto (bielectrónico) se simplifique a un hamiltoniano efectivo de un solo cuerpo. Además, los MOs no son soluciones únicas, y es posible encontrar infinitos sets de MOs que reproducen la energía variacional total. Las limitaciones de la MOT se manifiestan en predicciones erróneas, como la ausencia de estabilidad del dímero He_2.

Teoría de Enlace de Valencia Moderna

La alternativa más importante a la MOT es la teoría de enlace de valencia (VBT por sus siglas en inglés). La VBT se basa en orbitales atómicos, que combina linealmente para formar orbitales de enlace de valencia. La función de onda total es un producto antisimetrizado de orbitales de este tipo, que por lo general no son ortogonales. La

construcción de los orbitales se realiza en términos químicos, considerando estructuras covalentes (en las que los electrones involucrados en el enlace de dos átomos tienen espines apareados) e ionicas (en el que los electrones involucrados en el enlace ocupan los orbitales atómicos de un solo átomo). Se trata por tanto de una teoría atómica. La generación de las estructuras relevantes escala factorialmente, por lo que habitualmente debe ser truncada teniendo en cuenta las reglas estándar de estabilidad de formas resonantes. Las funciones de onda resultantes, minimizadas variacionalmente, son mejores que las del método HF (para una misma base finita) al contener más de un determinante.

Sin embargo, no capturan toda la correlación electrónica y son significativamente más difíciles de calcular debido a la falta de ortogonalidad. Los orbitales utilizados tienen una interpretación química clara, y su contribución en la función de onda, a través del respectivo coeficiente en la combinación lineal, encaja con la noción de la estructura química en términos de formas resonantes con distintas "probabilidades". En cualquier caso, los orbitales siguen sin estar definidos en la teoría exacta, y éstos son relativamente variables en función de la construcción de los orbitales atómicos.

Topología química cuántica

En lugar de utilizar orbitales para elaborar la interpretación química, es posible centrarse en la densidad electrónica, que en DFT determina la energía. La densidad electrónica es un campo escalar definido en un espacio tridimensional, por lo que la dimensionalidad del objeto de estudio se reduce sustancialmente respecto a la función de onda completa. Este tipo de campos escalares puede ser estudiado muy convenientemente utilizando la teoría de Morse, que se centra en los puntos críticos y sus variedades asociadas. En un sentido más amplio, este tipo de herramientas matemáticas pertenecen al área de la topología.

El campo escalar por excelencia es la propia densidad electrónica, $\rho(\mathbf{r})$. El estudio de ésta con herramientas topológicas se suele denominar teoría cuántica de átomos en moleculas (AIM, por sus siglas en inglés). Sólo hay cuatro tipos de puntos críticos distintos en la densidad electrónica, que se asocian con las posiciones nucleares (NCPs), enlaces químicos (BCPs), anillos (RCPs) y cajas (CCPs). El gradiente de la densidad electrónica particiona exhaustivamente el espacio en variedades estables asociadas a NCPs, que pueden interpretarse como átomos. Llamamos rutinariamente a estos subespacios "cuencas" atómicas o átomos topológicos. Si la acción de un operador lineal puede expresarse en términos de la densidad electrónica, podemos integrar dicha función en una cuenca atómica para obtener propiedades atómicas genuinas, como cargas atómicas.

Similarmente, podemos analizar otros campos escalares, como la función de localización electrónica (ELF, por sus siglas en inglés). La ELF se basa en la relación entre distintas densidades de energía cinética. Generalmente, se expresa en términos de $\eta_{ELF}(\mathbf{r})$ (Ecuación 4.47) que es una función acotada entre 0 y 1. De forma simplificada, $\eta_{ELF}(\mathbf{r})$ se aproxima a 1 en regiones en las que los electrones están apareados o localizados, y a 0 en regiones en las que los electrones están desapareados o muy poco localizados. El gradiente de la ELF también particiona exhaustivamente el espacio, dando como resultado cuencas que se asocian con núcleos (cuencas nucleares) y cuencas que se asocian con los electrones de valencia (enlaces y pares libres). Las cuencas nucleares contienen posiciones nucleares del sistema y son pequeñas y prácticamente esféricas. Las cuencas de valencia son clasificadas según el número de cuencas nucleares adyacentes, y difieren mucho en forma y volumen. Típicamente, una cuenca asociada a un enlace será adyacente a dos cuencas nucleares, lo que habitualmente se denomina

disináptica.

El método de átomos cuánticos interactivos (IQA, por sus siglas en inglés) se puede utilizar partiendo de cualquier particion exhaustiva del espacio. En este método se particionan las matrices de densidad reducidas de primer y segundo orden, lo cual permite descomponer la energía total de manera exacta en términos provenientes de las diferentes cuencas del espacio. Ésto se debe a que el hamiltoniano exacto sólo depende de dos partículas. Este método proporciona energías cuantitativas y con una interpretación directa, pero genera una gran cantidad de términos que deben ser reagrupados. Además, requiere integración numérica de múltiples términos. Esto es costoso computacionalmente, y no exento de riesgos. Pequeños errores en términos opuestos de gran magnitud producen errores cualitativos importantes. Además, el particionado condiciona la interpretación de los diferentes términos. Debido a estas limitaciones este método por ahora no se ha extendido mucho en la comunidad.

Resultados

Un Modelo de Carga de Enlace Moderno

Es posible describir la curva de energía potencial de una molécula homonuclear diatómica usando un potencial de Morse. Sin embargo, también es posible construir un potencial de la forma $W(R) = W_0 + W_1/R + W_2/R^2$ donde R es la distancia internuclear. Para un mismo número de parámetros empíricos, este modelo es capaz de proporcionar ajustes similares a resultados empíricos. Según el teorema del virial molecular podemos asumir que el término W_1/R proviene de la energía potencial, y el término W_2/R^2 de la energía cinética. Considerando esto, podemos construir un modelo de enlace de carga, que podemos describir considerando que el enlace químico es una partícula cargada negativamente confinada entre dos átomos de carga netamente positiva. Ambos átomos interaccionan de forma coulombica, es decir, $\propto 1/R$. La partícula de enlace tiene una carga negativa neta q, e interacciona coulombicamente con ambos átomos, siguiendo un factor proporcional a q/R. Además, el enlace tiene su propia energía cinética, que depende del espacio en el que está confinada. En una molécula diatómica, el volumen accesible es proporcional a R, similar a una partícula en una caja de potencial monodimensional. Por ello, podemos asumir que el término cinético escala como $\propto 1/\nu R^2$, siendo ν la fracción accesible del espacio.

Esto permite interpretar de forma cualitativa el origen de los distintos términos en la primera expresión. Parr y coautores utilizaron expresiones analíticas para derivar W_1/R y W_2/R^2 y usaron el modelo resultante para ajustar distintas propiedades experimentales. Cabe destacar que una vez conocida la expresión analítica de $W(R)$ es posible obtener la distancia internuclear de equilibrio R_{eq}; la constante de fuerza k_e, con la que se puede calcular la frecuencia armónica, y la energía de disociación. Sin embargo, al carecer de una forma empirica de cuantificar q, resulta difícil parametrizar el modelo de forma consistente. Para sistemas sencillos es posible obtener valores absurdos de los dos parámetros considerados, q y ν.

Sin embargo, el modelo tiene algunas propiedades particularmente interesantes. Para empezar, considera explícitamente el enlace y sus propiedades. Dicho de otro modo, desconecta los electrones de valencia de sus respectivos átomos. En ese sentido, es más flexible para incorporar correcciones. Por ejemplo, un enlace tensionado (e.g. ciclopropano) puede ser representado por una carga de enlace desviada del eje internuclear. También permite variar el orden de enlace formal de manera continua,

transferiendo carga de los átomos al enlace y viceversa. Un campo de fuerza atómico require potenciales distintos para distintos ordenes de enlace.

El Modelo de Carga de Enlace – Función de Localización Electrónica

Si calcular q es posible, varios de los problemas del modelo original se solucionan. Por un lado, resulta posible asegurar que q permanece racional. Por otro, permite incorporar la migración de densidad electrónica, entendiendo la variación dq/dR. Convenientemente, tanto q como ν pueden ser definidos a partir de la topología de la ELF. q es simplemente la integral de $\rho(\mathbf{r})$ en la cuenca correspondiente al enlace, y ν se puede obtener restando el radio de las cuencas nucleares a la distancia internuclear. Esto implica que los átomos son identificados claramente con las cuencas nucleares dadas por la ELF. Llamaremos a estos pseudoátomos nucleares simplemente núcleos, recordando que incluyen los electrones más próximos y no simplemente el núcleo atómico puntual.

Al ser q el término fundamental del modelo, podemos proponer una expresión de la forma $W = D + V + T + XC$, donde D es la energía del sistema con $R \to \infty$; V es la energía potencial, que incluye términos núcleo–núcleo proporcionales a $1/R$ y enlace–núcleo proporcionales a q/R. T es un término cinético, para el que proponemos una forma propocional a $q^{5/3}/R^2$ basándonos en una aproximación local. XC recoge efectos de correlación e intercambio relacionados con $E_{xc}[\rho]$. Asumimos que este término es pequeño y despreciable debido a que las cuencas de la ELF minimizan la repulsión de Pauli entre ellas.

Para validar el modelo, se realizaron cálculos utilizando la ELF y el método IQA. Equiparando los términos de nuestro modelo con términos rigurosos derivados de la descomposición IQA, es posible poner a prueba empíricamente las asunciones clave del modelo y la relativa falta de relevancia de XC. Usando datos de una serie de moléculas sencillas se confirma que las principales asunciones del modelo se cumplen para enlaces covalentes y parcialmente iónicos. Los enlaces casi perfectamente iónicos no son compatibles dado que la ELF no es capaz de asignar una cuenca al enlace, y los enlaces metálicos (e.g. Li_2) no están bien descritos. Esto último es coherente dado que el enlace metálico no se asemeja a la representación de partida. El carácter metálico de un enlace puede medirse de forma cuantitativa usando la Ecuación 5.28, que se basa en la homogeneidad de la densidad electrónica en el BCP asociado.

Por tanto, podemos concluir que el modelo es adecuado para describir enlaces covalentes con robustez.

Aplicación en enlaces C-C

Como ejemplo de aplicación, el modelo puede ser utilizado para predecir la energía de enlace intrínseca de enlaces C−C. La energía de enlace intrínseca es la energía de un enlace in situ, y por tanto una propiedad de equilibrio de un sistema químico, a diferencia de la energía de disociación.

Para ello es necesario refinar el término de energía cinética planteado anteriormente, ya que éste se basaba en una densidad electrónica homogénea. Incluimos un factor de apantallamiento para describir correctamente la energía cinética en un rango de R mayor. Como datos de referencia, calculamos q, R_{eq} y la energía de enlace intrínseca para 13 enlaces C−C característicos: C_3H_6, $H_3C{-}CH_3$, C_6H_6, $H_3C_4{-}C_4H_3$, $H_2C{=}CH_2$, $HC{\equiv}C{-}C{\equiv}CH$, $HC{\equiv}CH$ y C_2 para muestrear distintos ordenes de enlace, y las conformacionesr *gauche-* y *trans-* del 1,2-Difluoroetano, así como los isómeros *cis-* y *trans-* del 1,2-Difluoroeteno y el Tetrafluoroeteno para muestrear el efecto de distintos

sustituyentes. Esta base de datos pretende minimizar efectos de reorganización e interacciones entre los fragmentos que no sean fundamentalmente a través el enlace C−C en cuestión.

Usando un modelo analítico con tres parámetros, es posible ajustar esta base de datos con un coeficiente de determinación $r^2 = 0.992$ (a nivel ωB97XD/def2-QZVP). Otros niveles de teoría conducen a valores similares para el mismo modelo. Si, en lugar de limitarse a un solo nivel de teoría, se toman como datos los resultados obtenidos con 61 métodos distintos (59 DFAs, HF y MP2), el ajuste empeora a $r^2 = 0.985$, lo cual es en cualquier caso un resultado positivo. Esto implica que distintos métodos relacionan densidades de enlace y energías de forma similar. El método que conduce peor el ajuste es HF, lo cual es coherente ya que este método no describe la correlación adecuadamente y se basa en aproximaciones distintas al resto. El error asociado al modelo ajustado es similar al error estimado para DFAs contemporáneas, y por tanto lo bastante pequeño como para poder usarlo de forma semicuantitativa. Dos ejemplos de aplicación son proporcionados: la energía de enlace C−C del ciclopentadienilo se reduce en aproximadamente 14 kcal/mol cuando éste forma parte de una molécula de ferroceno. Por otra parte, estimamos que los enlaces del diamante son similares a otros enlaces C−C sencillos, mientras que los enlaces en el grafito son más débiles que los del benceno.

Densidades de enlace y energías

Una cuestión polémica en la comunidad de la DFT es la importancia de los errores en la densidad. La mayoría de las DFAs modernas contienen cierta cantidad de parámetros empíricos. Estos parámetros se ajustan habitualmente para reproducir algunas energías, absolutas o relativas. Algunos autores sugieren que esto puede conllevar que ciertas DFAs conduzcan a densidades electrónicas erróneas aunque las energías sean correctas. Ésto implica que el sistema estará mal descrito en general. Sin embargo, cuantificar los errores en la densidad electrónica no es trivial. Evaluar el error de la densidad en términos de la energía no es unívoco, ya que hay al menos dos caminos conectando la evaluación de una DFA en su densidad autoconsistente y la evaluación de otro DFA en su propia densidad autoconsistente.

La mayoría de la densidad se concentra en torno a los núcleos. Comparando la densidad autoconsistente dada por un método con una densidad de referencia, se aprecia que la mayor parte del error se concentra en las regiones nucleares también. Sin embargo, en términos relativos, este error es mínimo (1-2 %) mientras que en regiones de valencia, donde el error es pequeño en términos absolutos, puede suponer más de un 10% en términos relativos.

Debido a esto, se desaconseja usar descriptores globales de la calidad de la densidad electrónica, y se recomienda optar por descriptores locales usando herramientas topológicas. Por ejemplo, la población de las cuencas de enlace dadas por la ELF es un indicador intuitivo. Además, se puede calcular entre distintas geometrías, e interpretar su efecto sobre otras propiedades de enlace (R_{eq} y k_e por ejemplo). En general, HF lleva a un exceso de densidad de enlace en sistemas covalentes, lo que a su vez conduce a distancias de equilibrio excesivamente cortas y frecuencias armónicas demasiado elevadas. Ésto se debe a la falta de correlación electrónica. Las DFAs locales tienen un comportamiento opuesto debido al SIE, y tienden a distribuir la densidad de forma homogénea.

Las DFAs híbridas que utilizan una gran cantidad de intercambio exacto tienen un efecto similar a HF en la densidad, por lo que se desaconseja su uso a pesar de que sea posible obtener energías muy exactas. El SIE actúa de forma similar a la correlación

electrónica en las regiones de enlace, causando repulsión entre los electrones. Se aboga por la incorporación de más propiedades, en lugar de sólo energías y energías relativas, en la parametrización de nuevas DFAs.

Parámetros de celda

En los enlaces fuertemente iónicos, HF lleva a distancias de enlace mayores mientras que las DFA locales llevan a un acortamiento ficticio. Esto es debido al SIE una vez más. HF prefiere distinguir más claramente los dos iones, mientras que en DFT se obtienen densidades más extendidas.

Este error se manifiesta claramente en la optimización geométrica de sistemas periódicos iónicos. Las aproximaciones LDA llevan a parámetros de celda artificialmente pequeños, mientras que HF conduce a parámetros de celda demasiado elevados. En general, estos dos límites actuan como barras de error con respecto a otros métodos y a los resultados experimentales. En este caso, los resultados experimentales obtenidos por difracción de rayos-X tienen una gran precisión.

Conclusiones

En este trabajo se revisan de forma crítica los principales marcos conceptuales y modelos interpretativos de la química, con especial énfasis en la ubiquidad de la perspectiva atomistica.

Un modelo basado en el modelo de carga de enlace y la ELF ha sido propuesto y desarrollado. Posteriormente ha sido validado de forma empírica y se han racionalizado sus limitaciones en términos intuitivos. Un ejemplo concreto en el que el nuevo modelo puede ser utilizado son los enlaces $C-C$, claramente covalentes. En este caso, se han modelado las energías de enlace intrínsecas con precisión semicuantitativa. El modelo plantea posibles aplicaciones futuras en múltiples áreas de la modelización química.

Finalmente, se discuten los problemas asociados a la cuantificación de los errores de la densidad electrónica debido a las características locales de la misma. Desde este punto de vista, resulta coherente utilizar técnicas locales para estudiar ese tipo de errores. Entendidos correctamente, modelos distintos llevan a consecuencias coherentes e introducen errores cualitativos en la descripción del sistema. Esto se ejemplifica en las distancias internucleares asociadas con enlaces covalentes e iónicos.

Introduction

Quantum chemistry is a relatively recent discipline. As the name indicates, quantum chemistry combines chemistry with quantum mechanics: it deals with matter by considering its fundamental constituents, which can only be understood at a quantum level.

Humans interact with matter at a macroscopic level. In the context of our everyday experience, bound by time, space and a set of standard conditions, classical mechanics are suitable. However, not much beyond this well-behaved face of nature, a non-intuitive reality awaits. Matter is naught but change, nothing remains static unless the laws of thermodynamics enforce it.

Electrons, which determine the dynamics of matter, can not be apprehended to any macroscopic experience. To properly describe the electronic structure of matter, we let go of macroscopic intuition and embrace the principles of quantum mechanics. Once the step is taken, though, we realize that all certainty is gone: there is very little we can solve *exactly*. We are therefore limited to some models, arising from different approximations.

A model can be defined as a stylized description of a target system, usually constructed with a mathematical structure. Naturally, very different models can suitably describe the exact same underlying system, particularly so when our empirical evidence is limited. This is often the case when dealing with detailed quantum phenomena. Still, we critically examine different hypotheses and choose a model. Lacking any first hand experience of the motion of quantum particles, an approximate model of choice often grows into the empty space of intuition: the wave equation becomes radiation itself, the occupied orbital becomes the electron. As the model merges with the system, its conceptual apparatus and language becomes *real*. Consequently, as models diverge significantly communication between conceptual frameworks becomes impossible because reality itself diverges as dramatically as the different models we use. For instance, discussing the properties of phonons, or those of covalent bonds, seems adequate and representative to some and ridiculous to others.

The usefulness of a model is two-fold. We build models by apprehending and mathematizing an underlying corpus of evidence; then we manipulate them to acquire additional understanding. Consequently, models have a privileged standing in the scientific methods, and there is hardly any science to be done without effective models. Quite frequently, models are fictional or more specifically non-referring (i.e. they do not describe a *real* system), and have little predictive value for experimental observations. Alternatively, very detailed models can be built which provide quantitative predictions upon manipulation, but very little insight on the inner workings of the system under study. Simply put, the models that lead to the most accurate predictions are not necessarily the most faithful ones.

As of now, several conceptual frameworks and models coexist in the different branches of chemistry, among which quantum chemistry is a heavy hitting newcomer of

sorts. In the darkness of the electronic structure of matter, models substitute empirical experience. The simplified concepts that such models entail surge and decay in usage as the understanding that can be extracted from their two facets fluctuates. Many would argue that quantum mechanics, and its well-reputed descendants (i.e. the Standard Model of particle physics) are as strongly predictive as obscure; while others desperate in the apparent arbitrariness of many chemical principles (e.g. leaving group rankings) that have been taught and used for decades. Alas, the conundrum of chemical intuition is set.

A succinct example of this issue is given by the famous words of Charles Coulson: *"Sometimes it seems to me that a bond between two atoms has become so real, so tangible, so friendly, that I can almost see it. Then I awake with a little shock, for a chemical bond is not a real thing. It does not exist. No one has ever seen one. No one ever can. It is a figment of our own imagination"*. Many would find themselves agreeing wholeheartedly with the last sentence, yet it must be kept in mind that chemical bonds are not unlike other many concepts such as atoms, orbitals or wavefunctions. In this last regard, Erich Hückel wrote a brief poem (as translated by Felix Block),

> Erwin with his psi can do
> Calculations quite a few.
> But one thing has not been seen:
> Just what does psi really mean?

which dwells on the interpretation of Ψ, the wavefunction in Erwin Schrödinger's famed equations. A contemporary chemist may wonder, with all due legitimacy, whether the concept of wavefunction *or* the concept of chemical bond, as arising from different non-reducible models, offers more understanding.

It is in this context that this manuscript puts forward a proposal, which is a simple bond model that connects some long-standing concepts in chemistry with others that arise from the quantum description of the electronic structure. The proposed model is invaluably intuitive, semiquantitative and robust. By virtue of its simplicity, it stimulates thinking outside strictly atomistic conceptions.

In this sense, the mathematical foundations of our model are secondary to its conceptual foundations. For this reason, a significant effort will be devoted throughout this manuscript to the conceptual frameworks involved in our crucible. While such a detour is indeed both necessary and original, the main scientific advances are collected in Chapters 5 and 6, the former being devoted to the model this manuscript attempts to put forward, and the latter to a relevant aspect of modern quantum chemistry that can – and arguably should – be linked to our theoretical assumptions.

A brief outline of the objectives and contents of the different Chapters is offered below, not without a brief foreword by Erwin Schrödinger himself that synthesizes our overall intent: *"The task is, not so much to see what no one has yet seen; but to think what nobody has yet thought, about that which everybody sees"*.

Chapter 1

In order to justify and contextualize our proposed model, the reigning paradigm in chemical interpretation before the first quantum revolution (i.e. until the second half of the 20th century) will be presented and analysed critically. A succinct historical overview will be given whenever needed to illuminate contemporary usage. This

apparently naive effort is needed to understand why some apparently ill-defined concepts have been transferred to the parlance of quantum chemistry. Note that, in spite of the systematic application of quantum mechanics, quantum chemistry is not reducible to physics and draws heavily from pre-existing chemical concepts to construct its models.

The concept of atom, as an all-important concept that founds all atomistic approaches and leads to atomic properties, will be revisited in some detail. Chemical structure, as derived from atomistic perspectives, will also be reviewed. Finally, the key concept of chemical bond, which requires both a concept of atom and the foundations of chemical structure alike, will be analysed critically. In particular, the locality and categorization of chemical bonds as opposed to the non-locality and generality of quantum mechanics will be discussed.

Chapter 2

The foundations of quantum chemistry will be covered from a rather simple yet mostly mathematical point of view. While an effort has been made to prioritize clarity and generality, the objective of the Chapter is highlighting the deficiencies and assumptions of the most fundamental methods (which is attempted using an array of examples), as well as defining some key concepts in suitable terms that can be used in further discussion.

For a detailed exploration of the methods in quantum chemistry, readers are directed to reference manuals such as *Modern Quantum Chemistry: Introduction to Advanced Electronic Structure Theory* by Atila Szabo and Neil S. Ostlund, *Molecular Electronic-Structure Theory* by Trygve Helgaker, Poul Jorgensen and Jeppe Olsen, and *A Chemist's Guide to Density Functional Theory* by Wolfram Koch and Max C. Holthausen, which are far more complete and educational.

Chapter 3

Orbitals are a key concept in contemporary chemical parlance. Perhaps paradoxically, orbitals are also subjected to controversy. The objective of this Chapter is presenting the two most relevant theories that use orbitals, as introduced in the methods of quantum chemistry, and reviewing the uses, limitations, advantages and disadvantages of orbital-based approaches for interpretation.

The Chapter is structured quite educationally and uses numerous simple examples. For a more complete approach to molecular orbital theory, readers are directed to the very educational *Orbital Interactions in Chemistry* by Thomas A. Albright, Jeremy K. Burdett and Myung-Hwan Whangbo. An in-depth review of modern valence bond theory can be found in *Valence Bond Theory* by David Cooper.

Chapter 4

As an alternative to orbital-based theories, quantum chemical topology studies scalar fields derived from the wavefunction. Some relevant mathematical aspects are presented briefly in this Chapter. Then, the two most relevant scalar fields, the electron density and the electron localization function, are studied in some detail using the previously introduced mathematical methods. Again, the strong points and the limitations are highlighted in order to complete a panoramic of chemical interpretation frameworks, and a number of examples is given to guide the reader.

A rather complete outlook on topological methods applied to quantum chemistry is given in *Applications of Topological Methods in Molecular Chemistry* by Remi Chauvin, Christine Lepetit, Bernard Silvi and Esmail Alikhani. Several additional scalar fields are covered as well, which will not appear in this manuscript but may be of interest for the reader.

Chapter 5

In this Chapter a bond model based in a previous proposal by Rober Parr and coworkers is presented. First, attention is devoted to this pre-existent semiclassical approach and its limitations. Then, a connection with quantum chemical topology is developed, leading to a new coupled model which avoid parametrization issues.

Critically, we show that deficiencies from the original model are fixed in the new model, all while preserving an intuitive interpretation. The domain of applicability of the coupled model, which can be associated with local covalent bonds, is explored empirically and its limitations (i.e. metallic bonds) are understood. Hitherto unexplored conceptions of interaction potentials are straightforwardly derived from our model. At the same time, qualitative approaches that have been used with much success in the context of chemical structure find in our model a first approach to quantitative mathematization.

Finally, some exemplary applications are given, opening the door to future developments.

Chapter 6

In this Chapter, errors related to the electron density are shown to affect different chemical bonds qualitatively. Thus, following from our model that connects chemical bonds, energies and quantum chemical topology, an attempt is made to shed light on the connection between these errors and the underlying models. At the same time, some approaches in the literature that deal with density errors in non-local ways are examined critically. A local point of view is used to understand errors in chemical terms, while relating them to other interpretative frameworks (as those introduced in the previous Chapters).

Then, different models in quantum chemistry are shown to describe different regimes of chemical bonding differently. Some behaviour are regular over large chemical spaces and can be predicted intuitively once understood, an example of which is given in terms of calculated cell parameters in periodic systems.

Chapter 1

Chemical Interpretation

Contents

Parmenides argued that, as all there is is constant and nothing comes out of nothing, change is merely an illusion: no real change is possible. Democritus, among others, saw change as an emergent property that does not require *ex nihilo* creation. Something fundamental must exist, they argued, that rearranges in what we see as change.

Interestingly, the word *chemistry* derives from the word *alchemy*, which in turn may come from the ancient Greek $\chi\upsilon\mu\epsilon\acute{\iota}\alpha$, the craft of alloying metals. Indeed, perhaps since its inception, chemistry is a science of change and matter.

The problem of metallurgy bewildered ancient knowledge. Alloys, for instance, present a conceptual challenge. Two distinct materials – the first elementary metals available being copper, gold, silver and iron – are combined into something with different properties. Notably, bronzes and brasses have a lower melting point than elementary copper, which enables sophisticate casting, and boast better mechanical properties. Thus, different properties *emerge* from combination of other substances. The development of pottery and metallurgy were a historical cornerstone of human advancement for milennia.

Many of this ancient endeavors, which we now could arguably backtrace as chemistry, physics and natural philosophy alike, dealt with the dynamics of matter – to a certain degree, as opposed to the dynamics of astral bodies and human spirit. In spite of some current views, this unified past belongs to chemistry insomuch as chemistry has inherited a body of common unsolved problems. However, it seems adequate to take the first chemical revolution of the 17th and 18th centuries, championed by Lavoisier, as a starting point in chemical sciences, due to its surprising degree of current validity.

What is apparently clear is that chemistry, at least from the 18th century onwards, has a separate identity from physics, which can be characterized in a number of ways. Indeed, it is clear that chemical knowledge can not be derived from pure epistemic reduction of physics, in part due to an extremely rich conceptual framework that extends through different domains of expertise, time and scale. There is a genuine, fruitful notion of what benzene *is* that can not be grasped from quantum mechanics but has to do with a surprisingly large underlying conceptual framework, which includes a range of models of benzene.

Many unvaluable concepts in chemistry are hard to define satisfactorily within the ontology given by quantum chemistry. Such concepts are often described as fuzzy, but the language of chemistry would be no more without them: atoms, molecules, bonds, valence, and many other notions developed over centuries. These concepts stem from models that have very little to do with quantum mechanics, but are firmly grounded and intertwined with the pivotal periodic table, molecular structure and the representation and depiction systems used in chemistry. This corpus of historically accumulated knowledge, somewhat fuzzy yet practical, has been called Folk Molecular Theory (FMT) by some authors.[1, 2]

Nowadays, the conceptual apparatus of chemistry focuses on three major aspects: structure, properties and interaction (reactivity). An ideal framework ought to capture all three in that very order. If we can understand chemical structure (e.g. chemical bonds, molecular shape, conformations), because properties are emergent from the arrangement of fundamental entities (e.g. electrophile sites, aromaticity, acidity), we can understand their origin. If we understand properties of matter, we can rationalize the interactions of chemical species that we usually discuss as chemical reactions.

The Folk Molecular Theory, which incorporated significant advances in the first half of the 20th century, gives chemists a rich conceptual framework. Howere, one may ask: where do this concepts come from? Why do we use them, why – and to what extent – are they succesful? Which concepts necessitate which others to be effectively understood? How does quantum mechanics, and quantum chemistry in particular, deal with these

questions? And, finally: how do these complex questions influence the construction of the concepts of quantum mechanics?

A brief historical and critical introduction of several key concepts in classic chemical parlance will be given in the forthcoming Section, which aims to highlight the successes and failures of conceptual cornerstones of chemistry. Interpretation from 1960 onwards has to be understood with a quantum perspective, and therefore will be covered in the next Chapters, in which we will try to see whether FMT and quantum mechanics have to be seen as integrated or simply coexisting.

1.1 Quantum chemical epistemology

Before the first chemical revolution, Robert Boyle published his famous treaty *The Sceptical Chymist: or Chymico-Physical Doubts & Paradoxes*, which attempted to distinguish alchemy from the incipient scientific apparatus of chemistry. In this foundational text of chemistry, Boyle speaks about *"unmingled bodies"*, minimal entities of matter. For him, the nature of such bodies and their discrete interactions were responsible for the properties of matter.

Mechanical philosophers that succeeded him faced the problem of transdiction with renewed interest. They attempted to explain change as emerging from the properties and arrangements of the fundamental, impenetrable, *natural minima* within it. After the first chemical revolution, chemists theorized that a set of underlying principles ought to govern the dynamics of matter, and that such principles could be understood in a mathematical and precise way. Only nowadays, in the 21st century and with quantum mechanics to help us, have we begun to collectively tackle this issue in real systems down to the atomic level.

However, the gain in formal mathematization and precision brought by quantum mechanics, which very soon expanded into quantum chemistry and has been significantly developed since, is accompanied by stark loses in certainty and accesibility.

After the first quantum revolution of the 20th century, scientists have been limited to accessing observables: physical quantities that can be measured. Our access is mediated by a corresponding operator that follows the correspondence principle, ultimately linking with macroscopic properties.

In the mathematical formulation of quantum mechanics, and restricting ourselves to finite-dimensional state-spaces $\mathbb{H}$ (cf. Chapter 2), operators that represent physical properties are Hermitian (i.e. have real eigenvalues) which constitute the corpus of what we can access empirically. Notably, the spectra of Hamiltonian operators give us discrete energies with which statistical thermodynamics can express macroscopical properties. On the other hand, it must be noted that there is no consensus on any widely agreeable interpretation of the measurement operation yet.

Most of the concepts in chemistry are not – and most likely can not be – expressed as Hermitian operators or relations of expectation values thereof. Therefore, most of the concepts in chemistry are devoid of rigurous mathematical foundations in the quantum mechanical context or any subatomic effective field theory so far.

This is not particularly rare in physical sciences. The particularity of chemical epistemology is given by its domain of interest. In terms of size, chemical epistemology is bound from below with a quantum description it rarely respects, and bound from above from a macroscopic world that can rarely be described in atomic and molecular terms. Physics faces similar yet genuine problems of applicability as well.

In the following Section, we will examine some of the most relevant conceptual

apparatus in chemistry, examining the empirical foundation and definition of such concepts critically.

1.2 Concepts in chemistry

Concepts have to be analyzed considering three key notions. First of all, there is the *term* itself; in our particular case, covalent bond, atom or valence. Then, there is a *meaning* that is associated with the term. Some terms have one – or more – associated meanings that evolve with time. A notorious example is the concept of atom. Last, but not least, there is a *context*, which captures historical, philosophical and scientific circumstances: how much is or was known at a certain point of time, how useful the concept is or was.

Clarifying a concept requires careful attention to all three facets. This, however, is surely out of the scope of this manuscript. In this Section we will attemt to contextualize the current meanings of some fundamental terms of chemistry in the 21st century. For this very purpose, we will try to remark the current scientific context and the evolution of the meanings of such terms.

The context of quantum chemistry

Quantum chemistry is N-fermionic quantum mechanics and, as shown in depth in Chapter 2 and Section 2.4, in the absence of relativity, this means studying the external potential exerted by pointwise nuclei and the corresponding electron density that integrates to N.

The ontology of quantum chemistry is supported by the underlying quantum mechanics, which is an extremely successful framework from the qualitative and quantitative point of view. However, as discussed in the previous Section, quantum chemistry is very limited from the epistemological point of view: very few terms from FMT can be associated with an univocous meaning in this context.

Perhaps the most fundamental concept in FMT that has its meaning unchanged by the quantum revolution is that of *element*. An element is defined as a *"species of atoms; all atoms with the same number of protons in the atomic nucleus"*.[3] Note that the notion of element is associated with the external potential of pointwise nuclei. As coulombic decay is $\propto 1/R^2$ and therefore nuclear potentials are noticeable over large distances, any and all stable binding in chemistry must arise from the compensation of repulsive internuclear potentials due to electrons.

Therefore, the notion of element stems from the local properties of the spherical potential that nuclei exert, i.e. there is a specificity that has to do with the discrete augmentations of such potential. This comes to say that, were nuclear charges a continuum, there would not be a proper definition of element.

The chemistry of elements is thus the chemistry of the Born-Oppenheimer approximation (cf. Section 2.1): the chemistry of a discrete local external potential and the electron density. So far, the context of quantum mechanics within this approximation is respected. On the other hand, the concept of element is tightly bound to the concept of atom, which is far more ephemeral in the quantum context.

Indeed, as we will later see, defining atoms without a prior definition of element is quite complicated, and so the historical background of the concept merits some attention here.

1.2.1 Chemical elements

Mechanical corpuscularism of the 17th century held particle *shape* as a fundamental property. This is particularly well documented for acid-base reactions that resulted in salts, in part because inorganic acids were of interest in protochemical alchemy. Acids where considered elongated spear-like particles, hence aggresive and corrosive, which would become interlocked in the pores and holes of alkali substances. Matter was thought to be composed of different fundamental particles with a distinct shape.

Over the 18th century, dynamic atomism, as coined by Newton and others, replaced much of what was attributed to shape to interparticle forces. Quoting Newton directly: *"There are therefore Agents in Nature able to make the Particles of Bodies stick together by strong Attractions. And it is the Business of experimental Philosophy to find them out"*. Thus, shape becomes suitability for different forces.

In 1789, Antoine Lavoisier, introduced the modern notion (i.e. in the atomic context) of *element*. His list of known elements included *light* and *caloric*, but is remarkably successful in the classification of these newtonian *"particles of bodies"*.

Until the early 19th century an element would remain distinct from the unified category of atom. J. J. Berzelius devised a way to quantify atomic weights, which led to the first plausible classifications and finally to the periodic laws, generally attributed to D. Mendeleev and his publications in 1869. In his 1889 Faraday Conference before the (Royal) Chemical Society, Mendeleev would say: *"Certain characteristic properties of the elements can be foretold from their atomic weights"*. Naturally, the question of isotopes was not easily understood, "which for instance led to a dilemma in the case of Co ($Z_{Co} = 27$) and Ni ($Z_{Ni} = 28$), as cobalt has a larger atomic mass.

Henry Moseley would derive integer nuclear charges from his work on the X-ray diffraction pattern of elementary substances. This would eventually support the apparent arbitrary nature of atomic masses, and would later lead to the elucidation of nuclear structure. This advancements date from 1913 onwards. Thus, the current atomic notion of element is roughly ten years older than the Schödinger equation.

Classification of elements is an unsolved problem. While, in general, the division between metals and non-metals is accepted, the extent of metalloids and functional subdivisions of metals are contested. Most of these divisions are based in a few selected properties of elementary substances, which often do not hold under careful examination. For instance, we know that noble gas compounds exist, including the Na_2He solid under high pressures. The great variability in properties for transition metals has led to some further subdivisions, such as refractory or noble metals.

While this much seems naive, it is undoubtedly true that this conventional classification of elements is routinely used. The first thought spared by a chemist when reflecting on the elementary composition of a solid state system will almost always regard whether its components are more likely to form a binary solid salt (metals plus non-metals, hence ionic bonds) and be subsequently insulating, or not. Many other examples could be given in this same direction, hinting at the conceptual importance of these conventional cathegories. In the following Subsections this point will be showcased.

1.2.2 The need for atoms

Let us examine the current meaning of atom: *"Smallest particle still characterizing a chemical element. It consists of a nucleus of a positive charge (Z is the proton number and e the elementary charge) carrying almost all its mass (more than 99.9%) and Z*

electrons determining its size".[3] Unsurprisingly, the practical definition and the historical development of the term are intertwined, and the result is perhaps deliberately fuzzy: we do not have a satisfactory definition of atom that does not stem from the notion of element, which is a species of atoms.

The given definition immediately implies that, just as elements are classified in groups and blocks, atoms belong to the same groups and blocks as their parent elements. Atomistic theories, and FMT in many ways, are strictly mereological: substances borrow their properties from the wholes they belong to, and particularities are treated exceptionally.

Atomistic ontology has consequences in our rationalization. Some will be better showcased while discussing bonding and chemical structure, but combining the given definition of atom with the periodic table of elements, straightfowardly we assume that periodic properties apply to elements and their characteristic atoms, which is often false because atomic entities do not exist proper in molecular systems. As more chemical space is explored, areas further away from the guidelines of FMT are discovered and rationalized. In the best cases, this results in important notions being reinforced. In the worst cases, it leads to redundant categories and terminology.

We commonly put forward a series of atomic properties: atomic radius (or *size*, as referenced in the previous definition), electron affinity, ionization energy, electronegativity and oxidation states, among others; some of which we consider transferable when building chemical structures, and some of which we order periodically. Only the ionization energy is rigorously defined, albeit only for isolated model quantum systems that we can roughly assimilate with atoms.

Arguably, the concept of atom can be deemed neither necessary nor central. It could be said that chemistry – in the current context – is better expressed in terms of arrangements of point-wise nuclei and quantum electrons, which give rise to possible ideal arrangements: elementary substances and compounds, atoms and molecules, on a uniform ground. Change – reactivity – is then restricted to the rearrangement of nuclei and/or electrons. However, much accumulated chemical knowledge would be lost in this reduction, and atoms play a central role in chemistry.

Electronegativity

Originally, the notion of *elemental* electronegativity arose from an electrochemical approach. When a substance is decomposed electrochemically, negatively charged ions are liberated from the positive pole and vice versa. This comes to show that, qualitatively, the atoms of some elements attach electrons more strongly than others.

The concept of electronegativity owes its current form to Pauling, defined as *" the power of an atom in a molecule to attract electrons"*. He introduced a revolutionary scale of electronegativities in 1932. Values were refined by A. L. Allred in 1961.

We will use χ_A for Pauling's atomic electronegativity for *atom A* throughout this text. Due to its relative character, which runs on a scale from 0.79 (Cs) to 3.98 (F) in adimensional units.

The original method for the calculation of χ_A was:

$$|\chi_A - \chi_B| = (eV)^{-1/2}\sqrt{DH^0(AB) - \frac{DH^0(AA) - DH^0(BB)}{2}} \tag{1.1}$$

where eV are electronvolts, there to make the scale adimensional; $DH^0(AB)$ are the standart bond dissociation enthalpies for diatomic compounds (or else, depending on experimental availability) and $DH^0(H-H)$ is fixed at 2.20 as a reference. The

underlying assumption is that bonds with a certain ionic character are stronger than non-polar homonuclear bonds.

Notably, Pauling's method may trivially be expanded to substituents by calculating bond dissociation enthalpies. The only ingredient needed are $DH^0(AB)$, which are not necessarily easy to determine experimentally, but can be generalized to formal oxidation states, bonds with a particualr functional group, etc. to take into accound the molecular environment.

Note that, as defined by Pauling, electronegativities are a relational property: the definition concerns differences in electronegativity, not electronegativities themselves. Other definitions do give explicit expressions for atomic electronegativities.

Indeed, there are many alternative scales for electronegativities, such as Mulliken's and Allen's scales. However, they normally correlate well to Pauling's and present a similar periodic trend. Electronegativity, together with the concept of valence and derived rules, is a pillar of FMT.

1.2.3 Chemical structure

J. B. Richter proposed the law of definite proportions in 1792. Completed with the observations of J. L. Proust, and his introduction of the term stoichiometry, the resulting concepts are still valable in chemistry today. Lavoisier himself, and J. Dalton, participated in the development of the atomic theory: atoms are discrete and rearrangement leads to change.

Just as the periodic laws provided a causal relation of sorts between atomic mass and properties, stoichometry cements atomistic by allowing elementary substances and compounds. We will refer to the question of this fundamental arrangement of atoms in matter as chemical structure. This conceptual step is needed to understand atomistic models of bonding and structure, as opposed to mechanical models that preceded it.

It must be noted that most analytical techniques that are capable of atomistic resolution have been developed in the last 50 years. For a significant period of time, only physical and chemical separation and characterization techniques, together with elementary analysis, were available for the study of chemical structure.

For example, the structue of CH_4 can be derived with purely chemical means. Monosubstitution of methane with Cl leads to a single chemical species with a formula that matches CH_3Cl, hence all C–H bonds must be analogous. Disubstitution leads to CH_2Cl_2, which is a single species. Hence, a tetrahedral structure for methane can be put forward with symmetry considerations. This example reflects the state of affairs in the beginning of the XXth century.

Models that explain, justify and predict chemical structure have spearheaded development in the chemical sciences. Consequently, chemical structure is a central concept of contemporary chemical sciences. We routinely assume that substances are built by atoms that are held together by chemical bonds in ways that are governed by symmetry. The notion of atom is therefore necessary to discuss chemical structure.

As the atomistic ontology of chemistry has already been introduced from a historical and conceptual perspective, we will now focus on the purely structural point of view.

Valence

William Higgins developed a model of divided force theory, which can be understood in the framework of dynamic atomism. Quoting Higgins directly: *"Let us suppose iron or zinc to attract oxygen with the force of* 7*, sulphur to attract it with the force of* $6\frac{7}{8}$*,*

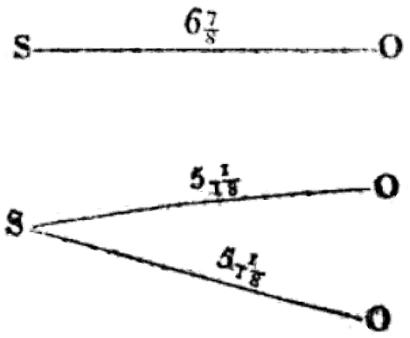

Figure 1.1: Chemical structures and bond *"forces"* as drawn by W. Higgins.

and hydrogen with the force of $6\frac{5}{8}$*"*, then this force would be due $\frac{1}{2}$ to oxygen and $\frac{1}{2}$ to sulphur. Then coherently, S–O bonds in the SO_2 molecule would have a force ≈ 5 instead of ≈ 6.9. Two of its structures are shown in Figure 1.1

The theory of chemical structures, and the concept of valence as we know it, evolved during the 19th century with notable contributions by E. Frankland, who coined combining power, and J. Loschmidt, to whom we owe the multiple line representation of double and triple bonds. The question of chemical structure is then put forward: if each atom has a limited combining power, or valence, how do atoms arrange themselves? And, furthermore, what is the interplay between chemical structure, as opposed to mere chemical composition, and properties?

Pioneering contributors to chemical structure theory, like A. M. Butlerov and A. Kekulé, suspected the tetravalency of carbon from 1860 onwards – the famous case of benzene needs no introduction. However, atomistic models so far did not incorporate electronic structure explicitely, while the atomic model of E. Rutherford was well on its way and studies on the electrical nature of matter by S. Arrhenius and others were being conducted.

G. N. Lewis is responsible for much of the contemporary parlance. In 1916 he identified chemical bonds with shared pairs of electrons. Together with I. Langmuir and W. Kossel, the octet rule and the electron-pair model were developed and boasted remarkable success. Valence became the concept we use nowadays. The resulting framework is sometimes referred to as the electronic theory, as it partially shifts focus from atoms to electrons.

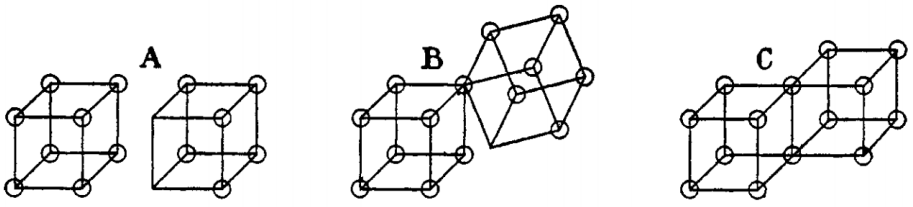

Figure 1.2: Mesomeric forms of the I_2 molecule as presented by G. N. Lewis. Accordingly, **A)** would correspond to an ionic situation I^-I^+, **B)** to an abhorrent one-electron bond, **C)** to the usual covalently bound I_2.

Ionic compounds were then understood on the basis of weakly bound electrons which

are transferred to satisfy octet rules, while covalent bonds are due to shared electrons from the atomic valence shells.

Atomic charges were expressed in terms of discrete polar numbers, from which the contemporary concept of oxidation state can be derived. Partial charges were introduced by C. Ingold and E. H. Ingold in 1926, who are also responsible for the terms electrophile and nucleophile as we know them today. Naturally, the concept of valence breaks down in several cases. Notable examples are what we now call hypervalent molecules (e.g. SF_6), which spark significant controversy even today.

As a small remark, a significant development of the Lewis-Langmuir octet rule and subsequent bonding model was put forward by J. W. Linnett from 1961 onwards, known as Linnett double-quartet theory.

Tautomery and resonance

The concept of mesomery is interpreted by the electronic theory of Lewis on the basis of different bonding possibilities among which structures may switch (see Figure 1.2 for his take on I_2 on the basis of cubic atoms).

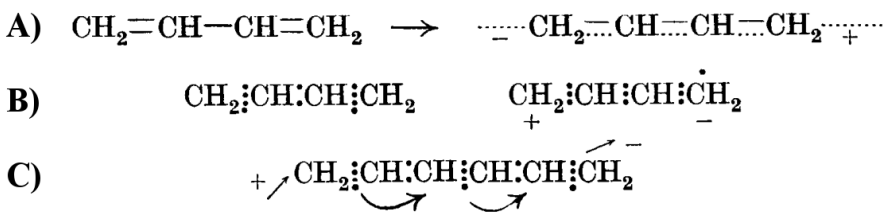

Figure 1.3: Three plausible depictions of conjugation in polyenes. **A)** showcases a partial valency depiction, **B)** represents a Lewis-Langmuir approach and **C)** includes curly arrows to explain delocalization. Adapted from early work by R. Robinson.

The concept of resonance would later be introduced (we will discuss the term in Section 3.2) which very nearly mirrors this feature, though mesomerism persists in chemical language through the work of Ingold among others. Arrow pushing (or curly arrows), as introduced by R. Robinson, also facilitate the understanding of resonance in terms of chemical structures, which made sense of some of the biggest flaws of the theories of valence.

Lewis structures are still commonly used and represented without much modification. However, his skeptical approach to quantum mechanics (*"the entering wedge of scientific bolshevism"*), in spite of his contemporaneity with several forerunners, meant that a true attempt at unification had to wait for L. Pauling and his seminal book *The Nature of the Chemical Bond* in 1939. By then, the contemporary notions of spin and quantum numbers were already introduced.

Note that Pauling himself had an atomistic take on bonding – in particular, through the atomic concept of valence – which led him to some notable misconceptions. His infamous calculation of the frequency at which benzene resonates between the two Kekulé structures suffices as an example. The fine line between isomerism and tautomerism is indeed an educational hassle at times, because we tend to associate structural properties to our conception of bonds. Therefore, two resonant structures with different bond orders might be incorrectly thought to be geometrically different.

The basic ideas of qualitative resonance theory can be outlined in few precepts that are founded in Lewis structures. Any chemical structure can be drawn using atoms – with their core electrons tightly bound – and valence electrons forming bonds. Covalent bonds connecting atoms are formed by pairs of electrons of opposite spin, free valence atoms couple to form lone pairs and unpaired electrons are localized on one or another atomic center. Ionic bonds can be formed by transferring valence electrons from one atom to another, which gives rise to localized positive and negative charges.

The "real" molecule is thought to be "resonating" between all structures, which are simply electronic configurations. Contributions from different structures depends on their relative stability. Many chemical species have a dominant Lewis structure. The stability of different Lewis structures is assessed using hierarchical qualitative rules:

- Compliance of the octet rule.
- Maximize the number and the strength of chemical bonds.
- Minimize the number of charged atoms, minimize and maximize separation between unlike and like charges respectively.
- Localize negative charges in electronegative atoms, positive charges in electropositive atoms.
- Maintain aromatic substructures locally.

It is inferred that having multiple relevant structures is energetically favorable. The behaviour and properties of the molecule will be governed by the weighted average of all contributing structures. Such approaches are succesful at explaining and predicting a wide array of effects, a notable example being electrophilic substitutions on benzene.

Most of the qualitative rules can be derived from classical physics and need no further explanation. The last one has to do with aromaticity. Current understanding of what aromaticity is or implies is somewhat poor and consequently open to an intense debate. We will avoid this topic for now, as it is far too vast to cover.

Valence shell electron pair repulsion

The Valence Shell Electron Pair Repulsion (VSEPR) model relates the electronic structure of the valence shell with molecular structure. As its name implies, it is deeply rooted in the concepts of valence shell and electron pair that were championed by Lewis, but implements some notable modifications that substantially improve its predictive power.

Notably, VSEPR theory seemlessly incorporates hypervalence or hypercoordination, and predicts accurate geometries for many different molecules. Geometries can be predicted by solving Thomson's problem using a Coulomb potential and considering the legitimate entity of *lone pairs* of electrons.

Many well-known phenomena in chemistry can be rationalized using the VSEPR model and are not trivial to understand by other means. A notable example is the anomeric effect in pyranose rings, which is attributed to the repulsion given by the tetrahedrally located lone pairs of oxygen atoms. Hence, hydroxyl substituents adjacent to the O atom in the ring favour axial orientations.

However, note that VSEPR fails for many transition metal complexes, species like $TeCl_6{}^{2-}$, and multiple isoelectronic series. Failure in molecules with heavy atoms is

usually attributed to the inert pair effect. Uneven number of electrons are also usually difficult to treat, and result in inconsistent treatments of $AB_3^\bullet$ radicals, for instance.

A fairly more substantial criticism could be made with respect to the choice of potentials for different coordinations. In the simple AX_n case, VSEPR-allowed geometries are solutions for Thomson's sphere problem for a given potential between lone pairs and bonds, which is arguably improvable by introducing specific potentials between such entities.

1.2.4 Atom in a molecule, functional group

Over the 19th century, the elucidation of chemical structures in terms of atoms and valence was progressively achieved. The underpinning is still an atomic theory, and furthermore, an atomic ontology. That is, electrons are *part* of an atom, their effect notably included in atomic properties assuming all-neutral atoms.

Therefore, the local properties of molecules are largely determined by their atomic composition, which conditions chemical bonding as well. In the early 19th century, the term radical was used to refer to a reactive fragment, mono or polyatomic, that preserved its chemical identity in different contexts. The influential work of C. Gerhardt solidified the notion of transferability on the basis of groups of atoms.

Much of what is (even today) understood as transferable is based on strict solution chemistry, and breaks down in other contexts. In any case, the concept of functional group, functionalization and transformation is still widely used in organic chemistry.

Some noteworthy features that can be considered transferable on the basis of atoms or functional groups are:

- Electronegativity – and nucleophilicity
- Bond length and angle, characteristic frequencies in infrarred spectra
- Pairwise bond energies, homolytic standard dissociation enthalpies $DH^0(AB)$
- Inductive and mesomeric effects, chemical shifts in nuclear magnetic resonance

In FMT, chemists rationalize chemical reactivity in terms of *moieties* or *sites* that have properties governed by their local (atomic, functional group) properties which are altered by the inductive and mesomeric effects of other moieties. The setup of (atomic) chemical structure theory is necessary to understand how we depict chemical bonds.

1.3 Chemical bonding

What do we consider a bond? An accepted definition reads: *"There is a chemical bond between two atoms or groups of atoms in the case that the forces acting between them are such as to lead to the formation of an aggregate with sufficient stability to make it convenient for the chemist to consider it as an independent "molecular species".*[3] Therefore, bonds are both based on atoms and convenience. As both convenience and atoms are quite vague concepts, the resulting definition is very fuzzy but useful nevertheless.

Usually chemists distinguish among different types of bonds. Notably, we orchestrate a difference between (discrete) molecules, separated by non-negligible distances with respect to their own size, and compounds. Reality is that everything is interacting with everything forming a vast heterogeneous aggregate that we call matter.

From a mathematical perspective, the interaction between molecular species can be treated using perturbation expansions of fragment wavefunctions (perturbation theory will be covered to a degree in Chapter 2). In a simplified way, we may split chemical bonds from weaker interactions by considering that chemical bonds are not, by definition, suitably described using perturbatory treatment. That is, chemical bonding plays a major role in the wavefunctions of the involved subsystems.

Let us generalize the notion of a chemical bond, in the context of quantum chemistry, to any situation in which the repulsive potential experienced by a nucleus A with respect to an arrangement of nuclei B, C, D, etc. is alleviated by the distribution of electron density between them, giving rise to a minima in the PES of the system that lies between the cusp of nuclear repulsion (when the two entities approach ($R \to 0$) and a constant energy ($R \to \infty$). If this feature of the PES can be projected as a function of the nuclear coordinates of two nuclei, $\mathbf{R}_A$ and $\mathbf{R}_B$ we will consider this bond to have "two-centers".

Consequently, we may define what non-bonded might be in the same spirit. Two non-bonded chemical species may have their respective degrees of freedom decoupled, and we may displace one or the other set of nuclei in the PES without altering the energy of the other fragment. Note that this definition is only possible if size-consistency holds, which will be defined in Section 2.3. It can be nevertheless inferred that such a situation is highly unlikely in most contexts, i.e. in solution chemistry all solute molecules affect each other through the solvent. Therefore, this meaning of non-bonded represents an extreme situation in which the function that couples the internal coordinates of the two chemical species is constant and equal to zero.

On the other hand, bond types are one of the key aspects that derive from the atomistic and electronic notions of FMT, and those are increasingly difficult to grasp in the context of quantum chemistry. In this Section we will critically examine the most distinct types of chemical bonds, and relate them to each other critically.

1.3.1 Covalent bonding

Covalent bonds could be called electron-sharing bonds in the framework of the electronic theory of Lewis. From a contemporary point of view, this sharing is understood to be observable through a significant electron density accumulation between the supposedly bonded nuclei, which alleviates the nuclear repulsion.

Coherently, more electrons being shared between atoms lead to larger density accumulation between nuclei and stronger – *multiple* – bonds. As electron pairs exist distinctly in the Lewis representation, multiple bonds may operate individually. Contemporary FMT explanations incorporate some orbital concepts (such as σ and π orbitals) in order to properly tackle these inconsistencies.

To assign a covalent bond a chemist often traverses two (atomistic) axes:

- Which atom pair is under consideration?
- Is the character of at least one of the atoms non-metallic?
- Is the electronegativity difference between them low?

Covalent bonds are only thought to exist between non-metallic atoms that have similar electronegativities. This requires an a prioristic knowledge of 1) which pairwise atoms should be considered; 2) metallic and non-metallic character, which are flexible as we have seen; 3) electronegativity values, which are quite ill-defined.

The first point is already troublesome, but the second point is fuzzy as it is. What should we call the bonds in aluminium carbide Al_4C_3 or aluminium nitride AlN_3? Should those be covalent enough, as in allotropic carbon forms? The third point is even worse. $\Delta\chi_{AB} = |\chi_A - \chi_B|$ is often taken as a criterion, but differences in atomic electronegativities very often fail. For instance, most alkali hydrides (LiH, KH, etc.) would be covalent, while molecules such as HF and PF_3 would be ionic.

All in all, FMT does not have any proper way to define covalent bonds on its own. The ideal case of covalent bond is simply any main-group homonuclear diatomic. Some reference values are $DH^0(HH) = 105$ kcal/mol in H_2 and $DH^0(NN) = 226$ kcal/mol for the triple bond in N_2.

1.3.2 Ionic bonding

Ionic bonds are usually considered opposite to covalent bonds. If the latter are based on sharing, ionic bonds are based on *transfering* electrons. Naturally, this is a Lewis-like atomic notion, which finds further foundations on the notion of atomic charge and oxidation number, which corroborates the notion of electron transfer or donation: an electron is transferred from one neutral atom to another neutral atom with higher electronegativity. The resulting cation and anion pair interact through electrostatics, and a significant dipole moment is generated along the bond axis.

The questions to solve in order to assign ionic bonds are similar to those seen for covalent bonds:

- Which atom pair is under consideration?
- Is the character of at least one of the atoms non-metallic?
- Is the electronegativity difference between them high?

Ionic bonds are thus thought to exist between pairs of non-metallic atoms with very different electronegativities, with $\Delta\chi_{AB} > 1.5$ at least. In this particular case, the first question is usually more troublesome, due to the ubiquity of ionic situations in the solid state. Take for example the cubic $Fm\bar{3}m$ halite (NaCl) lattice. Are there six ionic $Cl^- - Na^+$ bonds per Cl nuclei in the bulk? Note that the solid state community may prefer using global – and definitely not pairwise – concepts for describing "bonding" in such structures, as Madelung constants and lattice energies.

At the molecular level, ionic bonds are associated with strong electrolytes due to the historical background of solution chemistry. However, Pauling's scale classifies all H–X bonds as covalent except for H–F. Triflic (CF_3SO_3H) and fluorosulfuric (HSO_3F) acids are much stronger acids than sulfuric acid, which signals that the O–H bond is in fact extremely polarized.

It is generally quite accepted that a covalent ideal case exists, but no ideal ionic bond exists because, naturally, two charged particles of opposite sign should simply approach infinitely. Recall, however, that Pauling's electronegativity scale is based on the notion that ionic character makes covalent bonds stronger.

1.3.3 Metallic bonding

Metallic bonds fill the remaining gap in the three-question scheme outlined before, and gather all remaining possible pairs of metallic elements – which are the majority of the periodic table. The key concept in metallic bonding is delocalization. As such, we do not expect metallic bonds to be necessarily pairwise. The previous schemes reduce to:

- Which atom groups are under consideration?
- Is the character of these atoms metallic?

Interestingly, the IUPAC has no definition for metallic bond. In fact, the fundamental understanding of metals stems mostly from electrochemical studies which showcase their cationic properties in solution and their conductive properties in the solid state. The free electron and near free electron models were pioneered by Sommerfeld in the early 20th century, and have had a lasting impact. The domain of metallic materials has been historically abandoned by chemistry in favour of other specialities and their terminologies, albeit the blooming field of inorganic chemistry has recovered much of the current discourse.

Consequently, bonding in metals is often understood as a delocalized spread of conducting electrons and a fixed lattice of positive nuclei. This is very inconsistent with the atomistic pictures of covalent and ionic bonds, and FMT as a whole.

Metallic bonds are thought as inherently delocalized, giving rise to conduction bands in periodic systems. However, as per the last sentence, based on properties, graphene would be a notable example of metallic bonding, which would be in contradiction with the basic statement from which we have started. On the other hand, bonding in Li_2 can hardly be said to be conducting or delocalized, as a homonuclear diatomic, but is expected to be metallic as per our initial assumption. Metallic bonds are plagued by much of the same conceptual problems from which aromatic systems suffer: innately delocalized phenomena fail to fit into an atomistic view.

Alas, FMT gives no local representation of the bonding present in metals: it can not. On a sidenote, it is important to notice that relativistic effects have a significant weight on the properties of metallic elements; which is portrayed quite directly by the melting point of Au (1100^o C) and Hg (-39^o C).

1.3.4 Other bonding regimes

The aforementioned bonding regimes are well-respected. However, as we have signaled in the different Subsections, there are many cases that cannot be cathegorized a priori, nor based on properties. In any case, they mostly stem as slight variations from the schematic representations offered by FMT. We will cover some of them as such in the most general way.

Multicenter-multielectron covalent bonds

Perhaps the most clear case of a breakdown of the covalent bond model of Lewis is the diborane molecule (B_2H_6), in which two boron atoms are bridged by two hydrogen atoms, as shown in Figure 1.4 A. The Lewis picture simply does not hold, boron is attached to four atoms and hydrogen is attached to two atoms. The plausible pseudofolk explanation is what has been called a three-center two-electron bond, in which each bridging B−H bond is only "half" a bond. Agostic bonds, including the several documented cases of H_2 coordination to metallic centers, are another example of this type of situation.

Other non-Lewis stable structures have been rationalized with similar ideas, which we can call multicenter and multielectron bonds or, simply, non-Lewis bonds. Ozone (Figure 1.4 B) is accordingly considered a three-center four-electron bond, like the triiodide anion (Figure 1.4 C) and the bifluoride anion (Figure 1.4 D). Naturally, non-minima points of the PES may present similar features quite often, in particular during bond formation and bond breaking and other activated complex situations.

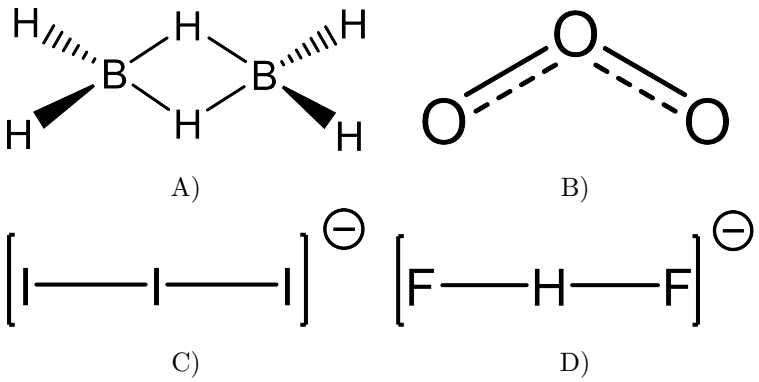

Figure 1.4: **A)** Diborane B_2H_6 **B)** Ozone O_3 **C)** Triiodide anion I_3^- **D)** Bifluoride HF_2^-

Many other examples of non-Lewis bonds exist. Simple molecules such as NO or ClO_2 are quite hard to rationalize in terms of pairs, leading to other hypothetical two-center N-electron bonds.

A proper comprehension of all such species is hardly possible from FMT. Quantum mechanics, and derived concepts, are necessary to understand for instance why ozone is bent and the triiodine anion is linear, which is not hard to picture by understanding σ and π systems and overlap integrals.

Dative bonds

Quite opposite to the bountiful examples in the previous Subsection, dative bonds are considered two-electron two-center bonds in which the electrons involved belong to the same atom. The paradigmatic example is the complex formed between borane BH_3 and ammonia NH_3, where the dative bond takes an electron pair that formally belongs to the nitrogen atom. This bond is of significant strength ($DH^0(BN) \approx 30$ kcal/mol). Other notable examples include tricarbon dioxide C_3O_2 and hexaphenylcarbodiphosphorane.

Presumably, this situation is similar to many coordination complexes, in which a ligand (e.g. H_2O) donates an available electron pair to a central metal with formal positive charge. In any case, the resulting bond is expected to be weaker and more ionic in nature than a standard covalent bond.

It results impossible to distinguish dative bonds from other covalent bonds with just FMT and without a causal explanation for bond formation (i.e. from a static molecular representation). A straightforward example is the SO_4^{2-} anion, which could be inferred to have four S−O dative bonds. This would seem bizarre to any organic chemist. However, combined with finer quantum details, some qualitative behaviors can be justified (e.g. the non-linear preference of C_3O_2).

Haptic bonds

Haptic bonds are a particular type of bond that is better exemplified by ferrocene and other metallocenes. Haptic bonds are thought to form between the π-system of a ligand and a central atom. In this sense, they are simply a multicenter generalization of dative bonds.

They are therefore pestered by the same conceptual issues in which an "origin" has to be assigned to electrons.

Hydrogen bonds

Hydrogen bonds are a very well known type of interaction arising from the proximity of a covalently bound hydrogen atom (i.e. with its single formal valence occupied) and an electron rich moiety in a separate atom. In spite of their typically reduced bond dissociation enthalpies when compared to formally covalent bonds (e.g. $DH^0(\text{H}\cdots\text{O}) \approx 5$ kcal/mol over 1.97 Å in water), they can be of great importance.

Due to the formal limit of one covalent bond for the single electron of hydrogen, the nature of this ubiquitous interactions has been a historical source of debate, in which they have been classified as anything from strictly electrostatic interactions to plainly covalent bonds.

At the same time, the abundance of situations in which hydrogen bonds may arise fosters the identification of subtypes, such as resonance assisted hydrogen bonds and symmetric hydrogen bonds.

In any case, the most identifying characteristic is the presence of hydrogen. For instance, dative explanations at the FMT level are also fitting of hydrogen bonding: a partially positive center receives an electron pair from an electron-rich moiety. Furthermore, symmetric hydrogen bonds can be understood as a three-center four-electron bonds.

Other *elementary* bonds

Mirroring hydrogen bonds, there are few more bonding regimes that are recognized mostly on the basis of the atomic participants. Notably, halogen bonds have the same definition as hydrogen bonds just exchanging the hydrogen atom for a halogen atom.

Subsequently, triel and tetrel bonds have been described based on similar principles, which in the end reduce to the identification of regions with positive electrostatic potential that are therefore susceptible to interact with regions with significant electron density.

Critically, many of such bonds respond to tautological premises, which in a way is also an issue with hydrogen bonds. In different situations, such bonds could probably be cathegorized using previous schemes, but the atomistic point of view favors an understanding based on transferability.

Chapter 2

Foundations of Quantum Chemistry

Contents

The wave function of an isolated non-relativistic quantum system abides to the time-dependent Schrödinger equation: [4]

$$i\hbar\frac{\partial\Psi(\mathbf{x},t)}{\partial t} = \widehat{\mathcal{H}}\Psi(\mathbf{x},t), \tag{2.1}$$

where $\widehat{\mathcal{H}}$ is the Hamiltonian operator of the system, and $\Psi(\mathbf{x},t)$ is the wave function of the N particle system, $\mathbf{x} = \{\mathbf{x}_1, \mathbf{x}_2, ..., \mathbf{x}_N\}$ represents the spin-space coordinates of all N particles and t is a parameter that accounts for time. More precisely, $\Psi(\mathbf{x},t)$ is a unit vector defined on a complex finite Hilbert space $\mathbb{H}$ and $\widehat{\mathcal{H}}$ is an hermitian operator acting upon $\mathbb{H}$.

The wave function contains all possible information about the system. First and foremost, it determines the probability density distribution $\rho(\mathbf{x},t)$ of the system

$$\rho(\mathbf{x},t) = |\Psi(\mathbf{x},t)|^2 \tag{2.2}$$

On the other hand, $\widehat{\mathcal{H}}$ accounts for the energetics of the physical system under inspection. The set of i eigenvectors of $\widehat{\mathcal{H}}$ constitutes a complete orthonormal basis for $\mathbb{H}$, and the corresponding spectrum of eigenvalues E_i are the real values of the energy of the system. In our particular case, $\widehat{\mathcal{H}}$ is time independent.

Equation 2.1 is a partial differential equation of first order in t and second order in $\mathbf{x}$. Let us focus on *separable* solutions, of the form

$$\Psi(\mathbf{x},t) = f(t)\psi(\mathbf{x}) \tag{2.3}$$

which can be used in Equation 2.1 to show

$$i\hbar\frac{f'(t)}{f(t)} = \frac{\widehat{\mathcal{H}}\psi(\mathbf{x})}{\psi(\mathbf{x})} = const. = \alpha \tag{2.4}$$

taking

$$f(t) = f(0)e^{-i\alpha t/\hbar} \tag{2.5}$$

$$\widehat{\mathcal{H}}\psi(\mathbf{x}) = \alpha\psi(\mathbf{x}) \tag{2.6}$$

As previously stated, the eigenvalues of $\widehat{\mathcal{H}}$ are the energies of the system, and hence the constant α is E. Then, due to the lack of time-dependence, and mirroring classical mechanics, quantum states in which Equations 2.5 and 2.6 hold are called *stationary states*. More precisely, the wave function can be expressed as

$$\Psi(\mathbf{x},t) = f(0)e^{-iEt/\hbar}\psi(\mathbf{x}) = e^{-iEt/\hbar}\Psi(\mathbf{x},0) \tag{2.7}$$

Therefore, a stationary state oscillates in time with a complex phase factor and angular frequency $E/\hbar$. Consequently, if we are interested in stationary states, only the eigenvalue problem of $\widehat{\mathcal{H}}$ has to be solved:

$$\widehat{\mathcal{H}}\psi(\mathbf{x}) = E\psi(\mathbf{x}) \tag{2.8}$$

Equation 2.8 is the time-independent Schrödinger equation. Solving and understanding this equation for N-electron systems is the underlying objective of most of this Chapter.

2.1 Born-Oppenheimer approximation

Using atomic units, in a system formed by N-electron system with M nuclei the non-relativistic Hamiltonian is given by

$$\widehat{\mathcal{H}} = \underbrace{-\frac{1}{2}\sum_{A}^{M}\frac{\nabla_A^2}{m_A} + \sum_{A>B}\frac{Z_A Z_B}{R_{AB}}}_{\widehat{\mathcal{H}}_{nuc}} \underbrace{-\frac{1}{2}\sum_{i}^{N}\nabla_i^2 + \sum_{i>j}\frac{1}{r_{ij}} - \sum_{A,i}\frac{Z_A}{r_{iA}}}_{\widehat{\mathcal{H}}_{el}} \tag{2.9}$$

where the indexes A, B and i, j run over nuclei and electrons respectively. ∇_i^2 and ∇_A^2 are the electron and nuclear Laplacian operators respectively. m_A is the mass of nucleus A, Z_A, Z_B are the nuclear charges of nuclei A and B respectively. r_i and R_A are the space coordinates of electron i and nuclei A, respectively. Distances are expressed as $r_{ij} = |r_i - r_j|$ with analogous notation for nuclei-nuclei and electron-nuclei terms. Spin coordinates are omitted because the non-relativistic Hamiltonian is spin-independent.

The first two terms in the definition of $\widehat{\mathcal{H}}$ in Equation 2.9 are the kinetic and electrostatic nuclear terms, $\widehat{T}_n$ and $\widehat{V}_{nn}$ respectively, which can be grouped into a nuclear term $\widehat{\mathcal{H}}_{nuc}$. The next two terms, $\widehat{T}_e$ and $\widehat{V}_{ee}$, are the kinetic and electrostatic operators for electrons. Together with the final term $\widehat{V}_{en}$ which accounts for the interaction of nuclei and electrons, they can be grouped as $\widehat{\mathcal{H}}_{el}$.

$$\widehat{\mathcal{H}}_{nuc} \quad = \widehat{T}_n + \widehat{V}_{nn} = \quad -\frac{1}{2}\sum_{A}^{M}\frac{\nabla_A^2}{m_A} + \sum_{A>B}\frac{Z_A Z_B}{R_{AB}} \tag{2.10}$$

$$\widehat{\mathcal{H}}_{el} \quad = \widehat{T}_e + \widehat{V}_{ee} + \widehat{V}_{en} = \quad -\frac{1}{2}\sum_{i}^{N}\nabla_i^2 + \sum_{i>j}\frac{1}{r_{ij}} - \sum_{A,i}\frac{Z_A}{r_{iA}} \tag{2.11}$$

The wave function $\Psi(\mathbf{r}, \mathbf{R})$ of such system must contain nuclear $\mathbf{R} = \{\mathbf{R}_1, ..., \mathbf{R}_M\}$ and electronic $\mathbf{r} = \{\mathbf{r}_1, ..., \mathbf{r}_N\}$ degrees of freedom. However, given the difference in the mass of electrons and nuclei ($\approx 10^3 - 10^5$) and that the forces exerted onto one another must be equal, nuclei must move considerably slower than electrons. Assuming that nuclear degrees of freedom remain constant with respect to electronic ones, $\widehat{T}_n = 0$ and $\widehat{V}_{nn} = const.$ Then the whole term $\widehat{\mathcal{H}}_{nuc}$ becomes a constant, and the wave function becomes separable such as

$$\Psi(\mathbf{r}, \mathbf{R}) = \Psi_{el}(\mathbf{r}; \mathbf{R})\Psi_{nuc}(\mathbf{R}) \tag{2.12}$$

where the electronic wave function $\Psi_{el}(\mathbf{r}; \mathbf{R})$ describes the electronic structure at a given nuclear configuration $\mathbf{R}$. It depends only parametrically on nuclear degrees of freedom. The aforementioned approximation that results in the factorization of the wave function in Equation 2.12 is known as the Born-Oppenheimer approximation.

The eigenvalue equation can then be solved only for the electronic wave function at a given $\mathbf{R}$

$$\widehat{\mathcal{H}}_{el}\Psi_{el}(\mathbf{r}; \mathbf{R}) = \left(\widehat{T}_e + \widehat{V}_{ee} + \widehat{V}_{ne}\right)\Psi_{el}(\mathbf{r}; \mathbf{R}) = E_{el}\Psi_{el}(\mathbf{r}; \mathbf{R}), \tag{2.13}$$

where E_{el} is the electronic energy. The total energy can be obtained by adding the nuclear potential energy $\widehat{V}_{nn}(\mathbf{R})$.

$$E(\mathbf{R}) = E_{el} + \widehat{V}_{nn} \tag{2.14}$$

Therefore, by sampling all possible nuclear arrangements it is possible to define a Potential Energy (*hyper*)Surface (PES) for a given N-electron system with M nuclei. In non-linear molecular systems with translational and rotational symmetry, the PES has $3M-6$ dimensions, which might be further reduced by symmetry elements.

In what follows, the main goal will be to solve the electronic structure problem as presented by Equation 2.13 in order to obtain (and, possibly, explore) the PES for any given molecular system.

Except whenever explicitly mentioned the *el* subscript will be dropped, as well as the parametric dependence on nuclear configuration. Thus, $\widehat{H}$ will the electronic Hamiltonian, Ψ (which shall become $|\Psi\rangle$ in Dirac notation) will represent a corresponding N-particle wavefunction, and E will simply be the electronic energy. In this notation, the electronic time-independent Schrödinger equation is just

$$\widehat{H}|\Psi\rangle = E|\Psi\rangle \tag{2.15}$$

and analogously the energy can be written as the expectation value of the Hamiltonian

$$E = \langle\Psi|\widehat{H}|\Psi\rangle \tag{2.16}$$

2.1.1 Many-electron systems

Equation 2.8 can only be solved analytically for systems with a single electron ($N=1$) such as the hydrogen atom. The analytical closed-form solutions to the one-electron case are functions called orbitals.

In the hydrogen atom, for a given combination of quantum numbers n, l and m the corresponding orbital can be expressed as a combination of a radial part R_{nl} and a Laplace spherical harmonic Y_{lm} in spherical coordinates,

$$\psi_{nlm}(r,\theta,\phi) = R_{nl}(r)Y_{lm}(\theta,\phi) \tag{2.17}$$

It suffices to mention here that the radial part has an exponential decay term e^{-cr} when moving away from the nuclei that exerts the radial potential, and recall that Laplace spherical harmonics form an orthonormal set.

Before moving onto more complex systems, it must be noted that electrons posses spin, an intrinsic angular momentum. Electrons are fermions known to have a value of the spin quantum number equal to $\frac{1}{2}\hbar$ with a z component of $\pm\frac{1}{2}\hbar$.

Under the non-relativistic model, spin coordinates (σ) are included on the wave function by two spin functions $\alpha(\sigma)$ and $\beta(\sigma)$, corresponding to eigenvalues of the z component of the spin operator equal to $+\frac{1}{2}\hbar$ and $-\frac{1}{2}\hbar$, respectively. These two spin functions are orthonormal by definition and form a complete set.

Therefore, the electronic wave function in Equation 2.13 must depend on spin coordinates $\mathbf{x} = \{\mathbf{r}, \sigma\}$ and parametrically on the nuclear coordinates $\mathbf{R}$.

Thus, spin functions have to be added to the spatial orbitals in Equation 2.17. Let us express the spatial part as $\psi_i(\mathbf{r})$, a function of a position vector $\mathbf{r}$, then spin orbitals take the form

$$\begin{aligned} \phi^{\alpha}(\mathbf{x}) &= \psi(\mathbf{r})\alpha(\sigma) \\ \phi^{\beta}(\mathbf{x}) &= \psi(\mathbf{r})\beta(\sigma) \end{aligned} \tag{2.18}$$

and thus two electrons *occupy* the same spatial part in spite of the one-electron nature of orbitals. For the most part this treatment will suffice for the inquiries of quantum

chemistry. In the following, we will refer to spatial orbitals simply as orbitals, $\phi_i(\mathbf{r})$ and will reserve the term spin orbital for whenever spin functions must be explicitly added due to significance.

Wavefunction ansatz

As a starting guess, many-electron systems can be described using combinations of the one-electron solutions. This is both convenient and intuitive: it gives a way to express the total wavefunction in terms of a known solution, and expects that every electron behaves in a similar way. For instance, a possible wavefunction Ψ for an N-electron system would be

$$\Psi(\mathbf{x}_1, \mathbf{x}_2, \dots \mathbf{x}_N) = \phi_1(\mathbf{x}_1)\phi_2(\mathbf{x}_2)\dots\phi_N(\mathbf{x}_N) \tag{2.19}$$

However, the fact that electrons are identical particles must be accounted for in the wavefunction. For instance, in a system with $N = 2$ and spin-coordinates $\mathbf{x}_1$ and $\mathbf{x}_2$ respectively, the probability of finding both electrons simultaneously in volume elements $d\mathbf{x}_1$ and $d\mathbf{x}_2$ around points $\mathbf{x}_1$ and $\mathbf{x}_2$ is given by $|\Psi(\mathbf{x_1}, \mathbf{x_2})|^2 d\mathbf{x}_1 d\mathbf{x}_2$. Were the two particles interchanged, the resulting probability $|\Psi(\mathbf{x}_2, \mathbf{x}_1)|^2 d\mathbf{x}_1 d\mathbf{x}_2$ ought to be the same since electrons are indistinguishable particles irrespective of our arbitrary tags 1 and 2. Hence,

$$|\Psi(\mathbf{x}_1, \mathbf{x}_2)|^2 = |\Psi(\mathbf{x}_2, \mathbf{x}_1)|^2 \tag{2.20}$$

which implies that the wavefunction is either symmetric or antisymmetric with respect to the exchange of electrons 1 and 2,

$$\begin{aligned} \Psi(\mathbf{x}_1, \mathbf{x}_2) &= \Psi(\mathbf{x}_2, \mathbf{x}_1) \text{ (symmetric)} \\ \Psi(\mathbf{x}_1, \mathbf{x}_2) &= -\Psi(\mathbf{x}_2, \mathbf{x}_1) \text{ (antisymmetric)} \end{aligned}$$

Electrons are fermions and follow Pauli's exclusion principle and thus the antisymmetric option has to be respected. More generally, the wavefunction of an N-electron system has to satisfy

$$\widehat{P}\Psi(\mathbf{x}_1, \mathbf{x}_2, \dots, \mathbf{x}_N) = (-1)^p \Psi(\mathbf{x}_1, \mathbf{x}_2, \dots, \mathbf{x}_N) \tag{2.21}$$

where $\widehat{P}$ is the permutation operator and p is the number of permuted electron pairs. The form of the wavefunction presented in Equation 2.19 does not comply and hence is generally not valid.

A general and compact way to construct a wavefunction for an N-electron system that satisfies the antisymmetry requirement was given by John C. Slater in 1929 [5] starting from an orthogonal set of orbitals $\phi_i(\mathbf{x}_i)$. It is nowadays known as a Slater determinant;

$$\Psi(\mathbf{x}_1, \mathbf{x}_2, ...\mathbf{x}_N) = \frac{1}{\sqrt{N!}} \begin{vmatrix} \phi_1(\mathbf{x}_1) & \phi_2(\mathbf{x}_1) & \dots & \phi_N(\mathbf{x}_1) \\ \phi_1(\mathbf{x}_2) & \phi_2(\mathbf{x}_2) & \dots & \phi_N(\mathbf{x}_2) \\ \vdots & \vdots & \ddots & \vdots \\ \phi_1(\mathbf{x}_N) & \phi_2(\mathbf{x}_N) & \dots & \phi_N(\mathbf{x}_N) \end{vmatrix} \tag{2.22}$$

where $1/\sqrt{N!}$ is a normalization factor.

Determinant expansion guarantees that Slater determinants satisfy the antisymmetry requirement in Equation 2.21. Every electron is indistinguishable. Whenever two rows or two columns corresponding to particles i and j are swapped, it holds that

$$\Psi(\mathbf{x}_1, \mathbf{x}_2, \ldots, \mathbf{x}_i, \mathbf{x}_j, \ldots, \mathbf{x}_n) = -\Psi(\mathbf{x}_1, \mathbf{x}_2, \ldots, \mathbf{x}_j, \mathbf{x}_i, \ldots, \mathbf{x}_n) \tag{2.23}$$

Furthermore, Pauli's exclusion principle is also implicitly satisfied: if $\phi_i = \phi_j$, two rows are identical and $\Psi = 0$. Therefore, there is a maximum of two electrons – with opposed spins – per orbital. However, limiting the wavefunction to this particular form has some underlying effects that will be examined in the following sections.

Variational principle

Given that the closed form solutions to the electronic problem are not analytically available, a computational approach is required to approximate the exact solution. Dirac notation will slowly be introduced from this point on in order to simplify notation. The variational principle states that the ground state energy E_0 is a lower bound to the expectation value of $\widehat{H}$ for any approximate wavefunction Ψ. Let us proove it for any normalized wavefunction composed by an orthonormal linear combination of orbitals ϕ_i, such as

$$\begin{aligned} \Psi &= \sum_i c_i \phi_i \\ \sum_i |c_i|^2 &= 1 \\ \int \phi_i(\mathbf{x}) \phi_j(\mathbf{x}) d\mathbf{x} &= \langle i|j\rangle = \delta_{ij} \end{aligned} \tag{2.24}$$

the expectation value of the Hamiltonian $\widehat{H}$, which is hermitian, can be written as,

$$\langle \Psi|\widehat{H}|\Psi\rangle = \sum_{i,j} c_i^* c_j \langle \phi_i|\widehat{H}|\phi_j\rangle = \sum_i |c_i|^2 E_i \tag{2.25}$$

which we can rewrite, using the conditions from Equation 2.24,

$$\langle \Psi|\widehat{H}|\Psi\rangle = |c_0|^2 E_0 + \sum_{i>0} |c_i|^2 E_i \tag{2.26}$$

Given that by definition E_0 is always the lowest energy solution,

$$\langle \Psi|\widehat{H}|\Psi\rangle \geq E_0 \tag{2.27}$$

in which the equality only applies if Ψ is exactly the ground state wavefunction. Naturally, the variational principle requires that $\widehat{H}$ is the exact electronic Hamiltonian.

2.2 The mean-field approximation

Using a single Slater determinant (Equation 2.22) as the form of the wavefunction, an attempt can be made to solve Equation 2.13. Given that the wavefunction is expressed as a combination of single-electron functions, it seems reasonable to rewrite the electronic Hamiltonian as

$$\widehat{H} = \sum_{i}^{N} \widehat{h}_i + \widehat{V}_{ee} \tag{2.28}$$

where $\widehat{h}_i$ is the one-electron operator, analogous for every electron i,

$$\widehat{h}_i = \widehat{T}_e + \widehat{V}_{en} \tag{2.29}$$

The expectation value of the energy of the electronic Hamiltonian with a Slater determinant we shall denominate Ψ_{HF} can be shown to be exactly

$$E_{HF} = \langle \Psi_{HF} | \hat{H} | \Psi_{HF} \rangle = \sum_{i}^{N} h_i + \frac{1}{2} \sum_{i}^{N} \sum_{j}^{N} (J_{ij} - K_{ij}) \tag{2.30}$$

where

$$h_i = \int \phi_i^*(\mathbf{x}) \widehat{h}_i \phi_i(\mathbf{x}) d\mathbf{x} = \langle \phi_i | \widehat{h}_i | \phi_i \rangle \tag{2.31}$$

represents the kinetic energy and potential energy for the electron described by ϕ_i. The two remaining terms, J_{ij} and K_{ij}, are two electron integrals that arise from the $\widehat{V}_{ee}$ term. They are called Coulomb and exchange integrals respectively,

$$J_{ij} = \int \int \phi_i^*(\mathbf{x}_1) \phi_i(\mathbf{x}_1) \frac{1}{r_{12}} \phi_j^*(\mathbf{x}_2) \phi_j(\mathbf{x}_2) d\mathbf{x}_1 d\mathbf{x}_2 = \langle \phi_i \phi_i | r_{12}^{-1} | \phi_j \phi_j \rangle \tag{2.32}$$

$$K_{ij} = \int \int \phi_i^*(\mathbf{x}_1) \phi_j(\mathbf{x}_2) \frac{1}{r_{12}} \phi_j^*(\mathbf{x}_2) \phi_i(\mathbf{x}_1) d\mathbf{x}_1 d\mathbf{x}_2 = \langle \phi_i \phi_j | r_{12}^{-1} | \phi_j \phi_i \rangle \tag{2.33}$$

J_{ij} represents the Coulomb interaction between electron i in ϕ_i and an average local potential given by the other electrons j in the system:

$$j_j(\mathbf{x}_1) = \int \left[\phi_j^*(\mathbf{x}_2) \frac{1}{r_{12}} \phi_j(\mathbf{x}_2) \right] d\mathbf{x}_2 \tag{2.34}$$

which defines a corresponding Coulomb operator $\hat{j}_j(\mathbf{x}_1)$ acting on $\phi_i(\mathbf{x}_1)$,

$$\hat{j}_j(\mathbf{x}_1) \phi_i(\mathbf{x}_1) = \int \left[\phi_j^*(\mathbf{x}_2) \frac{1}{r_{12}} \phi_j(\mathbf{x}_2) \right] d\mathbf{x}_2 \phi_i(\mathbf{x}_1) \tag{2.35}$$

On the contrary, there is no classical equivalent for the interpretation of the exchange term. It arises from the antisymmetry of Ψ_{HF}. However, analogously we may write the following exchange operator $\hat{k}_j(\mathbf{x}_1)$, by its action on a spin orbital $\phi_i(\mathbf{x}_1)$

$$\hat{k}_j(\mathbf{x}_1) \phi_i(\mathbf{x}_1) = \int \left[\phi_j^*(\mathbf{x}_2) \frac{1}{r_{12}} \phi_i(\mathbf{x}_2) \right] d\mathbf{x}_2 \phi_j(\mathbf{x}_1) \tag{2.36}$$

The Coulomb and exchange operators can be combined with the one electron operator, defining the Fock operator $\widehat{F}$ as

$$\widehat{F}_i = \widehat{h}_i + \sum_{j}^{N} \left[\hat{j}_j - \hat{k}_j \right] \tag{2.37}$$

where the subindex i can be removed, as the operator is equal for all the N-electrons in the system.

It is important to notice now that the Fock operator represents a mean-field approximation: the choice of Ψ_{HF} determines that $\widehat{V}_{ee}$ is only applied as a combination of a local Coulomb mean field term and the exchange which is strictly due to antisymmetry.

Analogously, it must be noted that the Hamiltonian (Equation 2.28) is not the Fock operator (Equation 2.37). Only the former returns the energy of the many-electron system, yet the second is retrieved naturally by assuming that a single Slater determinant is appropriate for the wavefunction.

2.2.1 Hartree-Fock equations

Under the premise of the variational principle, the Hartree-Fock (HF) method attempts to find the set of orbitals that minimize E_{HF} (Equation 2.30) of the Slater determinant wavefunction Ψ_{HF}. It was developed by Douglas Hartree, Vladimir A. Fock and others.

At the same time, it imposes an orthonormality constraint upon the orbitals through the overlap integral, which was introduced in Equation 2.24,

$$\langle i|j\rangle = \int \phi_i(\mathbf{x})\phi_j(\mathbf{x})d\mathbf{x} \tag{2.38}$$

upon which we impose $\langle i|j\rangle = \delta_{ij}$. The problem can be formulated in terms of Lagrange multipliers. Starting with the following Lagrangian;

$$\mathcal{L}_{HF} = E_{HF} - \sum_{ij}^{N} \lambda_{ij}(\langle\phi_i|\phi_j\rangle - \delta_{ij}) \tag{2.39}$$

where λ_{ij} are the Langrange multipliers, we enforce that $\mathcal{L}_{HF}$ is stationary with respect to small changes in orbitals

$$\delta\mathcal{L}_{HF} = \delta E_{HF} - \sum_{ij}^{N} \lambda_{ij}(\langle\delta\phi_i|\phi_j\rangle - \langle\phi_i|\delta\phi_j\rangle) = 0 \tag{2.40}$$

Solving Equation 2.40 leads to

$$\widehat{F}|\phi_i\rangle = \sum_{j}^{N} \lambda_{ij}|\phi_j\rangle \tag{2.41}$$

Since $\widehat{F}$ is an hermitian operator, the matrix formed by Langrange multipliers λ_{ij} is also hermitian and therefore can be diagonalized by a unitary transformation $\mathbf{U}$ such that

$$\mathbf{U}^{\dagger}\lambda\mathbf{U} = \lambda^{'} = \begin{cases} \lambda_{ij}^{'} = 0, \\ \lambda_{ii}^{'} = \epsilon_i \end{cases} \tag{2.42}$$

Using the same unitary transformation for every spin orbital ϕ_i, the above equation turns into a diagonal form, which is just the canonical HF equation

$$\widehat{F}|\phi_i\rangle = \epsilon_i|\phi_i\rangle \tag{2.43}$$

The corresponding orbitals are the canonical Hartree-Fock spin orbitals and the eigenvalues ϵ_i are known as molecular orbital energies or eigenvalues.

This equation is ruled by an effective one-electron operator, the Fock operator $\hat{F}$, which couples the N equations of the system together. However, each individual electron

does not feel the instantaneous field generated by the remaining $N-1$ electrons of the system.

For the moment, spin parts may be removed under the assumption that α and β orbitals have identical spatial parts, and thus only $N/2$ of them are needed for a total of N electrons. Limitations of the HF method will be covered extensively in Section2.3.

2.2.2 Roothaan-Hall equations

The eigenvalue problem outlined in Equation 2.43 is still quite hard to solve numerically. Clemens C. J. Roothan and George G. Hall developed a scheme to represent the HF equations in a non-orthonormal basis set.

Starting with the spatial part of the HF equations, each spatial function ψ_i can be expanded in a linear combination of N_{basis}, known as spatial functions χ_ν, and expansion coefficients $C_{\nu i}$:

$$\psi_i = \sum_{\nu}^{N_{basis}} C_{\nu i}\chi_\nu(\mathbf{r}) \tag{2.44}$$

If the functions of choice, $\chi_\nu(\mathbf{r})$, are atomic orbitals, the approach is called the Linear Combination of Atomic Orbitals (LCAO) method. The naming is usually preserved even though other convenient functions are often used instead.

Assuming that the set of basis functions is complete, the expansion 2.44 is exact. Usually, the expansion is limited to a finite set of N_{basis} functions, and the orbitals $\{\psi_i\}$ are just approximate solutions of the HF equations.

As a lower bound, note that N_{basis} must at least be as large as the number of spin orbitals under consideration $N_{basis} \geq N$. An empirical upper bound can be attained with ease by verifying the convergence of E_{HF} (Equation 2.30) with respect to N_{basis}.

Inserting the basis set expansion 2.44 into Equation 2.43 and multiplying by $\langle\chi_\nu|$ leads to

$$\sum_{\nu}^{N_{basis}} C_{\nu i}\langle\chi_\mu|\widehat{F}|\chi_\nu\rangle = \epsilon_i \sum_{\nu}^{N_{basis}} C_{\nu i}\langle\chi_\mu|\chi_\nu\rangle \tag{2.45}$$

For convenience, an overlap matrix $\mathbf{S}$ is defined with elements

$$S_{\mu\nu} = \langle\chi_\mu|\chi_\nu\rangle \tag{2.46}$$

and a Fock matrix $\mathbf{F}$ is defined with elements

$$F_{\mu\nu} = \langle\chi_\mu|\widehat{F}|\chi_\nu\rangle \tag{2.47}$$

With this in mind, Equation 2.43 may now be rewritten as

$$\sum_{\nu}^{N_{basis}} F_{\mu\nu}C_{\nu i} = \epsilon_i \sum_{\nu}^{N_{basis}} S_{\mu\nu}C_{\nu i} \tag{2.48}$$

These are the so-called Roothaan equations, that can be written more compactly as

$$\mathbf{FC} = \mathbf{SC}\epsilon \tag{2.49}$$

where $\mathbf{C}$ is the matrix of expansion coefficients $C_{\nu i}$ and ϵ is the diagonal matrix of orbital energies ϵ_i.

In order to calculate $\mathbf{C}$ and ϵ, we need an explicit expression for the Fock matrix elements,

$$F_{\mu\nu} = H_{\mu\nu}^{core} + \sum_{\sigma\lambda} P_{\sigma\lambda}[\langle\mu\lambda|\nu\sigma\rangle - \frac{1}{2}\langle\mu\lambda|\sigma\nu\rangle] \tag{2.50}$$

where $H_{\mu\nu}^{core}$ is an element of the core Hamiltonian matrix,

$$H_{\mu\nu}^{core} = \langle\mu|\widehat{h}|\nu\rangle, \tag{2.51}$$

and $P_{\mu\nu}$ are elements of density matrix $\mathbf{P}$,

$$P_{\mu\nu} = 2\sum_{j}^{N/2} C_{\mu j} C_{\nu j}, \tag{2.52}$$

Equation 2.49 is a non-linear eigenvalue problem due to the dependence of the Fock matrix on the expansion coefficients in the density matrix. Thus, the equation has to be solved by an iterative procedure. The iterative procedure is based on the fact that it is possible to orthonormalize the basis by using an unitary transformation $\mathbf{U}$ such as

$$\mathbf{U}^{\dagger}\mathbf{S}\mathbf{U} = \mathbf{I} \tag{2.53}$$

where $\mathbf{U}^{\dagger}$ is the adjoint matrix of $\mathbf{U}$, and $\mathbf{I}$ is the identity matrix. As long as $\mathbf{U}$ is non-singular, Equation 2.49 can be written as

$$(\mathbf{U}^{\dagger}\mathbf{F}\mathbf{U})(\mathbf{U}^{-\mathbf{1}}\mathbf{C}) = (\mathbf{U}^{\dagger}\mathbf{S}\mathbf{U})(\mathbf{U}^{-\mathbf{1}}\mathbf{C})\epsilon \tag{2.54}$$

If, once more, we define $\mathbf{F}^{'}$ and $\mathbf{C}^{'}$ as

$$\mathbf{F}' = \mathbf{U}^{\dagger}\mathbf{F}\mathbf{U} \tag{2.55}$$

$$\mathbf{C} = \mathbf{U}\mathbf{C}' \tag{2.56}$$

Equation 2.49 is transformed into

$$\mathbf{F}'\mathbf{C}' = \mathbf{C}'\epsilon \tag{2.57}$$

Equations 2.55-2.57 are the transformed Roothaan equations, which are once more non-linear. The problem is therefore solved iteratively: an initial guess is used to generate an approximate $\mathbf{C}$ and, through transformation, an $\mathbf{F}'$ matrix. A new set of orbitals is obtained, which can then be used to generate a new Fock matrix, and so on until self-consistency is achieved in the orbital energy matrix and in the density matrix.

The iterative approach herewith outlined is usually called the Self-Consistent Field (SCF) method, given its nature.

All the matrices that arise in the development of the Roothaan-Hall equations are of size $N_{basis} \times N_{basis}$. In our current formalism, the ground state wave function are constructed by taking the $N/2$ eigenvectors of $\mathbf{F}$ with lower orbital energies and discarding the remaining ones. These eigenvectors determine the spatial part of the occupied orbitals, while the remaining empty eigenvectors are known as virtual orbitals.

As only occupied orbitals are used in the construction of the Fock operator, they are the only ones which are optimized in the SCF procedure. Virtual orbitals are only implicitly optimized through their orthogonality with respect to the occupied ones.

Notes on the SCF procedure

In a very simplified form, the HF equations reduce to:

$$E = \min_{\phi_i} \langle \Psi_{HF} | \widehat{F} | \Psi_{HF} \rangle \tag{2.58}$$

While the Roothaan-Hall procedure gives a convenient way to solve this problem in matrix form, the SCF procedure is open to various improvements. A very basic technique is called F-mixing or just SCF damping, in which a contribution of $\mathbf{F}$ from a previous iteration is mixed with the newly calculated one during the SCF. Thus, at iteration n

$$\mathbf{F} = a\mathbf{F}_n + (1-a)\mathbf{F}_{n-1} \tag{2.59}$$

SCF damping can often improve the convergence of the procedure. Some other techniques that have to do with SCF convergence are Direct Inversion of the Iterative Subspace (DIIS) introduced by Peter Pulay in 1982, and shooting techniques.[6, 7]

A startling observation might be made with respect to the solutions to the Roothaan-Hall equations: SCF procedures select self-consistency, leading not necessarily to the lowest energy wavefunction. Hence, *in principle* excited states can be calculated in simple HF theory with a single Slater determinant. Avoiding collapse towards the ground state solution can be achieved using algorithms such as the Maximum Overlap Method (MOM) and SCF damping.

As a final remark, it was demonstrated by J. Harris [8] that the convergence of the energy is to the second order of the convergence of the density. This means that, in general, verifying that the density matrix $\mathbf{P}$ is converged suffices to ascertain that the energy is converged, while the opposite may not be true.

Basis sets in quantum chemistry

Appropriate selection of basis sets is not trivial. As highlighted previously, the radial part of nuclei-centered orbitals is akin to

$$\psi^{STO}(x,y,z) = Cx^a y^b z^c e^{-\xi r} \tag{2.60}$$

where C is a normalizing constant, x, y, z are Cartesian coordiantes with angular momentum controled by $n = a + b + c$, r is the distance from the nuclei and ξ is a proportionality constant that reflects the effective charge of the nucleus. n is a natural number that represents the principal quantum number.

Basis sets can be constructed using linear combinations of such radial functions, which are usually called Slater Type Orbitals (STO). STO basis sets are, in principle, very close to the spirit of the LCAO method: they constitute a very faithful one-electron basis set.

However, more generally, other functions are used which compromise physical rigor for ease of computation. The most widely used basis sets in quantum chemistry use Gaussian Type Orbitals (GTO), given by

$$\psi^{GTO}(x,y,z) = Cx^a y^b z^c e^{-\xi r^2} \tag{2.61}$$

Obviously, GTOs can not reproduce the correct behavior of STOs neither at $r \to 0$ nor at $r \to \infty$. Notably, the electronic wavefunction should have a discontinuity on top of nuclear positions. This is known as Kato's cusp condition, as pointed out by Tosio Kato in 1957. This condition is not respected by GTOs, which are cuspless at $r = 0$.

However, products and integrals of GTOs are much easier to compute. In order to compensate for their inaccuracies, several GTOs can be linearly combined into a Contracted GTO (CGTO) to mimic every atomic orbital,

$$\psi^{CGTO}(x,y,z) = \sum_i C_i x^a y^b z^c e^{-\xi_i r^2} \tag{2.62}$$

where the contraction coefficients C_i are normalized. The approach is represented in Figure 2.1.

Very often in chemical applications basis sets are categorized depending on the number of basis functions (with respective coefficients in the SCF procedure) used per atomic orbital. As such, minimal basis sets use a single (STO, GTO, CGTO or else) function per orbital, double-ζ basis sets use two, triple-ζ basis sets use three, and so on.

Many CGTO basis sets exist for different purposes in modern quantum chemistry, which will not be covered here. Different basis set expansions might be used as well, as plane waves or polynomials. In any case, the basis set limit can be retrieved by increasing N_{basis}.

2.2.3 Restricted and unrestricted formalisms

The Hartree-Fock equation (Equation 2.43) has been introduced for a general set of (spin)orbitals $\{\phi_i\}$, defined as the product of an orbital ϕ_i and an $\alpha(\sigma)$ or $\beta(\sigma)$ spin function.

In closed-shell chemical systems, with an even number of electrons N, spin polarization is 0 and the spatial part of α and β spin orbitals is identical. Within the single-determinant Hartree-Fock framework, this is known as the Restricted Hartree-Fock (RHF) formalism. However, in some cases it is convenient to have different spatial parts for α and β spin orbitals, in what is called the Unrestricted Hartree-Fock (UHF) formalism.

Notably, systems with an unpaired number of electrons are usually better represented by having a genuine orbital for the unpaired electron. With this in mind, and starting from Equation 2.43 in terms of the orbitals, in the UHF formalism we have

$$\widehat{F}^{\alpha}|\psi_i^{\alpha}\rangle = \epsilon_i^{\alpha}|\psi_i^{\alpha}\rangle \tag{2.63}$$

$$\widehat{F}^{\beta}|\psi_i^{\beta}\rangle = \epsilon_i^{\beta}|\psi_i^{\beta}\rangle \tag{2.64}$$

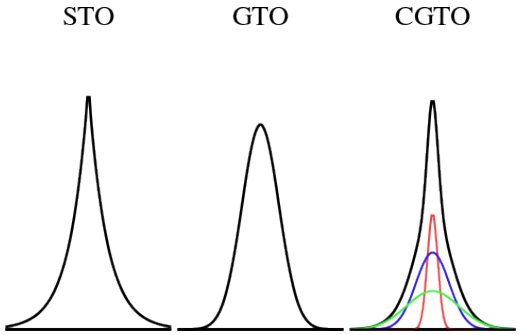

Figure 2.1: Schematic representation of an STO, a GTO and a CGTO basis function. Three colored GTOs are combined into the black-lined CGTO.

with a different Fock operator acting upon the α and β parts

$$\widehat{F}^{\alpha} = \widehat{h}_i + \sum_{j \neq i}^{N_\alpha} (\hat{j}_j^{\alpha} - \hat{k}_j^{\alpha}) + \sum_{j \neq i}^{N_\beta} \hat{j}_j^{\beta} \tag{2.65}$$

$$\widehat{F}^{\beta} = \widehat{h}_i + \sum_{j \neq i}^{N_\beta} (\hat{j}_j^{\beta} - \hat{k}_j^{\beta}) + \sum_{j \neq i}^{N_\alpha} \hat{j}_j^{\alpha} \tag{2.66}$$

The additional term in the spin-resolved Fock operators, $\widehat{j}_{ij}^{\alpha}$, acts upon $N_\alpha = N - N_\beta$ orbitals occupied by β electrons and vice-versa. Since $\widehat{F}^{\alpha}$ depends on the occupied β functions, ψ_i^{β}, and $\widehat{F}^{\beta}$ depends on the occupied α functions, ψ_i^{α}, the two equations must be solved simultaneously.

If the electronic state under consideration has an even number of electrons N, such that there are $N/2$ doubly occupied orbitals, we can consider α and β orbitals to be identical $\psi_i^{\alpha}(\mathbf{r}) = \psi_i^{\beta}(\mathbf{r}) = \psi_i(\mathbf{r})$. The number of occupied α and β orbitals are identical and equal to $N/2$ and thus only a single spatial part needs to be solved,

$$\widehat{F}_i |\psi_i\rangle = \epsilon_i |\psi_i\rangle \tag{2.67}$$

where

$$\widehat{F}_i = \widehat{h}_i + \sum_{j \neq i}^{N/2} (2\hat{j}_j - \hat{k}_j) \tag{2.68}$$

Through which we return to the formalism in Section 2.2.

If the electronic state under consideration does not have an even number of electrons N, the symmetry-breaking of the Slater determinant with respect to spin induces an energy lowering, a new analogous way of solving the HF equations has to be used which is analogous to two coupled Roothaan-Hall procedures, often called the Pople-Nesbet-Berthier equations.

As a consequence of the instability with respect to symmetry-breaking, note that the RHF formalism is often uncapable of dissociating covalent chemical bonds properly. If a molecule would break into two uneven electron fragments, RHF imposes that electrons will be paired irrespective of the bond length. For a hydrogen molecule in the ground state (Σ_g^+), the one-dimensional PES for nuclei at a distance R is shown in Figure 2.2. It can be clearly seen that the excited state with $S = 1$ is needed to describe the dissociated situtation at $R \to \infty$, where the spin of the two electrons is unpaired. This can be achieved by combining two UHF solutions, but simply cannot be described with RHF.

In the simple case in Figure 2.2, the point where symmetry-breaking induces additional stabilization is shown to be at $R \approx 1.6$ Å in what is sometimes called the Coulson-Fischer point.

The main drawback of lifting the symmetry restriction between α and β orbitals is that the single-determinantal wavefunction is no longer an eigenfunction of the total spin operator, $\langle \widehat{S^2} \rangle$. If the expectation value of the spin operator differs significantly from the initial spin, significant mixing from excited configurations has taken place and the results might not be accurate.

As a result, other formalisms exist based on the symmetry-breaking of the HF solutions, including the Restricted Open Hartree-Fock (ROHF) formalism and spin-constrained techniques, which result in quite involved methodologies. The

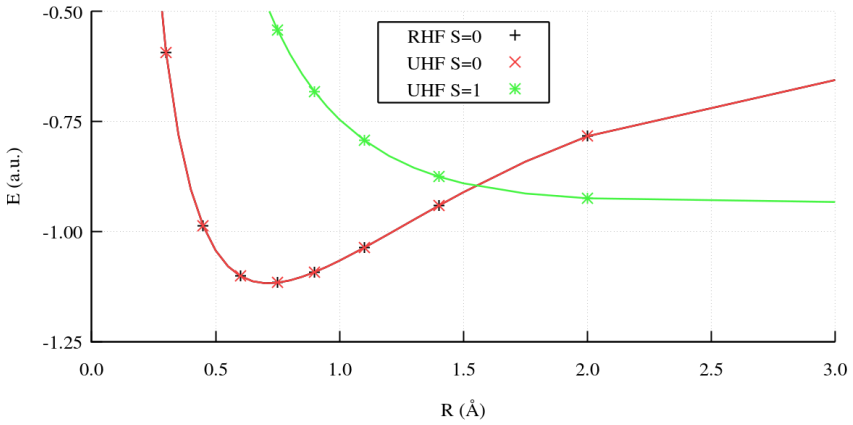

Figure 2.2: Dissociation curves for the H_2 molecule at different theory levels with a STO-3G basis set.

existence of such formalisms is noteworthy in a wider context because, as it will be shown later, HF is often used as the first stepping stone in more sophisticated calculations. However, they will not be covered in detail in this manuscript.

2.3 Electron correlation

HF theory is founded upon several assumptions. Other than the always implicit Born-Oppenheimer approximation and the non-relativistic treatment, HF equations constrain the wavefunction to a single Slater determinant and the true electronic Hamiltonian to the Fock operator.

Therefore, each electron can only interact with the averaged Coulomb potential of all other $N-1$ electrons, but not with their instantaneous positions. This introduces an error, which can be quantified by comparing the HF energy (E_{HF}) and the exact energy E_{exact} at the basis set limit.

$$E_{corr} = E_{exact} - E_{HF} \tag{2.69}$$

The difference, E_{corr}, is often called the correlation energy, and must always be negative. It accounts for the energy lowering that is achieved when electronic motion is instantaneously correlated instead of averaged.

For instance, near the basis set limit for the H_2 molecule, at an equilibrium bond length $R = 0.7609$ Å E_{HF} is -1.133141 a.u. and E_{exact} is approximately -1.173985 a.u. Thus, E_{corr} is merely -0.040846 a.u., a very small 3.4% of the energy. However, chemistry often arises from small differences in large quantities, and this small percentage is often the key. Indeed, we see that this E_{corr} is 25.63 kcal/mol, which is a significant energy in chemical terms. HF theory lies at the heart of quantum chemistry, but it turns out that this limitation makes it unsuitable for quantitative calculations on molecular systems.

This does not mean that the wavefunction is entirely *uncorrelated*, however. Electrons with parallel spins are correlated through the antisymmetry of the wavefunction. However, the term electron correlation is widely used to express the deficits of the HF approximation, which arise from a purely mathematical reason and have no *intrinsc* physical meaning.

Quite often, scientific literature distinguishes two types of electron correlation, which are called static and dynamic for an assortment of reasons that have to do mostly with their mathematical foundations. Utmost care will be taken through this manuscript to properly discuss the question of correlation. Hence, we will first showcase an explicit example for the H_2 molecule, then we will discuss some other simple examples, and only afterwards we will discuss possible categories.

2.3.1 Correlation in the hydrogen molecule

As it has been discussed in Subsection 2.2.3, the restricted HF method cannot dissociate bonds properly. The underlying reason is that constraining the wavefunction to a single Slater determinant is sometimes too crude of an approximation.

In fact, the HF method fails whenever several possible Slater determinants are similarly representative of the true wavefunction, which crudely means that they have similar energies. This was shown in Figure 2.2: in the Coulson-Fischer point the energy of the singlet and triplet determinants is very similar. To properly describe the system, one would need to include more than a single determinant in the wavefunction.

Following this intuition, let us expand the wavefunction as a linear combination such as:

$$|\Psi\rangle = \sum_i C_i |\Phi_i\rangle \tag{2.70}$$

where every Φ_i is generally a symmetry-adapted linear combination of Slater determinants of an N electron system, called a Configuration State Function (CSF). In many cases Φ_i is simply a single Slater determinant as defined in Equation 2.22. In Equation 2.70, C_i would be coefficients that can be obtained variationally by variationally minimizing the total energy.

Let us exemplify using the H_2 molecule. We express orbitals of the system as simple combinations of s-type atomic orbitals, $1s_A$ centered in one nucleus H_A and $1s_B$ centered in the other nucleus H_B, such as

$$\phi_1 = N_g\Big(1s_A + 1s_B\Big)$$
$$\phi_2 = N_u\Big(1s_A - 1s_B\Big)$$

where

$$N_g = \frac{1}{\sqrt{2(1+S)}}$$
$$N_u = \frac{1}{\sqrt{2(1-S)}}$$

and S is just the overlap integral between $1s_A$ and $1s_B$. Note that we are using a minimal basis set in this example. Typically, $1s_A$ and $1s_B$ would typically be expanded in as a linear combination of STOs or GTOs. Thus, ϕ_1 and ϕ_2 are the only two possible orthogonal combinations of the atomic orbitals: the *de facto* molecular orbitals.

In a RHF formalism, let us take the two molecular orbitals ϕ_i and build a wavefunction as a Slater determinant. For the ground state we have

$$|\Phi_0(\mathbf{x}_1,\mathbf{x}_2)\rangle = \frac{1}{\sqrt{2}}\Big(\psi_1(\mathbf{r}_1)\alpha(\sigma_1)\psi_1(\mathbf{r}_2)\beta(\sigma_2) - \psi_1(\mathbf{r}_1)\beta(\sigma_1)\psi_1(\mathbf{r}_2)\alpha(\sigma_2)\Big) = |\phi_1\alpha,\phi_1\beta\rangle \tag{2.71}$$

where $|\phi_i,\phi_j,\dots\phi_N\rangle$ is short hand notation for the Slater determinant of the N-electron system. In this case, it is straightforward to separate the spin part such as

$$|\phi_1\alpha,\phi_1\beta\rangle = \frac{1}{\sqrt{2}}\psi_1(\mathbf{r}_1)\psi_1(\mathbf{r}_2)(\alpha(\sigma_1)\beta(\sigma_2) - \beta(\sigma_1)\alpha(\sigma_2)) \tag{2.72}$$

which, as pointed before, cannot dissociate correctly as we increase the internuclear distance and the overlap becomes negligible. The expectation value of the energy would be the energy of a single H atom and 1/2 of the energy of an H^- anion.

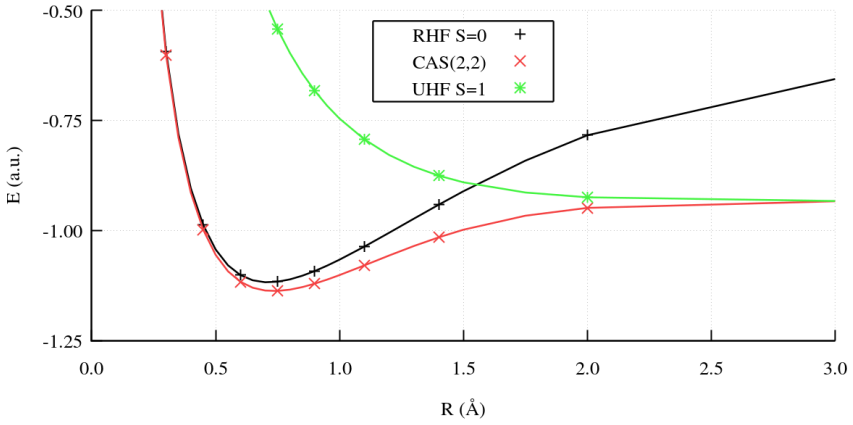

Figure 2.3: Dissociation curves for the H_2 molecule at different theory levels with a STO-3G basis set.

Instead, we can build a new multiconfigurational wavefunction using also the excited state of the same spin symmetry,

$$|\Psi_{MC}\rangle = c_0\Phi_0 + c_1\Phi_1 = c_0|\phi_1\alpha,\phi_1\beta\rangle + c_1|\phi_2\alpha,\phi_2\beta\rangle \tag{2.73}$$

and we devise a procedure to variationally minimize the expectation value of the energy with respect to the coefficients c_i:

$$E = \min_{c_i}\langle\Psi_{MC}|\widehat{H}|\Psi_{MC}\rangle \tag{2.74}$$

Such a wavefunction is able to dissociate the H_2 molecule correctly. This is shown in Figure 2.3, where the wavefunction in Equation 2.73 is represented by the CAS(2,2) method. At the Equilibrium distance, In fact, it turns out that the resulting wavefunction and E are exact for the minimal basis set. Adding CSFs to the wavefunction ansatz improves upon the HF result, correcting for the lack of electron correlation.

In the following section we will systematize this approach.

2.3.2 Configuration Interaction methods

To reach the exact result, all possible independent combinations of CSFs must be included in the wavefunction. If this is the case, the method is called Full Configuration Interaction (FCI) and it is the exact solution for a given basis set choice.

The appropiate expansion can be generated by exchanging occupied orbitals for virtual orbitals starting from a single reference CSF, for example, the RHF ground state. The FCI wavefunction can de written as:

$$|\Psi_{FCI}\rangle = c_0|\Phi_0\rangle + \sum_{ai} c_i^a|\Phi_i^a\rangle + \sum_{ai,bj} c_{ij}^{ab}|\Phi_{ij}^{ab}\rangle + \dots \tag{2.75}$$

In which the coefficients c_i^a applies to the different singly excited CSFs, the coefficients c_{ij}^{ab} apply to the double excited ones, and so on.

Continuing the example from the previous section, we would only need to consider single and double excitations in a 2 electron 2 orbital system. Starting from $\Phi_0 = |\phi_1\alpha\phi_1\beta\rangle$ we would have only one possible linearly independent double excitation, namely

$$|\Phi_{11}^{22}\rangle = |\phi_2\alpha, \phi_2\beta\rangle$$

because the single excitations are redundant. Thus, the expansion in Equation 2.73 is the FCI wavefunction for a minimal basis set, and the result is exact. The total number of CSFs N_{CSF} increases proportional to a binomial coefficient:

$$N_{CSF} \propto \binom{N_{basis}+1}{N} \tag{2.76}$$

Where N_{basis} is the number of basis functions and N is the number of electrons as usual. As N_{basis} increases, which is desirable to approach the basis set limit, the number of determinants explodes and the computational task at hand becomes impractical.

The expansion has to be truncated at some point for practical reasons, which leads to methods called Configuration Interaction (CI). Such methods are ranked hierarchically: Configuration Interaction with Single excitations (CIS), CI with Single and Double excitations (CISD) and so on.

In the H_2 system with a minimal basis set, FCI is the same as CISD and CID. If the basis set is not minimal, more terms arise because there are much many more unoccupied orbitals to which every electron can be excited. Several mathematical rules exist that limit the contribution of certain excitations, such as Brillouin's theorem and Slater's rules. We will not cover CI expansions in detail here.

2.3.3 Multireference methods

As stated in Equation 2.74, we can minimize with respect to the coefficients of the expansion, and obtain every determinant systematically through excitations starting from the HF reference.

However, we can also minimize the multideterminantal ansatz in Equation 2.70 with respect to the expansion coefficients of the basis $C_{\nu i}$ at set at the same time,

$$E = \min_{c_i, C_{\nu i}} \langle\Psi_{MC}|\widehat{H}|\Psi_{MC}\rangle \tag{2.77}$$

At the FCI level, both approaches give equivalent results, and thus the added complexity is not desirable. However, with a finite basis set, the legitimate question of whether adding more determinants or optimizing the expansion coefficients is better.

The general denomination for such methods is Multi-Configurational SCF (MCSCF). Very often, only some *active* part of the wavefunction is expanded in terms of several CSFs in order to reduce the computational effort. These methods are usually called Complete Active Space (CAS) methods and derivations thereof, such as Restricted Active Space (RAS) and others.

Such methods only treat a given number of electrons N and orbitals N_{orb} at the multideterminantal level, and thus carry a term (N,N_{orb}) to indicate the type of the expansion. A CAS(2,2) calculation would imply that a complete CSF expansion is used for 2 electrons in 2 orbitals. As such, in our previous example of minimal basis set H_2, this is once more a FCI calculation.

The selection of the CSFs to include in the expansion for more complex systems is usually subject to some mathematical and empirical constraints, and it is far from a solved problem that will not be covered here.

2.3.4 Coupled Cluster methods

Some desirable properties for any computational approach to solve Equation 2.15 are size-extensivity and size-consistency.

Supposing a method that can provide the wavefunction and corresponding value of the energy $E(A)$ of a given system A. The size-consistency requirement is required if, for two systems A and B that are not interacting – for instance, due to a distance $R_{AB} = \infty$ – it holds that

$$E(AB) = E(A) + E(B) \tag{2.78}$$

From the practical point of view, this condition is very important whenever interaction energies between subsystems have to be computed. Size extensivity has to do with the correct scaling of the electronic energy with the number of electrons N of the system. We will not elaborate further here.

Truncated CI methods are not size consistent. This can be easily seen by writing a CID expansion for our test case A, B and AB with distance $R_{AB} = \infty$ at all times,

$$\begin{aligned} \Psi_{AB} &= \Phi^0_{AB} + \Phi^D_{AB} \\ \Psi_{A} &= \Phi^0_{A} + \Phi^D_{A} \\ \Psi_{B} &= \Phi^0_{B} + \Phi^D_{B} \end{aligned}$$

and so the the condition in Equation 2.78 would hold if

$$\Psi_{AB} = \Psi_A \Psi_B \tag{2.79}$$

but in the CID case we have

$$\Psi_A \Psi_B - \Psi_{AB} = \Phi^D_A \Phi^D_B \tag{2.80}$$

Therefore, the CID wavefunction misses double excitations in the monomers, and Equation 2.78 does not hold. Coupled Cluster (CC) methods expand the wavefunction differently to avoid these issues:

$$|\Psi_{CC}\rangle = exp^{\widehat{T}}|\Phi_0\rangle = (1 + \widehat{T} + \frac{1}{2!}\widehat{T}^2 + \ldots \frac{1}{N!}\widehat{N}^2)|\Phi_0\rangle \tag{2.81}$$

where $\widehat{T} = 1 + \widehat{T}_1 + \widehat{T}_2 \ldots \widehat{T}_N$ is the cluster operator, and the corresponding $\widehat{T}_i$ operators generate excitations analogous to the ones covered in CI theory. CC methods also converge to the FCI result, but they are size-consistent and size-extensive, and are named in an analogous way: CC Single and Double excitations (CCSD), etc. Note that, again, CCSD is FCI for H_2 in a minimal basis set.

2.3.5 Perturbative methods

Electron correlation may also be recovered using perturbation theory. There are many possible approaches. For exemplary purposes, we will stick to non-degenerate Rayleigh-Schrödinger perturbation theory as a framework and Møller-Plesset (MP) perturbation theory as a method.

As often in perturbative approaches, the Hamiltonian of the system is divided in two pieces: a zero-order part, $\widehat{H}_0$, whose solution is known, and a perturbation $\widehat{V}$.

$$\widehat{H} = \widehat{H}_0 + \lambda\widehat{V}$$
$$\widehat{H}_0|\Psi_i^0\rangle = E_i^0|\Psi_i^0\rangle$$

where $\widehat{H}_0$ is the HF Hamiltonian which, again, we will use as reference. $|\Psi_i^0\rangle$, and E_i^0 are its ith eigenvector and eigenfunction respectively. λ is an ordering parameter.

$|\Psi_i\rangle$ and E_i are expanded in a Taylor series in λ that goes from the HF results ($\lambda = 0$) to the fully exact solution ($\lambda = 1$),

$$E_i = E_i^0 + \lambda E_i^1 + \lambda^2 E_i^2 + \ldots, \tag{2.82}$$
$$|\Psi_i\rangle = |\Psi_i^0\rangle + \lambda|\Psi_i^1\rangle + \lambda^2|\Psi_i^2\rangle + \ldots \tag{2.83}$$

Where E_i^n and $|\Psi_i^n\rangle$ are the nth order energy and wavefunction corrections, respectively. First order corrections to E_n and $|\Psi_i\rangle$ are given by

$$E_i^1 = \sum_{n>0} \frac{\langle\Psi_0^0|\widehat{V}|\Psi_n^0\rangle}{E_i^0 - E_n^0} \tag{2.84}$$

$$|\Psi_i\rangle = |\Psi_i^0\rangle + \sum_{n>0} \frac{\langle\Psi_0^0|\widehat{V}|\Psi_n^0\rangle}{E_i^0 - E_n^0}|\Psi_n^0\rangle \tag{2.85}$$

The 2^{nd} order correction (E^2) is the first term which improves upon the HF energy,

$$E_i^2 = \sum_{n>0} \frac{\langle\Psi_0^0|\widehat{V}|\Psi_n^0\rangle\langle\Psi_0^0|\widehat{V}|\Psi_n^0\rangle}{E_i^0 - E_n^0}. \tag{2.86}$$

HF enhanced with the 2^{nd} order correction from Equation 2.86 is often called the MP2 method. Further expansion is possible (MP3, MP4, etc.) but becomes increasingly expensive. Convergence is not trivial except for very small perturbations, as in usual

perturbation theory. In fact, the denominator in Equation 2.86 immediately means that if the energy of the different states is exactly the same the correction will diverge.

MP2 corrections are reasonably cheap and can account for a large percentage of the correlation energy in many situations. However, perturbative series often face problems due divergences. As the method is not variational, MP2 corrections may overestimate correlation effects and lead to artificially low energies beyond the exact limit.

2.3.6 Outlook on electron correlation

To finish this section, some exemplary calculations will be showcased for our model system so far, the H_2 molecule, using different basis sets. We will try to define some concepts related to electron correlation that will be used later on.

With a minimal basis set, as we have said previously, CAS(2,2), CISD and FCI are all exactly the same for H_2. This is shown in Figure 2.4. Notably, it can be seen that MP2 lags behind the exact solution with various degrees of success at different values of the internuclear distance R. Near the equilibrium distance $R \approx 0.76$ Å MP2 is very close to the exact solution.

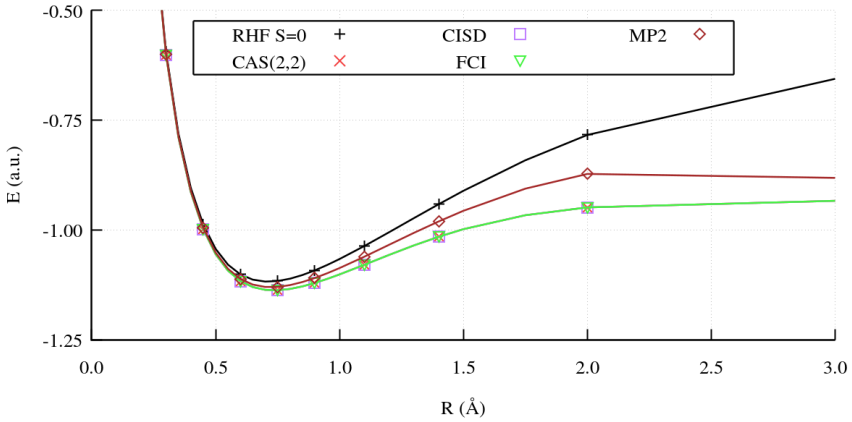

Figure 2.4: Dissociation curves for the H_2 molecule at different theory levels with a STO-3G basis set.

However, as we approach the Coulson-Fischer point, MP2 breaks down because the weight of the doubly excited configuration in the multideterminantal expansion is approximately the same as the weight of the HF reference. Therefore, the perturbation is not small at all: the reference wavefunction and determinant are *very* far from the proper multideterminantal wavefunction.

Let us increase the basis to a double-ζ quality to decouple the exact solutions. In Figure 2.5 we can now see that the dissociation curves properly tend to the energy of two hydrogen atoms (-1 a.u.) unlike Figure 2.4. This signals that we are approaching the basis set limit for this system. However, the Coulson-Fischer problem in MP2 is not fixed whatsoever. We start seeing some discrepancies between the FCI and CAS(2,2) curves, but they are not significant.

As a final test, let us increase the basis set to triple-ζ quality, shown in Figure 2.6. While the MP2 problem persists, the discrepancies between CAS(2,2) and FCI keep increasing. The increasing number of virtual orbitals means that there is an increasing

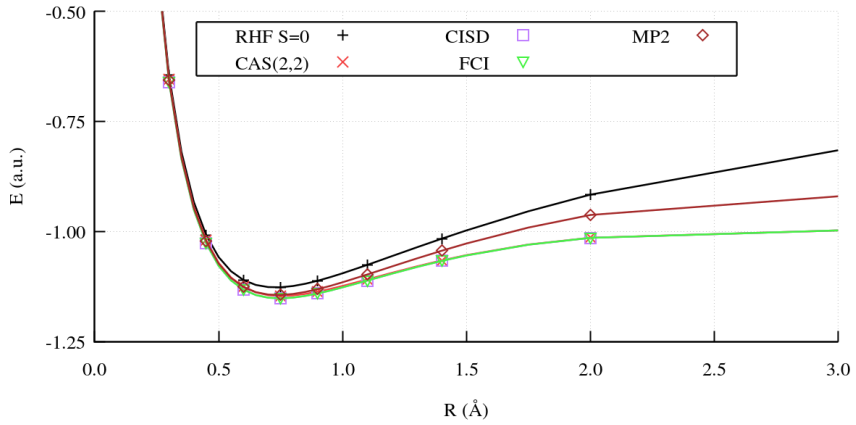

Figure 2.5: Dissociation curves for the H_2 molecule at different theory levels with a 6-31G basis set.

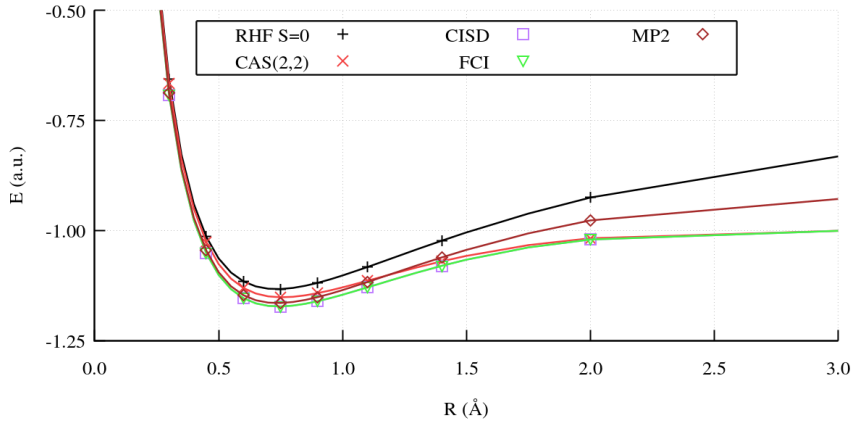

Figure 2.6: Dissociation curves for the H_2 molecule at different theory levels with a cc-PVTZ basis set.

number of excitations which are not accounted for in the CAS(2,2) expansion. These excitations must have a very small weight in the expansion, but contribute to the energy expression nevertheless.

In fact, in Figure 2.6, MP2 gives more accurate values than CAS(2,2) near the equilibrium distance. CAS(2,2) is better again after the Coulson-Fischer point. At the equilibrium distance, considering many excitations in the perturbative series gives a better energy than simply considering the main determinants in the multirreference wavefunction.

Note that correlated methods explore the virtual orbitals, unlike HF theory, and therefore the energy is lowered much more significantly for the MP2 curve than for the HF curve when moving from Figure 2.4 towards 2.6. In general, correlated methods require very large basis sets to converge to the basis set limit.

After considering the different situations and methods in this section, we can attempt to classify two *mathematical origins* of electron correlation:

- Strong correlation is the deficit of a single-reference wavefunction due to the fact that one or a few CSFs which would have large weights in the FCI expansion have not been included. Hence, the qualitative description of a strongly correlated system given by the single reference calculation will be wrong.

- Weak correlation is the error in which a single-reference wavefunction incurs due to the lack of many CSFs which would have small weights in the FCI expansion. The qualitative description of weakly correlated systems might be good, but is never quantitative at the single reference level.

Only FCI is able to treat strongly and weakly correlated systems accurately. For the most part, perturbative methods are better for weak correlation and multirreference methods are better for strong correlation.

The *de facto* golden standard is CCSD(T), which is a CCSD expansion with triple excitations treated perturbatively. The cost of such an approach scales very steeply with the number of electrons and orbitals, but it is the most used approach for benchmarking and comparison.

2.4 Density functional theory

In the previous section we have outlined several approaches that allow us to get increasingly accurate electronic wavefunctions and associated energies. However, the electronic wavefunction is a highly-dimensional mathematical object which we can hardly imagine or interpret. What we can interpret comfortably is, in fact, the probability density arising from the electronic wavefunction (cf. Equation 2.3): the electron density.

As we will see first, with a fast examination, the electron density bears a lot of information about the system. We will later show that, in fact, it formally bears enough information to calculate the exact electronic energy directly from it.

The theoretical framework that tries to express the exact electronic energy as a functional of the electron density is called Density Functional Theory (DFT).

2.4.1 The electron distribution

All the wavefunction expressions we have used in Section2.3 are constructed using spin orbitals, which are just mathematical objects. Only the square of the wave function has a true physical meaning.

Considering a single electron in orbital $\phi_i(\mathbf{r})$ with spin α, the wave function is $\Psi_i(\mathbf{x}) = \phi_i(\mathbf{r})\alpha$. The probability density of that electron is given by

$$\rho^\alpha(\mathbf{r}) = |\Psi_i(\mathbf{x})|^2 = |\psi_i(\mathbf{r})|^2 \tag{2.87}$$

Consequently, the probability of finding the electron in a volume d$\mathbf{r}$ is given by integration:

$$P(\mathbf{r}) = \int |\psi_i(\mathbf{r})|^2 d\mathbf{r} = \int \rho^\alpha(\mathbf{r}) d\mathbf{r} \tag{2.88}$$

If ψ_i is replaced by a normalized N electron wave function $\Psi(\mathbf{x}_1, \mathbf{x}_2, \ldots, \mathbf{x}_n)$, we can generalize. For any restricted wavefunction we can omit the spin part for simplicity. Then, the electron density becomes:

$$\rho(\mathbf{r}_1) = \Psi^*(\mathbf{r}_1, \dots \mathbf{r}_N)\Psi(\mathbf{r}_1, \dots \mathbf{r}_N) \tag{2.89}$$

Which integrates to N for a normalized wavefunction. If the wavefunction is a Slater determinant, then the electron density can be rewritten as a sum over molecular orbitals,

$$\rho(\mathbf{r}) = \sum_i n_i |\psi_i(\mathbf{r})|^2 \tag{2.90}$$

where n_i are the occupation numbers of the i-th molecular orbital. That is, the probability densities arising from different orbitals over space are additive.

Density matrices

The density matrix of a system is given by [9]

$$\Gamma(\mathbf{x}_1, \mathbf{x}_2, \dots \mathbf{x}_N; \mathbf{x}'_1, \mathbf{x}'_2, \dots \mathbf{x}'_N) = \Psi(\mathbf{x}_1, \mathbf{x}_2, \dots \mathbf{x}_N)\Psi^\star(\mathbf{x}'_1, \mathbf{x}'_2, \dots \mathbf{x}'_N) \tag{2.91}$$

where $\mathbf{x}_i$ are spin-spatial coordinates as before. The density matrix contains similar information to the wavefunction expanded in a given basis set. A more convenient expression can be obtained in terms of reduced density matrices.

The n-particle reduced density matrix can be expressed as

$$\Gamma^n(\mathbf{x}_1, \dots \mathbf{x}_n; \mathbf{x}'_1, \dots \mathbf{x}'_n) = n!\binom{N}{n}\int \Gamma(\mathbf{x}_1, \dots \mathbf{x}_N; \mathbf{x}'_1, \dots \mathbf{x}'_N)d\mathbf{x}_{n+1}, \dots, d\mathbf{x}_N \tag{2.92}$$

where we assume that integrating over space-spin coordinates is equal to integrating over spatial coordinates $\mathbf{r}_i$ and summing over spin coordinates σ. The one particle reduced density matrix is thus

$$\Gamma^1(\mathbf{x}_1; \mathbf{x}'_1) = N\int \Psi(\mathbf{x}_1, \mathbf{x}_2, \dots \mathbf{x}_N)\Psi^*(\mathbf{x}', \mathbf{x}_2, \dots \mathbf{x}_N)d\mathbf{x}_2, \dots, d\mathbf{x}_N \tag{2.93}$$

which is definite positive. Analogously, the two-particle reduced density matrix is

$$\Gamma^2(\mathbf{x}_1, \mathbf{x}_2; \mathbf{x}'_1, \mathbf{x}'_2) = N(N-1)\int \Psi(\mathbf{x}_1, \mathbf{x}_2, \dots \mathbf{x}_N)\Psi^*(\mathbf{x}'_1, \mathbf{x}'_2, \dots \mathbf{x}_N)d\mathbf{x}_3, \dots, d\mathbf{x}_N \tag{2.94}$$

Such compact expressions are useful for discussion. Reduced density matrices are also hermitian and symmetric with respect to particle permutations. Conveniently, they integrate to the corresponding number of combinations of n electrons,

$$\int \Gamma^1(\mathbf{x}_1; \mathbf{x}'_1)\Big|_{\mathbf{x}_1=\mathbf{x}'_1} d\mathbf{x}_1 = N \tag{2.95}$$

$$\int \Gamma^2(\mathbf{x}_1, \mathbf{x}_2; \mathbf{x}'_1, \mathbf{x}'_2)\Big|_{\substack{\mathbf{x}_1=\mathbf{x}'_1 \\ \mathbf{x}_2=\mathbf{x}'_2}} d\mathbf{x}_1 d\mathbf{x}_2 = N(N-1) \tag{2.96}$$

Both reduced density matrices can be rendered spin-less by integration of the spin part,

$$\gamma^1(\mathbf{r}_1; \mathbf{r}'_1) = \int d\sigma_1 \Gamma^1(\mathbf{x}_1; \mathbf{x}'_1) \tag{2.97}$$

and

$$\gamma^2(\mathbf{r}_1, \mathbf{r}_2; \mathbf{r}'_1, \mathbf{r}'_2) = \int d\sigma_1 \int d\sigma_2 \Gamma^2(\mathbf{x}_1, \mathbf{x}_2; \mathbf{x}'_1, \mathbf{x}'_2) \tag{2.98}$$

The diagonal parts of the one and two-particle reduced density matrices represent probability densities of finding just a set of n electrons in $d\mathbf{r}_1, \ldots d\mathbf{r}_n$, because this is analogous to integrating over all the N electrons of the system except the subset $n < N$ and noting that every electron is indistinguishable from any other electrons.

For $n = 1$, we formally retrieve the electron density ρ again (Equation 2.89).

$$\rho(\mathbf{x}_1) = \gamma^1(\mathbf{r}_1; \mathbf{r}_1) \tag{2.99}$$

For $n = 2$, the pair density $\rho_2(\mathbf{x}_1, \mathbf{x}_2)$ is obtained:

$$\rho_2(\mathbf{r}_1, \mathbf{r}_2) = \gamma^2(\mathbf{r}_1, \mathbf{r}_2; \mathbf{r}_1, \mathbf{r}_2) \tag{2.100}$$

Note that for single-determinant wavefunctions, the one-particle reduced density matrix can be written simply as

$$\gamma^1(\mathbf{r}_1; \mathbf{r}'_1) = \sum_i n_i \psi_i(\mathbf{r}_1) \psi_i^\star(\mathbf{r}'_1) \tag{2.101}$$

in terms of the molecular orbitals ψ_i that compose the wavefunction and their occupation number n_i. In any restricted formalism, occupation numbers are either 2 for occupied orbitals or 0 for virtual orbitals. Note that such one-particle reduced density matrix is both diagonal and idempotent.

2.4.2 Bright-Wilson argument

As pointed out in Section 2.2, the wavefunction must have a discontinuity on top of the nuclear positions $\mathbf{R}_i$ or all nuclei M_i with nuclear charge Z_i. Thus, the electron density must present this discontinuity as well. Kato's cusp condition states that:

$$\frac{d\overline{\rho}(\mathbf{r})}{d\mathbf{r}} = -2\overline{\rho}(\mathbf{r}) Z_i \tag{2.102}$$

when $\mathbf{r} = \mathbf{R}_i$ and where $\overline{\rho}$ is the electron density spherically averaged around R_i. Equation 2.102 is valid for Coulomb systems assuming the Born-Oppenheimer approximation and point-like nuclei. The electron density then decays exponentially, satisfying

$$\rho(\mathbf{r}) \propto e^{-(\sqrt{2I})\mathbf{r}}, \tag{2.103}$$

where I is the first ionisation potential, when $\mathbf{r}$ is far from the nuclear positions.

Therefore, just from the electron density we can get the positions of all nuclei as discontinuities, the nuclear charges through derivatives, and the number of electrons by integration (Equation 2.89). Therefore, the Coulomb potential of the system is completely determined just from the exact electron density ρ. [10]

In the rest of the section we will generalize this keen observation, due to E. Bright Wilson, to any potential. This, in turn, will proof that a functional may exist that recovers the exact energy from the electron density.

2.4.3 First Hohenberg-Kohn theorem

The first Hohenberg-Kohn theorem generalizes the previous reasoning. It is usually stated as the following: [11]

First Hohenberg-Kohn Theorem *For any system of N interacting particles in an external potential $V_{ext}(\mathbf{r})$, this potential is determined uniquely, except for a constant, by the ground state particle density $\rho(\mathbf{r})$.*

Thus, as the complete electronic Hamiltonian $\widehat{H}$ of the system is determined by $V_{ext}(\mathbf{r})$ and N, all the properties of the system are determined by $\rho(\mathbf{r})$. Therefore, the energy is uniquely determined by the ground state particle density.

While there are many refined and generalized ways to demonstrate this theorem, the classic *reductio ad absurdum* is given below.

Proof: Let us propose two different external potentials $V_{ext}^{(1)}(\mathbf{r})$ and $V_{ext}^{(2)}(\mathbf{r})$ which differ in more than a constant and lead to the same ground state density $\rho(\mathbf{r})$.

For each potential there will be a different Hamiltonian, $\widehat{H}^{(1)}$ and $\widehat{H}^{(2)}$, with different corresponding ground state wave functions, $\Psi^{(1)}$ and $\Psi^{(2)}$. Since $\Psi^{(2)}$ is not the ground state of $\widehat{H}^{(1)}$, from the variational principle it follows that

$$E^{(1)} = \langle\Psi^{(1)}|\widehat{H}^{(1)}|\Psi^{(1)}\rangle < \langle\Psi^{(2)}|\widehat{H}^{(1)}|\Psi^{(2)}\rangle \tag{2.104}$$

Where non-degeneracy of the ground state is assumed. The last term may be rewritten as

$$\begin{aligned}\langle\Psi^{(2)}|\widehat{H}^{(1)}|\Psi^{(2)}\rangle &= \langle\Psi^{(2)}|\widehat{H}^{(2)}|\Psi^{(2)}\rangle + \langle\Psi^{(2)}|\widehat{H}^{(1)} - \widehat{H}^{(2)}|\Psi^{(2)}\rangle \\ &= E^{(2)} + \int[\widehat{V}_{ext}^{(1)}(\mathbf{r}) - \widehat{V}_{ext}^{(2)}(\mathbf{r})]\rho(\mathbf{r})d\mathbf{r}\end{aligned} \tag{2.105}$$

and thus

$$E^{(1)} < E^{(2)} + \int[\widehat{V}_{ext}^{(1)}(\mathbf{r}) - \widehat{V}_{ext}^{(2)}(\mathbf{r})]\rho(\mathbf{r})d\mathbf{r} \tag{2.106}$$

The same procedure can be used to derive the analogous expression for E^2,

$$E^{(2)} < E^{(1)} + \int[\widehat{V}_{ext}^{(2)}(\mathbf{r}) - \widehat{V}_{ext}^{(1)}(\mathbf{r})]\rho(\mathbf{r})d\mathbf{r}. \tag{2.107}$$

and adding both Equation 2.106 and 2.107 yields a contradictory inequality $E^{(1)} + E^{(2)} < E^{(1)} + E^{(2)}$.

Therefore, there cannot be two different external potentials differing by more than a constant but giving rise to the same non-degenerate ground state electron density.

2.4.4 Second Hohenberg-Kohn theorem

The second Hohenberg-Kohn theorem completes the first one, and leads to the key result of this section. It states:

Second Hohenberg-Kohn Theorem *A functional for the energy $E[\rho]$ in terms of the density $\rho(\mathbf{r})$ can be defined valid for any external potential $V_{ext}(\mathbf{r})$. The exact ground state energy of the system is given by the global minimum value of such functional, and the exact ground state density is the one that minimizes it.*

Once again, there are many subtle ways of demonstrating this. The classic proof is given below.

Proof: Since all the properties are uniquely determined by $\rho(\mathbf{r})$, each energy term may be defined as a functional of $\rho(\mathbf{r})$

$$E[\rho] = F_{HK}[\rho] + \int V_{ext}\rho(\mathbf{r})d\mathbf{r} \tag{2.108}$$

where $F_{HK}[\rho]$ is a universal functional of the density which contains the kinetic and electron-electron interaction energy,

$$F_{HK}[\rho] = T[\rho] + V_{ee}[\rho] \tag{2.109}$$

Therefore, the ground state electronic energy of a system with ground state density $\rho^{(1)}(\mathbf{r})$, external potential $V_{ext}^{(1)}$ and wavefunction $\Psi^{(1)}$ is given by the energy functional $E^{(1)}[\rho^{(1)}]$,

$$E^{(1)}[\rho^{(1)}] = \langle\Psi^{(1)}|\widehat{H}^{(1)}|\Psi^{(1)}\rangle \tag{2.110}$$

As per the first Hohenberg-Kohn theorem, any trial electron density $\rho^{(2)}(\mathbf{r})$ uniquely determines its own external potential $V_{ext}^{(2)}$, Hamiltonian $\widehat{H}^{(2)}$ and wavefunction $|\Psi^{(2)}\rangle$.

The variational principle enforces that

$$E^{(1)}[\rho^{(1)}] = \langle\Psi^{(1)}|\widehat{H}^{(1)}|\Psi^{(1)}\rangle \leq \langle\Psi^{(2)}|\widehat{H}^{(1)}|\Psi^{(2)}\rangle = E^{(1)}[\rho^{(2)}]. \tag{2.111}$$

Which means that due to the unique correspondence $\rho \rightarrow V_{ext} \rightarrow \widehat{H} \rightarrow \Psi$, the variational principle can be used in terms of ρ. Any trial electron density different from the exact ground state one leads to a higher energy than the exact one.

A constraint has to be added to ensure that ρ integrates to N, which is sometimes expressed as the stationary principle:

$$\frac{d}{d\rho}\Big(E[\rho] - \mu\int\rho(\mathbf{r})d\mathbf{r}\Big) = 0 \tag{2.112}$$

where μ is a Lagrange multiplier. Other than that, the minimization problem is simply

$$E = \min_{\rho}\Big(F_{HK}[\rho] + \int\rho(\mathbf{r})V_{ext}d\mathbf{r}\Big) \tag{2.113}$$

and we can express the universal functional as

$$F_{HK}[\rho] = \min_{\Psi\rightarrow\rho}\langle\Psi|\widehat{T} + \widehat{V}_{ee}|\Psi\rangle \tag{2.114}$$

where the condition $\Psi \rightarrow \rho$ means simply that the following holds for the antisymmetric wavefunction Ψ:

$$\rho(\mathbf{r}) = N\int|\Psi(\mathbf{x}_1, \mathbf{x}_2, \ldots \mathbf{x}_N)|^2 d\mathbf{x}_1, d\mathbf{x}_2, \ldots d\mathbf{x}_N \tag{2.115}$$

So far, the task of finding the exact energy has been expressed as a double minimization problem. This is known as the constrained search approach. [12, 13, 14]

However, the exact form of $F_{HK}[\rho]$ is not known. This issue will be tackled in the next Section.

2.5 Kohn-Sham formulation

As the exact expression of $F_{HK}[\rho]$ is not known, and with what has been covered so far, the minimization problems in Equations 2.113 and 2.114 are very hard to solve.

A very effective approach was introduced in 1965 by Kohn and Sham (KS).[15] The KS approach is based on using a fictitious system of N non-interacting particles that has the exact same ground-state density as the true system. We will refer to this system as the KS system.

The non-interacting Hamiltonian $\widehat{H}_{KS}$ can be written as

$$\widehat{H}_{KS} = \widehat{T} + \widehat{V}_{KS} \tag{2.116}$$

where $\widehat{T}$ is the kinetic energy operator. $\widehat{V}_{KS}$ is the external potential term, which we will call the KS potential, so that $\widehat{V}_{KS} = \int v_{KS}(\mathbf{r})\rho(\mathbf{r})d\mathbf{r}$.

Because the KS system is non-interacting, we may enforce that the potential $v_{KS}(\mathbf{r})$ leads to a Slater determinant wavefunction Φ, from which the ground-state density $\rho(\mathbf{r})$ may be derived. We then require that the single-reference wavefunction Φ minimizes the expectation value of $\widehat{T}$;

$$T_s[\rho] = \min_{\Phi\to\rho}\langle\Phi|\widehat{T}|\Phi\rangle \tag{2.117}$$

We may now rewrite $F_{HK}[\rho]$ from Equation 2.114 as

$$F[\rho] = T_s[\rho] + E_H[\rho] + E_{xc}[\rho] \tag{2.118}$$

where the Hartree functional $E_H[\rho]$,

$$E_H[\rho] = \frac{1}{2}\int\int \frac{\rho(\mathbf{r}_1)\rho(\mathbf{r}_2)}{|\mathbf{r}_1 - \mathbf{r}_2|}d\mathbf{r}_1 d\mathbf{r}_2 \tag{2.119}$$

is a mean-field term, analogous to HF theory, and $E_{xc}[\rho]$ is an exchange-correlation functional that accounts for a supposedly small part

$$E_{xc}[\rho] = T[\rho] - T_s[\rho] + V_{ee}[\rho] - E_H[\rho] \tag{2.120}$$

that is, a term that accounts for electron correlation beyond the mean field approximation and the difference between the true kinetic energy functional $T[\rho]$ and the KS one $T_s[\rho]$. Let us assume for the time being that the exact expression of $E_{xc}[\rho]$ is known.

By noting that the explicit expression for the effective KS potential $v_{KS}(\mathbf{r})$ using the exchange-correlation potential $v_{xc}(\mathbf{r})$ and the external potential $v_{ext}(\mathbf{r})$ (usually simply due to nuclei):

$$\begin{aligned} v_{KS}(\mathbf{r}) &= v_{ext}(\mathbf{r}) + \frac{E_H[\rho(\mathbf{r})]}{d\rho(\mathbf{r})} + \frac{dE_{xc}[\rho(\mathbf{r})]}{d\rho(\mathbf{r})} \\ &= v_{ext}(\mathbf{r}) + v_H(\mathbf{r}) + v_{xc}(\mathbf{r}) \end{aligned}$$

Then we can rewrite the minimization problem in a self-consistent manner. The KS system is subject to a familiar eigenvalue equation (cf. Equation 2.43), as Φ can be built using a set of orbitals ϕ_i with eigenvalues ϵ_i,

$$\widehat{H}_{KS}|\phi_i\rangle = \epsilon_i|\phi_i\rangle \tag{2.121}$$

Again, there is no explicit $\widehat{V}_{ee}$ term in the Hamiltonian. We have chosen Φ to be a single Slater determinant, which can be treated using the LCAO method with Roothaan-Hall basis set expansion as we have shown before. $\hat{H}_{KS}$ depends on Φ through $\rho(\mathbf{r})$ in $\widehat{V}_{KS}$.

Where $E_{xc}[\rho]$ known, whenever self-consistency is achieved, $\rho(\mathbf{r})$ must be the exact ground state electron density, with which we can then calculate the exact energy. That is, given the exact $E_{xc}[\rho]$ we can get the exact result at the basis set limit with a very simple single-reference KS wavefunction and the even simpler electron density, a three-dimensional scalar field.

2.5.1 Physical content of the exchange-correlation functional

As pointed before, the exact form of $F_{HK}[\rho]$ is not known, and the exact form of $E_{xc}[\rho]$ is not known either. It is significantly easier to approximate the latter, because it only captures the physics beyond the mean-field problem, and we have seen in Section 2.2 that this is a small quantity in terms of energy.

Thus, the key problem in KS-DFT is finding a good approximation to $E_{xc}[\rho]$. Naturally, using an approximate exchange-correlation functional means that the theory so far is sadly rendered *inexact*.

Let us partition $E_{xc}[\rho]$ in order to better understand what is needed to emulate it. First of all, we can dissect it into $E_x[\rho]$ and $E_c[\rho]$, the exchange and correlation functionals respectively:

$$\begin{aligned} E_{xc}[\rho] &= E_x[\rho] + E_c[\rho] \\ E_x[\rho] &= \langle\Phi|\hat{V}_{ee}|\Phi\rangle - E_H \\ E_c[\rho] &= \langle\Psi|\hat{T} + \hat{V}_{ee}|\Psi\rangle - \langle\Phi|\hat{T} + \hat{V}_{ee}|\Phi\rangle \end{aligned}$$

where Ψ is the true wave function of the system and Φ is the wavefunction of the KS system as before. The correlation energy may be further decomposed into kinetic and potential components

$$E_c[\rho] = T_c[\rho] + V_c[\rho] \tag{2.122}$$

where $T_c[\rho] = T[\rho] - T_s[\rho]$ and $V_c[\rho] = V_{ee}[\rho] - (E_H[\rho] + E_x[\rho])$.

We can use the pair density as defined in Subsection 2.4.1, $\rho_2(\mathbf{r}_1, \mathbf{r}_2)$, to further simplify the spin-less expressions

$$V_{ee}[\rho] = \langle\Phi|\hat{V}_{ee}|\Phi\rangle = \frac{1}{2}\int\int \frac{\rho_2(\mathbf{r}_1, \mathbf{r}_2)}{r_{12}} d\mathbf{r}_1 d\mathbf{r}_2 \tag{2.123}$$

Let us reflect upon the significance of the exact pair density. In a non-interacting system, the pair density must be separable into one-particle densities. In a truly correlated system, it is not. We can express the difference as

$$\rho_2(\mathbf{r}_1, \mathbf{r}_2) - \rho(\mathbf{r}_1)\rho(\mathbf{r}_2) = \rho(\mathbf{r}_1)h_{xc}(\mathbf{r}_1, \mathbf{r}_2) = -\rho_{xc}(\mathbf{r}_1, \mathbf{r}_2) \tag{2.124}$$

where the term $h_{xc}(\mathbf{r}_1, \mathbf{r}_2)$ is usually called the exchange-correlation hole, and $\rho_{xc}(\mathbf{r}_1, \mathbf{r}_2)$ is called the exchange-correlation density. The normalization conditions showcased in Subsection 2.4.1 imply that

$$\int h_{xc}(\mathbf{r}, \mathbf{r}')d\mathbf{r}' = -1 \tag{2.125}$$

Coherently, we can define the exchange-correlation energy per electron $\epsilon_{xc}(\rho(\mathbf{r}))$.

$$\begin{aligned} E_{xc}[\rho] &= \frac{1}{2}\int\int \rho(\mathbf{r}_1)\frac{h_{xc}(\mathbf{r}_1, \mathbf{r}_2)}{r_{12}}d\mathbf{r}_1 d\mathbf{r}_2 \\ &= \int \rho(\mathbf{r}_1)\epsilon_{xc}(\rho(\mathbf{r}_1))d\mathbf{r}_1 \end{aligned}$$

Therefore, the search for $E_{xc}[\rho]$ may be reformulated in terms of $\epsilon_{xc}(\rho((\mathbf{r}))$, which is often subdivided into ϵ_x and ϵ_c, exchange and correlation contributions. In other words, we attempt to model a two-electron function in terms of one electron.

2.5.2 Density functional approximations

In the KS-DFT context, the approximate form of $F_{HK}[\rho]$ (Equation 2.109) is given solely by the approximate form of $E_{xc}[\rho]$, which is in turn determined by $\epsilon_{xc}[\rho]$. Therefore, the term Density Functional Approximation (DFA) is used indistinctly to refer to particular approximations to the exchange-correlation term or the universal functional.

Classically, such approximations are built on increasingly sophisticate sources of information, which have been historically compared to the rungs in the biblical ladder of Jacob. We will cover the main *families* now, and the final Subsection of the Chapter will be dedicated to current limitations of DFAs.

First rung: Local density approximations

One of the simplest N electron systems is given by a uniform electron gas, moving on a positive background charge distribution such that the total ensemble is electrically neutral. In these systems ρ is constant everywhere: this is the Homogeneous Electron Gas (HEG), also called jellium.

The Thomas-Fermi-Dirac model extensively studies the properties of such systems, and many accurate results are known. The kinetic energy of an HEG can be expressed as

$$T^{HEG}[\rho] = C_F \int \rho^{5/3}(\mathbf{r})d\mathbf{r} \tag{2.126}$$

where

$$\begin{aligned} C_F &= \frac{3}{10}(3\pi^2)^{2/3} \\ \epsilon_T^{HEG}(\rho) &= -C_F\rho^{2/3} \end{aligned}$$

where C_F is the Fermi constant. The exchange energy is also known, which leads to an expression of the exchange energy per particle $\epsilon_x^{HEG}(\rho)$:

$$E_x^{HEG}[\rho] = -C_x \rho^{4/3}(\mathbf{r}) d\mathbf{r} \tag{2.127}$$

where

$$\begin{aligned} C_x &= \frac{3}{4}\left(\frac{3}{\pi}\right)^{1/3} \\ \epsilon_x^{HEG}(\rho) &= -C_x \rho^{1/3} \end{aligned}$$

The exchange energy density $\epsilon_x^{HEG}(\rho)$ is sometimes called Slater exchange.

First rung DFAs, Local Density Approximations (LDAs) are defined using $\epsilon_x^{HEG}(\rho)$ to derive the exchange functional. The remaining $\epsilon_c^{LDA}(\rho)$ term has been very accurately derived from quantum Monte-Carlo simulations as a function of ρ and empirical parameters. Generally, an LDA DFA is expressed as

$$\begin{aligned} E_{xc}^{LDA}[\rho] &= \int \rho(\mathbf{r}) \epsilon_{xc}^{LDA} d\mathbf{r} \\ &= \int \rho(\mathbf{r})(\epsilon_x^{HEG}(\rho) + \epsilon_c^{LDA}(\rho)) d\mathbf{r} \end{aligned}$$

Examples of ϵ_c^{LDA} will be given later on. While, for the most part we will remain in a spinless formulation, spin may be trivially introduced in the LDA formulation using the spin-polarization density $\xi(\mathbf{r})$, defined as

$$\xi(\mathbf{r}) = \frac{\rho^\alpha(\mathbf{r}) - \rho^\beta(\mathbf{r})}{\rho(\mathbf{r})} \tag{2.128}$$

where the spin densities $\rho^\alpha(\mathbf{r})$ and $\rho^\beta(\mathbf{r})$ are calculated for electrons of the corresponding spin and satisfy that $\rho^\alpha + \rho^\beta = \rho$. Spin polarization modifies Equation 2.127 slightly to

$$\begin{aligned} E_x^{LSDA}[\rho] &= -2^{1/3}\frac{1}{2} C_x \int \rho^{4/3}(\mathbf{r}) \Big[(1+\xi(\mathbf{r}))^{4/3} + (1-\xi(\mathbf{r}))^{4/3} \Big] d\mathbf{r} \\ \epsilon_x^{LSDA}(\rho,\xi) &= \epsilon(\rho,0) + [\epsilon_x(\rho,1) - \epsilon_x(\rho,0)] f(\xi) \\ f(\xi) &= \frac{1}{2(2^{1/3}-1)} [(1+\xi(\mathbf{r})^{4/3} + (1-\xi(\mathbf{r})^{4/3}) - 2] \end{aligned} \tag{2.129}$$

The spin-polarized variant is known as the Local Spin-Density Approximation (LSDA).

In general, LDA and LSDA are appropiate for homogeneous electron densities, which very rarely arise in molecular systems but are not too far from the situation in a bulk metal. This is to be expected as per the construction of the approximation.

Some standard LDA DFAs have been proposed by fitting to accurate results. The flagship example is the SVWN DFA that combines Slater exchange with the VWN correlation functional of Vosko, Wilk, and Nusair.[16]

Second rung: Generalized gradient approximations

Starting from the LDA theory, a natural way of adapting to inhomogeneous densities is adding some dependency on density derivatives to $E_{xc}^{LDA}[\rho]$ trough a gradient expansion of E_{xc}. Thus, the Generalized Gradient Approximation (GGA) adds a source of information $\rho(\mathbf{r})$, but also derivatives of $\rho(\mathbf{r})$ in E_{xc}.

A typical GGA exchange energy functional is simply a modification from Equation 2.128:

$$E_{xc}^{GGA}[\rho] = \int \rho(\mathbf{r})\epsilon_{xc}^{LDA}(\rho)F_{xc}^{GGA}(\rho, s)d\mathbf{r} \tag{2.130}$$

where $F_{xc}^{GGA}(\rho, s) \geq 0$ is the enhancement factor, a function of the adimensional reduced density gradient $s(\mathbf{r})$, where the dependence on the gradient of the density lies,

$$s(\mathbf{r}) = \frac{|\vec{\nabla}\rho(\mathbf{r})|}{2(3\pi)^2)^{1/3}\rho(\mathbf{r})^{4/3}} \tag{2.131}$$

The enhancement factor can be decomposed as usual

$$F_{xc}^{GGA}(\rho, s) = F_{x}^{GGA}(s) + F_{c}^{GGA}(\rho, s) \tag{2.132}$$

and we impose both that $F_{xc}^{GGA}(\rho, s) \to F_{x}^{GGA}(s)$ as $\rho \to \infty$ and that $F_{x}^{GGA}(0) = 1$. Note that for an infinite HEG, $s(\mathbf{r}) = 0$. These are known as the high density and uniform density limits. This construction attempts to satisfy the properties of the exchange-correlation hole.

It can be said that, in general, GGAs do not achieve the accuracy that is required for widespread application in molecular systems. However, there are many ways to build a GGA DFA, including extensive parametrization at times.

Semiempirical approaches fit a few empirical parameters to reproduce the exact exchange energy of a reference system, usually atomic. Examples of this approach are the B88 exchange functional of Becke,[17] the PW91 exchange functional developed by Perdew and Wang,[18], and the one-parameter correlation functional LYP, developed by Lee Yang and Parr.[19]

Other DFAs attempt to be free of semiempirical parameters. A notable example is the PBE DFA developed by Perdew, Becke and Ernzerhof,[20] as well as the correlation functional of the aforementioned PW91 DFA.

We will not enter into too much detail at this point. Do note, however, that *all* DFAs are parametrized because the correlation energy of the homogeneous electron gas is fitted to a model, generally the VWN. Generally, the number of empirical parameters refers to the *additional* parameters which are fitted to actual systems, and not to the HEG.

Third rung: Meta-generalized gradient approximations

Naturally, more information may be added by considering the second derivatives of ρ as well. After all, such terms would arise in the gradient expansion of the LDA form after $|\vec{\nabla}\rho(\mathbf{r})|$. Meta-Generalized Gradient Approximation (mGGA) DFAs therefore include the Laplacian of $\rho(\mathbf{r})$, $\nabla^2\rho(\mathbf{r})$ as well as the gradient.

Very often, the Laplacian of the molecular orbitals ϕ_i of the KS system is a more interesting ingredient because it can be used to define several Kinetic Energy Densities (KED), i.e. integrands of the kinetic energy of the non-interacting system. A particularly popular one is the positive semidefinite KED, $\tau(\mathbf{r})$:

$$\tau(\mathbf{r}) = \frac{1}{2}\sum_i |\vec{\nabla}\psi_i(\mathbf{r})|^2 \tag{2.133}$$

where i runs over all doubly occupied KS orbitals. Some explicit dependency on $\tau(\mathbf{r})$ is usually introduced in the exchange enhancement factor, such as

$$E_x^{mGGA}[\rho] = \int \rho(\mathbf{r})\epsilon_x^{HEG}F_x(s,\tau,\tau_w)d\mathbf{r} \tag{2.134}$$

where $\tau_w(\mathbf{r})$ denotes the von Weizsäcker kinetic energy density, which is the kinetic energy density for a single-orbital system

$$\tau^W(\mathbf{r}) = \frac{1}{8}\frac{|\vec{\nabla}\rho(\mathbf{r})|^2}{\rho(\mathbf{r})} \tag{2.135}$$

Note that DFAs of this rung that profit from $\tau(\mathbf{r})$ are only *implicit* functionals of the electron density. However, the kinetic energy density has a clear physical interpretation, and the additional flexibility is in any case benefitial for fitting strategies.

Different meta-GGA functionals have been developed, for example the Perdew-Kurth-Zupan-Blaha (PKZB) exchange-correlation functional which depends on two fitted parameters,[21], the non-empirical Tao-Perdew-Staroverov-Scuseria (TPSS) exchange-correlation functional,[22] and the M06L DFA introduced by Truhlar and coworkers, which has 32 fitted parameters.[23]

These meta-GGA correlation functional are one-electron SIE free. The results obtained using meta-GGA are generally improved with respect to GGAs, but not always enough for finer chemical applications.

Fourth rung: Hybrids

Up to this point most of our attention has been devoted to the exchange functional $E_x[\rho]$. This is not casual, as it is known that the exchange contribution to $h_{xc}(\mathbf{r}_1,\mathbf{r}_2)$ is majoritary.

The exchange hole $h_x(\mathbf{r}_1,\mathbf{r}_2)$ may be computed from the HF wave function by Equation 2.33. Therefore, hybrid DFAs utilize HF-like exchange as a source of information as well.

Further justification for the need of hybrid functionals can be extracted from the adiabatic connection argument that follows. By starting from Equation 2.114 we can write

$$F_\lambda[\rho] = \min_{\Psi\to\rho}\langle\Psi|\widehat{T} + \lambda\widehat{V}_{ee}|\Psi\rangle \tag{2.136}$$

Where ρ is kept constant. λ is a coupling parameter that goes from 0 to 1 as the interacting term is included in the Hamiltonian. Let us assume that minimization renders a valid Ψ_ρ^λ for any value of λ. Note that

$$\begin{aligned} F_{\lambda=0}[\rho] &= T_s[\rho] \\ F_{\lambda=1}[\rho] &= T[\rho] + V_{ee} \end{aligned}$$

We can write an expression for the exchange-correlation functional in terms of λ:

$$\begin{aligned} E_{xc}[\rho] &= \int_0^1 d\lambda \frac{F_\lambda[\rho]}{d\lambda} - E_H[\rho] \\ &= \int_0^1 d\lambda \langle \Psi_\rho^\lambda | \widehat{V}_{ee} | \Psi_\rho^\lambda \rangle - E_H[\rho] \\ &= \int\int \rho(\mathbf{r}_1) \frac{h_{xc}^\lambda(\mathbf{r}_1, \mathbf{r}_2)}{r_{12}} d\mathbf{r}_1 d\mathbf{r}_2 \end{aligned}$$

Hybrid functionals can be pictured as interpolation schemes between the exact exchange ($\lambda = 0$) and the exact exchange-correlation functionals ($\lambda = 1$). Generally this is achieved through parametrization. A simplistic ansatz could be

$$E_{xc}^{hybrid}[\rho] = aE_x^{HF}[\rho] + (1-a)E_{xc,\lambda=1}^{GGA} \tag{2.137}$$

Where a is an empirical parameter. In this rung we find the most widely used DFA, B3LYP, which combines a previous GGA exchange functional with the LYP correlation functional: [24]

$$E_{xc}^{B3LYP} = aE_x^{HF} + (1-a)E_x^{LSDA} + bE_x^{B88} + cE_c^{LYP} + (1-c)Ec^{VWN} \tag{2.138}$$

where three parameters ($a = 0.2$, $b = 0.72$, $c = 0.81$) were adjusted to the G2 set of experimental data, and the LYP DFA was used for the correlation part. Other DFAs attempt to avoid empirical parametrization, such as the PBE0 DFA: [25]

$$E_{xc}^{PBE0} = E_{xc}^{PBE} + 0.25(E_x^{HF} - E_x^{PBE}) \tag{2.139}$$

Hundreds of hybrid DFAs coexist with various degrees of success, but this rung is responsible for the widespread popularity of DFT in molecular calculations. Other popular DFAs of this rung include the M06 and M062x functionals, with 32 and 35 empirical parameters on top of the fraction of exact exchange.[26]

Beyond Fourth rung: Range-separated hybrids and double hybrids

Further rungs elaborate on the adiabatic formulation. Generally, this is attempted real space-wise, giving birth to Range-Separated Hybrids (RSH) or virtual space-wise, which leads to Double Hybrids (DH).

In RSH, we separate electron-electron interactions into short and long range terms using the error function *erf* and its complementary *erfc*:

$$\frac{1}{r_{12}} = \frac{erf(\mu r_{12})}{r_{12}} + \frac{erfc(\mu r_{12})}{r_{12}} \tag{2.140}$$

where the parameter μ controls the separation between the long-range ($\mathrm{erf}(\mu r_{12})/r_{12}$) and the short-range ($\mathrm{erfc}(\mu r_{12}/r_{12})$ interactions. This is equivalent to representing E_{xc} as a short-range and a long-range effect.

$$E_{xc}^{RSH} = E_{xc}^{SR}(\mu) + E_{xc}^{LR}(\mu)$$

Thus it allows the treatment of different effects using different effective μ. The main justification is the difficulty of expressing all exchange-correlation effects as local or

semilocal. HF-like exchange terms are far less local than LDA or GGA derived ones. There are, however, too many complicated approaches to this development to consider here.

DHs include information from virtual orbitals, normally through perturbation theory. An example construction could be

$$E_{xc}^{DH} = (1-a)E_x^{GGA} + aE_x^{HF} + (1-b)E_c^{GGA} + bE_c^{MP2} \tag{2.141}$$

in which a and b are empirical parameters and the $MP2$ superindex corresponds to a second order perturbative correction calculated using the KS orbitals. Again, much can be said with respect to developments in this direction which does not concern us here.

Some examples of RSH are the famous CAM-B3LYP modification, based on the Coulomb attenuated method of Yanai and coworkers,[27] and the ωB97XD functional of the Head-Gordon group.[28] In spite of the complex formulation, the cost is not significantly increased with respect to hybrid DFAs.

DHs are somewhat less used due to the increased cost of MP2. Honorable menctions are the PBE0-DH DFA of Brémond and coworkers [29] and the B2PLYP DFA of the Grimme group.[30]

2.5.3 Current limitations of Density Functional Theory

There are some known constraints that apply to the exchange-correlation functional $E_{xc}[\rho]$ directly or indirectly. The mathematical derivations are far too extensive to be included here, but we will sketch a general perspective and some of the main concepts in terms of the errors that are understood and that, most of all, derive in qualitative discrepancies.

Note that, formally, errors in KS-DFT are analogous to the issue of electron correlation. The main difference is that, here, we start from a non-interacting system of particles and thus the exchange term is not naturally included. Crudely, it can be said that DFT has trouble describing systems which are not well defined by a single Slater determinant (strong correlation) nearly by definition.

Thus, we will focus on the errors that arise from the unphysical approximation of $E_{xc}[\rho]$, more than in the limitations of a single-reference method. In any case, the *exact* universal functional would fix any and all issues.

Self interaction error

Self Interaction Error (SIE) is one of the most well known errors in DFAs. For most DFAs there is no exchange term K_{ii} to counteract the Coulomb term J_{ii} for a given electron (for a reminder, see Equation 2.30). This is better seen in one-electron systems, where the following should hold in DFT.

$$E_H[\rho] = -E_{xc}[\rho] \tag{2.142}$$

Equation 2.142, which naturally holds in HF methods and derivations thereof, does not hold for most DFAs: electrons interact with themselves and one-electron systems are ill-described. In a one-electron system *all* of the Coulomb interaction that is not removed is purely SIE, because there are no other electrons. In N-electron systems *some* of the Coulomb interactions may arise for the same reason.

Quantifying this error exactly is not possible in general because the exact $V_{ee}[\rho]$ functional is unknown. A possible strategy for designing DFAs without SIE uses a combination of $\tau(\mathbf{r})$ and $\tau_w(\mathbf{r})$ to define it. Starting from the following expression:

$$\tau^W(\mathbf{r}) \leq \tau(\mathbf{r}) \tag{2.143}$$

The equality applies only if $\rho(\mathbf{r})$ is represented by a single orbital. We can therefore define an indicator of the form

$$\eta^{SIE}(\mathbf{r}) = 1 - \frac{\tau^W(\mathbf{r})}{\tau(\mathbf{r})} \tag{2.144}$$

and take advantage of the fact that $\eta^{SIE} \to 0$ when the system becomes single-orbital-like to correct for SIE. A straightforward way to correct SIE is to add HF-like exchange terms, which is in fact used in hybrid, RSH and DH DFAs.

These exchange terms help compensate the self-interacting Coulomb part. No DFA below third rung can properly account for SIE trivially.

Derivative discontinuity and fundamental gap

It can be shown that the energy and the density of a system (considering that the external potential is fixed) with respect to the number of electrons N, which may change fractionally, has to be a straight line between integers:

$$\begin{aligned} E(N+\delta) &= (1-\delta)E(N) + \delta E(N+1) \\ \rho(N+\delta) &= (1-\delta)\rho(N) + \delta\rho(N+1) \end{aligned}$$

Therefore, at integer values both linear piecewise series must show derivative discontinuities with respect to N.

The fundamental gap of a system of N particles, E_g, is given by the following equations assuming that the exact piecewise behaviour is respected. Note that both E_H and the external potential are continuous with N. Therefore, the discontinuity has to come from T_s and/or E_{xc}.

$$\begin{aligned} E_g &= [E(N-1) - E(N)] - [E(N) - E(N+1)] \\ &= \lim_{\delta\to 0}\Big[\Big(\frac{dE}{dN}\Big)_{N+\delta} - \Big(\frac{dE}{dN}\Big)_{N-\delta}\Big] \\ &= \lim_{\delta\to 0}\Big[\Big(\frac{dT_s[\rho]}{d\rho}\Big)_{N+\delta} - \Big(\frac{dT_s[\rho]}{d\rho}\Big)_{N-\delta}\Big] + \Delta_{xc} \end{aligned} \tag{2.145}$$

In which Δ_{xc} is the difference between the right and left derivatives with respect to N (taking $\rho \to N$) of the E_{xc} term.

In the $N = 1$ case it has been shown that the KS kinetic energy term in Equation 2.145 correspond to the difference between the highest occupied and lowest unoccupied KS eigenvalues. Assuming this may hold for other systems, it still means that Δ_{xc} has to be taken into account in the calculation of gaps. Furthermore, it means that the exchange correlation potential v_{xc} must have a discontinuity at integer N.

This is often not the case. Hence, gaps computed with most DFAs are significantly wrong. Deviations in the dE/dN line are the cause of many of the failures of DFAs.

Long range correlation

Long range interactions are particularly difficult to model in DFT. From the CI point of view, such interactions arise from the presence of determinants with low weights that correspond to CSF with *induced* electric momenta, i.e. long range excitations over large distances in atomic orbital space. A multideterminantal minimization procedure forces all such CSFs to interact and slightly modifies the PES of the system, which is enough to govern over nuclear repulsion at long distances.

It is very hard for any DFA to capture such long range interactions due to the local nature of $\rho(\mathbf{r})$. In fact, the asymptotic behaviour of the exchange-correlation potential v_{ext} should fulfil

$$v_{ext} \propto -\frac{1}{R} \tag{2.146}$$

but it decays significantly faster, as $1/R^2$, for most DFAs. This is extended to the decay rate of the density and the orbitals in space.

RSH tackle this issue explicitly, but a very popular solution is to add empirical corrections on top of $E_{xc}[\rho]$, which is generally inexpensive and robust.

A prototypical example are pairwise dispersion corrections parametrized per atom type (and DFA) by Grimme and coworkers.[31] These take the form

$$E^{2-body} = -\frac{1}{2}\sum_{A,B}\left(\frac{C_6^{AB}}{R_{AB}^6} + s_8\frac{C_8^{AB}}{R_{AB}^8}\right) \tag{2.147}$$

which gives the interaction energy for a pair of nuclei A, B in terms of some empirical coefficients. This form arises from the multipolar expansion of the potential between two electronic clouds. The first terms are considered to be included in the underlying calculation, the R^{-6} and R^{-8} are considered because they dominate when $R_{AB} \to \infty$, the $1/R^7$ factor is ignored and higher order terms are truncated out.

Often, a damping function is added to the denominators in Equation 2.147 to properly connect the asymptotic $\propto 1/R^6$ behaviour with the short range ($R \to 0$) effect of the DFA. A popular option is a Becke-Johnson damping of the form

$$R_{AB}^i \to R_{AB}^i + (c_1 R_{AB}^0 + c_2)^i \tag{2.148}$$

where R_{AB}^0 is a minimum distance and c_i are empirical parameters once more. The multipolar treatment breaks down when there is significant overlap between electron densities and therefore such damping extends the applicability of the corrections.

There are many schemes that attempt to correct for these issues, including other pairwise corrections. After all, molecular mechanics use Lennard-Jones potentials with great success. Another significant contribution to the accurate treatment of long range correlation effects in DFT is the exchange-hole dipole moment model.[32, 33]

Density errors

As we have seen, and remarkably from the constrained search perspective, DFT typically proceeds on two steps. A trial wavefunction is found that is well-behaved and satisfies the Kohn-Sham equations under the chosen exchange-correlation potential v_{xc}, which stems from $E_{xc}[\rho]$. Then, the energy is evaluated from ρ explicitly ($E_H[\rho], E_{xc}^{HEG}[\rho], \ldots$) or implicitly ($T_s, \tau, \ldots$) and the ground state energy is calculated.

However, as we have continuously mentioned, $E_{xc}[\rho]$ is often parametrized with respect to reference data. In this case, nothing guarantees that a very good exchange-correlation functional has to lead to a proper density or wavefunction. Only the *exact* functional gives the *exact* ground state energy for the *exact* ground state density ρ.

To decouple errors due to the functional evaluation from errors due to the approximate density, it has been proposed to write a density error metric ΔE^d assuming that the exact functional $E[\rho]$ is known

$$\Delta E^d = E[\rho'] - E[\rho] \tag{2.149}$$

where ρ' is a trial density and ρ is the exact one. We can also define a functional error metric ΔE^f, using an approximate $E'[\rho]$,

$$\Delta E^f = E'[\rho] - E[\rho] \tag{2.150}$$

As per the variational theorem, ΔE^{total} is never negative. Obviously, we can never fill in the data in Equation 2.149 from a practical point of view, because the only way we can generally get the exact energy is as the expectation value of the exact FCI wavefunction. However, the concepts of density-error and functional-error for an approximate DFA will be useful for discussion later on, in particular in Chapter 6.

2.5.4 Outlook on Kohn-Sham Density Functional Theory

As in Section 2.3, we will finish by showcasing some of the features and limitations of KS-DFT using the humble H_2 molecule.

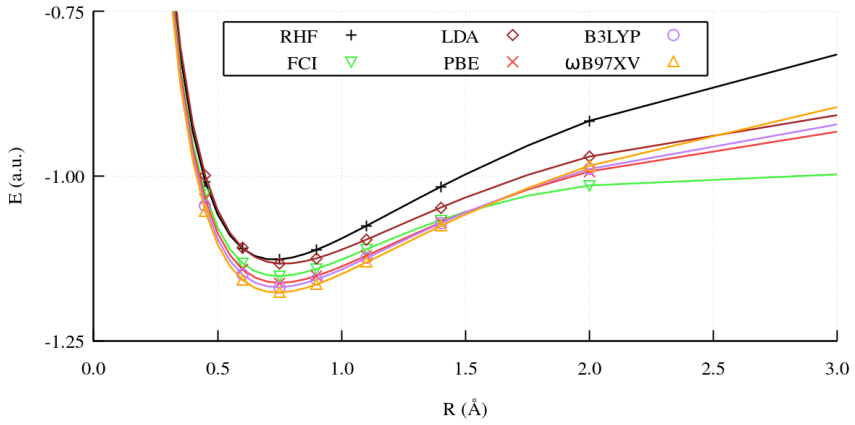

Figure 2.7: Dissociation curves for the H_2 molecule at different theory levels with a 6-31G basis set.

In Figure 2.7 several KS-DFT dissociation curves are shown with the RHF and FCI references as in 2.5. Results are surprisingly poor, but expected: a single-determinant reference still has troubles past the Coulson-Fischer point.

However, curves are significantly better than the HF one for a sigificant region of R, as they only break down past $R = 2.0$ Å. This signals that, in fact, some amount of strong correlation is being taken into account. Considering that the formal scaling of KS-DFT computation is analogous to HF, it seems that KS-DFT is indeed superior.

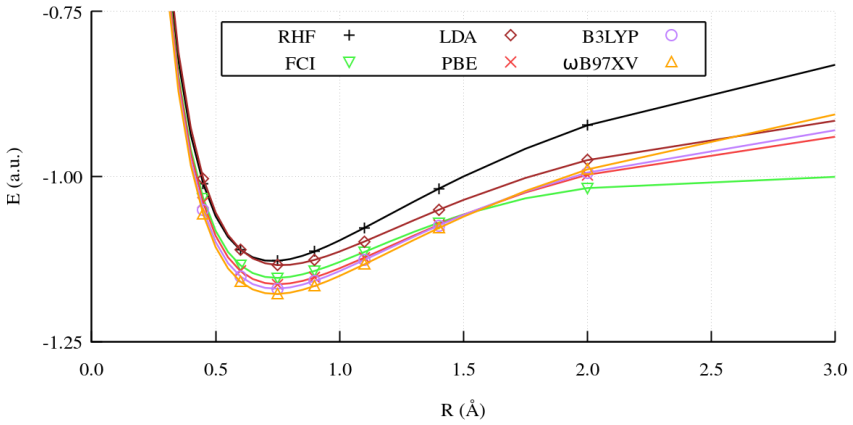

Figure 2.8: Dissociation curves for the H_2 molecule at different theory levels with a 6-311G basis set.

Results do not change qualitatively upon increasing the basis set (Figure 2.8): KS-DFT, like HF, converges faster with respect to basis set size than methods that explore virtual orbitals.

Let us simplify the test to the $H_2{}^+$ cation, for which the RHF and FCI methods give the same exact result. KS-DFT, however, fails miserably, as seen in Figure 2.9. Due to a combination of SIE and an incorrect concave behavior of dE/dN, all DFAs shown, irrespective of the rung, dissociate the cation to an abhorrent energy in a $2H^{+\frac{1}{2}}$ situation instead.

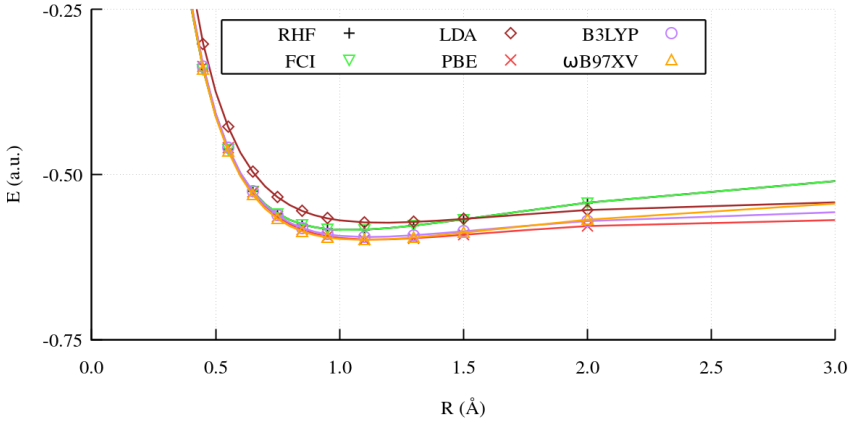

Figure 2.9: Dissociation curves for the $H_2{}^+$ molecule at different theory levels with a 6-31G basis set.

In the opposite direction, let us increase the complexity very slightly and study the He_2 molecule, a rare gas dimer in which there is no formal covalent bond. Coherently, the curve in Figure 2.10 does not have a deep well, i.e. it is *not* Morse-like.

However, being a stable dimer, the FCI curve does have a very shallow minima at $R = 3.200$ Å. HF has its minima at about $R = 3.225$ Å, which seems reasonable. The

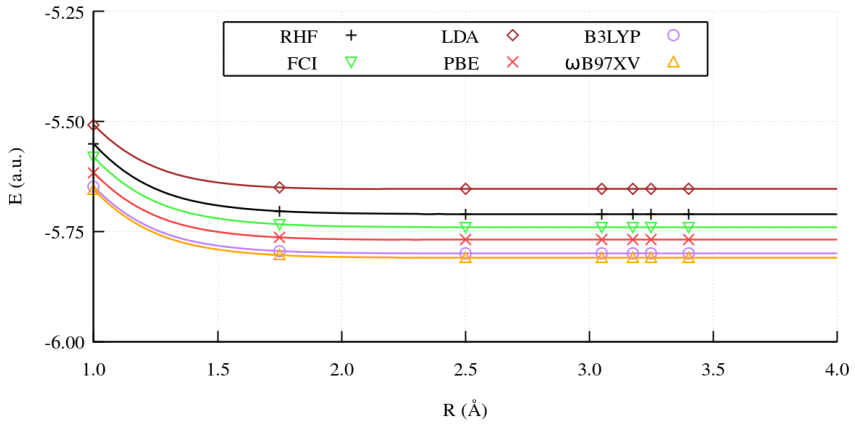

Figure 2.10: Dissociation curves for the He_2 molecule at different theory levels with a 6-31+G basis set.

LDA we have considered, PBE and ωB97XV have minima at $R < 2.75$ Å, which incurs in significant error. B3LYP does not seem to bind the He_2 molecule at this theory level.

This comes to show the underpinnings of locality: HF gets a very small qualitative detail acceptably, but DFT fails at describing the weak long-range interaction that binds the dimer. In fact, the popular B3LYP DFA is shown to be particularly bad in this aspect.

Chapter 3

Orbital-based chemical interpretation

Contents

As it has been highlighted in Chapter 2, the equations of quantum mechanics in many-electron chemistry are solved using a finite basis set and approximating the wavefunction in terms of one-particle functions called orbitals. As the orbitals are optimized in terms of the basis set, one obtains an approximate wavefunction that contains all information on the system of interests at a given theory level.

Traditionally, orbitals have been used as a foundation to discuss chemistry. However, many approaches exist from the theoretical point of view, which subsequently lead to different interpretations of chemical phenomena.

The two main frameworks that draw on orbitals are Molecular Orbital Theory and Valence Bond Theory. Both were developed during the XXth century, at the dawn of quantum mechanics, and competed for relevance in the community of the chemical sciences. There are several discrepancies between the two theories, but also significant agreement. Notably, they both converge to the same exact solution in a multiconfigurational expansion.

However, folk chemical concepts have usually been reinterpreted by using these theories at a qualitative level, and there the zeroth-order discrepancies outweight the similarities. Molecular Orbital Theory uses delocalized orbitals by definition, which are given an energetic relevance. Valence Bond Theory favors a significantly more local approach in chemical terms which mirror Lewis structures.

In this Chapter, both theories will be discussed. The foundations of the theories will be demonstrated for rigor, but our goal will rest with the concepts that can be defined from quantum mechanics and the notion of chemical bond in particular. As such, we will try to showcase the strengths and limits of both frameworks.

3.1 Molecular orbital theory

As explicitely developed in Chapter 2, and more specifically in Section 2.2, the fundamental single-determinant methods in quantum chemistry are based on the Roothaan-Hall equations (Equation 2.49). Therefore, the Molecular Orbitals (MOs) that build the wavefunction are expressed as a linear combination of basis functions.

In most cases, such basis functions will be Gaussians that mimic Atomic Orbitals (AOs), which will be placed on top of nuclear positions. However, as a simpler model, let us expand the spatial functions of the Hartree-Fock equations as:

$$\psi_\mu = \sum_{i}^{N_{basis}} C_{i\mu}\chi_i(\mathbf{r}) \tag{3.1}$$

Where $\chi_i(\mathbf{r})$ are simply atomic spatial orbitals, placed on different atoms. This is the so-called Linear Combination of Atomic Orbitals (LCAO) approach that we have reviewed in Section 2.2.

Every MO ψ_μ is formed by contributions of different AO $\chi_i(\mathbf{r})$. It is to be expected that some contributions will be dominant, and therefore an atomistic character is recovered for some MOs of the system. Then, perhaps the features of the wavefunction of the system can be predicted by observing the atomic wavefunctions of the constituents, or the wavefunctions of fragments (e.g. transferable functional groups).

However, note that this approach is quite delocalized in nature. The use of MOs is akin to treating the system from a "unified particle" limit. From the MO perspective, H_2 is quite similar to He, and both systems can be treated using the same basis functions if desired. In other words, we willingly sacrifice atomic identity towards molecular identity.

In any case, a theoretical and interpretative framework can be built stemming from these ideas. Such a framework places a great deal of importance on the orbitals that result from the minimization of the coefficient $C_{i\mu}$, which will be called Canonical Molecular Orbitals (CMOs). The resulting theory is often called Molecular Orbital Theory (MOT), and was pioneered by R. S. Mulliken, F. Hund and others in the late 1920's.

In this Section we will outline the core principles of MOT and the underlying mathematical justifications with the goal of underlining the advantages and disadvantages of this approach.

3.1.1 Principles of Molecular Orbital Theory

MOs form by linear combination of AOs. Both MOs and AOs are one-electron eigenfunctions. Therefore, we will assume that an effective one-body Hamiltonian $\widehat{H}_{eff}$ is known, a bright example of which is the Fock operator from Chapter 2.

Any effective one-electron Hamiltonian $\widehat{H}_{eff}$ may be used instead of the Fock operator. The interaction between two overlapping AOs is given by the hopping integral H_{ij}, defined as:

$$H_{ij} = \langle \chi_i | \widehat{H}_{eff} | \chi_j \rangle \tag{3.2}$$

The hopping integral H_{ij} takes negative values. Diagonal terms, H_{ii}, are simply AO energies.

If we limit ourselves to two centers, we can combine the AOs constructively by adding them, or we can substract them as in a destructive interference. MOT states that the number of orbitals must remain constant, so that the number of input AOs is the same as the number of MOs that must result from linear combination.

The linear combination of two atomic orbitals χ_i and χ_j that have well defined energies, such as:

$$\begin{aligned} E_i &= H_{ii} = \langle \chi_i | \widehat{H}_{eff} | \chi_i \rangle \\ E_j &= H_{jj} = \langle \chi_j | \widehat{H}_{eff} | \chi_j \rangle \end{aligned}$$

leads to two MOs, bonding and antibonding, according to

$$\begin{aligned} \phi_+ &= C_{i+}\chi_i + C_{j+}\chi_j \\ \phi_- &= C_{i-}\chi_i - C_{j-}\chi_j \end{aligned}$$

The constructive linear combination ϕ_+ will, through constructive interference, take significant values along the internuclear axis. Consequently, it increases the probability density for the electrons in this region. We use the term *bonding* to refer to such MOs, which are then labeled by symmetry (e.g. σ, π). The destructive interference, ϕ_-, anihiquilates all density in the internuclear axis: the MO has a nodal plane perpendicular to the H_A–H_B bond. Analogously, we use the term *antibonding* to refer to MOs with these features, and add a star to their labels (e.g. $\sigma^\star$, $\pi^\star$).

The MO energies ϵ that are variationally minimized with respect to the coefficients in the LCAO expansion:

$$\frac{\partial \epsilon_{\pm}}{\partial C_{i\pm}} = \frac{\partial \epsilon_{\pm}}{\partial C_{j\pm}} = 0 \tag{3.3}$$

which, taking a general normalized expression for MO energies,

$$\epsilon_{\pm} = \frac{\langle \phi_{\pm} | \widehat{H}_{eff} | \phi_{\pm} \rangle}{\langle \phi_{\pm} | \phi_{\pm} \rangle} \tag{3.4}$$

leads to a system of secular equations of the form

$$\begin{aligned}(E_i - \epsilon_{\pm})C_{i\pm} + (H_{ij} - \epsilon_{\pm}S_{ij})C_{j\pm} = 0 \\ (E_j - \epsilon_{\pm})C_{j\pm} + (H_{ij} - \epsilon_{\pm}S_{ij})C_{i\pm} = 0\end{aligned}$$

Such systems have a solution if the determinant is zero, therefore

$$(E_i - \epsilon_{\pm})(E_j - \epsilon_{\pm}) - (H_{ij} - \epsilon_{\pm}S_{ij})^2 = 0 \tag{3.5}$$

where S_{ij} are the overlap integrals between AOs χ_i and χ_j. This result holds for any number of AOs and MOs, by generalizing the system of secular equations to higher dimensions. These secular equations are central to MOT. We will restrain ourselves to the two-orbital case for clarity.

Molecular Orbital energies

If χ_i and χ_j lead to the same energies $E_i = E_j$ we get the following solutions for the energies $\epsilon_{\pm}$ of our MOs ϕ_+ and ϕ_-,

$$\epsilon_{\pm} = \frac{E_i \pm H_{ij}}{1 \pm S_{ij}} \tag{3.6}$$

These energies are symmetric with respect to $E_i = E_j$ if the overlap integral $S_{ij} \to 0$, but not in general. We can expand the previous expression approximately as

$$\epsilon_{\pm} \approx E_i \pm (H_{ij} - E_i S_{ij}) - S_{ij}(H_{ij} - E_i S_{ij}) \tag{3.7}$$

Generally, the term $(H_{ij} - E_i S_{ij})$ is negative and therefore we assume that the bonding MO is less distant from the original AO energies than the antibonding MO. In other words, the antibonding MO is more antibonding than the bonding MO is bonding. This is the MOT explanation for the fact that H_2 is covalently bound, but He_2 is only very weakly bound – and was thought, until relatively recently, to not bind at all.

If the AOs involved do not have the same energy, and assuming by convention that $E_j - E_i > 0$, the expression for the energies of the MOs becomes:

$$\epsilon_{\pm} = \frac{-b \pm \sqrt{D}}{2a} \tag{3.8}$$

where the terms a, b and D stand for:

$$\begin{aligned} a &= 1 - S_{ij}^2 \\ b &= 2H_{ij}S_{ij} - E_i - E_j \\ D &= b^2 - 4a(E_iE_jH_{ij}^2) \end{aligned}$$

The expression in Equation 3.8 can be approximately expanded to obtain

$$\begin{aligned} \epsilon_+ &\approx E_i + \frac{(H_{ij} - E_iS_{ij})^2}{E_i - E_j} \\ \epsilon_- &\approx E_j + \frac{(H_{ij} - E_jS_{ij})^2}{E_j - E_i} \end{aligned} \tag{3.9}$$

where it must be noted again that we assumed that χ_i is more stable than χ_j. Thus, the bonding orbital is stabilized with respect to χ_i, while the antibonding orbital is less stable than χ_j. These expressions are used very often to rationalize MO energies qualitatively in terms of simple integrals. Note that E_i and E_j must be different for such expressions to work. If the denominator is too large, the energies will be very close to those of the AOs: no mixing shall take place, the resulting MOs are just the original AOs.

Assuming that the separation is not too large, the bonding MO will be significantly closer to the lowest lying AO in terms of energy. The antibonding MO will be much closer to the highest lying AO.

The hopping integral between two AOs, H_{ij}, can be approximated in terms of the one-particle energies and the overlap integral. As an example, in the Wolfsberg-Hemholtz formula, used in the extended Hückel method, we assume

$$H_{ij} \propto \frac{1}{2}(E_i + E_j)S_{ij} \tag{3.10}$$

which therefore allows calculation of the energies of all MOs in analytical terms by fixing an arbitrary proportionality constant.

The qualitative basis of MOT stems from the rationalization of the interactions between AOs. The way AOs i and j interact can be predicted on the basis of the overlap integral, S_{ij}, and the AO energies, H_{ii}. Note that in this approximation the sign of H_{ij} will always be negative (stabilizing) if S_{ij} is positive.

Molecular Orbital coefficients

Following our two-orbital example, the coefficients of the LCAO expansion, $C_{i\pm}$ and $C_{j\pm}$ for the weights of AOs χ_i and χ_j in the MOs ϕ_+ and ϕ_-, can be derived from the secular equations and the normalization condition.

For the degenerate case $E_i = E_j$, we get simply the result shown in Subsection 2.3.1,

$$\begin{aligned} C_{i+} = C_{j+} &= \frac{1}{\sqrt{(2(1 + S_{ij})}} \\ C_{i-} = C_{j-} &= \frac{1}{\sqrt{(2(1 - S_{ij})}} \end{aligned}$$

Note that, if S_{ij} is positive, the coefficients of the bonding MO ϕ_+ ought to be smaller than the coefficients for ϕ_-. The antibonding MO is more diffuse.

For the other case in which $E_j - E_i > 0$, inserting the approximate result in Equation 3.9 in the secular equations leads to

$$\begin{aligned} C_{i+} &= t_i \frac{1}{\sqrt{1 + 2t_i S_{ij} + t_i^2}} \\ C_{j+} &= \frac{1}{\sqrt{1 + 2t_i S_{ij} + t_i^2}} \\ C_{i-} &= \frac{1}{\sqrt{1 + 2t_j S_{ij} + t_j^2}} \\ C_{j-} &= t_j \frac{1}{\sqrt{1 + 2t_j S_{ij} + t_j^2}} \end{aligned}$$

where the mixing coefficients t_i and t_j are defined as

$$\begin{aligned} t_i &= \left(\frac{H_{ij} - E_i S_{ij}}{E_i - E_j}\right) \\ t_j &= \left(\frac{H_{ij} - E_j S_{ij}}{E_i - E_j}\right) \end{aligned}$$

Note that, as per our initial assumption, the denominator in the mixing coefficients is negative and the numerator is negative as well, and thus the mixing coefficients are positive and generally larger than 1.

As we have seen when discussing MO energies, ϕ_+ must lie closer in energy to the most stable AO, χ_i. The mixing coefficients determines that the weight of χ_i will also be larger – by a factor of t_i – than the contribution of χ_j in ϕ_+. Therefore, the bonding MO is closer in energy and resembles closer the most stable AO. The opposite is true to the antibonding MO.

Additionally, note that χ_j is by definition less stable than χ_i. Therefore, the coefficients are indeed expected to be larger for the antibonding combination as per the numerator in the mixing coefficients.

Key principles of Molecular Orbital Theory

Due to the orthogonality constraints of spherical harmonics, the overlap of many AOs is 0 by definition. Other overlaps can be rationalized using molecular symmetry with relatively low effort. Let us examine the principles of Molecular Orbital Theory for two AOs that have been outlined in this section:

- MOs are formed by linear combination of AOs.
- Combining N AOs must produce N MOs.
- Mixing two AOs produces both a bonding (constructive interference) and an antibonding (destructive interference) MO.

- Mixing between two AOs χ_i,χ_j can only take place if $S_{ij} \neq 0$ and E_i is not very different from E_j.

- Bonding MOs are lower in energy than the originating AOs by some quantity proportional to S_{ij} and $|E_j - E_i|$.

- Antibonding MOs are higher in energy than the originating AOs by some quantity proportional to S_{ij} and $|E_j - E_i|$, which is larger than the one stabilizing bonding MOs for the same AO pair.

- Population of MOs determines the total energy and the bonding pattern of the system.

Minimization of the coefficients of the linear combination approximately justifies two additional rules:

- MOs resemble most the AO that originated them and which is closest in energy.

- Antibonding MOs are more diffuse than bonding MOs.

These rules suffice to build MO diagrams for any molecule at a qualitative level if the AOs of its atoms are known. Naturally, the framework outlined here can be extended to linear combinations of more than 2 AOs.

Furthermore, analogous analysis can be done starting with MOs from different fragments. We will not justify such generalizations mathematically, but they can be derived from the principles herewith and symmetry considerations. The other key aspect of MOT for fragment MOs is the notion of hybridization that is developed next.

Hybridization in Molecular Orbital Theory

While two-orbital MOT is very consistent, more numerous linear combinations often result in qualitative errors. For instance, the AOs on the carbon atom ($1s^2 2s^2 2p^4$) imply, according to Hund's rule, a ground state $S = 1$. From this starting diagram, overlap with four hydrogenoid $1s$ orbitals to lead to CH_4 can not be devised qualitatively.

Even if one of the $2s$ electrons is promoted to a $2p$ orbital, leading to a quintet spin state, which is energetically feasible as this state is not too energetic, this would predict three of the bonds to be identical (arising from degenerate $2p$ orbitals, hence with the same hopping integral) and one to be different (arising from the remaining $2s$ orbital). Obviously, this does not bode well with the fact that methane is completely apolar and tetraedrically symmetric.

This is a fundamental flaw, which has to do with the limitations of MOT, but can be addressed in the theory itself, albeit somewhat crudely. The basic assumption is that AOs on a single center are all orthonormal ($S_{ij} = 0$) and hence we can build normalized linear combinations of them.

Whenever needed, MOT assumes that AOs (or fragment MOs) can be combined into hybrid orbitals that are oriented towards the bonds. In the case of carbon, the quintet state is assumed to undergo hybridization: the close lying $2s$ and all $2p$ AOs combine to produce four identical sp^3 hybrids, as in

$$\begin{aligned}
\chi^1_{sp^3} &= \frac{1}{2}(\chi_{2s} + \chi_{2px} + \chi_{2py} + \chi_{2pz}) \\
\chi^2_{sp^3} &= \frac{1}{2}(\chi_{2s} + \chi_{2px} - \chi_{2py} - \chi_{2pz}) \\
\chi^3_{sp^3} &= \frac{1}{2}(\chi_{2s} - \chi_{2px} - \chi_{2py} + \chi_{2pz}) \\
\chi^4_{sp^3} &= \frac{1}{2}(\chi_{2s} - \chi_{2px} + \chi_{2py} - \chi_{2pz})
\end{aligned}$$

which can now interact identically with four hydrogen atoms. This approach is sometimes called the bond MO approach. Note that, however, the picture provided by this approach is elegant, matching the VSEPR model closely, but qualitatively wrong. From accurate calculation and spectoscopy we know that, in fact, the four C–H bonds are equal, but no four degenerate orbitals are found in any optimized wavefunction of methane.

Hybridization is thus a useful notion that, while theoretically belonging to Valence Bond Theory (VBT), can be conceptually useful in MOT. At the purely qualitative level, hybridization is often coupled to MOT for *a posteriori* analysis.

Note that photoelectron spectroscopy shows two distinct peaks for the ionization of methane, which correspond roughly to the two distinct valence MOs of the molecule. Hence, effectively, all four C–H bonds are *not* equivalent.

3.1.2 Fock operator in Molecular Orbital Theory

If a proper computational methodology exists that can evaluate all the required integrals, and optimize the MOs in terms of the basis set, the principles of MOT that have been outlined in the previous Subsection can be verified.

Let us bring back the example from Chapter 2 (Subsection 2.3.1) in which we expressed the wavefunction of the H_2 molecule using a LCAO approximation and the Hartree-Fock method.

By combining two s-type atomic orbitals, $1s_A$ and $1s_B$, each one centered in one hydrogen nuclei, we got two MOs $\phi_\pm = N_\pm(1s_A \pm 1s_B)$, where $N_\pm = 1/\sqrt{2(1 \pm S_{AB})}$ and S_{AB} is the overlap integral (cf. Equation 2.46) between the AOs.

Now, the overlap integral integral between such orbitals can be expressed as a function of the distance R between H_A and H_B due to the spherical symmetry they both present:

$$S_{AB}(R) = e^{-R}\Big(1 + R + \frac{R^2}{3}\Big) \tag{3.11}$$

Therefore, $S_{AB}(0) = 1$ and then decreases exponentially as R increases in this particular case. Recall that generally the overlap integral is bound between -1 and 1.

In HFT, the MO energy for the ith MO, ϵ_μ, is given by:

$$\epsilon_\mu = \langle\phi_\mu|\widehat{F}|\phi_\mu\rangle = h_\mu + \sum_{\nu=1}^{N}(J_{\mu\nu} - K_{\mu\nu}) \tag{3.12}$$

Where all terms are expressed in the notation from Chapter 2. Note that here naturally there are only two non-vanishing two electron integrals, J and K between ϕ_+ and ϕ_-, so that we can write:

$$\epsilon_{\pm} = h_{\pm} + (J - K) \tag{3.13}$$

Therefore, the energy difference between both MOs is due to the one-body term h_i, which we can evaluate here explicitely using the AOs, which are eigenvectors of the one-electron Hamiltonian with eigenvalue E_{1s}. Let us assume $S_{AB} \to 0$ for simplicity:

$$h_{\pm} = \langle \phi_{\pm} | \widehat{h} | \phi_{\pm} \rangle = \pm E_{1s} \tag{3.14}$$

E_{1s} is negative. Therefore, the constructive interference ϕ_+ has lower energy than ϕ_-. This is coherent with our interpretation: the constructive system has probability density in the internuclear axis and therefore should be more stable. It also matches our previously derived Equation 3.6, because the hopping integral here is naturally just E_{1s} again.

As pointed in Subsection 2.3.1(cf. Equation 2.71), in the ground state the spatial part of the wavefunction is simply

$$\Phi_0 = \frac{1}{\sqrt{2}} \phi_+(\mathbf{r}_1)\phi_+(\mathbf{r}_2) \tag{3.15}$$

which can be expanded in AOs, ignoring normalization constants, as

$$\Phi_0 = \Big[1s_A(\mathbf{r}_1)1s_A(\mathbf{r}_2) + 1s_B(\mathbf{r}_1)1s_B(\mathbf{r}_2)\Big] + \Big[1s_A(\mathbf{r}_1)1s_B(\mathbf{r}_2) + 1s_B(\mathbf{r}_1)1s_A(\mathbf{r}_2)\Big] \tag{3.16}$$

Recall that $1s_A$ is centered in nuclei A and $1s_B$ is centered in nuclei B. The first term in Equation 3.16 can be interpreted as an ionic term, in which both electrons are placed in an orbital sitting in A, or in *atom* H_A, or in H_B. The second term represents covalency, and has electrons shared between H_A and H_B.

From this perspective, we can say that the MOT description of H_2 has equal weights for the covalent and the ionic part. The dissociation problem that was showcased in Subsection 2.3.1 becomes significantly easier to understand: as $R \to \infty$ the wavefunction should become strictly covalent in an homolytic dissociation. However, the HFT wavefunction does not have this freedom, and the system incorrectly dissociates to $H^- + H^+$. Let this brief example showcase how naturally MOT and the HFT interact.

Mulliken population analysis

The analysis of the dissociation of H_2 in a minimal basis set in terms of ionic and covalent terms has an underlying assumption, which is rooted in the LCAO method: we have assigned electrons to atoms based on the allocation of basis functions. That is, we assume that the $1s_A(\mathbf{r}_1)$ term corresponds to an electron *belonging* to the H_A, an hydrogen atom, because the basis function $1s_A$ is centered in the nuclei A.

In other words, by analyzing the composition of the occupied MOs in terms of AOs, it is possible to derive *atomic charges*. Let us see a simple example. For the bonding MO of the previous example, ϕ_+, we can write a probability density as

$$\phi_+^2 = \Big[\frac{1}{\sqrt{2(1+S_{AB})}}(1s_A + 1s_B)\Big]^2 = C_{A+}^2 + C_{B+}^2 + 2C_{A+}C_{B+}S_{AB} = 1 \tag{3.17}$$

in which we have introduced explicit terms C_{A+} and C_{B+} for the coefficients of the two AOs in the bonding MO ϕ_+, which might naturally be different from each other. We

have assumed MOs to be normalized. From this expression, a possible interpretation is that one electron in this MO contributes by C_{A+}^2 to the population of AO $1s_A$, by C_{B+}^2 to the population of AO $1s_B$ and by $2C_{A+}C_{B+}S_{AB}$ to the overlap region between the two of them. The overlap term can be considered to be split equally between both MOs.

This notion can be generalized to any LCAO calculation in which basis functions have an intrinsic atomic character. This approach is often called Mulliken population analysis.

We define a population matrix $\mathbf{P}$ with terms

$$\mathbf{P}_{ij} = \mathbf{D}_{ij}\mathbf{S}_{ij} \tag{3.18}$$

running over the basis functions, which we can assume are AOs, and in which the density matrix $\mathbf{D}$ has elements

$$\mathbf{D}_{ij} = 2\sum_{\mu}^{occ.} C_{i\mu}C_{j\mu} \tag{3.19}$$

in which $C_{i\mu}$ are the coefficients of AO i in MO μ as before. This expression assumes a RHF formalism in which MO occupations are always 2 for occupied MOs. Note that S_{ij} must be the identity matrix if a set of orthonormal basis functions is used.

The terms of $\mathbf{P}$ sum to the number of electrons in the system, N:

$$\sum_i \sum_j P_{ij} = N \tag{3.20}$$

Diagonal elements are contributions that arise purely from one AO, while off-diagonal elements belong to overlap regions between pairs of AOs, and threfore should be split evenly. We define the Gross Orbital Population (GOP) of an AO as

$$GOP_i = \sum_i P_{ii} + \frac{1}{2}\sum_{i\neq j} P_{ij} \tag{3.21}$$

Note that the GOP might be unphysically negative. We can then add GOPs according to the atom on which the AOs – or basis functions – are centered. This term is sometimes called the Gross Atomic Population (GAP). The atomic charge of atom A, Q_A, is then derived by substraction

$$Q_A = Z_A - \sum_i GOP_i^A = Z_A - GAP^A \tag{3.22}$$

Due to Equation 3.20, the sum of all atomic charges Q_A must be equal to the net charge of the system. While this approach is quite crude, and is extremely inconsistent due to its initial premises – it *requires* that basis functions are assigned to atoms – it is a very natural way to obtain atomic charges from a LCAO framework.

On the same spirit, the bond order BO_{AB} between atoms A and B can be defined from $\mathbf{P}$ as

$$BO_{AB} = \sum_{i^A} \sum_{j^B} P_{i^A j^B} P_{j^B i^A} \tag{3.23}$$

in which sums run only over AOs centered in atoms A and B as indicated by the superscripts. This expression is sometimes called Mayer's bond order.

3.1.3 Frontier Molecular Orbital Theory

The Klopman-Salem model decomposes the interaction energy between two chemical species. We put forward the analytical expression of the energy variation in the Klopman-Salem model:

$$\Delta E = -A + B + \sum_{\mu}^{occ.} \sum_{\nu}^{vir.} \left[\frac{2C_{i\mu}^2 C_{j\nu}^2 H_{ij}^2}{\epsilon_\mu - \epsilon_\nu} \right] \tag{3.24}$$

where the same convention has been used as before for the indices of AOs i,j and MOs of the involved species follow indices μ,ν. Note that virtual MOs are included in the third term as well. The first two terms, A and B, model electrostatic and steric interactions and are not relevant here. The expression can be further generalized to interactions between several entities.

Equation 3.24 is governed by the third term in many chemical contexts, notably when steric or purely electrostatic effects are not very strong. It is controled by the closest occupied-unoccupied pair, that are usually called the Frontier MOs. Hence, reactivity can be modelled on the basis of the interaction between the Highest Occupied MO (HOMO) and the Lowest Unoccupied MO (LUMO).

As this is usually a two-orbital problem, the reasonings that have been put forward in this Section for the coefficients $C_{i\mu}$ and the hopping integral H_{ij} can all be applied.

Koopman's theorem

The particular importance of FMOs is coupled to a physical interpretation. The Ionization Potential (IP) of a chemical species M is defined as the energy required to go from M to $M^+ + e^-$, that is, to pull an electron from the system. The Electron Affinity (EA) is defined analogously for the monoanionic species, i.e. from M^- to $M + e^-$.

Suppose that the MOs of a chemical species with N electrons have been optimized with respect to the energy in HFT. The total energy is then given by

$$E_N = \sum_{i}^{N} \epsilon_i - \frac{1}{2} \sum_{i}^{N} (J_{ij} - K_{ij}) \tag{3.25}$$

If we assume that the cationic and anionic species might be accurately described by the same set of MOs as the neutral species, the energy for the same species with an more or one less electron is simply

$$E_{N-1} = \sum_{i}^{N-1} \epsilon_i - \frac{1}{2} \sum_{i}^{N-1} (J_{ij} - K_{ij})$$

and hence

$$E_{N-1} - E_N = -\epsilon_N \tag{3.26}$$

which represents the IP as defined before. Therefore, the IP can be approximated as the negative of the energy of the HOMO. An analogous procedure equiparates EA with the negative of the energy of the LUMO.

According to this view, the energies of the HOMO and the LUMO also determine the disposition of a molecule to accept or donate electrons. If the IP of a chemical species is similar to the EA of a different chemical species, it seems rational to expect that an interaction is possible in which one electron is transferred between the two.

Hence, it is coherent to picture interactions between chemical entities as arising from HOMO-LUMO interactions, and such interactions as controlled by the usual concepts from MOT, namely the hopping integral and the overlap integral. As we have seen before (cf. Equation 3.10), the hopping integral can be approximated in terms of orbital energies and overlap integrals as well.

The regioselectivity and viability of many reactions can be rationalized by the maximization of the overlap between the HOMO-LUMO pair that is closest in energy, and the resulting MOs from the interaction can be rationalized using the precepts from general 2-orbital MOT as well. Such approaches are notably popular in chemisty.

In general, the more electrophile species is expected to react through its LUMO to *accept* electrons, and nucleophiles are expected to react through their HOMO. Sometimes the interaction is allegedly two-fold, as in σ-donation–π-backdonation in coordination complexes.

3.1.4 Limitations of Molecular Orbital Theory

The applications of MOT and MO diagrams, including MO correlation diagrams, are far too vast and well-known to cover. As a sidenote, MOT has no problem describing delocalized bonds and hypervalent molecules (e.g. SF_6) that can not be easily understood from the Lewis picture.

Our interest, however, concerns the limitations of the framework at the quantitative and qualitative levels.

Routinely, MOs are not rationalized from scratch using constituent AOs, which would quickly become cumbersome. Instead, MOs are derived from any one-particle effective Hamiltonian theory expressed in terms of a finite basis set using the Roothaan-Hall method. Alternatively, the MOs of the Kohn-Sham system might be used, while in principle those do not represent the variationally minimized wavefunction of the real system.

The resulting MOs are expressed as linear combinations of the basis functions of choice. Note that the coefficients are optimized in order to minimize the energy, which is not explicitely a function of any unoccupied MOs. Only the occupied MOs are optimized.

The MOs that result from the minimization procedure, so-called Canonical MOs (CMOs), must diagonalize the Fock matrix, which is adequate for the computation in terms of matrix algebra. On the other hand, this requirement makes them progressively delocalized. This means that most MOs, in particular those of higher energies, have contributions from some of the basis functions on every nuclei of the molecule. In other words, CMOs are very delocalized.

Hence, interpretation of CMOs is very often quite hard. This is the main qualitative issue the theory faces from the practical point of view. Other issues and some specific examples will be covered in what follows.

Mathematical limitations

MOT is a one-electron theory. While it might be possible to write the two-body electronic Hamiltonian as an effective one-body $\widehat{H}_{eff}$, we do not know how.

The immediate consequence is that MOT can not be quantitative. This shortcoming is coherently shared by HFT, which arises from similar assumptions (see Section 2.3 of Chapter 2). Indeed, homolytic dissociation can not be properly described in MOT, as seen in the extensive discussion concerning the Coulson-Fischer point.

In other words, MOT is *a priori* not defined in the exact many-body wavefunction, which as we have seen in Chapter 2 would require a linear combination of many configuration state functions.

Quantum chemistry tipically evaluates the quality of wavefunctions, and MOs therein, using the variational theorem for the exact Hamiltonian. For instance, it could be said that MOs for H_2 near the equilibrium position are quite representative of the exact wavefunction. Past the Coulson-Fischer point this can hardly be said: the MOs are not representatve at all.

The most notable practical consequence of the mathematical limitations of MOs is their non-uniqueness. That is, there can be infinitely as many MOs that lead to the same energy in the minimization problem highlighted in Chapter 2 (cf. Equation 2.58). Let us start from the canonical HF method (Equation 2.43) and define

$$\eta_m = \sum_\mu U_{m\mu}\phi_\mu \tag{3.27}$$

where U_{mi} are elements of a unitary matrix $\mathbf{U}$, the eigenvalue problem becomes

$$\widehat{F}|\eta_m\rangle = \epsilon^\eta_\mu|\eta_m\rangle \tag{3.28}$$

where the new matrix of eigenvalue energies is

$$\epsilon^\eta = \mathbf{U}\epsilon\mathbf{U}^\dagger \tag{3.29}$$

The sum of all MO energies will not change because the trace is invariant under any unitary transformation. Therefore, the total energy will not change: both wavefunctions will be equally good or bad.

From the energetic point of view, both sets of MOs will be exactly as good. From the interpretative point of view, however, this has twofold consequences. On one hand, it questions any reasoning based on individual MO energies and shapes. On the other hand, it means that one can choose a unitary transformation according to some criteria to obtain a wavefunction with some advantageous properties. This will be exemplified later on.

The rationalization of molecular structure in terms of overlap integrals and energies is thus rendered inadequate, because there are infinitely many ways to represent MOs with equal accuracy. FMO is equally troubled by this fact: the shape of the frontier MOs can be modified freely.

Practical limitations

As highlighted before, MOT – and HFT – can never be quantitative. In fact, the simplistic foundations of MOT given in this Chapter cannot justify any bonding in He_2, which was also discussed in Section 2.3.

As seen in the previous Subsection, two-orbital four-electron interactions are predicted to be unstable in MOT: two electrons will end up in the resulting bonding MO, two electrons will end up in the antibonding MO, and the net energy change will be destabilizing.

While quantitative inconsistencies that are due to the mathematical underpinnings that have been evidenced so far, there are other situations in which MOT is not intuitive. A bright example is the CO molecule, which is known to have a dipole moment of 0.122 D that points toward the carbon atom. This is in principle counterintuitive because

oxygen is more electronegative than carbon, and hence is expected to polarize the charge distribution towards itself.

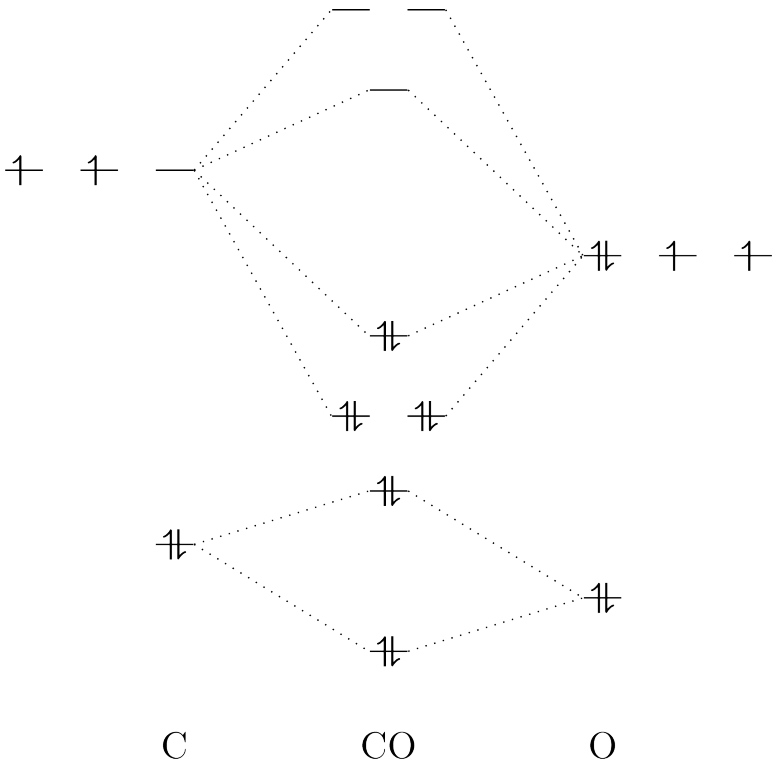

Figure 3.1: Qualitative valence MO diagram of the CO molecule.

In MOT, CO is expected to have two core MOs, belonging to the unmixed $1s$ AOs of each atom. Then, a pair of σ and $\sigma^\star$ as arising from the combination of $2s$ orbitals. Then, two π MOs and a σ MOs arising from the interaction between the $2p$ MOs of both atoms. This results in a total of 7 MOs, to be occupied by the 14 electrons of the molecule (see Figure 3.1). As oxygen is in the same row as carbon but has a larger nuclear charge, its AOs are lower in energy (this can be easily verified).

Hence, and according to the principles of MOT that we have developed in Subsection 3.1.1, the bonding orbitals resulting from the interaction of the $2p$ AOs should be definitely closer in shape to the oxygen AOs. Thus, the probability density of such MOs should be higher in the vicinity of the oxygen atom, and the dipole moment should point towards it. This is not the case. This error is corroborated by HFT, which gives a wrongly signed dipole moment. Furthermore, no interpretation can be given in terms of *intra*-molecule orbital interactions, since the CMOs are strictly orthonormal with one another.

As in this example, MOT sometimes gives wrong qualitative predictions of ground state equilibrium properties. From the quantitative point of view, including other CSFs improves the wrong dipole moment of HFT until the FCI limit, which gives the correct direction and magnitude.

On the other hand, this situation is far more troublesome than the strong correlation problems due to the lack of some relevant CSFs, because the MO single CSF is relatively

good energetically, but fails qualitatively in a property that is highly relevant for our understanding of its chemistry.

Ontological limitations

A more precise way to state the fact that MOs are approximate mathematical constructions is to say that the concept of orbital is *non-referring*.

If we accept that the epistemology of chemistry is bound by the laws of quantum mechanics, MOs do not refer to any ulterior physical object: they are purely mathematical constructions that are useful as a coarse approximation. Electrons in a molecule can not be assigned to orbitals, nor quantum numbers at all.

Of course, the same can be said for most chemical concepts, including the notion of atom, molecule, molecular *shape* and so on. The underlying question is whether chemical sciences are epistemologically – and ontologically – reductible to quantum mechanics. The details of such discussion are far beyond the scope of this manuscript.

3.1.5 Localization schemes

CMOs are delocalized in nature. Hence, they are hard to interpret with ease. As the energy is invariant with respect to unitary transformations of the MOs, it is plausible to select a particular unitary transformation that produces MOs that have advantages over CMOs.

One of the main objectives of such transformations is localization, because a set of localized orbitals is easier to interpret using MOT and related concepts. Some examples will be given later on. Tipically, this is attempted as a search over unitary transformations that maximize or minimize the expectation value of an operator, which is tuned by modifying the MOs of the wavefunction.

In this Subsection, some examples of localization schemes will be presented in order to better understand the limitations of CMOs and the interpretative framework of MOT.

Foster-Boys localization

The Foster-Boys localization procedure is based on the minimization of the spatial extent of the orbitals, as given by the expectation value of the $|\mathbf{r}_1 - \mathbf{r}_2|$ operator, expressed as

$$L_1^{FB}(\phi) = \sum_{\mu}^{N} \langle \phi_\mu(\mathbf{r}_1)\phi_\mu(\mathbf{r}_1)|\mathbf{r}_1 - \mathbf{r}_2|\phi_\mu(\mathbf{r}_2)\phi_\mu(\mathbf{r}_2)\rangle \tag{3.30}$$

which can be shown to reduce to a simpler maximization procedure, in which the operator $\overline{r}$ is the operator associated to the distance between the MO centroid and the arbitrarily chosen origin of the molecular coordinate system,

$$L_2^{FB}(\phi) = \sum_{\mu}^{N} \left[\langle \phi_\mu|\overline{r}|\phi_\mu\rangle\right]^2 \tag{3.31}$$

The maximization of $L_2^{FB}(\phi)$ is far simpler because it requires less computation of integrals. Let us showcase the application for a two-orbital case, starting from a pair of MOs ϕ_1 and ϕ_2 towards a new pair ξ_1,ξ_2 through a standard 2×2 unitary matrix in terms of the angle γ:

$$\begin{aligned}\xi_1 &= (cos\gamma)\phi_1 + (sin\gamma)\phi_2 \\ \xi_2 &= (-sin\gamma)\phi_1 + (cos\gamma)\phi_2\end{aligned}$$

We can express the maximization function of Equation 3.31 for the new orbitals

$$L_2^{FB}(\xi) = L_2^{FB}(\phi) + A_{12} + \sqrt{A_{12}^2 + B_{12}^2}cos[4(\gamma - \alpha)] \tag{3.32}$$

where a simplified notation has been used to define the following integrals

$$\begin{aligned}\overline{r}_{\mu\nu} &= \langle\phi_\mu|\overline{r}|\phi_\nu\rangle \\ A_{12} &= \overline{r}_{12}^2 - \frac{1}{4}(\overline{r}_{11} - \overline{r}_{22})^2 \\ B_{12} &= \overline{r}_{12}^2(\overline{r}_{11} - \overline{r}_{22})\end{aligned}$$

and the angle α is defined bound as $0 \leq \alpha < \pi/2$ and satisfying

$$\begin{aligned}cos(4\alpha) &= -\frac{A_{12}}{\sqrt{A_{12}^2 + B_{12}^2}} \\ sin(4\alpha) &= \frac{B_{12}}{\sqrt{A_{12}^2 + B_{12}^2}}\end{aligned}$$

The function is maximal when the cosine term is equal to 1, which arises when $\gamma = \alpha + n\frac{\pi}{2}$ with $n \in \mathbb{N}$. In principle, it suffices to iterate pairwise through all MOs until the unitary transformation matrix converges to a value γ. We will not comment on the convergence of the procedure.

As the matrix of MO energies ϵ is diagonal, it can be split into two blocks: occupied and virtual MOs. Then, occupied and virtual MOs can be localized using this scheme.

Pipek-Mezey localization

Another popular strategy to obtain localized MOs is the one proposed by Pipek and Mezey. In this case, the value to maximize is

$$L^{PM}(\phi) = \frac{1}{N}\sum_\mu GOP_\mu^2 \tag{3.33}$$

That is, we want to maximize the square of all Mulliken's GOPs in the system (see Subsection 3.1.2 for details on GOPs). This function can be expressed as the expectation value of an operator for computational implementation.

It suffices to say that this procedure suffers from the same basis set dependency as Mulliken's partial charges, notably the need for atom-based basis functions. Again, the procedure can be applied blockwise to occupied and virtual MOs.

Natural Orbitals

Natural Orbitals (NOs) are eigenfunctions of the one-particle reduced density matrix $\gamma^1(\mathbf{r})$, which was introduced in Chapter 2. NO η_i is an eigenfunction of $\gamma^1(\mathbf{r})$ with eigenvalue n_i, which is thereafter called the occupation number of the i-th NO;

$$\gamma^1(\mathbf{r}_1;\mathbf{r}_1')\eta_i = n_i\eta_i \tag{3.34}$$

Note that NOs diagonalize the one-particle reduced density matrix as per the previous statement,

$$\gamma^1(\mathbf{r}_1;\mathbf{r}_1') = \sum n_i\eta_i^\star\eta_i \tag{3.35}$$

Furthermore, note that CMOs in LCAO HFT are also NOs. In RHF all occupation numbers are either 0 or 2, with the α and β μ-th MO being degenerate. In correlated theories, NOs are a compact way of expressing the wavefunction.

Recalling Mulliken's population analysis, which was covered in Subsection 3.1.2, note that it assumed that off-diagonal elements in the AO basis density matrix are split evenly between two AOs. This is a coarse assumption. The easiest way to correct this issue is orthogonalizing the AO basis to ensure that the density matrix in terms of the AO basis is diagonal. This is achieved by using a symmetric orthogonalization.

GAPs can then be obtained as sums of occupation numbers of all AOs with the same center, with no off-diagonal terms.

3.2 Valence bond theory

Valence Bond Theory (VBT) is arguably the greatest competitor of MOT in chemical interpretation. During much of the 20th century both theories competed, argued and fought over conceptual significance. [34]

In VBT, the wavefunction is built from *structures*. Structures are CSFs (cf. Section 2.3) that might not be proper spin eigenfunctions. Covalent bonds arise from the overlap of valence atomic orbitals, generally two unfilled orbitals to produe a spin pair. Such bonds must be directional, belonging to the axis of maximum overlap between such AOs.

For the most part, MOT triumphed, largely due to the convenience of orthogonal MOs obtained from LCAOs from the computational point of view (i.e. HFT, KS-DFT). However, many concepts from VBT still permeate chemical parlance – or vice-versa. This section is an attempt to delineate such concepts and highlight their mathematical origin.

3.2.1 Modern valence bond theory

MOT can be coupled to any one-particle effective Hamiltonian. However, as the procedure does become quite involved when the number of electrons and orbitals increases, MOT is usually coupled to HFT. In other words, HFT (with finite basis set expansions) permeates MOT because it pushes its mathematization forward by providing solutions. Analogously, VBT is as of today linked to its genuine computational framework.

Although VBT was developed analytically during a significant period of time, it is nowadays feasible to solve the electronic structure problem for a Valence Bond (VB) wavefunction. We will outline the fundamentals of the approach here.

A general VB wavefunction is expressed as a linear combination of CSFs,

$$\Psi^{VB} = \sum_i w_i\Phi_i \tag{3.36}$$

where w_i are coefficients of the linear combination, often called weights in VBT, and each CSF might be written as a product

$$\Phi_i = \widehat{\mathcal{A}}\Omega_0\Theta_i \tag{3.37}$$

where the spatial part Ω_0 is a product of VB orbitals, which are AOs of some type, and Θ_i is the spin part, which may be approached with the Rumer method (cf. Subsection 3.2.2, Equation 3.52).

Optimal coefficients may be determined by solving a matrix equation of the form

$$\mathbf{HC} = \epsilon\mathbf{Sw} \tag{3.38}$$

in which Hamiltonian matrix elements are of the form

$$H_{ij} = \langle\Phi^i|\widehat{H}|\Phi^j\rangle \tag{3.39}$$

and overlap matrix elements are of the form

$$S_{ij} = \langle\Phi^i|\Phi^j\rangle \tag{3.40}$$

VB orbitals are ultimately expressed as a linear combination of atomic basis functions, generally CGTOs as in the Roothaan-Hall method.

Although the procedure will not be covered extensively in this manuscript, we will assume that VBSCF is the generic procedure through which the optimized wavefunction is obtained, which involves simultaneous minimization of basis coefficients and coefficients of AOs – and thus, the CSFs – in the wavefunction. There are other possible approaches to quantitative VBT, but for the purpose of this Section we will stay within this mathematical framework.

3.2.2 Principles of Valence Bond Theory

The main features of the approach can once more be exemplified using the H_2 system, for which it was developed by Heitler, London and others.

Starting once again from two hydrogenoid atomic orbitals $1s_A$ and $1s_B$ centered in H_A and H_B respectively, a VBT-like wavefunction can be built by taking the expanded ground state wavefunction given by MOT (Equation 3.16) and building a linear combination of covalent and ionic terms.

For the spatial part, this yields

$$\begin{aligned}\Phi^{VB} = w_c\Big[1s_A(\mathbf{r}_1)1s_B(\mathbf{r}_2) + 1s_B(\mathbf{r}_1)1s_A(\mathbf{r}_2)\Big] \\ +w_i\Big[1s_A(\mathbf{r}_1)1s_A(\mathbf{r}_2) + 1s_B(\mathbf{r}_1)1s_B(\mathbf{r}_2)\Big]\end{aligned} \tag{3.41}$$

where w_c and w_i are the weights of the covalent and ionic terms respectively. Naturally, normalization must be imposed upon the weights and/or the CSFs.

Compared to the MOT ground state spatial part of the wavefunction in Equation 3.16, the VBT wavefunction has an additional degree of freedom through the variational optimization of the coefficients.

Recalling Chapter 2 and Subection 2.3.1 in particular, and noticing that ionic and covalent terms are indeed CSFs, this can be thought of as a multiconfigurational approach.

In fact, the terms arising from the expansion of Φ^{VBT} in terms of AOs are analogous to the terms arising from the CI expansion in Equation 2.73, for which the spatial part would be

$$\Phi^{MC} = c_0\Big[1s_A(\mathbf{r}_1)1s_B(\mathbf{r}_2) + 1s_B(\mathbf{r}_1)1s_A(\mathbf{r}_2) + 1s_A(\mathbf{r}_1)1s_A(\mathbf{r}_2) + 1s_B(\mathbf{r}_1)1s_B(\mathbf{r}_2)\Big]$$
$$+c_1\Big[1s_A(\mathbf{r}_1)1s_A(\mathbf{r}_2) + 1s_B(\mathbf{r}_1)1s_B(\mathbf{r}_2) - 1s_B(\mathbf{r}_1)1s_A(\mathbf{r}_2) - 1s_A(\mathbf{r}_1)1s_B(\mathbf{r}_2)\Big] \tag{3.42}$$

which, as discussed before, can dissociate the molecule correctly because all the ionic terms are anhiquilated when $c_0 = c_1$. Analogously, Φ^{VBT} can dissociate correctly because the weight of the ionic term, w_i, can drop to zero as R increases: both wavefunctions are the same. However, the splitting of terms in the VBT wavefunction has a natural interpretation: the optimized weights of the two CSFs represent how much the wavefunction is akin to the ionic or covalent situation. From the quantitative point of view, both wavefunctions are exactly the same, as shown in Figure 3.2 for the VBSCF wavefunctions.

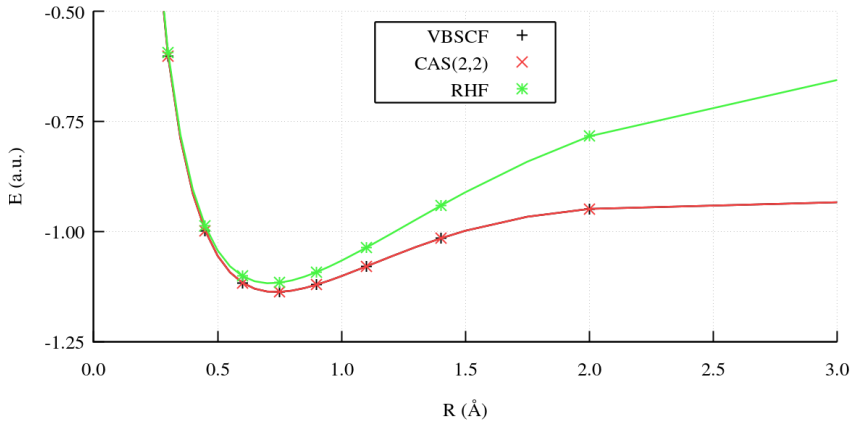

Figure 3.2: Dissociation curves for the H_2 molecule at different theory levels with a STO-3G basis set.

VBT is significantly more localized than MOT because it does not use molecular orbitals *per se*. Instead, CSFs are built from atomic orbitals – in a broad sense –, which hopefully will simplify the interpretation.

In more specific terms, the valence bond wavefunction should be built as a linear combination of Slater determinants of atomic orbitals, $1s_A$ and $1s_B$ centered in H_A and H_B, such as

$$|1s_A\alpha, 1s_B\beta\rangle = \frac{1}{\sqrt{2}}\Big(1s_A(\mathbf{r}_1\alpha)1s_B(\mathbf{r}_2\beta) - 1s_B(\mathbf{r}_1\beta)1s_A(\mathbf{r}_2\alpha)\Big) =$$
$$= \frac{1}{\sqrt{2}}1s_A(\mathbf{r}_1)1s_B(\mathbf{r}_2)(\alpha(1)\beta(2) - \beta(1)\alpha(2))$$
$$|1s_A\alpha, 1s_A\beta\rangle = \frac{1}{\sqrt{2}}\Big(1s_A(\mathbf{r}_1\alpha)1s_A(\mathbf{r}_2\beta) - 1s_A(\mathbf{r}_1\beta)1s_A(\mathbf{r}_2\alpha)\Big) =$$
$$= \frac{1}{\sqrt{2}}1s_A(\mathbf{r}_1)1s_A(\mathbf{r}_2)(\alpha(1)\beta(2) - \beta(1)\alpha(2))$$
$$|1s_B\alpha, 1s_B\beta\rangle = \frac{1}{\sqrt{2}}\Big(1s_B(\mathbf{r}_1\alpha)1s_B(\mathbf{r}_2\beta) - 1s_B(\mathbf{r}_1\beta)1s_B(\mathbf{r}_2\alpha)\Big) =$$
$$= \frac{1}{\sqrt{2}}1s_B(\mathbf{r}_1)1s_B(\mathbf{r}_2)(\alpha(1)\beta(2) - \beta(1)\alpha(2))$$

in which spin coordinates σ_1 and σ_2 have been simplified to 1 and 2 for conciseness. This leads to the VB wavefunction,

$$\Phi^{VB} = w_1\Big(|1s_A\alpha, 1s_B\beta\rangle - |1s_A\beta, 1s_B\alpha\rangle\Big) + w_2|1s_A\alpha, 1s_A\beta\rangle + w_3|1s_B\alpha, 1s_B\beta\rangle \quad (3.43)$$

where, following our previous reasoning, a covalent term has been devised with weight w_1 that includes both spin couplings for generality, and two ionic terms with weights w_2 and w_3 represent the two extreme cases of polarization. In VBT, the term structure is usually reserved for such terms from which a Lewis-like depiction of the molecule is inferred. Hence, w_1 is the weight of the covalent structure and so on, and we can write the same wavefunction in terms of structures as

$$\Phi^{VB} = w_1\Phi^{cov} + w_2\Phi^{ion}_A + w_3\Phi^{ion}_B \quad (3.44)$$

The given expression is general for any two-center two-electron situation. Naturally, the previous expression simplifies in the strictly symmetric case of H_2 to the expression given in Equation 3.41.

$$\Phi^{VB} = w_{cov}\Phi^{cov} + w_{ion}\Phi^{ion} \quad (3.45)$$

VB wavefunctions might be built for any system in terms of structures. Structures are composed of one or more Slater determinants of atomic orbitals that mirrors a chemically sound structure. In general, atomic orbitals of any type might be used, but for ease of interpretation it is recommended that only localized one-center functions are included. Like in Mulliken population analysis, the basis set expansion is embroidered in the theory.

Non-orthogonality

It must be noted that in VBT, CSFs are not orthogonal, because AOs are not generally orthogonal between different atoms. In fact, overlap between different structures – and between determinants in a single structure – might be high, and must be evaluated to calculate both the energy of a given structure and the coupling between structures.

For instance, starting from the wavefunction for H_2 in Equation 3.45, the overlap integral is

$$S_{ion-cov} = \langle \Phi^{ion} | \Phi^{cov} \rangle = \frac{2S_{AB}}{1 + S_{AB}} \tag{3.46}$$

where $S_{AB} = \langle 1s_A | 1s_B \rangle$ as given in Equation 3.11, which is a function of the distance R between H_A and H_B. However, the general rule is that the overlap between two AO-based N-dimensional CSFs requires $N!$ AO overlap integrals. While this cost might be reduced using symmetry, as in our model system, the factorial scaling quickly becomes computationally intractable as the basis set is expanded.

In our model case, the energies for the ionic and covalent structures are relatively simple:

$$\langle \Phi^{cov} | \widehat{H} | \Phi^{cov} \rangle = -1 + \frac{1}{R} + \frac{2KS_{AB} + 2J + J' + K'}{1 + S_{AB}^2} \tag{3.47}$$

$$\langle \Phi^{ion} | \widehat{H} | \Phi^{ion} \rangle = -1 + \frac{1}{R} + \frac{2KS_{AB} + 2J + 5/8 + K'}{1 + S_{AB}^2} \tag{3.48}$$

where the integrals J, J', K and K' have been introduced,

$$\begin{aligned} J &= \langle 1s_A | - \frac{1}{r_{B1}} | 1s_A \rangle \\ K &= \langle 1s_A | - \frac{1}{r_{B1}} | 1s_B \rangle \\ J' &= \langle 1s_A 1s_B | \frac{1}{r_{12}} | 1s_A 1s_B \rangle \\ K' &= \langle 1s_A 1s_B | \frac{1}{r_{12}} | 1s_B 1s_A \rangle \end{aligned}$$

where r_{B1} is the distance between nuclei H_B and electron 1, and the coupling between ionic and covalent terms is given by the so-called resonance integral,

$$\langle \Phi^{ion} | \widehat{H} | \Phi^{cov} \rangle = \frac{2}{1 + S_{AB}^2} \Big[K + JS_{AB} + S_{AB}(-1 + \frac{1}{R}) + Q \Big] \tag{3.49}$$

where another term Q has been introduced,

$$Q = \langle 1s_A 1s_B | \frac{1}{r_{12}} | 1s_A 1s_A \rangle$$

Furthermore, the weights of the linear combination must satisfy

$$2w_{ion}^{\star} w_{cov} S_{ion-cov} + w_{ion}^2 + w_{cov}^2 = 1 \tag{3.50}$$

Thus, the overlap integrals are shown to be absolutely ubiquitous. In any case, we do not require the analytic expression of all integrals, to review the concepts that arise from VBT, and so we will consider structures to be fully non-orthogonal.

Valence Bond Structures

There are several ways to build structures in VBT. One of the most chemically intuitive ones is the so-called perfect pairing approach, which stems from a fundamental assumption: spin-coupling, leading to covalent bonds, is the most important factor in chemical structure.

Assuming this, covalent structures can be expressed as products of two-center bond wavefunctions, under the assumption that the two-center bond is the proper minimal element. Thus, the covalent structure for a linear H_4 molecule with atoms H_A to H_D and corresponding orbitals $1s_A$ to $1s_D$ would be

$$\begin{aligned}\Phi^{cov} = \Big(|1s_A\alpha, 1s_B\beta\rangle - |1s_A\beta, 1s_B\alpha\rangle\Big)\Big(|1s_C\alpha, 1s_D\beta\rangle - |1s_C\beta, 1s_D\alpha\rangle\Big) = \\ = |1s_A\alpha, 1s_B\beta, 1s_C\alpha, 1s_D\beta\rangle + |1s_A\beta, 1s_B\alpha, 1s_C\beta, 1s_D\alpha\rangle \\ -|1s_A\alpha, 1s_B\beta, 1s_C\beta, 1s_D\alpha\rangle - |1s_A\beta, 1s_B\alpha, 1s_C\alpha, 1s_D\beta\rangle\end{aligned} \tag{3.51}$$

which leads to four Slater determinants to which a normalization constant $1/\sqrt{4}$ would be added. In general, for n-centers with n-electrons, the perfect pairing approach generates 2^n determinants.

A general procedure to construct a linearly independent set of atomic Slater determinants was proposed by Yuri Rumer for singlet states. The spin part of the wavefunction becomes

$$\Theta_i = \prod_{i,j} \frac{1}{\sqrt{2}}\Big[\alpha(i]\beta(j] - \beta(i)\alpha(j)\Big] \prod_k \alpha(k) \tag{3.52}$$

where i, j run over all presumed "bonds" and k runs over all unpaired electrons. The procedure involves spreading AOs in a circle, then finding all possible combinations of lines connecting interacting centers that do not intersect one another. The number of Rumer structures N_{Rumer} for a closed shell system of an $N = 2A$ electron system is expected to be

$$N_{Rumer} = \frac{2A!}{A!(A+1)!} \tag{3.53}$$

This comes to show, without further detail, that the number of Slater determinants becomes very large as the number of electrons increases. This further aggravates the factorial scaling of overlap integrals. Therefore, as it will be argued later (see Subsection 3.2.3), the expansion is often truncated, in particular for ionic structures. In fact, given that the mightiest advantage of VBT is its interpretative character, usually structures can be selected in chemical terms.

Note that sometimes the key assumption of the perfect pairing method will fail because, as it has been covered with some detail in Subsection 1.3.4, some molecules cannot be written as naive Lewis structures. It is perfectly possible, however, to include three-electron two-center bonds as structures in VBT, as well as other exotic combinations. However, it should be noted that this is quite cumbersome.

Weights

In general, due to normalization, we know that

$$\sum_{ij} w_i^\star w_j S_{ij} = 1 \tag{3.54}$$

where w_i are weights of structures and S_{ij} is the overlap integral between such structures (e.g. the $S_{ion-cov}$ that has been used in Equation 3.50).

However, it is desirable to express weights intuitively so that they mirror the interpretation of coefficients in the linear combination of MO-based Slater

determinants, in which the normalization constraint is simply $\sum_i |c_i|^2 = 1$. Several proposals coexist in this regard.

The simplest approach is simply renormalizing the square of the absolute value of the weights to obtain renormalized weights w^{rn},

$$w_i^{rn} = \frac{|w_i|^2}{\sum_i |w_i|^2} \tag{3.55}$$

which is sometimes not very representative because it treats positive and negative coefficients on the same footing.

A more reputed standard approach is to use the weights w_i^{cc} defined by Chirgwin and Coulson,

$$w_i^{cc} = w_i^\star \sum_j w_j S_{ij} \tag{3.56}$$

Although these are not guaranteed to be real nor positive, they are still quite present in the literature.

Other approaches use the so-called inverse weights w_i^{inv} defined as

$$w_i^{inv} \propto \frac{w_i^2}{S_{ii}^{-1}} \tag{3.57}$$

and then renormalized so that $\sum_i w_i^{inv} = 1$.

Several other approaches exist, many of which use orthogonalization procedures. The three examples provided suffice for discussing VBT.

3.2.3 Resonance theory in Valence Bond

The expectation value of the Hamiltonian on the Φ^{VBT} wavefunction in Equation 3.45 can be obtained as a linear combination of the expressions given in Subsection 3.2.2 for the covalent and ionic structures (Equations 3.47 and 3.48 respectively).

The difference between both energies is simply

$$\langle \Phi^{cov} | \widehat{H} | \Phi^{cov} \rangle - \langle \Phi^{ion} | \widehat{H} | \Phi^{ion} \rangle = \frac{J' - 5/8}{1 + S_{AB}^2} \tag{3.58}$$

as we know that S_{AB} is bound between 0 and 1 in this simple case, the leading factor will be J', which represents the Coulomb repulsion between two charge distributions. At long R, such term tends to a point charge $1/R$ term, at short R it explodes to infinity. Hence, the covalent structure bonds more than the ionic structure on its own as J' decreases, while the ionic structure is expected to be more stable at short R: the minimum is at a lower distance but the energy is slightly higher. This is shown in Figure 3.3.

Note that, on the other hand, both structures have exactly the same electron density, and only differ in their two-electron densities.

While the covalent curve is quite accurate, improved results are achieved when the ionic structure is included. As the covalent structure is variationally bound by the exact result, we can safely say that the mixing of the ionic structure contributes to the stability of the molecule.

This provides an underlying mathematical foundation to the concept of resonance which can be generalized to larger systems with increasingly numerous structures. Adding

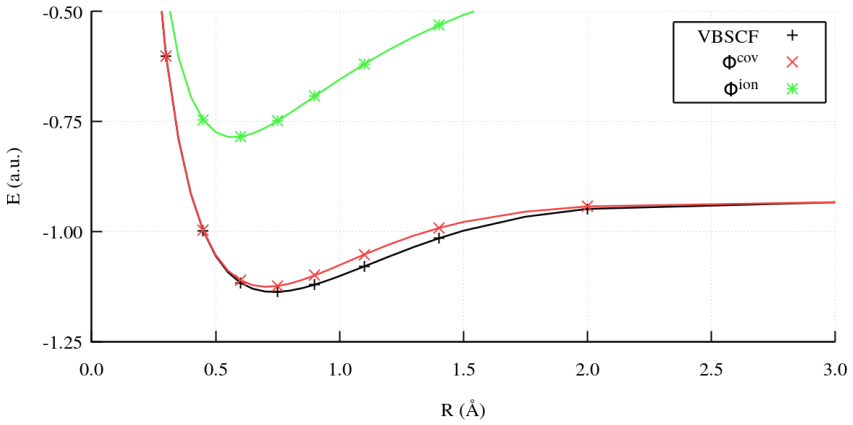

Figure 3.3: Dissociation curves for the H_2 molecule for the different valence bond CSFs with a STO-3G basis set.

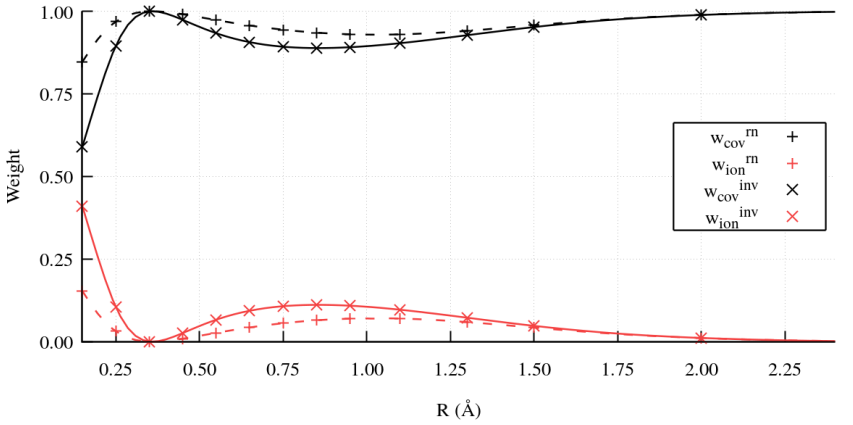

Figure 3.4: VBSCF weights of the ionic and covalent structures along the dissociation curve of the H_2 molecule calculated with a STO-3G basis set.

structures to the wavefunction must lower the energy; if the lowering is not noticeable the weight of such a structure must be negligible – in that particular point of the PES.

The evolution of the weights of the two structures (see Subsection 3.2.2 for details) as the H_2 molecule dissociates further underlines this point. The weight of the ionic structure is only slightly relevant near the equilibrium geometry and when $R \to 0$. When $R \to \infty$, it quickly becomes 0 and thus $\Phi^{VBT} = \Phi^{cov}$.

Concepts such as the Resonance Energy (RE) are easily defined in VBT. In chemical terms, the resonance energy is usually defined as the difference in energy between the main Lewis structure of the system (e.g. Kekulé's benzene) and the fully delocalized system, the so-called resonance hybrid. In terms of our model, RE is simply written as

$$RE = \langle \Phi^{Lewis} | \widehat{H} | \Phi^{Lewis} \rangle - \langle \Phi^{VBT} | \widehat{H} | \Phi^{VBT} \rangle \tag{3.59}$$

which, as per the variational theorem, must be positive. RE in H_2 is be the difference between the red and black lines in Figure 3.3, which, as expected, is quite small.

Thus, VBT captures the concepts of the theories of resonance and mesomerism which are perfectly useful nowadays and which were covered in Subsection 3.2.3.

Analogously, one might use the rules of resonance theory to select structures for a self-consistent valence bond calculation. This feedback loop between the qualitative theory and the computational approach is convenient.

Note that selecting which excited Slater determinants in terms of MOs to include in a multiconfigurational calculation (cf. Section 2.3) is far more difficult to rationalize intuitively.

This is due to the heavily engrained atomistic, Lewis-based character of VBT.

Atomic orbitals and hybridization in Valence Bond Theory

As it has been shown, VBT is far more atomistic and local than MOT, largely because it rejects the notion of delocalized MOs and preserves the atomic character of the AO basis as much as possible.

However, there are two major reasons that lead to the modification of the AO basis.

The first, major reason belongs to the practical realm: on the one hand onorthogonality simplifies calculations, and on the other, delocalized basis sets improve the energy.

The first point has been tackled in Subsection 3.2.2 where the $N!$ number of overlap integral evaluations has been put forward.

The second point is quite easy to understand from a finite basis set perspective. Orthogonalization generally generates "tails" of AOs within the spatial domain of other AOs. As such, the basis set usually spawns more space, which confers more freedom to the wavefunction. Atomic basis sets are usually not optimized for VBT calculations. If basis functions are allowed to AOs from different centers (i.e. to be semilocal), significant additional stabilization is achieved. However, this compromises the validity of ionic structures in particular because charges are allowed to delocalize using these unlike-centered basis functions or tails.

The second major reason is hybridization, which was introduced in the MOT framework (see Subsection 3.1.1) as a rationalization tool. That is, building new AOs from linear combinations of like-centered existing ones to better depict overlaps. In VBT it is possible to use hybrid AOs to describe structures. Note that the basis functions will remain unchanged: only the description of the structures will be different. However, this preserves the interpretative advantages of the theory.

To better exemplify this point, let us revisit the case of minimal basis set CH_4 from Subsection 3.1.1.

We assume that the valence AOs of methane are orthogonal sp^3 hybrids $\chi^1_{sp^3}$ to $\chi^4_{sp^3}$. Let us assume as well that the core AO for C is a $1s_C$ AO that is kept orthogonal with respect to the valence AOs. The effect from core orbitals is introduced into the effective Hamiltonian for the valence block and vice-versa. Alternatively, core orbitals might be kept frozen (i.e. not optimized) during the procedure. This methodological approach will be highlighted in Section 3.3. The AOs for the different hydrogen atoms are $1s_1$ to $1s_2$ in a minimal basis set.

We can write a perfect pairing wavefunction for the valence block of CH_4 as the product of four covalent structures

$$\Phi^{cov}_{val} = \prod_i^4 \Big(|\chi^i_{sp^3}\alpha, 1s_i\beta\rangle - |\chi^i_{sp^3}\beta, 1s_i\alpha\rangle \Big) \tag{3.60}$$

to which ionic structures can be added. However, the description in covalent terms might suffice for CH_4. Now, not only the description of the system has become more compact thanks to the use of sp^3 hybrids. However, if AOs are expressed as linear combinations of basis functions, for instance nuclei-centered GTOs, all sp^3 hybrids will enjoy the increased flexibility of s and p type functions. If the basis set is large enough, a formally ionic structure might lead to an orbital that is localized *away* from its center.

In a VBSCF procedure, where both the weights of structures and the basis coefficients are optimized, this will result in a significantly lower energy. In MOT, hybridization does not formally change the total energy.

The physical interpretation of hybridization is quite important. It is usually assumed that an energetic cost is *paid* by the atom (or fragment), which assumes a hybrid AO electronic structure with the proper multiplicity, which is then recovered with gains by bond formation. Do note that hybridization must not be understood as a *process* since we have removed time evolution from our approach. However, this notion of "preparation energy", which is manifest in VBT, will be mirrored in other frameworks.

3.2.4 Limitations of Valence Bond Theory

As in MOT, the applications and success stories derived from VBT are far too many to cover in this manuscript. Some of its triumphs over MOT have been highlighted, which can be synthetized in two main points: VBT overcomes the monoconfigurational limitations of MOT, and has a much clearer chemical interpretation in terms of Lewis structures.

Expanded octets and other abhorrent species in the folk Lewis picture can be treated with VBT, which accomodates general N-center N-electron bonds through structures. If all possible structures and spin couplings are entered in the VB calculation, and basis set coefficients and structure weights are optimized, the FCI result is obtained because the complete space is covered.

Hence, in the exact limit both theories give the same result, but they approach this limit differently. Compared to multideterminantal approaches, methods derived from VBT, such as VBSCF, have an advantage through the chemical interpretation of CSFs. On the other hand, the increased cost of VB calculations due to non-orthogonality strongly limits the number of basis functions and determinants far more than other multireference approaches.

Very often, the VB treatment has to be reserved for a subset of valence electrons, while the rest are treated using orthogonal MOT including coulomb effects from VB orbitals in the effective Hamiltonian.

Other than this practical limitations, we will examine other issues critically. The ordering is slightly altered with respect to Subsection 3.1.4 for clarity.

Mathematical limitations

VBSCF is formally analogous to CAS methods (see Subsection 2.3.3 for details) in the sense that it is able to take into account qualitatively important strong correlation effects. However, truncated VBSCF is often lackluster at describing weak correlation because it is an effective one-particle theory. This is particularly troublesome given the increase in computational cost.

Arguably, proper systematic inclusion of all CSFs is less systematic and efficient in VBT, because different determinants overlap while FCI calculations using Slater determinants of MOs are strictly efficient.

It is interesting to note that situations in which the single reference HFT method fails dramatically are usually attributed to strong correlation. However, a chemical interpretation has been attributed to situations in which the main Lewis VB structure (generally, the ensemble of covalent structures) is quite lackluster and requires from ionic configurations to properly describe the electronic structure. This has sometimes been called a "charge-shift bond".

Approaches that improve the accuracy of the VBSCF method by including weak correlation effects exist, such as the Breathing Orbital Valence Bond (BOVB) approach,[35] but will not be covered here.

Ontological limitations

As in the case of MOT, orbitals are *non-referring* mathematical objects. However, in this sense interpretation is hampered even further because interpretation is given from a localization perspetive rather than from an energetic standpoint (cf. Koopman's theorem, Subsection 3.1.3).

As noted before, this is a Mulliken-like approach, and as such it is plagued by the same deficiencies as Mulliken's analysis: it requires a properly localized basis set and it depends strongly in the basis set size.

Furthermore, as highlighted in Subsection 3.2.3 when discussing hybridization, the definition of atomic orbitals is highly volatile. Attention has to be drawn to this point. In VBT, structures are often "drawn" instead of explicitely expressed as determinants. This highlights the strong side of the framework. However, the exact composition of AOs in terms of basis functions must always be kept in mind.

3.3 Molecular Orbital Theory and Valence Bond Theory

After critically examining the two main wavefunction based interpretative frameworks, both of which place a great deal of importance in orbitals that build up the antisymmetrized wavefunction, it is necessary to highlight some of the explicit impact that accepting one or another theory have.

We will point at the things that both frameworks have in common, and some of the successful combinations that still exist. It must be noted that current (post-folk) chemical theory juggles between both theories constantly. There is no HOMO-LUMO interaction without MOT, there are no resonant structures without VBT, and there is no organic chemistry that can rationalize reactivity of π systems without both.

3.3.1 Combined approaches

From the practical point of view, MOT has undergone much more development than VBT over the last 50 years. Consequently, VBT draws on MOT approaches more than MOT does on VBT.

The more significant example is the treatment of core electrons in VBSCF calculations (and other derived approaches), which is routinely done to reduce the computational cost. Formally, this is akin to some procedures that are used in MOT, namely active space and frozen orbital approaches.

Uninteresting orbitals are separated from active orbitals blockwise, which produces the following form of the wavefunction

$$\Psi_{tot} = \widehat{\mathcal{A}}(\Phi_{core}\Phi_{val}) \tag{3.61}$$

where $\widehat{\mathcal{A}}$ is the antisymmetrization operator.

The wavefunction is thus blockwise separated between a core and a valence part. Generally, core orbitals are treated at the RHF level and kept doubly occupied. VBT or any other multiconfigurational approach can be used to propose a wavefunction for the valence part. Alternatively, the coefficients of the basis functions in core orbitals might be kept completely frozen.

3.3.2 Numerical comparison

MOT and VBT, from the mathematical point of view, converge to the FCI result as the CSF basis increases. Let us compare performances, energy-wise, for a realistic system; none other than benzene (C_6H_6).

In both cases we will treat all core electrons and σ bonds at the RHF level. Then, on the one hand we will treat the 6 valence electrons in the 6 frontier MOs to build a CAS(6,6) wavefunction, and on the other hand we will generate a multideterminantal VB valence wavefunction using π AOs centered in the carbon atoms.

With a minimal STO-3G basis set, the CAS wavefunction includes 400 Slater determinants and the total energy is -227.947399 a.u., which is slightly lower than the RHF result of -227.890481 a.u. The VBSCF result with the same number of determinants, and delocalized AOs is -227.947399 a.u., the same as the CAS wavefunction because they are identical. However, the interpretation is significantly hampered in VBSCF using semilocal AOs, as pointed out before.

If, instead, we limit π orbitals to contain GTOs with the same nodal plane centered in a single carbon atom, and σ orbitals to contain none of those functions, the resulting electronic energy is -226.923080, which is now much higher than the RHF result – in spite of using 400 determinants. Furthermore, if we only include covalent structures, which reduces the wavefunction down to 20 determinants, the total energy is -225.475762 a.u., which is quite high. The mixing of the ionic structures is thus responsible for a significant energy lowering.

Hence, we can conclude that a judicious use of VBT must be made, lest the resulting wavefunction, which might be highly multideterminantal, is considered to be a guaranteed improvement over humble HFT. The localized nature of AOs, when implemented through basis set construction – or else, i.e. constraints on the SCF procedure – have an associated energetic cost, and a higher energy generally means a less representative wavefunction.

Chapter 4

Quantum chemical topology

Contents

In the previous Chapter we have discussed the interpretation of orbitals thoroughly. The relevance of orbitals is justified in Chapter 2 due to the impossibility of solving Schrödinger's equations. However, we also introduced a different approach to the electronic structure problem in DFT.

While DFT in chemical applications is often reduced to KS-DFT, formally there is no need for orbitals. In fact, orbital-free DFT boasts remarkable success in other fields. The fundamental object in DFT is the electron density, $\rho(\mathbf{r})$, and not the wavefunction. Coherently, any interpretative framework that aspires to be applied to the apparatus of DFT should focus on the study of $\rho(\mathbf{r})$.

In principle, this change of paradigm implies a loss of information. After all, orbitals are defined in a many-dimensional space $\mathbb{H}$ and the electron density is a humble three-dimensional scalar field in $\mathbb{R}^3$. On the other hand, this is advantageous because three-dimensional objects are far more intuitive and easier to navigate both conceptually and mathematically.

When discussing DFT (cf. Section 2.4) we introduced several other scalar fields that are often used in DFAs. As long as they are defined in $\mathbb{R}^3$, similar mathematical tools can be used to treat them. The ensemble of techniques that study and interpret the electron density and other fields defined from the application of quantum mechanics in chemistry has been called Quantum Chemical Topology (QCT).

The purpose of this Chapter is twofold. We will introduce the key mathematical aspects that are general, and then demonstrate the application and the interpretative theory that arises from the topological study of two scalar fields in particular, the electron density and the Electron Localization Function.

4.1 Methods of Quantum chemical topology

We have introduced Quantum Chemical Topology (QCT) [36] quite generally as the study of a given scalar field. In mathematics, topology is the term used to refer to the study of aspects of space that are independent from geometry metrics. In our context, we will assume that the scalar functions of interest are continuous and differentiable at any point, and thus we can use the mathematical tools of topology to study them.

Indeed, in differential topology, differentiable functions of a manifold may be used to study its topology. This approach is often called Morse theory. Owing to this fact, the gradient vector field is an immediate source of information about the shape and key features of the scalar field to be investigated.

4.1.1 Morse theory

In strict mathematical terms, Morse theory relates the critical points of a smooth function and the global topology of the manifold in which the function is defined. In our case, the manifold $\mathbb{M}$ can be thought to be simply a three-dimensional Euclidean space $\mathbb{R}^3$ for the most part. Mathematically, smooth manifolds resemble Euclidean spaces locally so that our analysis can be kept intuitive by thinking in terms of n-dimensional Euclidean spaces.

The smoothness of a function has to do with the number of continuous derivatives the function has over a space. As we stated before, the functions of interest in QCT are at the very minimum differentiable at any point, and thus continous.

For instance, we know that as per Kato's cusp condition (cf. Equation 2.102) there should be discontinuities on top of nuclei, and the density should spread approximately

exponentially from those discontinuities on. If the wavefunction is built using CGTOs as basis functions, unavoidably the density will be differentiable everywhere as well as its gradient.

Usually, having defined first and second derivatives is enough to qualify as a smooth function.

Thus, assuming this degree of smoothness, we may define the gradient of f, $\vec{\nabla} f$, in terms of its first order derivatives $f : \mathbb{M}^n \to \mathbb{R}$,

$$\vec{\nabla} f = \Big[\frac{\partial f}{\partial r_1} \dots \frac{\partial f}{\partial r_n}\Big]^T \tag{4.1}$$

so that the gradient is a column vector per convention, and the total derivative is a row vector with the same components.

The gradient of a scalar function is a vector field. If the function is smooth as per the aforementioned usual requirement, it is also continuous. From any given point, it points towards the direction of steepest ascent. Given a point $p \in \mathbb{R}^n$, $p = r_1, r_2, \dots, r_n$, it is said to be a regular point of f if $\nabla f(p) \neq 0$, and a Critical Point (CP) p_c if the following holds

$$\vec{\nabla} f(p_c) = \frac{\partial f}{\partial r_1}(p_c) = \frac{\partial f}{\partial r_2}(p_c) = \dots = \frac{\partial f}{\partial r_n}(p_c) = 0 \tag{4.2}$$

The value of a function in a CP, $f(p_c)$, is called a *critical value* of f; the image elsewhere are *regular values* of f.

To further distinguish between different types of CPs the second derivatives can be studied at p_c. The matrix of second derivatives a a given point p is the Hessian of f. In $\mathbb{R}^3$:

$$\mathbb{H}(p) = \begin{pmatrix} \frac{\partial^2 f}{\partial x^2} & \frac{\partial^2 f}{\partial x \partial y} & \frac{\partial^2 f}{\partial x \partial z} \\ \frac{\partial^2 f}{\partial y \partial x} & \frac{\partial^2 f}{\partial y^2} & \frac{\partial^2 f}{\partial y \partial z} \\ \frac{\partial^2 f}{\partial z \partial x} & \frac{\partial^2 f}{\partial z \partial y} & \frac{\partial^2 f}{\partial z^2} \end{pmatrix}_p \tag{4.3}$$

CP p_c is *non-degenerate* if the Hessian of that point $\mathbb{H}(p_c)$ is non-singular, i.e. $det\mathbb{H}(p_c) \neq 0$. Then, all its eigenvalues must be non-zero. Otherwise, the CP is *degenerate* and at least one of the eigenvalues of the matrix is 0.

Morse functions

In Morse theory, a smooth function $f : \mathbb{M} :\to \mathbb{R}$ is considered a Morse function if all its CPs are non-degenerate. Therefore, the Hessian matrix at any CP can be diagonalized to render n eigenvalues $\lambda_1, \dots \lambda_n$. In QCT, the eigenvalues of $\mathbb{H}(p_c)$ are ordered from negative to positive so that $\lambda_1 < \lambda_2 \leq \dots \leq \lambda_n$.

Morse functions have some characteristic properties that can be useful for our interests. The Morse lemma guarantees that given a Morse function in $\mathbb{R}^d$, $f : \mathbb{R}^d \to \mathbb{R}$, its behavior in the surroundings of a CP p_c is such that there can not be another CP in the immediate vicinity of the point. Thus, CPs in Morse functions are said to be isolated.

A non-degenerate CP p_c can thereafter be classified by the number of negative eigenvalues of the Hessian $\mathbb{H}(p_c)$, which is called the index q of the said CP. This is akin to the number of directions along which the CP is a maxima. In $\mathbb{R}^3$ there are four possibilities: minima, which have 0; 1-saddles, which have 1; 2-saddles, which have 2;

and maxima, which have 3. This criterion can be rigorously derived from the expansion of a diffeomorphic map in the neighbourhood of the CP, which will not be covered here.

In QCT, however, CPs are usually classified in terms of their rank r, and their signature, s, using the notation (r, s). For non-degenerate CP p_c, the rank is the number of non-zero eigenvalues of $\mathbb{H}(p_c)$ and the signature is the difference between the number of positive and negative eigenvalues,

$$s = \sum_i \frac{\lambda_i}{|\lambda_i|} \tag{4.4}$$

Consequently, in $\mathbb{R}^3$, maxima, 2-saddles, 1-saddles and minima are denoted by $(3, -3)$, $(3, -1)$, $(3, +1)$ and $(3, +3)$ respectively. Note that the existence of CPs with $r \neq 3$ would imply that the function is not a Morse function anymore.

A different notion of index, which we shall designate as I, is often used in the mathematical framework of dynamical systems to characterize CPs. I is the number of positive Lyapunov exponents of an hyperbolic CP. The equivalence of this nomenclature is summarized in Table 4.1, and is reported for completeness due to the historical usage of the term.

Critical Point	I	q	(r, s)
Maximum (attractor)	0	3	(3,-3)
2-saddle	1	2	(3,-1)
1-saddle	2	1	(3, 1)
Minimum (repeller)	3	0	(3, 3)

Table 4.1: Classification of the critical points in $\mathbb{R}^3$ in different nomenclatures. I is the index used in dynamical systems, q is the index in Morse theory and (r, s) notation is used in QCT.

Since non-degenerate CPs are isolated, the topology of any isosurface – or level set – of the Morse function is determined by its CPs. Roughly, this implies that two spaces are homeomorphic if they have the same CPs structure, and diffeomorphic if they do not.

Morse inequalities

The total number of CPs of a Morse function $f : \mathbb{M} \to \mathbb{R}$ is limited by Morse inequalities. The weak Morse inequality states that the number of CPs c_q of some index q are bound by

$$c_q \geq \beta_q(\mathbb{M}) \qquad \forall q \tag{4.5}$$

in which β_q is the qth Betti number of the space. For our interest, it suffices to know that β_0 corresponds to the number of connected components, β_1 corresponds to the number of circular holes, and β_2 to the number of two-dimensional cavities. For instance, in a 2-sphere (Figure 4.1 A) we find $\beta_0 = 1$, $\beta_1 = 0$ and $\beta_2 = 1$. In a 2-torus (Figure 4.1 B), however, $\beta_0 = 1$, $\beta_1 = 2$ and $\beta_2 = 1$, because β_1 takes into account both the hole in the center of the torus and the circular hole inside the surface. Betti numbers of $q \geq 3$ are all 0 in both cases.

If all Betti numbers are finite and 0 beyond a certain q, the alternating sum of all Betti numbers for a topological space gives the Euler-Poincaré characteristic $\chi(\mathbb{M})$:

$$\chi(\mathbb{M}) = \beta_0(\mathbb{M}) - \beta_1(\mathbb{M}) + \beta_2(\mathbb{M}) - \beta_3(\mathbb{M}) \dots \tag{4.6}$$

The number of CPs of different indices is connected to $\chi(\mathbb{M})$ as

$$\sum_q (-1)^q c_q = \chi(\mathbb{M}) \tag{4.7}$$

This condition is analogous to the Poincaré-Hopf theorem in the field of dynamical systems, in which it is defined in terms of the index I (see Table 4.1 for equivalences) of all i isolated CPs p_c^i:

$$\sum_i (-1)^{I(p_c^i)} = \chi(\mathbb{M}) \tag{4.8}$$

Following the previous example, $\chi(\mathbb{R}^3)$ is 2 for a 2-sphere – and all spherical polyhedra– but 0 for a 2-torus.

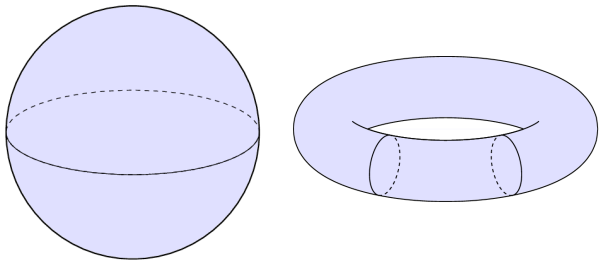

A) B)

Figure 4.1: **A)** 2-sphere **B)** 2-torus

In QCT, the Euler-Poincaré characteristic $\chi(\mathbb{M})$ is formally 1 for isolated systems – because the gradient field is defined in $\mathbb{R}^3$ – and 0 for periodic systems. Hence, for most applications in this manuscript, the following rule must be followed for any Morse scalar function:

$$c_3 - c_2 + c_1 - c_0 = 1 \tag{4.9}$$

where, as previously stated, c_3 is the number of $(3,-3)$ maxima, c_2 is the number of $(3,-1)$ 2-saddles, c_1 is the number of $(3,1)$ 1-saddles and c_0 is the number of $(3,3)$ minima.

4.1.2 Partitioning of space

The gradient flow may be used to decompose a manifold into submanifolds. With this purpose in mind, we introduce the notion of integral line. Given a Morse function $f : \mathbb{M} \to \mathbb{R}$, a curve $\gamma(t)$ is an integral line of f if $\frac{\partial \gamma(t)}{\partial t} = \nabla f(\gamma(t))$ for all $t \in \mathbb{R}$. That is, integral lines are tangent to the gradient field at every point.

Integral lines have several interesting properties. First of all, as per the definition, f increases along the curve. Furthermore, as the integral line is defined for all $t \in \mathbb{R}$, $\gamma(t)$

must have an origin $orig(\gamma(t))$ and a destination $dest(\gamma(t))$, and both must be $\pm\infty$ or an open-ended CP of the Morse function.

It can be shown that two integral lines are either disjoint or the same. Integral lines spawn all $\mathbb{M}$, and subsequently every regular point of $\mathbb{M}$ is traversed by exactly one integral line.

Given these properties, it seems coherent to partition space into unions of integral lines according to some criteria, for example their origin and destination. Therefore we define

- The stable manifold of a CP p_c of f, $S(p_c)$, is the point itself together with all regular points whose integral lines end at p_c.
- The unstable manifold of p_c, $U(p_c)$, is the point itself together with all regular points whose integral lines originate at p_c.

as

$$\begin{aligned} S(p_c) &= p_c \cup x \in \mathbb{M} | \text{dest}(\gamma(x)) = p_c \\ U(p_c) &= p_c \cup x \in \mathbb{M} | \text{orig}(\gamma(x)) = p_c \end{aligned}$$

The Morse function f increases as γt goes from $orig(\gamma(t))$ to $dest(\gamma(t))$ and therefore

$$\begin{aligned} f(p_c) &\geq f(x) \quad \forall x \in S(p_c) \\ f(p_c) &\leq f(x) \quad \forall x \in U(p_c) \end{aligned}$$

Hence, $S(p_c)$ and $U(p_c)$ might be referred to as the *descending* and *ascending* manifolds of the CP p_c.

Intuitively, they can be pictured as "hills" and "valleys". They can also be understood as the dual of each other. For example, in $\mathbb{R}^3$, the stable or descending manifold $S(p_c)$ of a local minimum is just the CP itself, p_c; while the unstable manifold will be a volume with p_c inside and bound by a set of maxima, saddle points and the integral lines connecting them. The exact opposite is found for a local maxima. In more general terms, there will always be a q-sphere of directions along which integral lines approach a CP of index q.

The Morse complex is formed by all descending manifolds of a Morse function $f : \mathbb{M} \to \mathbb{R}$. Each descending manifold will naturally contain a CP that is a local maxima, and be bound by a set of minima, saddle points and integral lines that connect them.

Restraining ourselves to $\mathbb{R}^3$, in dynamical systems parlance the descending manifold of a maximum p_M is called the *basin*, Ω_{p_M}, of the CP. The stable manifolds of 2-saddles are surfaces, those of 1-saddles are integral lines, and those of minima are the CP itself. Because the combination of these surfaces, saddle points and integral lines partition space between basins, they are often called *separatrices*.

Generally speaking, the partitioning of the system given by the Morse complex reigns supreme in QCT, as it will be shown in the next Section.

Morse-Smale complex

It is possible to define a complex akin to the Morse complex for the ascending manifolds of a Morse function. However, it is more interesting to define the more general Morse-Smale complex. For it, we require that the Morse function satisfies some further conditions, which can be crudely said to be:

- No pair of CPs of the function with the same index are connected by an integral line.
- The index q of the CP at $orig(\gamma(t))$ must be less than the index at $dest(\gamma(t))$.

More formally, the requirement is that stable and unstable manifolds intersect transversally. A function in which this holds is called a Morse-Smale function.

Then, we can define the Morse-Smale complex of such function $f : \mathbb{M} \to \mathbb{R}$ as the intersection of the Morse complex of f and the Morse complex of $-f$. We could analogously say that it is the intersection of all ascending and descending manifolds.

The Morse-Smale complex tesselates the topological space so that all points inside a cell belong to integral lines with the same $orig(\gamma(t))$ and $dest(\gamma(t))$.

4.2 Topology of the electron density

The electron density was introduced in Chapter 2, Subsection 2.4.1. As we have pointed out in the previous Section, we can assume that the electron density resulting from a calculation is a Morse function. Hence, all the mathematical concepts introduced may be applied for the topological analysis of the electron density, $\rho(\mathbf{r})$.

It must be kept in mind at all times that the electron density is well defined in exact many-body theory because the one-particle reduced density matrix is defined at any theory level, unlike orbitals. It does not suffer from particular basis set dependencies or requires any a priori information. It is also, within the DFT framework, enough to calculate the exact energy of the system due to its relation with the external potential. The electron density can also be obtained from both an approximate wavefunction and experiments, through the structure factors from X-ray diffraction experiments. All things considered, it is a pretty handy observable compared to the very abstract wavefunction.

In many ways, the resulting analysis and the interpretation thereafter owes to the work of R. F. W. Bader and others.[37, 38] Due to this, the name "Quantum Theory of Atoms In Molecules", or more simply "Atoms In Molecules" (AIM) is often used to refer to any technique that uses the topological analysis of the electron density. These names point at an important virtue, which is no other than the retrieval of a definition for atoms in a molecular environment, which, as detailed in Chapter 1 is not a trivial matter.

4.2.1 Critical points of the electron density

Our goal is the study of a Morse function, $\rho : \mathbb{R}^3 \to \mathbb{R}$, for which we will use Morse theory.

The gradient of $\rho(\mathbf{r})$, the vector field $\vec{\nabla}\rho(\mathbf{r})$, can be written as a column vector

$$\vec{\nabla}\rho(\mathbf{r}) = \begin{pmatrix} \frac{\partial\rho(\mathbf{r})}{\partial x} \\ \frac{\partial\rho(\mathbf{r})}{\partial y} \\ \frac{\partial\rho(\mathbf{r})}{\partial z} \end{pmatrix} (\vec{i}, \vec{j}, \vec{k}) \tag{4.10}$$

in which we have expanded the spatial coordinates $\mathbf{r} = \{x, y, z\}$ in Euclidean space $\mathbb{R}^3$. As introduced before, there are four distinct types of CPs of $\rho(\mathbf{r})$ given by $\vec{\nabla}\rho(\mathbf{r}) = 0$.

AIM theory attempts to assign a chemical interpretation to each type of CP of $\rho(\mathbf{r})$. In the Born-Oppenheimer framework N-fermionic systems are just point-like nuclear

charges and quantum electrons moving in the resulting external potential. Thus, it seems logical for the probability density to be maximal near nuclei. This is empirically found to be true: $\rho(\mathbf{r})$ has maxima on top of nuclear positions. Recall that, in fact, the electron density should be discontinuous on top of nuclear positions, as given by Kato's cusp theorem (Equation 2.102). It can be safely assumed that a maximum will be found near nuclear positions instead.

Thus, $(3, -3)$ CPs of $\rho(\mathbf{r})$ are often called Nuclear Critical Points (NCPs) or nuclear attractors. Generally, every nucleus has a corresponding NCP on the exact same position. This implies that every nuclei has its own stable manifold, or basin.

As an example, the electron density of the H_2 molecule is shown in Figure 4.2 (and in the surface in Figure 4.4 A), and the corresponding gradient is shown in Figure 4.3. Note that in this case only one coordinate, z, has been taken into account due to the axial symmetry of the molecule – and the internuclear axis has been aligned with the z-axis. The position of each hydrogen nucleus matches exactly the position of the maximum in ρ and hence has an associated CP, i.e. $\vec{\nabla}\rho = 0$. Going back to $\mathbb{R}^3$, any step towards the x or y axis will make the value of $\rho(\mathbf{r})$ decrease. Note as well that the stable manifold of each maximum can be projected on the internuclear axis as the intervals $(-\infty, 0)$ and $(0, +\infty)$.

Between the two maxima, another CP is found at $z = 0$ (cf. Figure 4.3), which is a local minimum in the z axis, but a $(3, -1)$ saddle point in $\mathbb{R}^3$. That is, it is a minimum only in one coordinate, but a maximum with respect to the x or y-axes. As it can be infered from classical arguments, but also from previously covered theoretical frameworks (cf. Subsection 3.1.1, for instance, with the notions of constructive and destructive linear combination of atomic orbitals), bonding is associated with the region between nuclei. Hence, $(3, -1)$ CPs are often called Bond Critical Points (BCPs) in AIM theory. The stable manifold of such CPs is a surface that we often call the *separatrix*. In the example of Figure 4.2, the separatrix is composed by all points with $z = 0$.

In the same spirit, $(3, +1)$ CPs are called Ring Critical Points (RCPs), because they appear, for instance, in the middle of a perfect square of H atoms. Their stable manifold is a single integral line. They are local minima in two perpendicular directions, but local maxima in the remaining one – the direction perpendicular to the "ring". Analogously, $(3, +3)$ CPs are local minima in all directions. They are usually referred to as Cage Critical Points (CCPs).

Summarizing, the AIM interpretation of CPs of $\rho(\mathbf{r})$ is:

- $(3, -3)$ CPs are Nuclear Critical Points (NCPs) that match nuclear positions.
- $(3, -1)$ CPs are Bond Critical Points (BCPs) that signal bonds between atoms.
- $(3, 1)$ CPs are Ring Critical Points (RCPs) that arise in molecular rings.
- $(3, 3)$ CPs are Cage Critical Points (CCPs) that arise in molecular cavities.

Molecular graph

Several examples of CPs in the AIM context are given in Figure 4.5. Note how the pattern of NCPs and BCPs matches the expected Lewis connectivity of the molecule quite well. In simple cases, as in H_2 (cf. Figure 4.2), the integral lines that join NCPs and BCPs match the expected position of the chemical bond. Hence, the integral lines joining two NCPs through a BCP are often called *bond paths*.[39] In fact, the CPs and bond paths are usually depicted together in what is usually called the *molecular graph*.

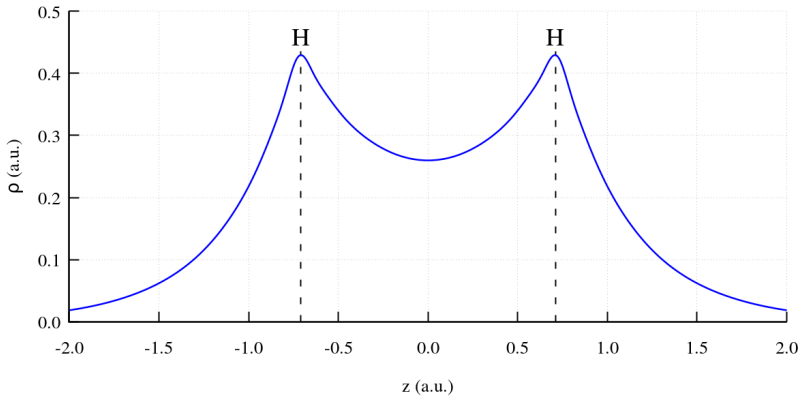

Figure 4.2: $\rho(z)$ along the internuclear axis of H_2. Calculated at the FCI/aug-cc-pwCVQZ level. Dashed lines indicate the position of each nucleus.

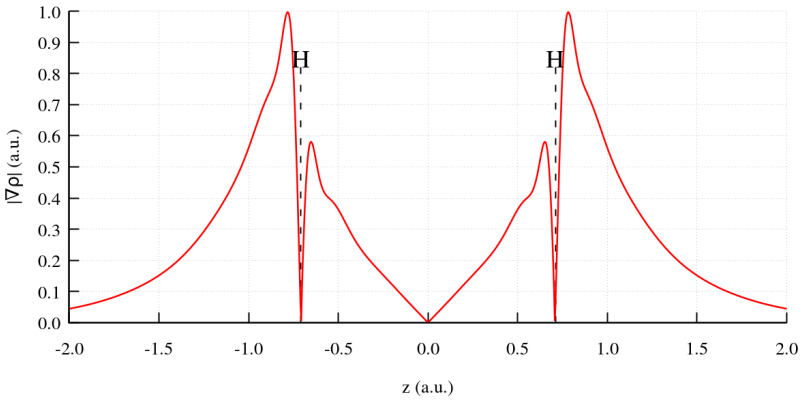

Figure 4.3: $|\vec{\nabla}\rho(z)|$ along the internuclear axis of H_2. Calculated at the FCI/aug-cc-pwCVQZ level. Dashed lines indicate the position of each nucleus.

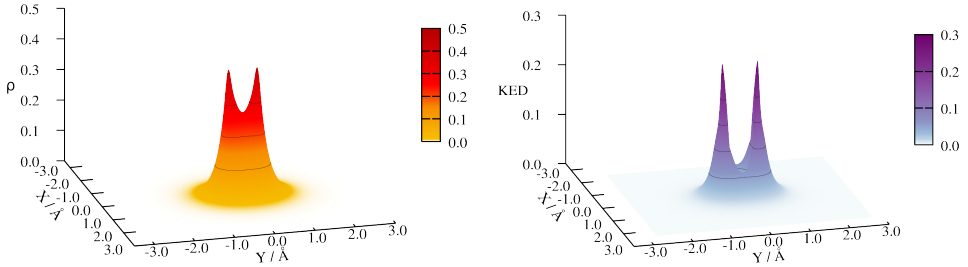

Figure 4.4: Functions calculated over the σ_v plane of the H_2 molecule at the FCI/aug-cc-pwCVQZ level: **A)** $\rho(\mathbf{r})$ **B)** $\tau(\mathbf{r})$ (Equation 2.133).

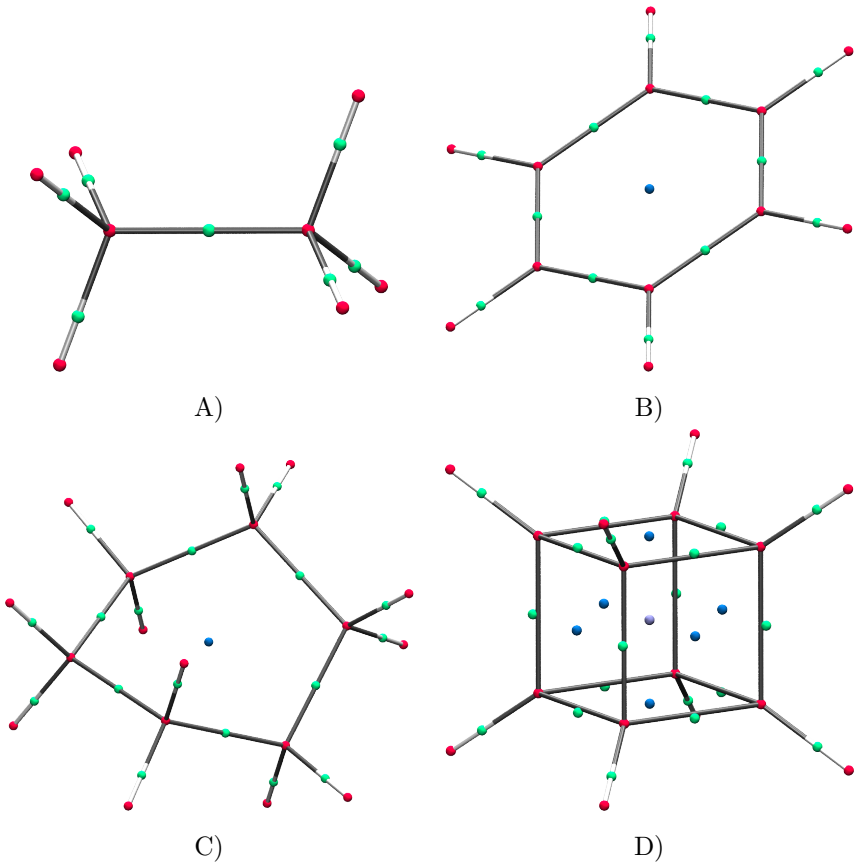

Figure 4.5: CPs of $\rho(\mathbf{r})$ for different molecules calculated at the HF/6-31$G^\star$ level: **A)** Ethane **B)** Benzene **C)** Cyclohexane **D)** Cubane. CPs are shown as spheres. NCPs, BCPs, RCPs and CCPs are colored red, green, blue and violet respectively.

In the most straightforward cases, the bond paths that connect NCPs and BCPs are almost strictly straight and match the folk notion of chemical bonds as in the least-distance connection between two adjoint nuclei. Notable exceptions are strained hydrocarbons, such as the ones shown in Figure 4.6, in which the integral line is longer than the geometrical distance between nuclei. The difference between the two distances may be used as an indicator of strain for such contexts.

Therefore, the chemical "structure" may be derived strictly ab initio from the study of the CPs of $\rho(\mathbf{r})$, condensed in the molecular graph. Similar information is enclosed in level sets of $\rho(\mathbf{r})$ (Figure 4.7) in a less compact way.

Being able to define and analyze chemical structure from the electron density is a forte of AIM theory.

Chemical bonds

The chemical bond is signaled by the presence of a BCP and its corresponding bond path, and hence might be characterized by the properties of $\rho(\mathbf{r})$ in those points. First and foremost, the critical value of the electron density at the BCP, ρ_{BCP}, is used as an

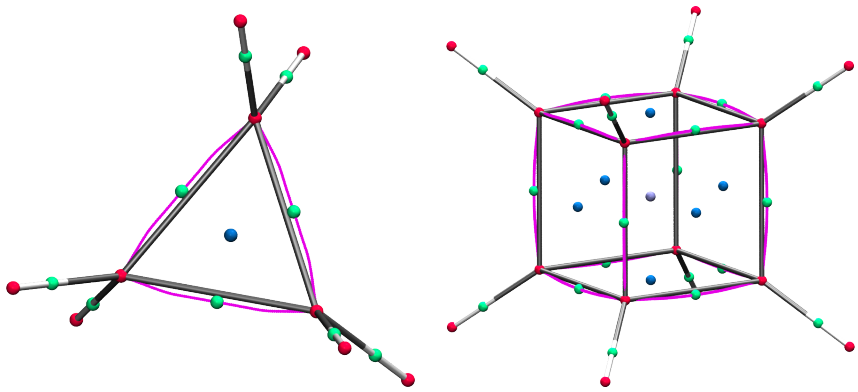

A) B)

Figure 4.6: CPs and integral paths of $\rho(\mathbf{r})$ for different molecules calculated at the HF/6-31$G^\star$ level: **A)** Cyclopropane **B)** Cubane. Integral paths connecting NCPs and BCPs have been drawn in magenta. CPs are colored with the color scheme of Figure 4.5.

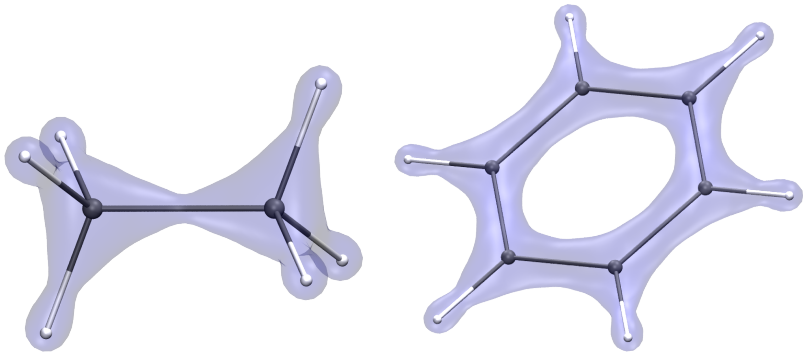

A) B)

Figure 4.7: Isosurfaces of $\rho(\mathbf{r}) = 0.25$ a.u. for different molecules calculated at the HF/6-31$G^\star$ level: **A)** Ethane **B)** Benzene. Isosurfaces colored blue.

indicator of bond strength.

A typical example is the increase in density with formal bond order in the ethane, ethene and ethyne series. For instance, the C−C BCP of ethane has $\rho_{BCP} \approx 0.26$ a.u., whereas the formal double bond of thene has $\rho_{BCP} \approx 0.36$ a.u. and ethyne has $\rho_{BCP} \approx 0.41$ a.u., with small variations due to the theory level and basis set combination. This gives a proportion of $1-1.4-1.6$ for single, double and triple bonds, with have equilibrium bond lengths of of 1.54 Å 1.33 Å and 1.20 Å respectively. Taking the inverse square of the bond lengths $(1/R^2)$ we find an extremely similar proportion of $1-1.3-1.6$. This comes to say that equilibrium bond lengths and ρ_{BCP} bear approximately the same information. CPs for the three molecules are shown in Figure 4.8.

To asses π-character, which in MOT and VBT is associated with out-of-plane overlap of π AOs, the bond ellipticity is defined as an adimensional ratio;

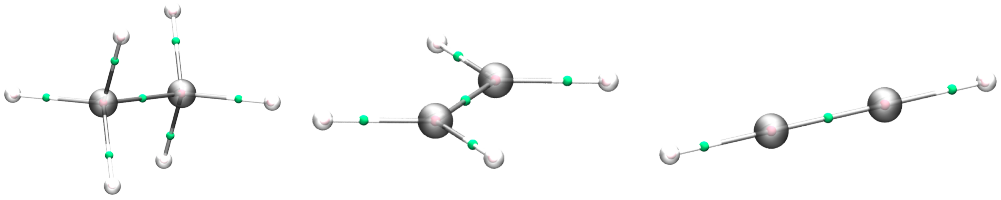

A) B) C)

Figure 4.8: CPs of $\rho(\mathbf{r})$ for different molecules calculated at the HF/cc-PVTZlevel: **A)** Ethane **B)** Ethylene **C)** Ethyne. CPs are shown as spheres. NCPs, BCPs, RCPs and CCPs are colored red, green, blue and violet respectively.

$$\epsilon_{BCP} = \frac{\lambda_1}{\lambda_2}\Big|_{BCP} - 1 \tag{4.11}$$

where λ_1 and λ_2 are the two first eigenvalues of the Hessian of the electron density at the BCP, which are chosen to be perpendicular to the bond path, i.e. the direction of space towards which the double partial derivative is positive. As per the ordering convention, in a BCP both $\lambda_1 < 0$ and $\lambda_2 < 0$ and $|\lambda_1| < |\lambda_2|$ so that the ellipticity ϵ_{BCP} is bound between 0 – for a cylindrically symmetric bond where $\lambda_1 = \lambda_2$ – and infinity for very asymmetric bonds with π-character.

As a paradigmatic example, $\epsilon_{BCP} \approx 0.25$ in the C–C bonds of benzene, indicating moderate π-character, and $\epsilon_{BCP} \approx 0.45$ for ethene. This matches chemical insight because the bond order of ethene is superior, while the bond in benzene only has 1/2 π-bonds. However, naturally $\epsilon_{BCP} = 1.0$ in acetylene, which should then be understood as no π-character at all, while MOT suggests that π AOs are involved in the bond.

In general, these approaches can be applied in many contexts but have important limitations. On the one hand, the density (and its derivatives) at those points is highly dependant on the geometry, which may or may not be governed by the specific interaction. On the other hand, different atoms have different valence densities, i.e. very "soft" atoms will naturally induce richer densities in adjacent BCPs than other "hard" electronegative ones. In short, this means that ρ_{BCP} and other properties evaluated at BCPs are not usually transferable between different chemical environments.

4.2.2 Atom in a molecule

The Morse complex given by the gradient vector field $\vec{\nabla}\rho(\mathbf{r})$ satisfies the zero-flux condition at the separatrices of the stable manifold of $(3,-3)$ CPs:

$$\vec{\nabla}\rho(\mathbf{r}) \cdot \vec{n}(\mathbf{r}) = 0 \qquad \forall \mathbf{r} \in S \tag{4.12}$$

where $\vec{n}(\mathbf{r})$ is a normal vector to the surface at point $\mathbf{r}$ and $\vec{\nabla}\rho(\mathbf{r})$ is the gradient of $\rho(\mathbf{r})$ at $\mathbf{r}$. S is the separatrix surface, which is given by the stable manifold of the CPs that surround the NCP. As introduced in the previous Section, the stable manifold of $(3,-3)$ NCPs is often called a *basin*.

Recalling that $(3,-3)$ CPs of $\rho(\mathbf{r})$ are NCPs associated with nuclei, the basin of the NCP on top of nuclei A is the basin Ω_A that identifies the *topological atom* A. As per the Morse complex partitioning, all space – $\mathbb{R}^3$ – is partitioned into basins Ω_I, belonging to

the atoms of the system, and stable manifolds of BCPs and RCPs which are just surfaces or integral lines.

An important property of atomic basins is that the integral of the Laplacian of the density is guaranteed to be 0 by the divergence theorem and Equation 4.12:

$$\int_{\Omega_I} \nabla^2 \rho(\mathbf{r}) d\mathbf{r} = \oint_S \vec{\nabla} \rho(\mathbf{r}) \cdot \vec{n}(\mathbf{r}) d\mathbf{s} = 0 \tag{4.13}$$

The concept of atom is thus retrieved in the AIM context: atoms *are* the basins Ω_I that arise in the electron density from the NCP of every nuclei. A simple example is shown in Figure 4.9 for the ethene molecule, which was previously shown in Figure 4.8. Note that in this particular case all basins spawn infinite volumes because the separatrices die at $\pm\infty$. However, there is a distinct, non-overlapping region of space that can be considered to belong to every atom.

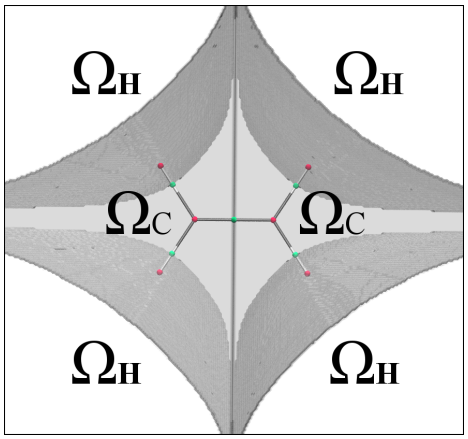

Figure 4.9: CPs of $\rho(\mathbf{r})$ and separatrices delimitating the stable manifold in the ethene molecule. Calculated at the HF/cc-PVTZ level.

The partitioning resembles the geometrically inspired patterns that arise when visualizing isosurfaces of $\rho(\mathbf{r})$, as in Figure 4.7, where carbon atoms were bound by a surface resembling a tetrahedron.

Recall that the partitioning given by the Morse complex is exhaustive: all points of space belong to a stable manifold. It follows that the stable manifolds of BCPs and RCPs, i.e. all separatrices, integral lines and surfaces, are infinitesimally thin. Usually a finite discrete grid is used to treat the function numerically, and as a result all regular points of space are attributed to atomic basins. Thus, in practice space is exhaustively partitioned in terms of topological atoms.

Atomic properties

Once that atoms have been defined and delimited as the stable manifolds of NCPs, we can assign properties to atoms. More specifically, a (topological) atomic property may be defined as

$$\langle \widehat{\mathcal{A}} \rangle_{\Omega_A} = \int_{\Omega_A} \rho_{\mathcal{A}}(\mathbf{r}) d\mathbf{r} \tag{4.14}$$

where $\rho_{\mathcal{A}}$ is the density of the property associated with a one-particle operator $\widehat{\mathcal{A}}$. The perhaps most enticing atomic property, the atomic charge, can be trivially recovered by integrating the electron density. For an atom A with an associated basin Ω_A, we define its electronic population $\overline{N}_A$ as

$$\overline{N}_A = \int_{\Omega_A} \rho_{\mathcal{A}}(\mathbf{r}) d\mathbf{r} \tag{4.15}$$

which substracted to the atomic number Z_A leads to the atomic charge Q_A,

$$Q_A = Z_A - \overline{N}_A \tag{4.16}$$

Due to the exhaustivity of the partitioning, the sum of all M atomic populations is the total number of electrons in the system, N,

$$\sum_A^M \overline{N}_A = N \tag{4.17}$$

Analogously, atomic spin densities may be used to define atomic spins. Many other atomic properties can be defined, with notable examples such as atomic volumes or dipoles.

Pair properties

Equation 4.14 may be generalized using two-particle pair functions as an integrand. As an example, integrating the pair density

$$\overline{\Pi}_{A,B} = \int_{\Omega_A} \int_{\Omega_B} \rho_2(\mathbf{r}, \mathbf{r}') d\mathbf{r} d\mathbf{r}' \tag{4.18}$$

gives the average number of electron pairs in the region $\Omega_A \cup \Omega_B$. This holds because in this particular case $\Omega_A \cap \Omega_B = 0$, i.e. the AIM partition is exhaustive and non-overlapping.

If we integrate the exchange-correlation density $\rho_{xc}(\mathbf{r}, \mathbf{r}')$, as defined in Section 2.5, we can define what is often called the delocalization index $\delta_{A,B}$, as

$$\delta_{A,B} = 2 \int_{\Omega_A} \int_{\Omega_B} \rho_{xc}(\mathbf{r}, \mathbf{r}') d\mathbf{r} d\mathbf{r}' \tag{4.19}$$

and the analogous localization index, Λ_A,

$$\Lambda_A = \int_{\Omega_A} \int_{\Omega_A} \rho_{xc}(\mathbf{r}, \mathbf{r}') d\mathbf{r} d\mathbf{r}' \tag{4.20}$$

which gives a neat decomposition of the total electron number N;

$$N = \frac{1}{2} \sum_{B, A \neq B} \delta_{A,B} + \sum_A \Lambda_A \tag{4.21}$$

$\delta_{A,B}$ is a pairwise property: it relates pairs of topological atoms by integrating $\rho_{xc}(\mathbf{r}, \mathbf{r}')$, which is a measurement of how correlated electrons are. Hence, it is akin to a bond order. Alternatively, we may define the total delocalization of a given atom, δ_A, as

$$\delta_A = \frac{1}{2} \sum_{B, A \neq B} \delta_{A,B} \tag{4.22}$$

which is akin to a formal valence of the atom, i.e. the number of "shared" electrons a topological atom has. In single-determinant wavefunctions, localization and delocalization indices are bound as

$$\begin{aligned} 0 \leq \quad \delta_{A,B} \quad &\leq min(\overline{N}_A, \overline{N}_B) \\ 0 \leq \quad \Lambda_A \quad &\leq \overline{N}_A \end{aligned}$$

and are therefore guaranteed to have a feasible chemical interpretation. These definitions will also be used to a certain extent in the next Subsection.

4.2.3 Interacting Quantum Atoms

As it has been shown, we can use the AIM partitioning of space to decompose one and two-particle properties. Naturally, partitioning the electronic energy is of interest. A quantitative theory based in the AIM scheme, called the Interacting Quantum Atoms (IQA) approach attempts to do this in an exact way. We will introduce the theoretical framework here, coupled to the AIM partitioning, but note that the method is valid for any exhaustive non-overlapping partition of space.[40]

For simplicity, we define a step function $\Theta_A(\mathbf{r})$ associated with basin Ω_A for every basin in the system,

$$\Theta_A(\mathbf{r}) = \begin{cases} 1 & \forall\ \mathbf{r} \in \Omega_A \\ 0 & elsewhere \end{cases} \tag{4.23}$$

which in the AIM context equates a basin for every topological atom A. Then, the one and two-particle reduced density matrices (introduced in Chapter 2, Section 2.4, here with spin-coordinates integrated out) can be partitioned as

$$\Gamma^1(\mathbf{r}_1;\mathbf{r}'_1) = \sum_A \Gamma^1(\mathbf{r}_1;\mathbf{r}'_1)\Theta_A(\mathbf{r}'_1) = \sum_A \gamma^1_A \tag{4.24}$$

and

$$\rho_2(\mathbf{r}_1,\mathbf{r}_2) = \rho_2(\mathbf{r}_1,\mathbf{r}_2)\frac{1}{2}\Big[\Theta_A(\mathbf{r}_1)\Theta_B(\mathbf{r}_2) + \Theta_B(\mathbf{r}_1)\Theta_A(\mathbf{r}_2)\Big] = \sum_{A,B}\gamma^2_{A,B} \tag{4.25}$$

in which we have taken only the diagonal part of the two-particle reduced density matrix. The electronic energy can be computed as

$$E_{el} = \int \widehat{h}\gamma^1(\mathbf{r}_1;\mathbf{r}'_1)d\mathbf{r}_1 + \frac{1}{2}\int\int \rho_2(\mathbf{r}_1,\mathbf{r}_2)\frac{1}{r_{12}}d\mathbf{r}_1 d\mathbf{r}_2 \tag{4.26}$$

in which we have assumed the non-diagonal part of the one-particle reduced density matrix for the application of the one-body operator $\widehat{h}$, but not for integration. The one-body operator itself can be assumed to be defined as in Hartree-Fock theory (Section 2.2) for the time being.

Let us decompose every part of the Hamiltonian explicitely. The kinetic energy term in the one-particle operator $\widehat{h}$ is trivially partitioned because AIM basins satisfy the zero-flux condition (Equation 4.12), and thus

$$T = \sum_A T^A = \sum_A \int_{\Omega_A} -\frac{\nabla^2}{2}\gamma^1(\mathbf{r}_1;\mathbf{r}'_1)d\mathbf{r}_1 \tag{4.27}$$

Analogously, the V_{en} term is easily partitioned in terms of the electron density, as it can be expressed as

$$V_{en} = \sum_{A,B} V_{en}^{A,B} \tag{4.28}$$

where

$$V_{en}^{A,B} = -\int_{\Omega_A} \frac{\rho(\mathbf{r}_1)Z_B}{r_{B1}}d\mathbf{r}_1 \tag{4.29}$$

which gives the Coulomb attraction between electrons in a basin Ω_A and a nuclei B with atomic number Z_B, as well as the one-atom term $V_{en}^{A,A}$.

Finally, the V_{ee} term is partitioned as

$$V_{ee} = \frac{1}{2}\int\int \rho_2(\mathbf{r}_1,\mathbf{r}_2)\frac{1}{r_{12}}d\mathbf{r}_1 d\mathbf{r}_2 = \sum_A V_{ee}^{A,A} + \frac{1}{2}\sum_A \sum_{B\neq A} V_{ee}^{A,B} \tag{4.30}$$

and hence has just one-atom $V_{ee}^{A,A}$ and two-atom $V_{ee}^{A,B}$ contributions as well. Note that in HFT the two-particle reduced density matrix can be expressed as the product of one-particle terms.

As nuclear repulsion energy is trivially partitioned into pairwise contributions in the Born-Oppenheimer framework, by partitioning the electronic energy we have successfully partitioned the total energy into one-atom and two-atom terms.

Grouping of terms

The IQA method gives many terms which are extremely large in chemical terms. They must generally be grouped to be understood intuitively. In the IQA framework – and arguably in quantum mechanics as a whole – chemistry arises from cancellation of large, opposite terms.

The total energy is written as a sum over atoms and pairs of atoms, i.e.

$$E = \sum_A E_{intra}^A + \frac{1}{2}\sum_{A,B\neq A} E_{inter}^{A,B} \tag{4.31}$$

where E_{intra} contains all *intra*-atomic terms: $V_{ee}^{A,A}$, $V_{en}^{A,A}$ and T_A. On the other hand, E_{inter} contains all pairwise terms: $V_{ee}^{A,B}$, $V_{en}^{A,B}$ (and $V_{en}^{B,A}$, which is not generally symmetric) and $V_{nn}^{A,B}$.

Note than the "preparation energy", which we previously associated with hybridization (cf. Subection 3.2.3), can be defined quite simply from this framework by comparing E_{intra}^A with the energy for the isolated atom,

$$E_{def}^A = E_{intra}^A - E_{isolated}^A \tag{4.32}$$

where E_{intra}^A is calculated in a chemical environment of interest, and $E_{isolated}^A$ is the energy of the isolated atom. The deformation energy E_{def}^A represents the energetic "cost" paid by the atom to adapt to the potential of the chemical environment.

Extension to Density Functional Theory

As discussed in depth in Section 2.4, DFT models the two-particle reduced density matrix in terms of a one-body operator through the expression of the exchange-correlation energy $\epsilon_{xc}(\rho(\mathbf{r}))$. The partition of such term is quite straightforward due to locality, but seems counterintuitive because one would expect that exchange-correlation effects must exist also between electrons of different atomic basins.

In general, we may rewrite $V_{ee}^{A,B}$ in pair-wise terms as

$$V_{ee}^{A,B} = \int_{\Omega_A}\int_{\Omega_B} \rho(\mathbf{r}_1)\rho(\mathbf{r}_2)\frac{1}{r_{12}}d\mathbf{r}_1 d\mathbf{r}_2 - E_{xc}^{A,B} = V_{Coul}^{A,B} - E_x^{A,B} - E_c^{A,B} \tag{4.33}$$

where $E_x^{A,B}$ and $E_c^{A,B}$ are pairwise terms for the exchange and correlation energies, that might be combined into $E_{xc}^{A,B}$. These terms are unknown at this point. The first term, $V_{elec}^{A,B}$, can be considered to be strictly Coulombic and hence bears the subscript *Coul*. Note that this decomposition applies to both E_{intra}^{A} and $E_{inter}^{A,B}$.

In the same spirit, we may decompose $E_{inter}^{A,B}$ into semiclassical "electrostatic" (subscripted as *elec*) terms and strictly quantum exchange and correlation factors,

$$E_{inter}^{A,B} = V_{elec}^{A,B} + \epsilon_{xc}^{A,B} \tag{4.34}$$

We may write an explicit HF-like expression (note the subscript) for E_x in atomic terms by summing over occupied MOs (from HFT or KS-DFT alike);

$$E_{x,HFX}^{A,B} = -\sum_{i,j}\int_{\Omega_A}\int_{\Omega_B} \psi_i(\mathbf{r_1})\psi_j(\mathbf{r_2})\frac{1}{r_{12}}\psi_i(\mathbf{r_1})\psi_i(\mathbf{r_2})d\mathbf{r}_1 d\mathbf{r}_2 \tag{4.35}$$

and we can therefore define a total exchange energy of any atom as

$$E_{x,HFX}^{A} = E_{x,HFX}^{A,A} + \frac{1}{2}\sum_{A,B\neq A} E_{x,HFX}^{A,B} \tag{4.36}$$

We can model an intra-atomic exchange-correlation contribution by calculating the exchange-correlation contribution given by the DFA through simple integration over Ω_A and the HF-like exchange with the same orbitals (assuming a KS-DFT context).

With this goal in mind, we define a weight factor λ_A for the atomic basin Ω_A, as

$$\lambda_A = a + \frac{1}{E_{x,HFX}^{A}}\int_{\Omega_A}\rho(\mathbf{r})\epsilon_{xc}d\mathbf{r} \tag{4.37}$$

where ϵ_{xc} is the exchange-correlation energy given by the DFA of choice, and a is the fraction of exact exchange in the DFA formulation (see Section 2.5 for details)

Finally, we put forward working expressions for the partitioning of $E_{xc}^{A,B}$,

$$E_{xc}^{A,B} = \frac{1}{2}\Big[\lambda_A + \lambda_B\Big]E_{x,HFX}^{A,B} \tag{4.38}$$

Which is an exchange-based partitioning that includes a formal correlation contribution. However, it fits in our partitioning scheme and it is therefore used.

4.3 Topology of the electron localization function

The Electron Localization Function (ELF) was originally derived in the framework given by HFT.[41] Arising from a monodeterminantal one-electron context, the probability of finding two particles with spin σ in the same point $\mathbf{r}$ is given by

$$D_\sigma(\mathbf{r},\mathbf{r}') = \rho_\sigma(\mathbf{r})\rho_\sigma(\mathbf{r}') - |\gamma^1_\sigma(\mathbf{r}_1;\mathbf{r}'_1)|^2 \tag{4.39}$$

where the σ-spin densities and the sigma one-particle reduced density matrix have been denoted with σ subindices. As a reminder, the definition for the one-particle reduced density matrix of σ spin is given below for this context as introduced in Equation 2.101:

$$\gamma^1(\mathbf{x}_1;\mathbf{x}'_1) = \sum_i n_{i\sigma}\psi_{i\sigma}(\mathbf{r}_1)\psi^\star_{i\sigma}(\mathbf{r}'_1) \tag{4.40}$$

which is exactly the same for $\sigma = \alpha, \beta$ in the restricted formalism with $n_{i\sigma} = 1$.

From Equation 4.39 we define the conditional pair probability, in which an electron of σ-spin is fixed at $\mathbf{r}$, as

$$P_\sigma(\mathbf{r},\mathbf{r}') = \rho_\sigma(\mathbf{r}') - \frac{|\gamma^1_\sigma(\mathbf{r}_1;\mathbf{r}'_1)|^2}{\rho_\sigma(\mathbf{r})} \tag{4.41}$$

which we may now expand around $\mathbf{r}$ in a spherically averaged fashion. The first term is 0 due to Pauli repulsion, and therefore the leading term is quadratic in s.

$$p_\sigma(\mathbf{r},s) = \frac{1}{3}\Big[\sum_i |\vec{\nabla}\psi_{i\sigma}|^2 - \frac{1}{4}\frac{|\vec{\nabla}\rho_\sigma(\mathbf{r})|^2}{\rho_\sigma(\mathbf{r})}\Big]s^2 + \dots \tag{4.42}$$

where ($\mathbf{r}$,s) denotes spherically averaged on a shell of radius s around the reference point $\mathbf{r}$. We may rewrite this expression, truncating at the quadratic term, as

$$p_\sigma(\mathbf{r},\mathbf{s}) = \rho_\sigma(\mathbf{r})\Big[\frac{2}{3}\frac{\tau_\sigma(\mathbf{r}) - \tau^W_\sigma(\mathbf{r})}{\rho_\sigma(\mathbf{r})}\Big]\mathbf{s}^2 \tag{4.43}$$

where the σ-spin positive semidefinite KED $\tau_\sigma(\mathbf{r})$ has been used as defined in Equation 2.133. Analogously, the von Weizsäcker kinetic energy density $\tau^w(\mathbf{r})$ was defined in Equation 2.135. Note that in this case only σ-spinned orbitals are considered.

From this last expression, we put forward the spinwith ELF kernel $\chi^{BES}_\sigma(\mathbf{r})$ as introduced by Becke and Edgecombe and generalized by Savin; [42]

$$\chi^{BES}_\sigma(\mathbf{r}) = \frac{\tau_\sigma(\mathbf{r}) - \tau^W_\sigma(\mathbf{r})}{\tau^{HEG}_\sigma(\mathbf{r})} \tag{4.44}$$

in which, again, we draw from Subsection 2.5.2 for the definition of the kinetic energy density of the homogeneous electron gas, which is simply

$$\tau^{HEG}_\sigma(\mathbf{r}) = C_F\rho^{5/3}(\mathbf{r}) \tag{4.45}$$

In a closed-shell system, since $\rho_\alpha(\mathbf{r}) = \rho_\beta(\mathbf{r}) = \frac{1}{2}\rho(\mathbf{r})$, the spin-independent ELF kernel simplifies to $\chi^{BES}(\mathbf{r})$, which is simply

$$\chi_{BES}(\mathbf{r}) = \frac{\tau(\mathbf{r}) - \tau^W(\mathbf{r})}{\tau^{HEG}(\mathbf{r})} = \frac{\tau^P(\mathbf{r})}{\tau^{HEG}(\mathbf{r})} \tag{4.46}$$

where a new kinetic energy density has been introduced: $\tau^P(\mathbf{r})$ is the kinetic energy due to the effect of the Pauli exclusion principle, that is, the fermionic nature of electrons in the non-relativistic model.

There are different suitable definitions for the ELF kernel, particularly so for the spin-dependent case. In this work we will adopt $\chi_{BES}(\mathbf{r})$ as defined in Equation 4.46 as the default one. Having chosen the ELF kernel, we can define the ELF itself as

$$\eta_{ELF}(\mathbf{r}) = \frac{1}{1+\chi^2_{BES}(\mathbf{r})} \tag{4.47}$$

which is a straightforward transformation that bounds the function to the interval $(0, 1)$ for visualization purposes. The mapping given by Equation 4.47 preserves all topological features of the ELF kernel $\chi_{BES}(\mathbf{r})$, since it is monotonically increasing.

We will begin by examining the information borne in this function. The topological features of $\eta_{ELF}(\mathbf{r})$ will be discussed in depth later in this Section.

4.3.1 Kinetic energy densities in chemical bonding

The ELF has been defined but no explicit interpretation of it has been put forward yet. There are many different conceptual ways to analyze this function. Perhaps the most fundamental notions stem from the virial theorem. The stabilization of the total energy that takes place in chemical bonds is given by a compensation of potential and kinetic energy.

The kinetic energy density of the interacting region is thought to decrease significantly: the electrons must be localized there in order to properly shield the nuclear repulsion. [43] As such, kinetic energy densities are quite useful as local descriptors of chemical bonding. [44, 45, 46, 47] There is a plethora of suggestions in this regard. We will outline some of them while attemtping to provide a clear picture of the ELF.

Let us examine the components of $\chi_{BES}(\mathbf{r})$ – and the relations between them – as presented in Equation 4.46.

First of all, note that the term $\frac{\tau_w(\mathbf{r})}{\tau(\mathbf{r})}$ was introduced when discussing SIE in DFT (cf. Subsection 2.5.3). $\tau_w(\mathbf{r})$ is a good approximation to the kinetic energy density of the system whenever the system has single-orbital character, and a lower bound otherwise. Hence, the term goes to zero as the system is further from a single-orbital character.

The numerator in the ELF kernel (Equation 4.46), that is, the Pauli kinetic energy density $\tau^P(\mathbf{r})$, draws on a similar idea. $\tau^P(\mathbf{r}) = 0$ only in single-orbital points $\mathbf{r}$, and is positive otherwise. The greater the value it takes, the further the system is from single-orbital character.

The two split quotients can be interpreted indivdually on their own right, which helps understand the ELF kernel.

Localized Orbital Locator

The kernel of the Localized Orbital Locator (LOL) is defined as:

$$t_{LOL}(\mathbf{r}) = \frac{\tau^{HEG}(\mathbf{r})}{\tau(\mathbf{r})} \tag{4.48}$$

which is then bound to define the LOL function $\eta_{LOL}(\mathbf{r})$,

$$\eta_{LOL}(\mathbf{r}) = \frac{t_{LOL}(\mathbf{r})}{1 + t_{LOL}(\mathbf{r})} = \frac{1}{1 + t_{LOL}^{-1}(\mathbf{r})} \tag{4.49}$$

preserving all topological features again. The interpretation of the LOL kernel $t_{LOL}(\mathbf{r})$ is quite straightforward. If the kinetic energy density of the system under consideration is much lower than the one given by $\tau_{HEG}(\mathbf{r})$, which is to say that the electrons are more "localized", then $t_{LOL}(\mathbf{r}) \to \infty$. On the contrary, if the kinetic energy density is very high compared to the HEG, $t_{LOL}(\mathbf{r}) \to 0$.

After transformation (Equation 4.49), localization is mapped to $\eta_{LOL}(\mathbf{r}) > 1/2$, and complete delocalization (i.e. *fast* electrons) is associated with $\eta_{LOL}(\mathbf{r}) < 1/2$. If $\tau(\mathbf{r})$ and $\tau^{HEG}(\mathbf{r})$ match exactly, $\eta_{LOL}(\mathbf{r}) = 1/2$. Only perfect localization ($t_{LOL}(\mathbf{r}) \to \infty$) or delocalization ($t_{LOL}(\mathbf{r}) \to 0$) reach the extremes of the function.

In this sense, it must be noted that the kinetic energy density (as defined in this text or otherwise) is always maximal for the electrons near nuclei, which are under the effect of a high local potential. Therefore, any bonding indicator requires some sort of renormalization that removes or rescales core densities.

Bosonic Kinetic Energy Density

The last missing connection is given by the bosonic kinetic energy density, $t_B(\mathbf{r})$, which may be defined as

$$t_B(\mathbf{r}) = \frac{\tau^W(\mathbf{r})}{\tau^{HEG}(\mathbf{r})} \tag{4.50}$$

and subsequently bound as $\eta_B(\mathbf{r})$,

$$\eta_B(\mathbf{r}) = \frac{1}{1 + t_B(\mathbf{r})} \tag{4.51}$$

$t_B(\mathbf{r})$ is a lower bound to $t_{LOL}^{-1}(\mathbf{r})$, and hence $\eta_B(\mathbf{r})$ is an upper bound to $\eta_{LOL}(\mathbf{r})$. In nuclear regions, $\eta_B(\mathbf{r})$ is extremely similar to $\eta_{LOL}(\mathbf{r})$ because, as expected, $\tau^P(\mathbf{r}) \approx 0$. In all other regions, it highlights localization in a stark way due to the gradient term in $\tau^W(\mathbf{r})$, which will naturally be zero in regions with constant density.

As a sidenote, $t_B(\mathbf{r})$ is related with the reduced density gradient, $s(\mathbf{r})$, which was introduced in the enhancement factor of GGA DFAs (cf. Equation 2.131), as

$$t_B(\mathbf{r}) = \frac{5}{3} s^2(\mathbf{r}) \tag{4.52}$$

and can henceforth be interpreted in terms of the inhomogeneity of the density as well. This has notable consequences for the analysis of non-covalent interactions which will not be covered here.[48, 49]

Pauli Kinetic Energy Density and Electron Localization Function

Having discussed all of its ingredients, it is apparent that the Pauli kinetic energy density $\tau^P(\mathbf{r})$ is quite simply a measurement of the single-orbital character of the system.

The denominator $\tau^{HEG}(\mathbf{r})$ is thus simply used to rescale both terms, as in the explicit expression

$$\chi_{BES}(\mathbf{r}) = t_{LOL}^{-1}(\mathbf{r}) - t_B(\mathbf{r}) \tag{4.53}$$

so that it measures the effect of non-bosonic character *in localization*. It is therefore straightforward to see that $\chi_{BES}(\mathbf{r})$ is always positive and mandatorily small in nuclear regions – but not strictly due to what we understand as chemical localization

Expanding the transformed expression, we get

$$\eta_{ELF}(\mathbf{r}) = \frac{1}{1 + t_{LOL}^{-2}(\mathbf{r}) + t_B^2(\mathbf{r}) + 2t_{LOL}^{-1}(\mathbf{r})t_B(\mathbf{r})} \tag{4.54}$$

from which we can easily see that $\eta_{ELF}(\mathbf{r}) = 1$ only whenever $t_{LOL}^{-1}(\mathbf{r}) = t_B(\mathbf{r})$ or $\eta_B(\mathbf{r}) = \eta_{LOL}(\mathbf{r})$, i.e. $\tau^P(\mathbf{r}) = 0$. This will only happen in one-orbital regions. Localization, as given by $t_{LOL}(\mathbf{r})$, might be arbitrarily large or small in this sense.

However, if $t_{LOL}(\mathbf{r})$ is very large, that is, the kinetic energy density of the system is very small compared to that of the HEG, then $t_{LOL}^{-1}(\mathbf{r})$ will be very small. $t_B(\mathbf{r})$ is a lower bound of the latter, and therefore $\eta_{ELF}(\mathbf{r}) \approx 1$ forcefully. In this sense, the ELF measures localization due to fermionic character but also localization that has to do strictly with the kinetic energy density itself.

On the other hand, $\chi_{BES}(\mathbf{r})$ will be large whenever the system has a character that is significantly different from the single-orbital model in a way that is significant compared to the homogeneous kinetic energy density for that region. Then, $\eta_{ELF}(\mathbf{r}) \to 0$.

That is, if the Pauli kinetic energy density $\tau^P(\mathbf{r})$ is large with respect to $\tau^{HEG}(\mathbf{r})$, which scales with the density, this can be interpreted as a lack of localization due to Pauli's exclusion principle.

Hence, $\eta_{ELF}(\mathbf{r})$ is often said to be maximal (i.e. nearly 1) for spin-paired regions, minimal (nearly 0) for spin-unpaired regions, and takes the value 1/2 when the system resembles the localization of the HEG model.

A comparison of the three bound functions is shown in Figure 4.10 for the CO_2 molecule. Note that in this case all three functions are quite similar. However, as per the nuanced interpretation that we have presented, this might not always be the case.

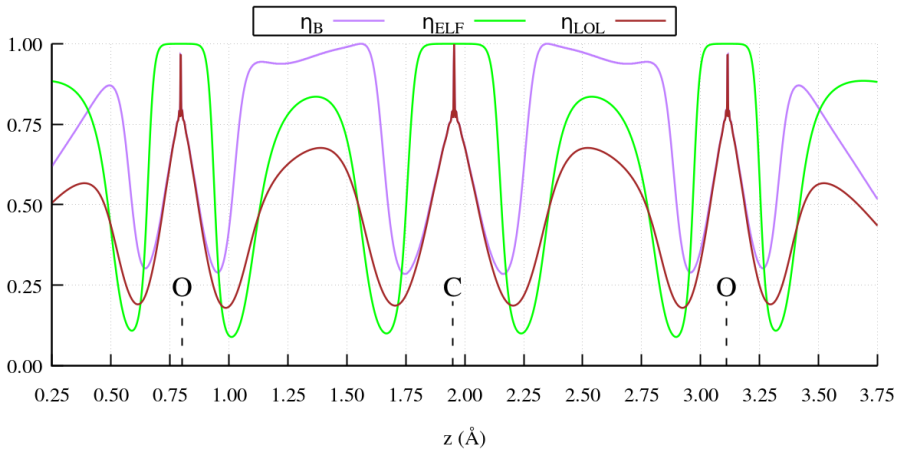

Figure 4.10: $\eta_b(\mathbf{r})$, $\eta_{ELF}(\mathbf{r})$ and $\eta_{LOL}(\mathbf{r})$ along the internuclear axis of CO_2. Calculated at the B3LYP/def2-SVP level. Dashed lines indicate the position of each nuclei.

As a final remark, the reader is encouraged to realize the effect of the bounding transformation critically. In particular, the effect of squaring the kernel function in Equation 4.47, which normalizes the $\eta_{ELF}(\mathbf{r}) = 0.5$ and preserves the topology, but

alters the shape of the function. Other plausible transformations have been proposed that share these properties. For instance, a family of hyperbolic bounding transformations is given by

$$\eta^n_{hELF}(\mathbf{r}) = \frac{1}{2}[1 + tanh(\chi^{-n}_{BES}(\mathbf{r}) - \chi^n_{BES}(\mathbf{r}))] \tag{4.55}$$

where $n \geq 1$ in order to achieve a steeper transformation. It must be noted that the measurement of localization itself is not under judgment here, as all information arises purely from $\tau^P(\mathbf{r})$, but the representation obtained might differ significantly.

4.3.2 Critical points of the Electron Localization Function

Analogous to the case of the electron density $\rho(\mathbf{r})$ in Subsection 4.2.1, we will attempt to the study a Morse function, $\eta_{ELF} : \mathbb{R}^3 \to \mathbb{R}$, using Morse theory. As it will be shown later, sometimes η_{ELF} will not be Morse function in practice. However, let us assume it always is for the time being.

Again, we will commence with the vector field to find the CPs of the function. Similarly, the vector field $\vec{\nabla}\eta_{ELF}(\mathbf{r})$ will be zero locally at the CPs, which will be of four distinct types. Recall that all the bounding transformations that have been considered are devised to maintain the position of CPs.

$(3, -3)$ maxima in the ELF context are often called *attractors*. The stable manifold of an attractor is, as in the AIM framework, a basin that occupies a given volume. As given by its interpretation, such basins identify regions of space in which electron pairs are localized. First and foremost, this situation is associated with the position of nuclei. However, in the case of the ELF topology, attractors are also found in covalent chemical bonds and in lone pairs – any region with spin-pairing. Thus, the resulting topology is significantly richer from the chemical and mathematical perspective.

Generally speaking, CPs of the ELF other than local maxima do not have a clear interpretation. This is consequent with what has been discussed in the previous Subsection: $\chi_{BES}(\mathbf{r})$ is only properly bound from below. Therefore, usually CPs are not rigorously characterized for this function.

A glimpse at the CPs of $\eta_{ELF}(\mathbf{r})$ is shown in Figure 4.11 for the same molecules as Figure 4.8. Note that the placement of maxima does indeed match chemical intuition with respect to electron pairing: every nuclei has one on top of itself, accounting for core electrons, and covalent bonds have at least one as well. C–H bonds have only one maxima because the core electrons are involved in the bond in this case. It must be noted that there is a typical error in Figure 4.11 C), where the $D_{\infty h}$ symmetry of the molecule (and thus, potential and wavefunction) is *not* respected. This is due to the use of a finite grid. However, this is a typical problem in the representation of the ELF that we will discuss in some depth in the next Subsection.

More usually, the representation of the topology of $\eta_{ELF}(\mathbf{r})$ is given by using a proper isosurface (usually $0.75 < \eta_{ELF}(\mathbf{r}) < 0.85$) which faithfully divides the different basins of all attractors. Obviously, the isovalue is bound between 0 and 1 in all cases, and a different bounding transformation may modify this approximate range. The molecules that were shown before are presented with $\eta_{ELF}(\mathbf{r}) = 0.85$ isosurfaces in Figure 4.12. Note that this procedure naturally merges the artificial CPs that rose due to symmetry breaking in ethyne.

The interpretation of symmetry-broken ELF basins is quite involved. A successful explanation has been given in terms of Lewis structures. The triple bond in ethyne is expected to be composed by a σ-bond on the interatomic C–C axis and two out of plane

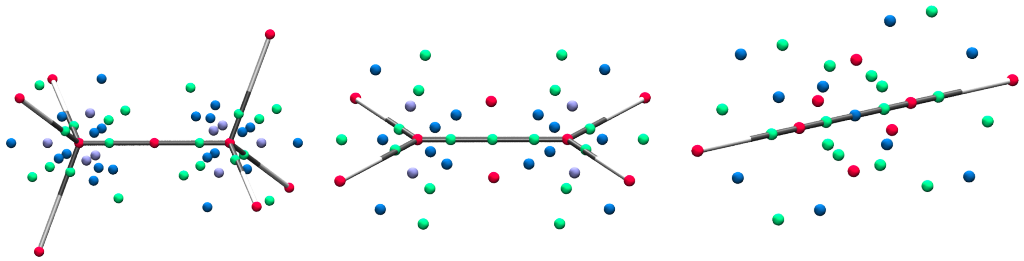

A) B) C)

Figure 4.11: CPs of $\eta_{ELF}(\mathbf{r})$ for different molecules calculated at the HF/cc-PVTZ level: **A)** Ethane **B)** Ethylene **C)** Ethyne. CPs are shown as spheres. $(3,-3)$, $(3,-1)$, $(3,+1)$ and $(3,+3)$ CPs are colored red, green, blue and violet respectively. Note the symmetry-breaking issue in C) (see text)

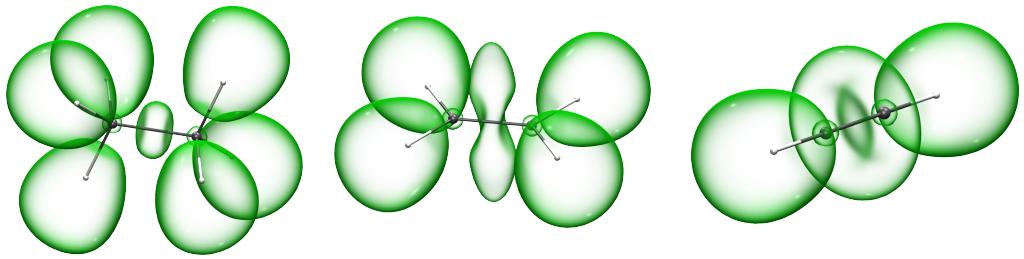

A) B) C)

Figure 4.12: Isosurfaces of $\eta_{ELF}(\mathbf{r}) = 0.85$ a.u. for different molecules calculated at the HF/cc-PVTZ level: **A)** Ethane **B)** Ethylene **C)** Ethyne. Isosurfaces colored green.

π-bonds. However, the $D_{\infty h}$ symmetry of the molecule forbids choosing a proper nodal plane for the π-orbitals, and hence the ELF gives an average depiction of the π-bonds over the symmetry elements of the molecule. Hence, the ring-shaped basin in Figure 4.12 C) can be understood as an averaged triple bond.

4.3.3 Lewis entities in a molecule

Finding all local maxima of $\eta_{ELF}(\mathbf{r})$ in a system allows to differentiate two types of basins, which are commonly called core and valence basins for ease of interpretation.

Core basins arise from the single-orbital character in the vicinity of the nuclear point charges and are subsequently quite small and spherical. Several notations exist for core basins, including $C(A)$, where A stands for nuclei on which the attractor is placed, and Ω_A^C where the superscript stands for *core*.

Valence basins fill the rest of the space exhaustively. The corresponding attractors usually match the electron pair arrangements of Lewis and, in a more general sense, the VSEPR model (see Subsection 1.2.3 for a critical introduction). Therefore, it provides a proper quantum support for concepts of such theories, including lone pairs. Valence basins are often denoted by $V(A, B)$, where A and B correspond to the nuclei whose core basins are contiguous to the valence basin. In most cases, A and B will simply match chemical intuition: they are the atoms *bonded* by $V(A, B)$. We will also introduce the notation $\Omega_{A,B}^V$ for generality. Note that, by definition, valence basins do not contain nuclei, and hence their classification requires notions on their connectivity.

We define the synaptic order of a valence basin as the number of core basins which have a common separatrix with it.[50] Valence basins are usually classified by their synaptic order: asynaptic basins (synaptic order zero), monosynaptic (synaptic order one), disynaptic (synaptic order two) or polysinaptic (see Table 4.2). Asynaptic and polysinaptic basins are quite rare. The $C(A)$ and $V(A, B)$ nomenclature that has been introduced, equivalences of which are captured in Table 4.2 as well, is used for interpretative purposes but may turn out to be ill-defined mathematically.

Synaptic order	Name	Basin symbol	ELF nomenclature
–	Core	Ω_A^C	$C(A)$
0	Asynaptic	Ω^V	–
1	Monosynaptic	Ω_A^V	$V(A)$
2	Disynaptic	$\Omega_{A,B}^V$	$V(A, B)$
3	Trisynaptic	$\Omega_{A,B,C}^V$	$V(A, B, C)$
>3	Polisynaptic	$\Omega_{A,B,C,\ldots}^V$	$V(A, B, C, \ldots)$

Table 4.2: $\eta_{ELF}(\mathbf{r})$ valence basin classification according to their nature and synapticity.

An example of asynaptic basin is found in NH_4^- due to the excess of electron density and in F-centers in solid state systems. Lone pairs are the typical example of monosynaptic basins, as found in the extremes of the CO_2 molecule (cf. Figure 4.10). Two-center covalent bonds are usually associated with disynaptic basins centered between them, while higher synaptic orders appear in non-Lewis bonding situations, as for example agostic bonds with coordination metals.

While polisynaptic basins can be associated with multicenter bonds, note that

asynaptic basins have no possible Lewis-like interpretation. Usually, covalent bonds appear as disynaptic basins, and increased bond order results in more than one basin or, as in the case of ethyne that was discussed before, a larger basin.

Perfectly ionic bonds lack associated ELF basins, which is coherent because there is no electron pairing associated with the bond. Metallic bonds are associated with large polisynaptic basins due to the fact that bonding is not localized and the ELF value is moderately high in all interatomic regions. Thus, a qualitative understanding of bonding regimes can be gained by the analysis of the basins and level sets of $\eta_{ELF}(\mathbf{r})$.[51]

Atomic shells

In isolated atoms, several local maxima of $\eta_{ELF}(\mathbf{r})$ arise. Rigorously, in any spherically symmetric potential with more than two electrons, subsequent spherically symmetric basins appear, which resemble the orbital concept of atomic shells. This is another context in which mono and asynaptic valence basins may arise.

While we are not particularly concerned about such features, it must be acknowledged as a notably succint example of the utility of the ELF. The $\eta_{ELF}(\mathbf{r})$ profiles of C and O (in two multiplicities each) are collected in Figure 4.13 for reference.

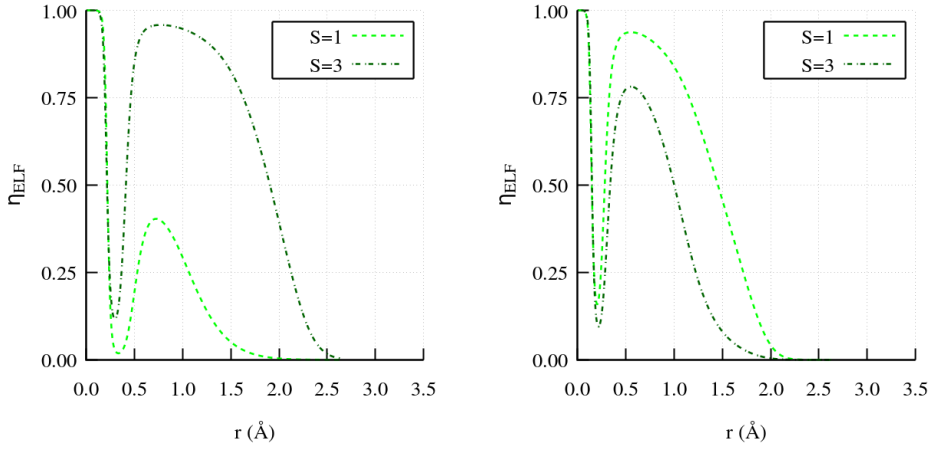

Figure 4.13: $\eta_{ELF}(\mathbf{r})$ a.u. along the distance r to the nuclear poisition of: **A)** carbon atom, **B)** oxygen atom. Data calculated at the CCSD/cc-PVTZ level.

Note how the trend on the $\eta_{ELF}(\mathbf{r})$ values of the second shell invert when passing from C to O: in O atom it could be suggested that the higher values of $\eta_{ELF}(\mathbf{r})$ for the second shell for the $S = 1$ are due to an increased electron pairing. This is shown to be inconsistent in the case of C, and hence not true. Let this example showcase how the interpretation of the ELF solely in terms of electron pairs, if used acritically, might lead to errors.

Basin properties

The Morse complex $\eta_{ELF}(\mathbf{r})$ is, once again, an exhaustive non-overlapping partitioning of space. Hence, all the basin properties introduced in Subsection 4.2.2 by the general

expressions in Equations 4.14 and 4.18 for the AIM framework may be used in the ELF context as well.

In fact, due to the reduced relevance of CPs in the analysis of the ELF, basin properties play a major interpretative role. For instance, we can calculate *ab initio* valence states for an atom by substracting the core population $\overline{N}_A^C$ from the formal number of electrons of the atom. $\overline{N}_A^C$ represents the average number of electrons in the core shell of an atom, which can be calculated by integrating over the core basin associated with the nuclei;

$$\overline{N}_A^C = \int_{\Omega_A^C} \rho(\mathbf{r}) d\mathbf{r} \tag{4.56}$$

and we can analogously integrate over any valence basin to calculate its electron population. The total number of valence electrons associated with an atom will be given by a sum of the valence basins that have a separatrix in common with the core basin of the nuclei;

$$\overline{N}_A^V = \int_{\Omega_A^V} \rho(\mathbf{r}) d\mathbf{r} + \sum_{A \neq B} \int_{\Omega_{AB}^V} \rho(\mathbf{r}) d\mathbf{r} + \dots \tag{4.57}$$

Thus, we can also calculate the total number of electrons associated with an atom as

$$\overline{N}_A^{CV} = \overline{N}_A^C + \overline{N}_A^V \tag{4.58}$$

and we expect this number to be quite stable in different chemical environments in order to verify the famed octet rule. We would also expect a total number of electrons of approximately 2 for hydrogen basins. Both these assumptions generally hold. Hence, a quantum mechanical theory of chemical structure can be built upon the topology of the ELF, which retrieves the notion of valence and Lewis entities.

Naturally, two-basin properties – as delocalization and localization indices – can also be defined in terms of ELF basins. Furthermore, the whole IQA approach can be coupled to the ELF partitioning with the caveat of having to choose a kinetic energy density to integrate. The total energy is recovered nevertheless.

Variance of pairs of Lewis entities

In ELF language, the concepts of variance are more popular than other two-basin properties. Hence, we will introduce them with respect to the previously defined delocalization and localization indices, $\delta_{A,B}$ and Λ_A respectively in Equations 4.19 and 4.20.

The variance σ_A^2 of the electron population of a basin A is given by

$$\sigma_{\Omega_A}^2 = \overline{N}_{\Omega_A} - \Lambda_{\Omega_A} \tag{4.59}$$

and can be decomposed into pairwise terms as

$$\sigma_{\Omega_A}^2 = \sum_{A \neq B} \left[\overline{N}_{\Omega_A} \overline{N}_{\Omega_B} - \int_{\Omega_A} \int_{\Omega_B} \rho_2(\mathbf{r}_1, \mathbf{r}_2) d\mathbf{r}_1 d\mathbf{r}_2 \right] = \frac{1}{2} \sum_{A \neq B} \delta_{\Omega_A, \Omega_B} \tag{4.60}$$

The interpretation of the contributions to the variance is quite straightforward given the nomenclature. The variance of the electron population of a given basin Ω_A – which might be of any given kind – is due to fluctuation towards other basins. Generally,

adjacent basins will present significant delocalization indices, while further away ones will not.

As in the AIM framework, delocalization indices between ELF basins give a sort of bond order, or a notion on the degree of interaction between them through formally shared electrons.

Chapter 5

A Modern Bond Charge Model Ansatz

Contents

As we have discussed in some detail over the previous Chapters, the chemical bond is a central concept in chemistry. The bond types covered in Chapter 1, and, to a lesser extent, the attribution of degrees of character to bonds, are absolutely fundamental to discuss chemical phenomena. On the other hand, chemical bonds – and subsequently, types of chemical bonds – are not rigorously defined whatsoever in the context of quantum chemistry.

Critically, in quantum chemistry bonds can only be defined between molecules, i.e. associated with nuclear displacement in the PES. However, in FMT bonds are entities associated with the interaction of atoms. This is the key reason why theoretical frameworks that retain atomistic properties tend to support the notion of chemical bond best.

However, there is yet another approach to the chemical bond that is not strictly based on atoms or nuclei: we can treat chemical bonds as distinct entities, with distinct properties, that may interact with *other* chemical bonds as well as with pseudoatoms.

There is much to be said in this direction. This Chapter will be devoted to a particular approach to distinct chemical bonds: we will put forward a semiclassical model, we will try to justify it quantitatively, and we will try to put our model to test.

5.1 The Bond Charge Model

It has been known for a very long time that the potential energy curve of an homonuclear diatomic can be modeled using a Morse potential. In fact, coupled with corrections and experimental parameters, a Morse potential might be more accurate than certain levels of quantum mechanical calculations with the advantage of being fully analytical. For an homonuclear diatomic molecule A_2 with internuclear distance R, a Morse potential takes the form

$$W(R) = W_{R=\infty} + D_e(1 - e^{-\beta(R-R_{eq})})^2 \tag{5.1}$$

in which R_{eq}, the equilibrium internuclear distance, D_e, the well depth, and β controls the width of the well. Hence, four parameters are needed to model the potential energy $W(R)$. Another analytical model that achieves similar success for the same situation is the following

$$W(R) = W_0 + \frac{W_1}{R} + \frac{W_2}{R^2} \dots \tag{5.2}$$

which, truncated at second order, gives reasonably accurate potential energy curves. This expression requires one parameter less than Equation 5.1, and does not require explicit knowledge of the equilibrium region. Note that, $W_0 = W_{R=\infty}$ and both can be set to zero for $W(R)$ in relative terms.

Attemtping to assign a physical meaning to Equation 5.2, we may try to rearrange the expression into potential $V(R)$ and kinetic $T(R)$ terms and satisfy the molecular virial theorem, that is

$$V(R) = 2W + R\Big(\frac{dW}{dR}\Big)$$

and

$$T(R) = -W - R\Big(\frac{dW}{dR}\Big)$$

which, when coupled with Equation 5.2 lead to the following

$$\begin{aligned} V(R) &= 2W_0 + \frac{W_1}{R} \\ T(R) &= -W_0 - \frac{W_2}{R^2} \end{aligned}$$

As forces are obtained by taking derivatives of $W(R)$, the term W_0 is unimportant for dynamic properties, and we can assume that it can be split subsequently. For our interest, it suffices to put forward that the $V(R)$ term and the $T(R)$ term have distinct forms so that we can build an interpretation on them.

5.1.1 Homonuclear Bond Charge Model

The energy associated with the bond can thereafter be expressed approximately using a semiclassical approach. For the simplest case, which is a homonuclear diatomic molecule A_2 with internuclear distance R, the potential energy curve $W(R)$ can be modeled as a sum of three terms in the spirit of Equation 5.2:

$$W(R) = D + V(R) + T(R) = D + C_V^{BN}\frac{q}{R} + C_V^{NN}\frac{1}{R} + C_T^B\frac{q}{R^2} \tag{5.3}$$

D is a bond-specific constant accounting for the internal energy of the participating atoms, hence system-specific and additive (i.e. $D = D_A + D_A$ in this case). In agreement with the virial development of Equation 5.2, $V(R)$ is a Coulomb term and T is a kinetic energy term. C_V^{BN}, C_V^{NN} and C_T^B are just proportionality constants whose interpretation will be clarified later.

Owing to Equation 5.3, the Bond Charge Model (BCM) is a simple proposal by Parr and coauthors [52, 53, 54, 55] in which the description of a chemical bond is likened to that of a negatively charged particle between two pseudo-atoms. These pseudo-atoms have, in principle, positive net charge: pseudo-atom here implies that the bond is "formed" by valence density from the constituent atoms, and hence the remaining part of the atom has a significant deficit of electron density. For instance, a chemical representation would be the nuclei surrounded by only core electrons. For brevity, we shall use the term core to refer to the pseudo-atom, following this reasoning. The core will naturally behave like an atomic nuclei shielded by core electrons.

In the BCM chemical bonds are assumed to be well described by a negative electronic charge or *bond charge* q placed somewhere between two pseudo-atoms – including a nucleus – with effective positive charge Z. The bond charge must therefore interact with the two cores electrostatically, which assuming it is centered in the middle of the bond means over a distance $R/2$. Analogously, the two cores must interact with each other over the internuclear distance R. The zeroth order term in a plausible multipole expansion is a Coulomb force between point charges, which leads to a $2qZ/R$ and Z^2/R dependencies for the bond-core and nucleus-nucleus terms in $V(R)$. Hence, written in a compact way, we have

$$V(R) = \frac{(Z^2 - 4qZ)}{R} = \frac{Z^2}{R} - 2\frac{qZ}{R/2} = C_V^{NN}\frac{1}{R} + C_V^{BN}\frac{q}{R} \tag{5.4}$$

In which the atomic charges have been grouped into constants which we may devise to be nuclei or atom-specific.

The kinetic term is somewhat harder to picture. The original proposal assumes that the bond particle is moving in a one-dimensional box between two infinite potentials that exist in the vicinity of the pseudoatoms. The energy of a particle in a 1D box of length L follows $E \propto 1/L^2$. Accordingly, a q/R^2 dependency for T, which suits Equation 5.3 and justifies the following

$$T(R) = \frac{qh^2}{8m_e R_B^2} = \frac{qh^2}{8m_e \nu^2 R^2} = C_T^B \frac{q}{R^2} \tag{5.5}$$

where h is Planck constant, m_e is the mass of the electron, and ν is a variable such that $\nu R = R_B$, where R_B is the effective bond length. It is implied that the bond charge moves in a limited fraction of the total internuclear distance so that $R_B < R$ and hence $\nu < 1$.

So far, we have assigned a meaning to the different terms in Equation 5.3. Assuming that q must compensate the nuclear charges, Z, to the net molecular charge, i.e. both terms represent the same parametric degree of freedom, the only model parameters that do not vanish in the expression of the force dW/dR are q and ν. The model is schematically presented in Figure 5.1.

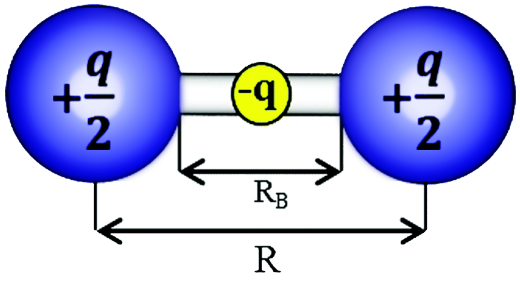

Figure 5.1: Schematic representation of an homonuclear diatomic molecule in the BCM.

Thus, $W(R)$ can be expressed in terms of a coefficient of the core-bond potential C_V^{BN}, a coefficient of the core-core potential C_V^{NN}, and a bond kinetic energy coefficient C_T^B, noting that in principle C_V^{BN} and C_V^{NN} are related by $C_V^{NN} = (C_V^{BN})^2/16$ and therefore only two parameters are needed. The superscript B will be used to refer to the bond charge, and the superscript N is used for the core, which is a nucleus plus some core electrons.

Recall that, as per the expression in Equation 5.3,

$$W_{R=\infty} = D \tag{5.6}$$

that is, D is a constant that shifts the potential energy but is non-important in the relative description. Thus, we can safely drop this variable for most of our analysis.

5.1.2 Heteronuclear Bond Charge Model

Once the interpretation of the model has been put forward, some modifications are needed for the model to be valid in heteronuclear diatomics – and other asymmetric chemical environments thereafter.

Formally, this can be achieved in several different ways. Let us remark the two most straightforward modifications to what has been stated so far.

Naturally, the effective charge of the two cores must differ now. Assuming neutral net charge, we may write a charge equalization condition between cores and bond charge for an homonuclear diatomic A_2 as

$$2Z - q = 0 \tag{5.7}$$

where we have assumed that q is written positive but represents a negative charge. Obviously, $q = Z/2$ in this model.

This condition may be extended to an heteronuclear diatomic molecule AB as

$$Z_A + Z_B - q = Z(1 - \delta_{AB}) + Z(1 + \delta_{AB}) - q = 0 \tag{5.8}$$

in which we have assumed that the most electronegative "atom", with core A, will attract more electron density than B. Hence, the net positive charge in the core B is larger by a factor δ_{AB} that is related to the electronegativity difference between A and B. Z is thus an averaged effective nuclear charge here,

$$Z = \frac{1}{2}\Big(Z_A + Z_B\Big) = \frac{q}{2} \tag{5.9}$$

and the net charge of both cores may be rewritten in terms of the bond charge q as

$$q = Z_A + Z_B = Z(1 - \delta_{AB}) + Z(1 + \delta_{AB}) = \frac{q - \delta}{2} + \frac{q + \delta}{2} \tag{5.10}$$

where the unspecified δ is the deviation between the effective core charges and $q/2$.

Given that the Coulomb terms between both cores and the bond charge will be different now, the position of the centroid of the bond charge might not be in the middle of the internuclear distance. Consequently, we may split R into two distances $R = r_1 + r_2$ where r_1 is the distance between atom B and the bond charge and r_2 is the distance between the bond charge and atom A. The heteronuclear situation is presented schematically in Figure 5.2.

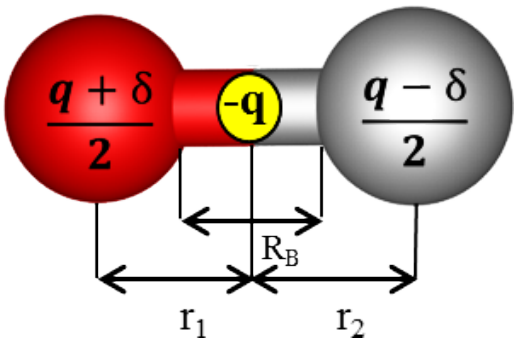

Figure 5.2: Schematic representation of an heteronuclear diatomic molecule in the BCM.

Thus, we may update the expression in Equation 5.3 to include these developments as

$$W_{AB}(R) = D_A + D_B + V_{AB}(R) + T(R) = D + C_{V1}^{BN}\frac{q}{R} + C_{V2}^{BN}\frac{q}{R} + C_V^{NN}\frac{1}{R} + C_T^B\frac{q}{R^2} \tag{5.11}$$

in which we have $D = D_A + D_B$ as suggested before, and the potential energy term contains two distinct bond-core terms and a core-core term, which can be expanded as

$$\begin{aligned} C_{V1}^{BN}\frac{q}{R} &= Z(1+\delta_{AB})\frac{1}{\alpha_1}\frac{q}{R} \\ C_{V2}^{BN}\frac{q}{R} &= Z(1-\delta_{AB})\frac{1}{1-\alpha_1}\frac{q}{R} \\ C_{V}^{NN}\frac{1}{R} &= \Big(Z^2 - Z^2\delta_{AB}^2\Big)\frac{1}{R} \end{aligned}$$

where $\alpha_1 R = r_1$ and thus $(1-\alpha_1)R = r_2$. Thus, two additional parameters are needed, α_1 and δ_{AB}.

The ratio of the two core-bond potential terms can be expanded as

$$\frac{C_{V1}^{BN}}{C_{V2}^{BN}} = \frac{\delta_{AB}+1}{\delta_{AB}-1} - \frac{1}{\alpha_1}\frac{\delta_{AB}+1}{\delta_{AB}-1} \tag{5.12}$$

which has a root for $\delta_{AB} = -1$ assuming $\alpha_1 \neq 0$ and also for $\alpha_1 = 1$ whenever $\delta_{AB} \neq 1$.

It is worth to notice that, to avoid excessive complexity, one of the two additional parameters presented may be set to the value of the homonuclear model, that is $\delta_{AB} = 0$ or $\alpha_1 = 1/2$ i.e. $r_1 = r_2 = R/2$. According to our assumptions, α_1 does not affect the core-core term and thus seems less important.

The series expansion of the ratio in Equation 5.12 around $\delta_{AB} = 0$ is simply

$$\frac{C_{V1}^{BN}}{C_{V2}^{BN}} = \Big(\frac{1}{\alpha_1} - 1\Big) + \delta_{AB}\Big(\frac{2}{\alpha_1} - 2\Big) + \delta_{AB}^2\Big(\frac{2}{\alpha_1} - 2\Big)\ldots \tag{5.13}$$

and thus, truncating to the first order, which should be valid for small δ_{AB} (i.e. electronegetivity differences), we have

$$\alpha_1 = \frac{C_{V2}^{BN}}{C_{V1}^{BN} + C_{V2}^{BN}} = \frac{r_1}{R} \tag{5.14}$$

upon which we may improve by including higher order terms.

However, as shown in Equation 5.11, both heteronuclear parameters may be merged into the proportionality constants in Equation 5.3 for the time being without loss of generality simply by adding an extra $\propto q/R$ term. Thus, for the most part, we will remain within the homonuclear model in this Section for simplicity.

5.1.3 Properties from the Bond Charge Model

In what follows, we will drop the dependency on R from the energy terms for simplicity. As anticipated, the BCM analytical expression of W allows for the advantageous calculation of equilibrium bond lengths R_{eq}, harmonic oscillator strengths k_e, and bond energies dissociation energies BDE (Equations 5.15-5.17), among others:

$$(\partial W/\partial R)_{R=R_{eq}} = -\frac{1}{R_{eq}^3}\Big(C_V^{BN}q + C_V^{NN} + 2C_T^B\frac{q}{R_{eq}}\Big) = 0 \tag{5.15}$$

$$(\partial^2 W/\partial R^2)_{R=R_{eq}} = \frac{2}{R_{eq}^3}\Big(C_V^{BN}q + C_V^{NN} + 3C_T^B\frac{q}{R_{eq}}\Big) = k_e \tag{5.16}$$

$$W_{R=R_{eq}} - D = C_V^{BN}\frac{q}{R_{eq}} + C_V^{NN}\frac{1}{R_{eq}} + C_T^B\frac{q}{R_{eq}^2} = -BDE \tag{5.17}$$

Conversely, these expressions can be used to fit experimental R_{eq}, k_e and BDE values. [56] For instance, using

$$R_{eq} = -\frac{2qC_T^B}{qC_V^{BN} + C_V^{NN}} \tag{5.18}$$

or

$$2\omega_h^2 = \frac{1}{\pi^2 c^2 \mu^2 R_{eq}^3}\left(C_V^{BN}q + C_V^{NN} + 3C_T^B\frac{q}{R_{eq}}\right) \tag{5.19}$$

where c is the speed of light, μ is the reduced mass of the system and ω_h is the harmonic frequency of the bond that results from the force constant k_e.

However, without the use of additional constraints the model leads to unphysical parameters which hamper interpretation.[55] Notably, very large effective bond lengths may be obtained for simple molecules (reported value of $\nu = 2.3$ for H_2). We will explore this issue in some depth later in this Subsection with an example. Naturally, from the interpretative point of view, bond charges must remain relatively close to the expected number of electrons in play, that is, $q \approx 2$ for a typical covalent bond and $\nu < 1$ at all times.

It must be noted that several local minima could coexist in the parametric space of the original model in Equation 5.3: several different combinations of q and ν may achieve similarly good fits to a dataset. On the other hand, were q known ab initio, an optimized fit to data could be performed using expressions in terms of C_V^{BN}, C_V^{NN} and C_T^B if the dependencies of the different terms with respect to q and R hold.

If q were available from empirical data, fitting would be completely justified in the case of C_T^B given that the value of ν is unknown. On the other hand, both C_V^{BN} and C_V^{NN} are in principle completely determined. Furthermore, an independent scaling factor for each term may be added. This additional degree of freedom can be understood as a shielding effect: charges are not strictly punctual, particularly so in bonds. Therefore, the effective Coulomb term for the C_V^{BN} and C_V^{NN} terms should be different. In this regard, the weight of the bond-core term is expected to be higher than that of the core-core term, both because it is an electrostatic interaction over a shorter distance and because bonding does take place after all.

Obviously, increasing the parameters of the model leads to improved fits. Our goal, however, is achieving good fits with an insightful model. The number of parameters – or constraints thereof – will be interrogated thoroughly in the following Subsections.

Obtaining model parameters

We will exemplify the procedure through which model parameters may be obtained, and its limitations, using a simple example. In this case, we will use the original model and the charge normalization condition.

At the B3LYP/def2-TZVP level of theory, the N_2 molecule has an equilibrium internuclear distance R_{eq} of 1.091 Å, which is very close to the experimental value of 1.098 Å. We can check the possible values of ν and q for this system using a simplified form of Equation 5.18 in which we respect the original model

$$R_{eq} = \frac{4\pi^2}{7}\frac{1}{q\nu^2} \tag{5.20}$$

which, for $R_{eq} = 2.0749193$ a.u. has a solution whenever $\nu \neq 0$ and $q = 2.71807/\nu^2$. For instance, for $\nu = 1.0$ we obtain $q = 2.71807$ which seems coherent for the formal triple bond of N_2.

Let us add another source of information using Equation 5.19. At the same level of theory as before, we obtain a harmonic frequency of 2452.9 cm^{-1} which is not too far from the experimental frequency of 2358.1 cm^{-1}. The corresponding force constant is $k_e = 3.1879$ a.u. for this system. Subsequently, we can use the following simplified combination of Equation 5.19 and Equation 5.20:

$$k_e R_{eq}^5 = \frac{4\pi^2}{7}\frac{1}{q\nu^2}\Big(\frac{3\pi^2 q}{\nu^2} - \frac{7q^2 R_{eq}}{2}\Big) \tag{5.21}$$

which may be rewritten as a polynomial assuming ν, q, R_{eq} and k_e are positive, which happens to be our case,

$$14\pi^2 q\nu^2 R_{eq} + 7\nu^4 q^5 k_e - 12\pi^4 = 0 \tag{5.22}$$

We may now fix $R_{eq} = 2.0749193$ a.u. and $k_e = 3.1879$ a.u. and find the roots in terms of q and ν. The solutions are quite involved, but there are multiple equally valid roots. This is an important point that must be kept in mind throughout this Section: fitting a simple model may lead to several combinations of parameters.

Using the experimental values, the original model of Parr can be fitted to obtain $q = 2.73$ and $\nu = 1.00$ for the nitrogen molecule,[55] which is as expected very close from our first approximation in terms of Equation 5.20. As per the closeness of the calculated values, the parameters do not change noticeably when using calculated values for R_{eq} and k_e, that is, the fit is expected to be very good for the harmonic frequency of the system.

Let us use this pair of values to express the potential energy curve of N_2 as

$$W = D + V + T = D + 4\frac{2.73^2}{R} - 8\frac{2.73^2}{R} + \frac{\pi^2}{2}\frac{2.73}{R^2} = D - \frac{29.81}{R} + \frac{13.47}{R^2} \tag{5.23}$$

which has a root at $R = 0.45$ a.u., which is quite coherent as a stability limit. At $R = R_{eq}$ we get $W_{R=R_{eq}} = D - 11.30$ in atomic units. That is, with these parameters we obtain a BDE of approximately 7091 kcal/mol, a whole order of magnitude larger than the BDE – experimental or calculated – of N_2, irrespective of D (cf. Equation 5.17).

This comes to show an important notion to keep in mind: a fitted model can very hardly contain more information than it took in. R_{eq} and k_e are equilibrium properties. The BDE is *not* an equilibrium property: there is no way to know the BDE associated to a dissociation from the equilibrium properties of the system because we can not express bond energies as an operator to obtain an expectation value from the wavefunction.

Arguably, the failure showcased here is more of a failure of the parametrization strategy than a failure of the model itself. Hence, the parametrization of a model must be carefully selected according to the properties we want to extract.

We could now devise a more sophisticate parametrization strategy and include an experimental or calculated BDE value. However, this would lead to a plethora of possible solutions for this case due to overdetermination of the model. In the following Section 5.2 we will put forward a different approach.

Conceptual advantages of the Bond Charge Model potential

Having covered some of the difficulties in the obtention of parameters, one may wonder why this model is more desirable than a simple Morse potential. More gravely so, simple harmonic potentials are well-established as the classical representation of chemical bonds in force fields, which are routinely used to perform atomistic simulations of chemical systems.

The main advantage that the BCM offers is interpretation. Quite often, chemical behaviour is determined by non-classical terms (e.g. exchange or correlation), which are not easily captured in these potentials. The BCM offers a change of paradigm because it has an interpretation, and thus can accept corrections with a physical, rather than mathematical, meaning.

For instance, Morse potentials are often corrected in longer ranges in order to properly reproduce non-covalent interactions at long R. Such features are absent from the default Morse parametrization scheme, and hence missing in the analytical expression of the potential. Similarly, force fields usually consider bonded terms and non-bonded terms separately, using harmonic potentials for the former and Lennard-Jones potentials for the latter.

In fact, atomistic models in force fields usually require specific parametrization for different formal coordinations (e.g. C–C single bonds and C=C double bonds have completely different potentials with no seamless connection between them) This stems from the fact that electrons (i.e. bonds) are the ones being re-allocated during a reaction. Consequently, the static view of electrons belonging to one atom, and hence its oxidation state, can be avoided if the electron pair is taken as the main unit. This is also the reason why the qualitative VSEPR model has strong predictive power in spite of disregarding other foundational concepts: valence electrons are not formally "assigned" to atoms, but rather shared between pointwise sites.

Note that these deficiencies do not arise in the BCM treatment, because bonds are not constrained to a certain bond order and may smoothly incorporate or donate electron density to become stronger or weaker with respect to an optimum that depends on the specific parameters of the bond and its environment. A significant part of the problems that arise in the development of reactive force fields is simply absent in the BCM.

The use of electron pairs in bonds as a fundamental entity also provides a simpler link to quantum mechanics. Perfectly paired electrons minimize Pauli correlation between them, so that exchange-correlation effects, which ought to be harder to model from a classical perspective, may be minimized.

5.2 The Electron Localization Function - Bond Charge Model

Were q known, it would be possible to parametrize the BCM in terms of C_V^{BN}, C_V^{NN} and C_T^B, using the very general expressions in Equations 5.15-5.17. The advantages would be twofold. First of all, we could guarantee the physical interpretation of q, and hence constrain ν among the many possible solutions in certain cases. On the other hand, we could possibly extend our model from equilibrium properties onwards using the dependency of dq/dR.

However, defining and calculating the bond charge q is not trivial, just like defining bonds is far from a solved problem.

As it has been discussed in Chapter 4, and Section 4.3 in particular, a possible approach to localized bonding is given by the ELF, whose topology defines basins, with an associated electron population, and pseudo-atoms that contain nuclei and core electrons. Indeed, the localized depiction of chemical bonding given by this model resembles the partitioning of real space given by the ELF quite strikingly, so that we may propose a coupled model that uses some of the concepts as defined by the topology of the ELF and the fundamental ideas of the BCM.

5.2.1 Coupling Localized Bond Charges

Including the extension to heteroatomic bonds, which we will skip for the time being, the two model parameters of the BCM can be defined and obtained from the topology of the ELF.

First of all, the bond charge q associated with a covalent bond A–A is given by the integration of the electron density $\rho(r)$ in the disynaptic ELF basin $\Omega^V_{A,A}$. Effective core charges Z_A correspond to the integral over the core basins of the respective bonded atoms, Ω^C_A plus the nuclear charge, analogous to how atomic charges were obtained in the AIM framework. Thus, the electrostatic components may all be obtained. These equivalences may be applied in any context, noting that the charge equalization condition is no longer respected.

On the other hand, the effective bond path, $R_B = \nu R$, can be calculated as the length of the disynaptic bond basin $\Omega^V_{A,A}$, which will naturally be bound by the two axial core basins Ω^C_A as per its synaptic order. Simply put, it can be calculated by subtracting the radii of each of the two core basins from the total internuclear distance. Note that multiple bonds may lead to multiple disynaptic basins, each accounting for an electron pair, in agreement with the detailed discussion in Section 4.3.

Each family of terms in Equation 5.3 is discussed in depth below.

Core terms

Bearing in mind that the term D plays a minor role, as it is not determinant in relative energies and hence independent of R, it does present certain conceptual difficulties from the coupling point of view that merit some discussion.

We are attempting to couple two models in which bonds are depicted as localized entities. Accordingly, in both representations "bonds" ought to disappear when the internuclear distance R is increased enough. This much is perfectly coherent.

However, both representations do not necessarily converge when $R \to \infty$. In the BCM ansatz, D is the energy of the isolated pseudo-atoms, which we have been calling "cores" so far. In a diatomic molecule, this is pretty straightforward to interpret: there is no bond over an infinite distance, and $W(R) = D$ which must be an additive constant of atomic self-energies.

In the ELF representation, however, we may find that the topology of $\eta_{ELF}(\mathbf{r})$ changes. Recall that in the Born-Oppenheimer approximation we disregard nuclear motion: we are limited to snapshots at fixed nuclear positions. Taking two discrete values of R, the partitionings of space given by $\eta_{ELF}(\mathbf{r})$ at each R may not be isotopological. That is, basins may merge, disappear and appear freely.

Isolated atoms have distinct attractor basins, as highlighted in Subsection 4.3.3 of Section 4.3. Hence, in the coupled model D must be interpreted not as the "core" energy, even if Z represents effective "core" charges; it represents the total energy of the atomic system, including the core basin, the valence basins (which have kinetic self-energies)

and the interactions between those, with proportionality constraints such that the total energy is indeed the atomic energy for a diatomic molecule.

In general we will restrict ourselves to bond stretching and compressing around equilibrium distances, which generally turns out to be isotopological in terms of $\eta_{ELF}(\mathbf{r})$. It must be kept in mind, still, that these modifications in the topology will take place during chemical reactions.

Electrostatic terms

The formulation may be extended to heteronuclear bonds A–B without a term δ_{AB}, as we may calculate Z_A and Z_B explicitly. r_1 or α_1 may be calculated by using the position of the attractor of the bond basin $\Omega^V_{A,B}$ as a reference. However, this last point will be clarified later on, as other proposals could be valid as well (e.g. using BCPs as reference).

We may now bring back Equation 5.3 for a chemical bond as represented by a disynaptic basin connected to core basins containing two distinct nuclei A and B, thus giving an A–B bond potential as

$$W = D + V + T + XC = D + C^{BN}_{V1}\frac{q}{R} + C^{BN}_{V2}\frac{q}{R} + C^{NN}_{V}\frac{1}{R} + C^{B}_{T}\frac{q}{R^2} + XC \qquad (5.24)$$

where we expect the dependencies with respect to q and R to hold if our approach is to be of use, and a new term $XC(R)$ has been added to represent quantum effects – as well as higher order couplings – that can not be taken into account in the other terms. Explicitely written, the bond charge associated with this bond is

$$q = \int_{\Omega^V_{AB}} \rho(\mathbf{r}) d\mathbf{r} \qquad (5.25)$$

We disregard the effective core charges Z_A and Z_B because in the ELF representation core basins have almost always constant populations (cf. Equation 4.56) for a given nucleus, irrespective of the chemical environment. On the contrary, bond populations q may migrate towards lone pairs or other bonds in polyatomic systems which are not directly involved in the bonding interaction. This is why it must be underlined that charge equalization between Z and q may not be sufficient in the context of the ELF-BCM.

Kinetic terms

With respect to ν and α_1, we may merge them into the proportionality constants for the time being due to several reasons. First and foremost, we may suspect that the notion of effective bond length in 1D is limited if we are to expand the model to larger chemical systems. Hence, a new kinetic energy term must be devised that is compatible with the 3D representation of bonds given by the ELF.

In any case, we may estimate r_1 – and, by definition, r_2 – using Equation 5.14 to see whether it matches chemical intuition. That is, even in cases where $Z_A \approx Z_B$ (e.g. C and N) we expect the more electronegative atom to have more electron density polarized towards its nuclei depending on the chemical environment.

As a first approximation, for a spherical basin of radius r and volume V, we may put forward a kinetic term inspired in the homogeneous electron gas (cf. Equation 2.126):

$$T(R) = C_F \int \rho^{\frac{5}{3}}(\mathbf{r}) dV = 4\pi C_F \int \left(\frac{q}{r^3}\right)^{\frac{5}{3}} r^2 dr = 4\pi C_F q^{\frac{5}{3}} \int \frac{1}{r^3} dr = -\frac{4\pi}{3} C_F \frac{q^{\frac{5}{3}}}{r^2} = C^B_{T0}\frac{q^{\frac{5}{3}}}{R^2} \qquad (5.26)$$

in which we have assumed that the radius of the sphere $r = R_B$ and merged everything into a proportionality constant once again. Thus, the key addition is the power in q, but the dependency on the internuclear distance R is kept.

5.2.2 Validation of model assumptions

As we have put forward in the previous Subsection, we want to use ELF-derived parameters coupled to the BCM in order to have a semiclassical model in chemical terms. In this Subsection the coupled model will be tested empirically using quantitative methods from Chapter 4.

Before, it must be noted that our proposed model is, so far, semiclassical at best. As previously discussed, we hope that the usage of electron pairs as the basis of representation will minimize quantum effects or include them implicitely. On the other hand, we may safely assume that exchange and correlation effects, quantum in nature, are required for an accurate representation of chemical bonds. This is the final assumption of the model so far, which has to be added to the points discussed before.

Let us now summarize the key assumptions of the ELF-BCM approach, as presented in Equation 5.24 and anotated in Equation 5.26:

- **Atomic terms :** $D \neq f(R), \qquad D = \sum_i D_i$
- **Electrostatic terms :** $V \propto \frac{1}{R}$
- **Kinetic terms :** $T \propto \frac{q^{5/3}}{R^2}$
- **Quantum terms :** $XC \approx 0$

If all these assumptions hold for a given chemical space, we can at least assure that the foundations of the coupled model are reasonable.

With this goal in mind, we may now study the dependency of the different terms by doing a relaxed scan (i.e. a constrained geometry optimization) along a particular internal coordinate, an internuclear distance which we shall call R for simplicity. The necessary reduced density matrices can be calculated at each geometry, and the topology of $\eta_{ELF}(\mathbf{r})$ can be explored in order to partition the system exhaustively.

Afterwards, the ELF partitioning can be coupled to the IQA method, which was introduced with some detail in Subsection 4.2.3, to decompose the total energy in one-basin and two-basin terms. Recall that the total energy decomposition (cf. Equation 4.31) in the ELF-IQA approach, at the HF level, is given by

$$E = \sum_A E_{intra}^{C_A} + \sum_A E_{intra}^{V_A} + \frac{1}{2}\sum_{A,B\neq A} E_{inter}^{C_A,C_B} + \frac{1}{2}\sum_{A,B\neq A} E_{inter}^{V_A,V_B} + \sum_{A,B} E_{inter}^{C_A,V_B} \quad (5.27)$$

in which the C_A and V_A superindices indicate the nature of the ELF basin, core or valence, respectively. Recalling that only core basins contain nuclei, we may further decompose each term as

Term	Assumption
$\sum_A E_{intra}^{\Omega_A^C}$	$\approx const.$
$E_{inter}^{\Omega_A^C,\Omega_B^C}$	$\propto \frac{1}{R}$
$E_{inter}^{\Omega_A^C,\Omega_{A,B}^V}$	$\propto \frac{1}{R}$
$T_{\Omega_{A,B}^V}$	$\propto \frac{q^{5/3}}{R^2}$
$E_{xc}^{\Omega_A^C,\Omega_{A,B}^V}$	≈ 0

Table 5.1: Summary of model assumptions of the ELF-BCM approach in ELF-IQA terms.

$$
\begin{aligned}
E_{intra}^{C_A} &= V_{en}^{C_A,C_A} + V_{ee}^{C_A,C_A} + T_{C_A} \\
E_{intra}^{V_A} &= V_{ee}^{V_A,V_A} + T_{V_A} \\
E_{inter}^{C_A,C_B} &= V_{ee}^{C_A,C_B} + V_{en}^{C_A,C_B} + V_{en}^{C_B,C_A} + V_{nn}^{C_A,C_B} \\
E_{inter}^{V_A,V_B} &= V_{ee}^{V_A,V_B} \\
E_{inter}^{C_A,V_B} &= V_{ee}^{C_A,V_B} + V_{en}^{C_A,V_B}
\end{aligned}
$$

We will assume that the kinetic energy density in Equation 4.27 suffices for our interests, and all other terms have been explicitely presented in Subsection 4.2.3. In particular, our attention will be focused in the terms that arise in the simplest cases: we will consider the disynaptic $\Omega_{A,B}^V$ as the valence basin of interest, corresponding to a bond, and two core basins Ω_A^C and Ω_B^C, that are adjacent to the bond.

Let us examine now what the assumptions of the ELF-BCM approach imply for these energy terms. The core intrabasin energies $E_{intra}^{\Omega_A^C}$ must approximately be an additive constant independent from R.

Then, all the interaction terms between cores and other entities, which are electrostatic in nature, must evolve proportional to $1/R$. The electron-electron terms here are the sensitive part, because the nucleus in every core basin is effectively a point charge. Therefore, the assessment in this regard is whether the core basin can be treated as an effectively shielded nuclei. In fact, the coulombic dependency of the $E_{inter}^{\Omega_A^C,\Omega_B^C}$ term is a given considering the very small size of core basins and the predominance of the nucleus-nucleus $V_{nn}^{\Omega_A^C,\Omega_B^C}$ term. Hence, we can safely infer that this condition is always met in any reasonable chemical situation.

The kinetic energy term for the bond is perhaps the most difficult assumption, because our model infers a $1/R^2$ dependency quite a priori. However, the kinetic energy of the bond has an immediate equivalent in $T_{\Omega_{A,B}^V}$, whose evolution with R we can evaluate.

Last but not least, we did not include any quantum effects in our model. Hence, exchange and correlation terms must be zero. In ELF-IQA terms the exchange-correlation term, $E_{xc}^{C_A,V_B}$, which was introduced in Equation 4.38 but not considered for clarity in the expansion in this section, must be negligible compared to the other terms.

A summary of these assumptions has been collected in Table 5.1.

For simplicity, let us put foward a unified notation for the merged terms in the ELF-BCM approach: we shall denote $E_{intra}^{\Omega_A^C}$ as E_{intra}^{A} due to the straightforward

interpretation. We will use E_{inter}^{A-b} for $E_{inter}^{\Omega_A^C,\Omega_{A,B}^V}$, where A will now use the atomic symbol of the nuclei in the corresponding core basin, and b stands for "bond". Analogously, we will use E_{xc}^{A-b} for $E_{xc}^{\Omega_A^C,\Omega_{A,B}^V}$ and we will use T^b for $T_{\Omega_{A,B}^V}$. This notation is less rigorous but simpler to interpret as far as the association of the "bond" with a disynaptic ELF basin $\Omega_{A,B}^V$, and the interpretation of core basins as pseudoatoms, are kept in mind. Note that E_{inter}^{A-b} is a purely electrostatic term if the corresponding E_{xc}^{A-b} is negligible.

We have thus devised a way to test the key assumptions of our model in a quantitative and rigorous way, which we will use in the following Subsections. We may now explore a variety of chemical systems to ascertain whether these assumptions hold in a significant chemical space. The assumptions of our model may be appropiate for some systems and completely lackluster for others due to the sheer variability of chemical space.

Subsequently, our attempt will be twofold: validation on one hand, and acquisition of a proper domain of application in the other.

5.2.3 Empirical testing of model assumptions in covalent bonds

As a first test, we tackle a symple heteronuclear covalent bond, namely the C–X bond in a series of CH_3–X molecules. Following the proposed methodology, the geometry of the molecules was optimized at different C–X internuclear distances R at a given theory level. Then, the total energy was decomposed using a modified version of the `PROMOLDEN` code.

Calculations on methanamine

We shall commence our exploration in a single system, namely methanamine CH_3NH_2, and we will present other systems afterwards in order to be succint. In particular, we want to assure at this point that our observations are not biased by the level of theory of the electronic structure calculations, be it DFA or basis set. This is not unusual, but it is a gratuitous assumption even in this relatively simple systems. We must also assure that the ELF-IQA approach is not introducing errors that might obscure our observations.

While the IQA decomposition is exact in principle, there are numerical errors associated with the integration. The errors in the total energy are generally small ($< 1\%$) in relative terms, but such inaccuracies might be determining in our analysis if they are particularly sensitive to R. Therefore, we report the total energies and the ELF-IQA energies for methanamine at the B3LYP/6-31G(d) level in Table 5.2, which show that this does not seem to be the case for this system.

This is coherent because the energy density is clearly maximal where the density is maximal, and thus the integration error is expected to originate mostly from core densities which are relatively inactive. However, it must be noted that the errors are enough to be chemically meaningful. This issue has to be kept in mind from the practical point of view.

In terms of the ELF topology, the methanamine molecule has, as chemical intuition would infer, a disynaptic $\Omega_{C,N}^V$ basin connected to the core basins of the carbon and nitrogen nuclei, Ω_C^C and Ω_N^C respectively. A graphical representation is given in Figure 5.5 B further on. The interpretation of the ELF-IQA terms is therefore straightforward as presented in the previous Subsection.

First of all, we will examine several trends with respect to R with different basis sets and using the B3LYP DFA for CH_3NH_2. The data is presented in Table 5.3 for the

R (Å)	E DFT (a.u.)	E ELF-IQA (a.u.)	ΔE (a.u.)	ΔE (%)
1.30	-95.8337	-95.1726	0.66	-0.69
1.40	-95.8507	-95.1947	0.66	-0.68
1.50	-95.8526	-95.1844	0.67	-0.70
1.60	-95.8460	-95.1882	0.66	-0.69
1.70	-95.8348	-95.1661	0.67	-0.70
1.80	-95.8214	-95.1501	0.67	-0.70
1.90	-95.8072	-95.1484	0.66	-0.69
1.47	-95.8497	-95.1939	0.66	-0.68

Table 5.2: Energies and integration errors for the CH_3NH_2 molecule at the B3LYP/6-31G(d) level.

kinetic energy term, $T_{\Omega^V_{C,N}}$ that we shall denote T^b for simplicity, which we expect to evolve as $\propto 1/R^2$, as per our previous reasoning (cf. Equation 5.26).

R (Å)	$1/R^2$ (a.u.$^{-2}$)	B3LYP			
		6-31G(d)	6-311G(d,p)	cc-PVDZ	cc-PVTZ
1.30	0.166	3.089	3.127	3.108	3.129
1.40	0.143	2.540	2.540	2.548	2.538
1.50	0.124	2.138	2.137	2.148	2.137
1.60	0.109	1.830	1.828	1.845	1.823
1.70	0.097	1.570	1.566	1.576	1.565
1.80	0.086	1.342	1.330	1.341	1.333
1.90	0.078	1.091	1.097	1.101	1.098

Table 5.3: Internuclear distance R and kinetic energy values T^b (a.u.) for the CH_3NH_2 molecule and the B3LYP DFA using different basis sets.

Our assumption is confirmed in this case, as least-squares fits to $const. + const./R^2$ lead to very high Pearson correlation coefficients. For the different basis sets in Table 5.3, the coefficients of determination r^2 (i.e. the squared Pearson correlation coefficients), are in all cases > 0.998. The corresponding equations and coefficients are

$$\begin{aligned}
\text{6-31G(d)} &: y = 22.124x - 0.596 \quad r^2 = 0.999 \\
\text{6-311G(d,p)} &: y = 22.472x - 0.632 \quad r^2 = 0.999 \\
\text{cc-PVDZ} &: y = 22.256x - 0.602 \quad r^2 = 0.999 \\
\text{cc-PVTZ} &: y = 22.476x - 0.633 \quad r^2 = 0.998
\end{aligned}$$

that is, very similar independently of the basis set choice. Let us now examine the two

critical electrostatic terms, that is, the Coulombic interactions between the bond basin $\Omega^V_{C,N}$ and the two core basins. The data is reported in Table 5.4 for the carbon basin Ω^C_C and Table 5.5 for the nitrogen basin Ω^C_N.

R (Å)	$1/R^1$ (a.u.$^{-1}$)	B3LYP			
		6-31G(d)	6-311G(d,p)	cc-PVDZ	cc-PVTZ
1.30	0.407	-5.382	-5.395	-5.386	-5.401
1.40	0.378	-4.570	-4.567	-4.585	-4.563
1.50	0.353	-3.951	-3.948	-3.968	-3.942
1.60	0.331	-3.450	-3.445	-3.468	-3.438
1.70	0.311	-3.031	-3.027	-3.046	-3.019
1.80	0.294	-2.655	-2.653	-2.672	-2.645
1.90	0.279	-2.304	-2.301	-2.317	-2.289

Table 5.4: Internuclear distance R and carbon core-bond electrostatic energy values E^{C-b}_{inter} (a.u.) for the CH_3NH_2 molecule and the B3LYP DFA using different basis sets.

R (Å)	$1/R^1$ (a.u.$^{-1}$)	B3LYP			
		6-31G(d)	6-311G(d,p)	cc-PVDZ	cc-PVTZ
1.30	0.407	-7.809	-7.895	-7.841	-7.908
1.40	0.378	-6.527	-6.523	-6.542	-6.520
1.50	0.353	-5.572	-5.570	-5.591	-5.569
1.60	0.331	-4.800	-4.796	-4.824	-4.785
1.70	0.311	-4.131	-4.124	-4.141	-4.122
1.80	0.294	-3.512	-3.496	-3.513	-3.500
1.90	0.279	-2.852	-2.867	-2.860	-2.866

Table 5.5: Internuclear distance R and nitrogen core-bond electrostatic energy values E^{N-b}_{inter} (a.u.) for the CH_3NH_2 molecule and the B3LYP DFA using different basis sets.

Again, we see that the obtained values correlate very well with a simple *const.* + *const.*$/R$ equation, with $r^2 > 0.997$ in all cases. In particular, the equations for each case are

$$\begin{aligned}
\text{6-31G(d)} &: y = -23.623x + 4.313 \quad r^2 = 0.998 \\
\text{6-311G(d,p)} &: y = -23.763x + 4.316 \quad r^2 = 0.997 \\
\text{cc-PVDZ} &: y = -23.616x + 4.291 \quad r^2 = 0.997 \\
\text{cc-PVTZ} &: y = -23.827x + 4.390 \quad r^2 = 0.997
\end{aligned}$$

for E^{C-b}_{inter} with respect to R, and

$$
\begin{aligned}
\text{6-31G(d)} &: y = -37.637x + 7.619 \quad r^2 = 0.998 \\
\text{6-311G(d,p)} &: y = -38.094x + 7.763 \quad r^2 = 0.997 \\
\text{cc-PVDZ} &: y = -37.817x + 7.664 \quad r^2 = 0.998 \\
\text{cc-PVTZ} &: y = -38.160x + 7.785 \quad r^2 = 0.997
\end{aligned}
$$

for E_{inter}^{N-b} with respect to R. In both cases the fitted equations are quite similar independently from the basis set choice, and in all cases follow the desired dependency with R. Note that the interaction with the nitrogen core is approximately 60% larger (at $R = 1$) than the interaction with the carbon core.

This is apparently counterintuitive. Intuitively, we expect N to be more electronegative than C, and hence its effective positive charge should be more shielded. On the other hand, nitrogen has a larger atomic number (by a mere 16%) and a similar core configuration $1s^2$. We may rationalize that the additional electron density pulled by the nitrogen atom is not shielding the interaction effectively because it is invested in the lone pair. Using Equation 5.14, we would obtain a distance of approximately 60% of R between the bond charge and the nitrogen core at $R = 1$.

However, the superiority of the nitrogen term depends starkly on R, becoming significantly reduced as it increases, in a way trending towards the atomic number increase. We can interpret this from a chemical point of view in this case, assuming shielding effects due to the chemical environment must disappear as the bond is progressively stretched until it breaks homolytically. We could expect such effects to diminish less dramatically in more ionic bonds, which tend to break heterolytically.

In any case, we may now investigate the exchange correlation term in E_{inter}^{C-b}, reported in Table 5.6, and the analogous term for the nitrogen core, reported in Table 5.7. At first glance, note that the E_{xc}^{C-b} and E_{xc}^{N-b} terms are quite insignificant compared to the classical interaction terms.

R (Å)	$1/R^2$ (a.u.$^{-2}$)	B3LYP			
		6-31G(d)	6-311G(d,p)	cc-PVDZ	cc-PVTZ
1.30	0.166	-0.062	-0.062	-0.063	-0.062
1.40	0.143	-0.052	-0.052	-0.052	-0.051
1.50	0.124	-0.043	-0.043	-0.044	-0.043
1.60	0.109	-0.037	-0.037	-0.037	-0.037
1.70	0.097	-0.032	-0.032	-0.032	-0.031
1.80	0.086	-0.027	-0.027	-0.028	-0.027
1.90	0.078	-0.023	-0.023	-0.024	-0.023

Table 5.6: Internuclear distance R and carbon core-bond exchange-correlation energy values E_{xc}^{C-b} (a.u.) for the CH_3NH_2 molecule and the B3LYP DFA using different basis sets.

The tiny contribution of the exchange-correlation terms to the interbasin energies is in agreement with our assumption. However, it is also found that the term scales

R (Å)	$1/R^2$ (a.u.$^{-2}$)	B3LYP			
		6-31G(d)	6-311G(d,p)	cc-PVDZ	cc-PVTZ
1.30	0.166	-0.086	-0.088	-0.087	-0.088
1.40	0.143	-0.068	-0.068	-0.069	-0.068
1.50	0.124	-0.055	-0.055	-0.055	-0.055
1.60	0.109	-0.045	-0.045	-0.046	-0.045
1.70	0.097	-0.037	-0.037	-0.037	-0.037
1.80	0.086	-0.030	-0.029	-0.029	-0.030
1.90	0.078	-0.021	-0.022	-0.022	-0.022

Table 5.7: Internuclear distance R and nitrogen core-bond exchange-correlation energy values E_{xc}^{N-b} (a.u.) for the CH_3NH_2 molecule and the B3LYP DFA using different basis sets.

proportional to $1/R^2$ very neatly ($r^2 \approx 0.999$). In the spirit of the previous terms, the fitted equations are reported below, first for the carbon-bond case, E_{xc}^{C-b}

$$\begin{aligned} \text{6-31G(d)} &: y = -0.436x + 0.011 \quad r^2 = 0.999 \\ \text{6-311G(d,p)} &: y = -0.439x + 0.011 \quad r^2 = 0.999 \\ \text{cc-PVDZ} &: y = -0.434x + 0.010 \quad r^2 = 0.999 \\ \text{cc-PVTZ} &: y = -0.439x + 0.012 \quad r^2 = 0.999 \end{aligned}$$

and for the E_{xc}^{N-b} term with respect to R,

$$\begin{aligned} \text{6-31G(d)} &: y = -0.714x + 0.033 \quad r^2 = 0.999 \\ \text{6-311G(d,p)} &: y = -0.734x + 0.035 \quad r^2 = 0.998 \\ \text{cc-PVDZ} &: y = -0.726x + 0.034 \quad r^2 = 0.999 \\ \text{cc-PVTZ} &: y = -0.731x + 0.035 \quad r^2 = 0.998 \end{aligned}$$

Once more, the coefficients in the fitted equation are 60% larger for the nitrogen core, in agreement with what was observed before. The basis set choice does not seem to play an important role either, so that we can assume that basis set effects are not relevant for our interests as long as a reasonable basis set is used (i.e. double-ζ or larger).

Figure 5.3 collects all the different terms at the B3LYP/6-31G(d) level, including the complete intrabasin term for the bond, E_{intra}^{b}. It can be readily appreciated how minuscule the exchange-correlation terms are with respect to the other major components. For more details, Figure 5.4 A presents the kinetic term of the bond, T^b directly versus $1/R^2$, showcasing the correlation and the accuracy of the fit. Analogously, Figure 5.4 B presents the two electrostatic terms, E_{inter}^{C-b} and E_{inter}^{N-b} against $1/R$. Once more, the fit is remarkably accurate.

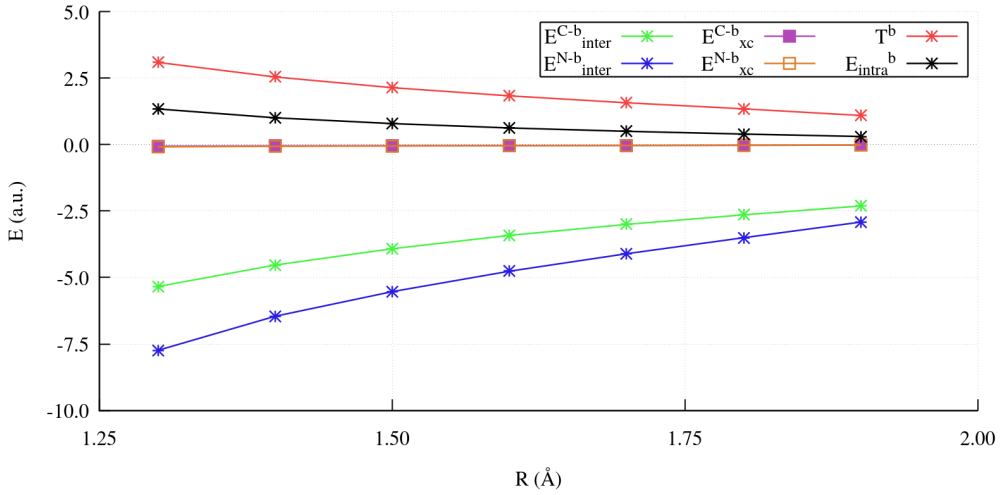

Figure 5.3: Energy terms at different internuclear distances R for the CH_3NH_2 molecule at the B3LYP/6-31G(d) level of theory.

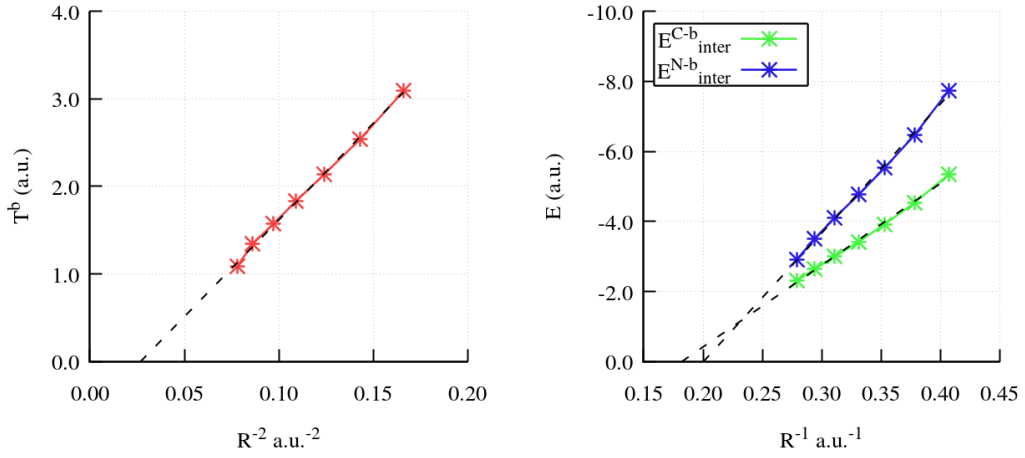

A) B)

Figure 5.4: Energy terms at different internuclear distances R for the CH_3NH_2 molecule at the B3LYP/6-31G(d) level of theory. **A)** Intrabasin kinetic energy, **B)** bond-core electrostatic energy terms.

Last but not least we need to ascertain that the core energies are indeed approximately constant with respect to R. Table 5.8 collects the values for the carbon and nitrogen core basins. The energy values are quite high due to the strong electron-nuclei interactions. There is a certain degree of fluctuation, but we can safely assume that most of it is due to numerical errors, as no significant trends can be appreciated in any direction. Core populations are also extremely stable independently of R.

Note that, far from trivial, the fact that these energies are stable implies that all the shifting additive constants in the fits to the kinetic and the interaction energies may be gathered in the shifting term D of the BCM. Were this not the case, we would have to fit our dependencies to unshifted equations ($\propto 1/R^2$ and $\propto 1/R$) without any shifting in the origin. Luckily, we find that cores are relatively stable in this context, and thus our usage of additive constants (i.e. $const. + const./R$ and $const. + const./R^2$) is justified.

R (Å)	E^C_{intra} (a.u.)	E^N_{intra} (a.u.)
1.20	37.322	51.318
1.30	37.284	51.293
1.40	37.265	51.288
1.50	37.256	51.297
1.60	37.254	51.317
1.70	37.256	51.334
1.80	37.259	51.354
1.90	37.261	51.368

Table 5.8: Internuclear distance R and intrabasin core energy values, E^C_{intra} and E^N_{intra} for the CH_3NH_2 molecule at the B3LYP/6-31G(d) level.

Thus, at least for the methanamine molecule, our assumptions as presented and interpreted in Subsection 5.2.2 all seem to hold remarkably well.

Covalent CH_3-X bonds and lone pairs

The same methodology was used to study another three CH_3-X bonds, with various degrees of polarity and different ELF topologies: CH_3CH_3, CH_3OH and CH_3F. The ELF topologies of all systems, including CH_3NH_2, are represented in Figure 5.5 for reference. The ELF representation matches, once again, chemical insight at first glance, and thus we can identify the ELF-IQA terms without problems.

Integration errors are, as in the previous case, relatively small with respect to the total energies. The values for all three systems are reported in Tables 5.9 to 5.11. Once more, the errors are relatively small and do not show trends with respect to R, and therefore we can safely assume that the decomposition is quantitative.

We may now explore the dependency of the different terms with R as before, in this case in a rigorous interval of points between $0.9R_{eq}$ and $1.1R_{eq}$. Analogous results were obtained for all systems: the assumptions that have been presented in detail for CH_3NH_2 before all hold for the other molecules here considered. We will tackle the terms in an ordered manner once again. In this case, we will also include the terms corresponding to lone pairs, which will be denoted by the lp superscript.

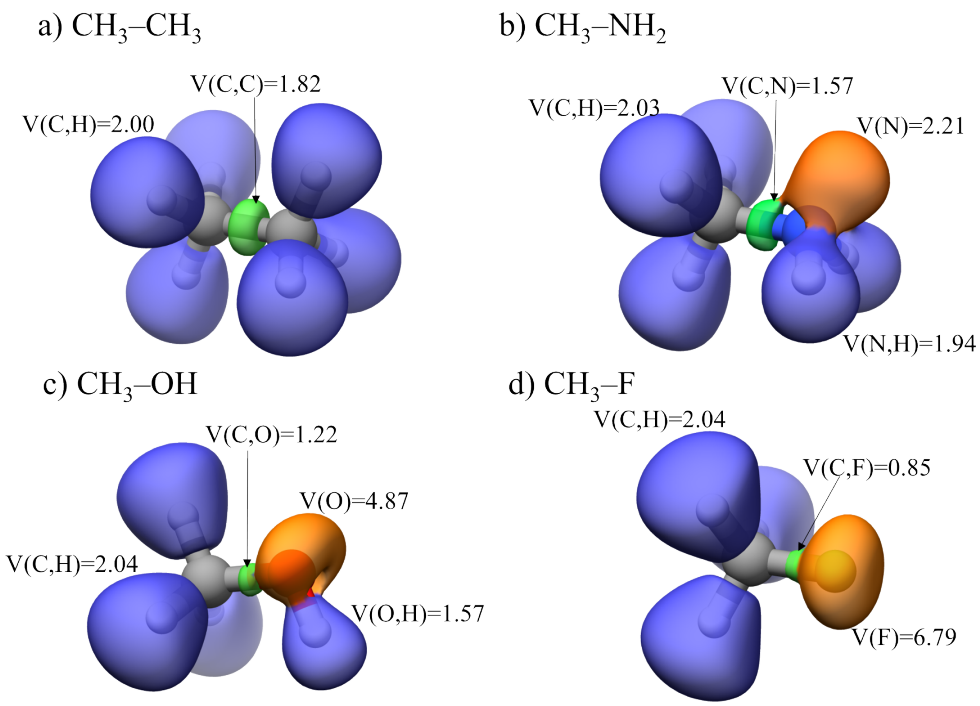

Figure 5.5: Isosurfaces of $\eta_{ELF}(\mathbf{r}) = 0.80$ a.u. for different molecules calculated at the B3LYP/6-31G(d) level: **A)** CH_3CH_3 **B)** CH_3NH_2 **C)** CH_3OH **D)** CH_3F. ELF basins are colored according to their classification: hydrogenoid basins are colored blue, core basins are colored purple, monosynaptic basins are colored orange and disynaptic basins are colored green. Basin populations in electrons are reported assigned to the respective basins.

R (Å)	E DFT (a.u.)	E ELF-IQA (a.u.)	ΔE (a.u.)	ΔE (%)
1.20	-79.7309	-79.1050	0.63	-0.78
1.30	-79.7910	-79.1681	0.62	-0.78
1.40	-79.8200	-79.2057	0.61	-0.77
1.50	-79.8299	-79.2150	0.61	-0.77
1.60	-79.8284	-79.2051	0.62	-0.78
1.70	-79.8200	-79.1952	0.62	-0.78
1.80	-79.8080	-79.1819	0.63	-0.78
1.53	-79.8304	-79.2060	0.62	-0.78

Table 5.9: Energies and integration errors for the CH_3CH_3 molecule at the B3LYP/6-31G(d) level.

R (Å)	E DFT (a.u.)	E ELF-IQA (a.u.)	ΔE (a.u.)	ΔE (%)
1.20	-115.6712	-114.9549	0.72	-0.62
1.30	-115.7043	-115.0152	0.69	-0.60
1.40	-115.7142	-115.0347	0.68	-0.59
1.50	-115.7112	-115.0398	0.67	-0.58
1.60	-115.7013	-115.0416	0.66	-0.57
1.70	-115.6877	-115.0305	0.66	-0.57
1.80	-115.6727	-115.0368	0.64	-0.55
1.90	-115.6573	-114.9960	0.66	-0.57
1.41	-115.7144	-115.0451	0.67	-0.58

Table 5.10: Energies and integration errors for the CH_3OH molecule at the B3LYP/6-31G(d) level.

Bond kinetic energies T^b fitted agains $const. + const./R^2$ give rise to very good determination coefficients, in all cases $r^2 > 0.997$. Lone pair kinetic energies, T^{lp}, are notably worse, orbiting $r^2 \approx 0.99$. This implies that the approximate dependency we have chosen for the bond is suitable, but not necessarily so for the lone pairs on either end of the scrutinized bond. Then again, this is to be expected. In any case, the slopes on the lone pair contributions are significantly lower, while the intercept values are larger. That is, in relative terms, the kinetic energies of lone pairs do not change dramatically as the adjacent bond elongates. Fitted equations are presented in Table 5.12.

In fact, for $R = R_{eq}$, the kinetic energies of lone pairs are quite small, at least one order of magnitude smaller than those of bonds in spite of the somewhat comparable integrated electron density. Interestingly, the slopes decrease from N to F, while the intercepts increase. This suggests that the lone pair in the less electronegative nitrogen is more sensitive to the bond to the carbon atom, while lone pairs in more electronegative

R (Å)	E DFT (a.u.)	E ELF-IQA (a.u.)	ΔE (a.u.)	ΔE (%)
1.10	-139.6398	-138.9749	0.66	-0.48
1.20	-139.7030	-139.0135	0.69	-0.49
1.30	-139.7288	-139.0521	0.68	-0.48
1.40	-139.7337	-139.0445	0.69	-0.49
1.50	-139.7272	-139.0372	0.69	-0.49
1.60	-139.7146	-139.0368	0.68	-0.49
1.70	-139.6991	-138.9389	0.76	-0.54
1.38	-139.7339	-139.0410	0.69	-0.50

Table 5.11: Energies and integration errors for the CH_3F molecule at the B3LYP/6-31G(d) level.

atoms are less involved in the interaction.

	CH_3CH_3	
T^b	$y = 15.635x + 0.264$	$r^2 = 1.000$
	CH_3NH_2	
T^b	$y = 21.946x - 0.585$	$r^2 = 0.997$
T^{lp}	$y = -9.295x + 4.551$	$r^2 = 0.984$
	CH_3OH	
T^b	$y = 23.582x - 1.329$	$r^2 = 1.000$
T^{lp}	$y = -5.629x + 5.877$	$r^2 = 0.992$
	CH_3F	
T^b	$y = 22.259x - 1.819$	$r^2 = 0.999$
T^{lp}	$y = -3.754x + 6.808$	$r^2 = 0.982$

Table 5.12: Fitted equations for bond kinetic energy values T^b (a.u.) and lone pair kinetic energy values T^{lp} (a.u) *versus* $1/R^2$ (a.u.$^{-2}$). Coefficients of determination r^2 are given for each fitted equation.

	CH_3CH_3	
E_{inter}^{C-b}	$y = -21.717x + 2.860$	$r^2 = 0.999$
	CH_3NH_2	
E_{inter}^{C-b}	$y = -23.366x + 4.246$	$r^2 = 0.995$
E_{inter}^{N-b}	$y = -37.311x + 7.535$	$r^2 = 0.996$
E_{inter}^{N-lp}	$y = 20.609x - 16.949$	$r^2 = 0.994$
	CH_3OH	
E_{inter}^{C-b}	$y = -23.329x + 5.375$	$r^2 = 0.996$
E_{inter}^{O-b}	$y = -46.533x + 11.693$	$r^2 = 0.999$
E_{inter}^{O-lp}	$y = 16.219x - 20.700$	$r^2 = 1.000$
	CH_3F	
E_{inter}^{C-b}	$y = -20.205x + 5.369$	$r^2 = 0.997$
E_{inter}^{F-b}	$y = -47.220x + 13.608$	$r^2 = 0.998$
E_{inter}^{F-lp}	$y = 10.664x - 22.138$	$r^2 = 0.988$

Table 5.13: Fitted equations for bond-core interaction energy values E_{inter}^{A-b} (a.u) and lone pair-core interaction energy values E_{inter}^{A-lp} (a.u) *versus* $1/R$ (a.u.$^{-1}$). Coefficients of determination r^2 are given for each fitted equation.

As a final remark, note that the fitted equation for methanamine is nearly identical to the one reported previously, which is to be expected since the only difference is the range of R considered.

Interbasin terms are fitted to *const.* + *const.*/R once again. Interactions between bonds and cores E_{inter}^{A-b} all present excellent coefficients of determination $r^2 > 0.995$. The corresponding equations and r^2 values are reported in Table 5.13 for all molecules. Noteworthily, terms with the carbon core are all relatively similar in slope and intercept,

suggesting a degree of transferability. Terms in which the heteroatom is involved show a definite increase in magnitude as we move from N to F, which then again is expected given the increased electronegativity and atomic charge.

As in the previous case, examining the behavior of lone pairs is more difficult due to the slightly worsened coefficients of determination ($r^2 < 0.99$ for the lone pair in CH_3F). However, for the most part it seems that the reasoning in the kinetic term applies as well: slopes are significantly reduced, as expected due to the limited interplay of the lone pair upon bond elongation, while intercepts skyrocket.

We may tentatively incorporate the empirical values of the bond charge q_1 and shielding electron density q_2 into our model, calculated by integrating the electron density over the corresponding basins, i.e. q_1 in $\Omega^V_{A,B}$ (or Ω^V_A for lone pair terms) and q_2 in Ω^C_A. The resulting fits are collected in Table 5.14 and exhibit analogous features.

Most notably, intercepts in all interaction terms between cores and bonds are significantly reduced and coefficients of determination are well kept over the $r^2 = 0.995$ mark. Proportions are kept across the dataset. Lone pair terms are significantly worse in this case, while intercepts increase notably. We may infer that lone pairs are affected by R more starkly through q_1, that is, the electron density transfer to or from the bond. Not much can be said at this point, however.

CH_3CH_3		
E^{C-b}_{inter}	$y = -2.672x + 1.085$	$r^2 = 0.998$
CH_3NH_2		
E^{C-b}_{inter}	$y = -2.785x - 0.712$	$r^2 = 0.999$
E^{N-b}_{inter}	$y = -4.422x - 0.369$	$r^2 = 0.997$
E^{N-lp}_{inter}	$y = 13.387x - 32.141$	$r^2 = 0.956$
CH_3OH		
E^{C-b}_{inter}	$y = -2.953x - 0.441$	$r^2 = 1.000$
E^{O-b}_{inter}	$y = -5.851x + 0.169$	$r^2 = 0.997$
E^{O-lp}_{inter}	$y = 5.441x - 25.311$	$r^2 = 0.992$
CH_3F		
E^{C-b}_{inter}	$y = -2.960x - 9.292$	$r^2 = 1.000$
E^{F-b}_{inter}	$y = -6.700x + 0.358$	$r^2 = 0.999$
E^{F-lp}_{inter}	$y = 3.581x - 24.768$	$r^2 = 0.954$

Table 5.14: Fitted equations for bond-core interaction energy values E^{A-b}_{inter} (a.u) and lone pair-core interaction energy values E^{A-lp}_{inter} (a.u) *versus* q_1q_2/R (e^2/a.u.). Coefficients of determination r^2 are given for each fitted equation.

CH_3CH_3		
E^{C-b}_{xc}	$y = -0.360x + 0.068$	$r^2 = 0.998$
CH_3NH_2		
E^{C-b}_{xc}	$y = -0.329x + 0.072$	$r^2 = 0.989$
E^{N-b}_{xc}	$y = -0.538x + 0.132$	$r^2 = 0.986$
E^{N-lp}_{xc}	$y = 0.233x - 0.223$	$r^2 = 0.980$
CH_3OH		
E^{C-b}_{xc}	$y = -0.305x + 0.077$	$r^2 = 0.989$
E^{O-b}_{xc}	$y = -0.502x + 0.142$	$r^2 = 0.991$
E^{O-lp}_{xc}	$y = 0.102x - 0.222$	$r^2 = 0.980$
CH_3F		
E^{C-b}_{xc}	$y = -0.301x + 0.088$	$r^2 = 0.988$
E^{F-b}_{xc}	$y = -0.452x + 0.144$	$r^2 = 0.983$
E^{F-lp}_{xc}	$y = 0.087x - 0.232$	$r^2 = 0.935$

Table 5.15: Fitted equations for bond-core interaction energy values E^{A-b}_{xc} (a.u) and lone pair-core interaction energy values E^{A-lp}_{xc} (a.u) *versus* $1/R^2$ (a.u.$^{-2}$). Coefficients of determination r^2 are given for each fitted equation.

Finally, fitted equations for the exchange-correlation terms are reported in Table 5.15. At a first glance, the proportionality constants are shown to be greatly reduced with respect to all other terms, in agreement with our previous reasoning and our model assumption. While coefficients of determination are still reasonably high, not much can be said about them. In any case, not much ought to be said about them because our main concern is that the terms are negligible with respect to the other terms, and this seems to be the case.

Therefore, the key assumptions of the ELF-BCM approach are shown to be valid for the chemical space herewith, which spawns different CH_3-X covalent bonds with different polarities and topological features. Consequently, we can expect the model to be a reasonable choice for describing covalent bonds as the ones reported here.

5.2.4 Empirical testing of model limitations

In the previous Subsection we have empirically validated our model using ELF-IQA energy decomposition, which justifies its usage within a certain chemical space. On the other hand, it seems coherent to think that the ELF-BCM simply can not describe certain chemical bonds properly.

Such an idea does not arise from mathematical or formal limitations as much as it does from purely conceptual reasons: we are representing bonds as negatively charged particles confined between two Coulombic potentials. While this seems reasonable – and valid, so far – for covalent bonds, we can expect it to break down in other bonding regimes.

Thus, just like in the previous Subsection we have attempted to validate our model empirically, we will now try to find and understand when and why our assumptions break down. We will use the same methodology that was presented in Subsection 5.2.2, but focus in far wilder chemical species: BH_3NH_3, a classic example of dative bonding; BeH_2NH_3, CH_3Li and Li_2. Our investigation will be focused in the B–N, Be–N, C–Li and Li–Li bonds respectively. The ELF representations of these four systems is given in Figure 5.6. Coherently, we expect more delocalized bonds to strain our model further from ideality, and we happily note that some of the bond basins have significantly increased volumes, notably those involving Li atoms.

Ideal ionic bonds will not be considered for the time being because they are formally unattainable and do not present proper ELF topologies that we can use with our ELF-IQA scheme. The question of ionicity and ideal ionic bonds will be discussed in Chapter 6.2.

The raw data for these four systems is collected in Table 5.18, for the kinetic and exchange-correlation parts, and Table 5.19 for the electrostatic terms. The corresponding fitted equations are given in Table 5.16 and 5.17. Let us begin with the first three systems and reserve Li_2, which is clearly anomalous, for last.

In the kinetic term, we observe remarkably good fits for the C–Li bond in CH_3Li and the Be–N bond in BeH_2NH_3, both of which present a coefficient of determination $r^2 > 0.995$. The dative B–N bond in BH_3NH_3 is substantially worse, being the worst fit so far even with respect to lone pairs in the previous Subsection, not approaching the $r^2 = 0.99$ mark at all. Therefore, we can safely assume that the $\propto 1/R^2$ dependency is not valid in this case. In the case of CH_3Li we see that the slope of the fitted model is of the same magnitude as the ones reported in the previous Subsection. Following previous observations, we can suggest that the C–Li bond is more polarized than any of the previous ones. Recall that a small slope can be related with less effect of bond stretching on the electronic structure of the bond, and thus points to heterolytic bond breaking and strongly polarized bonds.

Regarding the electrostatic interbasin terms, we find good fits for all three systems as well except for the interaction between the bond basin and the Li core, which is once again much worse. On the other hand, this interaction is shown to be far less important than the one arising from the carbon core in CH_3Li, and the interbasin term so far by about an order of magnitude. This further corroborates our hypothesis regarding the polarity of the bond. If we use the values around $R = 1$ Å (close to R_{eq}) in Equation 5.14, we obtain

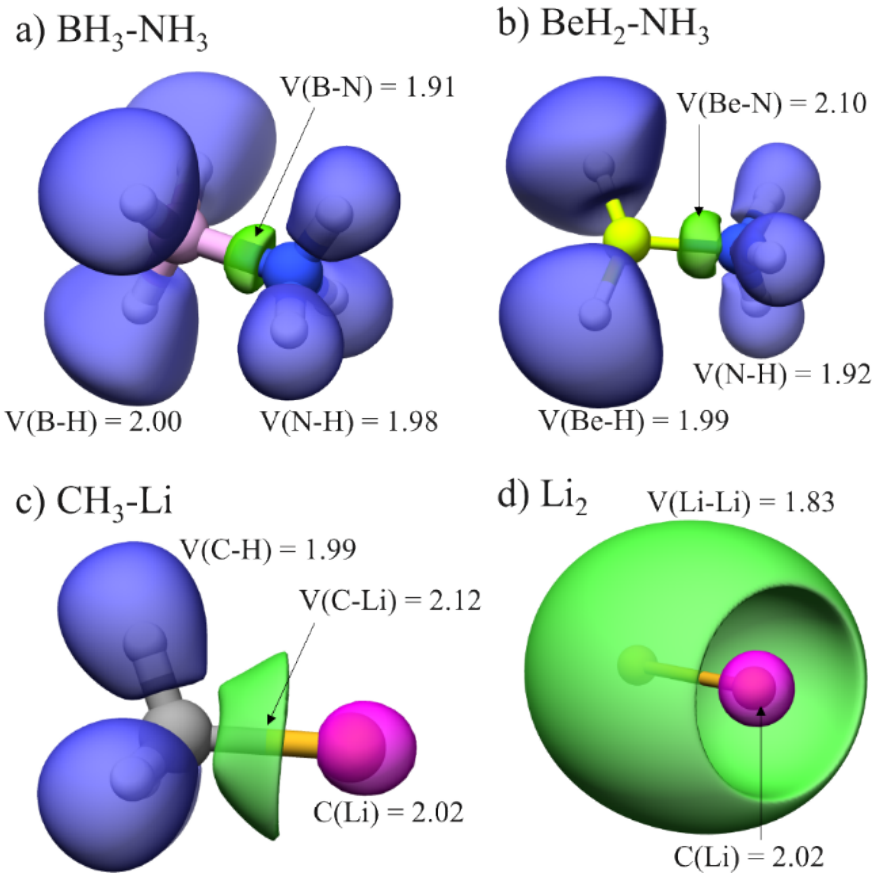

Figure 5.6: Isosurfaces of $\eta_{ELF}(\mathbf{r}) = 0.80$ a.u. for different molecules calculated at the B3LYP/6-31G(d) level: **A)** BH_3NH_3 **B)**BeH_2NH_3 **C)** CH_3Li **D)** Li_2. ELF basins are colored according to their classification: hydrogenoid basins are colored blue, core basins are colored purple, monosynaptic basins are colored orange and disynaptic basins are colored green. Basin populations are reported with arrows.

a $r_1/R = 0.85$ approximately, suggesting a strongly displaced bond charge placement. The slope for the term arising from the carbon core is similar to that of CH_3F.

The slopes in BH_3NH_3 are significantly smaller than those reported before, suggesting that the electrostatic interaction is less important in bond stability in this case. On the other hand, note that the interbasin term for lone pairs is positive, as seen in the previous Subsection. Thus, the fact that the interactions with both cores is now stabilizing can be understood as arising from the dative interaction, and thus highlights an interpretation on the dative reactivity of lone pairs which may be explored in the future. Values are significantly reduced in BeH_2NH_3, which is surprising considering the increase in q at R_{eq}. Note that also the corresponding kinetic energy term was smaller than in BH_3NH_3. In a way, we could expect the terms related to the bond to be lesser in the beryllium adduct considering that BeH_2 is a weaker Lewis acid than BH_3.

Finally, exchange-correlation terms are shown to be, once more, approximately two orders of magnitude smaller than the corresponding interbasin and kinetic terms. Consequently, we may consider such effects as negligible in the first three molecules in

this Subsection. All things considered, the ELF-BCM assumptions seem reasonably well founded for these systems.

	BH_3NH_3	
T^b	$y = 8.596x + 1.966$	$r^2 = 0.966$
	BeH_2NH_3	
T^b	$y = 6.286x + 2.378$	$r^2 = 0.995$
	CH_3Li	
T^b	$y = 15.157x + 0.542$	$r^2 = 0.998$
	Li_2	
T^b	$y = 0.019x - 0.000$	$r^2 = 0.980$

Table 5.16: Fitted equations for bond kinetic energy values T^b (a.u.) *versus* $1/R^2$ (a.u.$^{-2}$). Coefficients of determination r^2 are given for each fitted equation.

	BH_3NH_3	
E_{inter}^{B-b}	$y = -13.479x + 1.698$	$r^2 = 0.998$
E_{inter}^{N-b}	$y = -12.130x - 4.234$	$r^2 = 0.950$
	BeH_2NH_3	
E_{inter}^{Be-b}	$y = -6.603x + 0.563$	$r^2 = 0.998$
E_{inter}^{N-b}	$y = -8.269x - 6.116$	$r^2 = 0.992$
	CH_3Li	
E_{inter}^{C-b}	$y = -19.650x - 0.423$	$r^2 = 0.999$
E_{inter}^{Li-b}	$y = -3.686x + 0.260$	$r^2 = 0.958$
	Li_2	
E_{inter}^{Li-b}	$y = -0.003x + 0.000$	$r^2 = 0.564$

Table 5.17: Fitted equations for bond-core interaction energy values E_{inter}^{A-b} (a.u) *versus* $1/R$ (a.u.$^{-1}$). Coefficients of determination r^2 are given for each fitted equation.

The Li_2 molecule

The case of Li_2, however, is a clear outlier. Strikingly, the values for all the relevant terms (cf. Tables 5.18 and 5.19) are several orders of magnitude (up to five) smaller than all other reported values. In other words, the molecule is fundamentally atomic, in the sense that the total energy is given almost strictly by the sum of the intrabasin core terms.

Figure 5.7 summarizes the inadequacies quite directly: the significant reduction in all terms makes the exchange-correlation term significantly more relevant in relative terms. This is in spite of the fact that the exchange-correlation term is also reduced, albeit less dramatically, with respect to other systems. On the other hand, the trends in the T^b and E_{inter}^{Li-b} adjust to the proposed dependencies with R far worse than any other terms considered so far ($r^2 = 0.980$ and 0.564, respectively). Consequently, we can not deem the ELF-BCM approach suitable for the Li_2 molecule.

On a brighter note, this is hardly surprising. As shown in Figure 5.6, the ELF depiction of Li_2 is significantly different from the expected representation. The Li–Li bond is far more delocalized, surrouding the cores as one would expect in a metallic bonding regime. This is also in agreement with our observation regarding the energy terms: Li_2 is a metallic bond, and thus better described as an atomic system in which some electron density is delocalized over space, as in the sea of electrons depiction that was discussed in Chapter 1. Therefore, it seems perfectly coherent that a localized model such as the BCM does not resemble this situation.

Other details, as the lengthy equilibrium distance of Li_2, the far superior volume estimate of the ELF bond basin, and the fact that the bond charge q obtained by integration is nearly independent from R all suggest that the physics underlying the Li–Li bond are nothing like our semiclassical depiction of a localized bond charge.

R (Å)	$1/R^2$ (a.u.$^{-2}$)	BH_3NH_3 T^b (a.u.)	E_{xc}^{B-b} (a.u.)	E_{xc}^{N-b} (a.u.)
1.40	0.143	3.231	-0.038	-0.118
1.50	0.124	3.007	-0.029	-0.112
1.60	0.109	2.871	-0.021	-0.109
1.70	0.097	2.794	-0.016	-0.109
1.80	0.086	2.752	-0.011	-0.011
1.67	0.101	2.818	-0.017	-0.109
R (Å)	$1/R^2$ (a.u.$^{-2}$)	BeH_2NH_3 T^b (a.u.)	E_{xc}^{Be-b} (a.u.)	E_{xc}^{N-b} (a.u.)
1.50	0.124	3.169	-0.027	-0.125
1.60	0.109	3.053	-0.021	-0.122
1.70	0.097	2.987	-0.016	-0.120
1.80	0.086	2.927	-0.012	-0.118
1.90	0.078	2.866	-0.009	-0.117
1.79	0.087	3.010	-0.017	-0.122
R (Å)	$1/R^2$ (a.u.$^{-2}$)	CH_3Li T^b (a.u.)	E_{xc}^{C-b} (a.u.)	E_{xc}^{Li-b} (a.u.)
1.70	0.097	1.997	-0.086	-0.043
1.80	0.086	1.853	-0.081	-0.037
1.90	0.078	1.726	-0.077	-0.031
2.00	0.070	1.616	-0.072	-0.027
2.10	0.063	1.508	-0.067	-0.023
2.20	0.058	1.415	-0.063	-0.019
2.30	0.053	1.330	-0.060	-0.016
1.98	0.071	1.632	-0.073	-0.028
R (Å)	$1/R^2$ (a.u.$^{-2}$)	Li_2 T^b (a.u.)	E_{xc}^{Li-b} (a.u.)	
2.40	0.0486	0.000698	-0.0000790	
2.50	0.0448	0.000636	-0.0000730	
2.60	0.0414	0.000583	-0.0000680	
2.70	0.0384	0.000515	-0.0000610	
2.80	0.0357	0.000424	-0.0000510	
2.90	0.0333	0.000413	-0.0000510	
3.00	0.0311	0.000395	-0.0000490	
3.10	0.0291	0.000318	-0.0000410	

Table 5.18: Internuclear distance R and bond kinetic energies T^b (a.u.) and core-bond exchange-correlation energy values E_{xc}^{A-b} (a.u.) at the B3LYP/6-31G(d) level.

Estimation of model limitations

It has been shown that, as somewhat expected, the ELF-BCM approach is suitable for localized bonding regimes, stretching all the way to dative bonds but failing completely in metallic systems. However, as metallic and localized character are somewhat diffuse, it is desirable to find quantitative descriptors from the wavefunction or the electron density that we can use to anticipate when our model is suitable and when it is not.

From the local point of view, as extensively discussed in Chapter 4, chemical bonds have historically been characterized by studying the properties of the corresponding BCP (e.g. the bond ellipticity defined in Equation 4.11). Among them, a bond metallicity descriptor ξ_{BCP}^m has been previously defined in the literature [57] as:

$$\xi_{BCP}^m = \frac{36}{5}(3\pi^2)^{2/3}\ \frac{\rho(\mathbf{r}_{BCP})^{5/3}}{\nabla^2\rho(\mathbf{r}_{BCP})} \tag{5.28}$$

which is only defined for positive values of the Laplacian at the BCP, $\nabla^2\rho(\mathbf{r}_{BCP})$. A

R (Å)	$1/R$ (a.u.$^{-1}$)	BH_3NH_3 E^b_{intra} (a.u.)	E^{B-b}_{inter} (a.u.)	E^{N-b}_{inter} (a.u.)
1.40	0.378	1.430	-3.417	-8.915
1.50	0.353	1.290	-3.045	-8.454
1.60	0.331	1.195	-2.742	-8.157
1.70	0.311	1.135	-2.493	-7.988
1.80	0.294	1.103	-2.290	-7.916
1.67	0.317	1.153	-2.567	-8.039
R (Å)	$1/R$ (a.u.$^{-1}$)	BeH_2NH_3 E^b_{intra} (a.u.)	E^{Be-b}_{inter} (a.u.)	E^{N-b}_{inter} (a.u.)
1.50	0.353	1.397	-1.918	-9.054
1.60	0.331	1.331	-1.768	-8.824
1.70	0.311	1.287	-1.641	-8.676
1.80	0.294	1.254	-1.529	-8.567
1.90	0.279	1.219	-1.425	-8.420
1.79	0.295	1.293	-1.650	-8.704
R (Å)	$1/R$ (a.u.$^{-1}$)	CH_3Li E^b_{intra} (a.u.)	E^{C-b}_{inter} (a.u.)	E^{Li-b}_{inter} (a.u.)
1.70	0.311	1.046	-5.659	-0.911
1.80	0.294	0.954	-5.361	-0.833
1.90	0.279	0.862	-5.065	-0.754
2.00	0.265	0.786	-4.807	-0.689
2.10	0.252	0.714	-4.544	-0.665
2.20	0.241	0.649	-4.302	-0.640
2.30	0.230	0.588	-4.068	-0.614
1.98	0.267	0.800	-4.852	-0.702
R (Å)	$1/R$ (a.u.$^{-1}$)	Li_2 E^b_{intra} (a.u.)	E^{Li-b}_{inter} (a.u.)	
2.40	0.220	0.000003	-0.000878	
2.50	0.212	0.000003	-0.000867	
2.60	0.204	0.000003	-0.000853	
2.70	0.196	0.000002	-0.000819	
2.80	0.189	0.000002	-0.000780	
2.90	0.182	0.000002	-0.000760	
3.00	0.176	0.000002	-0.000735	
3.10	0.171	0.000002	-0.000692	
2.72	0.194	0.000002	-0.000815	

Table 5.19: Internuclear distance R, bond intrabasin energies E^b_{intra} (a.u.) and core-bond electrostatic energy values E^{N-b}_{inter} (a.u.) at the B3LYP/6-31G(d) level.

simple interpretation is that a very small positive value for the Laplacian implies that the electron density is quite flat in the interaction region, BCP and surroundings. We expect this to be the case for metallic bonds, and thus $\xi^m_{BCP} >> 0$ for metallic bonds. If the Laplacian is negative, we identify the situation with covalent bonds, in which there is significant charge accumulation in the bonding region. Naturally, we may expect $\xi^m_{BCP} << 0$ for a strongly covalent bond, resulting from a negative Laplacian and a substantial value for $\rho(\mathbf{r})$.

The values of $\rho(\mathbf{r})$, $\nabla^2\rho(\mathbf{r})$ and ξ^m_{BCP} for the bonds studied in the different systems covered both in Subsection 5.2.3 and in this Subsection are presented in Table 5.20. As expected, the Li–Li bond in Li_2 is a clear outlier, with $\xi^m_{BCP} = 12.780$, to be compared with values in the negative values for conventional covalent bonds and the 1.631 value of the B–N bond. Therefore, the bond metallicity approach is able to detect situations in which the ELF-BCM approach is not appropiate with relative ease.

The bonds in the molecules in Subsection 5.2.3 all present negative values, which

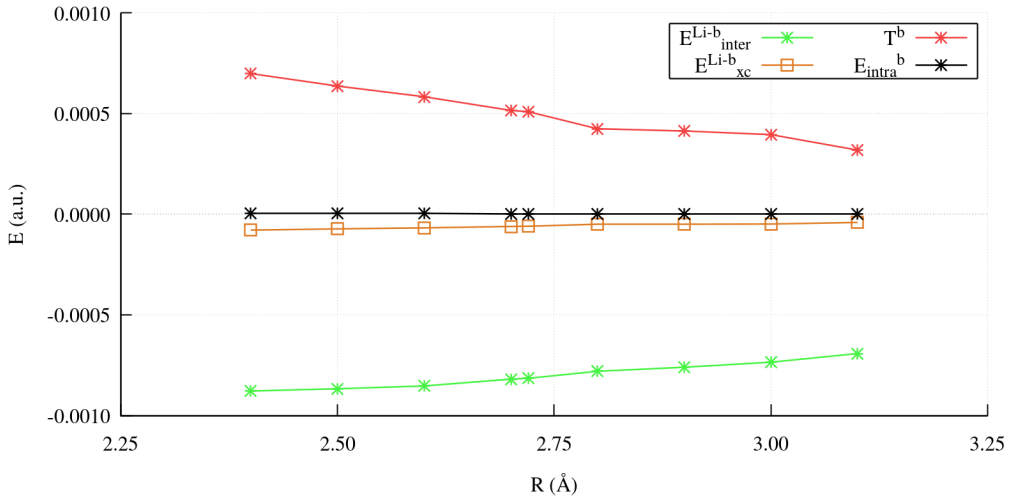

Figure 5.7: Energy terms at different internuclear distances R for the Li_2 molecule at the B3LYP/6-31G(d) level of theory.

agrees with our interpretation. The bonds that we have covered in this Subsection are, in general, less appropiate. This was partially showcased by the slight worsening of the fits. However, density values are still in the same approximate order of magnitude. Laplacian values at the BCP, while positive instead of negative, present values that are also in the same order of magnitude as the first covalent bonds.

The simple diatomic LiF molecule was also calculated and its descriptors at the BCP were extracted as well, as reported in Table 5.20 for completeness. The Laplacian takes a positive yet large value, resulting in a non-metallic ξ^m_{BCP} value. However, LiF does not present a disynaptic bond basin except for a very limited range of R, which means that it is fundamentally ionic and thus not meant to be tackled with the ELF-BCM approach.

Summarizing, we propose that the ELF-BCM approach can be used semi-quantitatively to describe localized bonds. The degree of localization of a chemical bond may be estimated by, at least, the ELF topology and the local characteristics of the BCP. Considering our starting point, which is firmly grounded in quantum chemical topology, we will not investigate further as an estimate of model limits based on the same grounds is sufficient.

Naturally, we expect other descriptors based on molecular orbitals (cf. Chapter 3) to be effective in this regard. For instance, it is reasonably to suggest that chemical bonds with a majoritary ionic contribution in valence bond terms will not be very suitable. Neither will be bonds in which the hopping integrals are small or the overlap integrals between atomic orbitals are very small. Such systems are predominantly metallic, because bonding is very limited.

5.3 Bond Properties from Equilibrium Properties

In Section 5.1 we have put forward a number of properties that may be calculated if a properly fitted analytical BCM-type potential is available. Equation 5.17 relates Bond Dissociation Energy (BDE) to the BCM ansatz.

Bond	$\rho(\mathbf{r}_{BCP})$	$\nabla^2\rho(\mathbf{r}_{BCP})$	ξ^m_{BCP}	q
C−C	0.238	0.532	5.518	1.82
C−H	0.273	−0.904	−4.089	2.00
C−N	0.261	0.670	5.116	1.62
C−O	0.256	0.504	6.560	1.24
C−F	0.233	0.022	130.6	0.90
B−N	0.099	0.420	1.631	1.89
Be−N	0.057	0.337	0.801	2.06
C−Li	0.044	0.213	0.821	2.06
Li−Li	0.013	0.002	12.780	1.82
Li−F	0.074	0.754	0.559	2.45

Table 5.20: Descriptors evaluated at the BCP of the bonds of interest in the systems reported in Figure 5.5 and Figure 5.6 and LiF. Data calculated at the B3LYP/6-311G(d,p) level and equilibrium geometries. All values in atomic units.

As the original BCM was combined with experimental data on equilibrium bond lengths and frequencies, an application in which the ELF-BCM based approach is used to model and predict bond energies will be given in this Section in order to exemplify a possible use of the model.

In the forthcoming application, equilibrium properties will be related to bond strength. As bonds are fuzzily defined, two pragmatic questions must be answered first thing: what do we mean exactly by bond strength, and why should our notion of bond strength be related with equilibrium properties whatsoever? Therefore, before we move onto the application itself we will devote some efforts to clarify what the BCM-ELF approach should be able to model, in the spirit of the critical perspective of Subsection 5.1.3.

This does not mean, however, that the ELF-BCM approach may not be used in other applications with different conceptual schemes in mind. What must be noted with our careful explanation herewith is that, as with any model, attention must be paid to the parametrization strategy and the underlying connections between input and output.

5.3.1 Bond Energy and Bond Strength

In this work, we have used BDEs several times as a property associated to a chemical bond. Unmistakingly, insomuch as they are defined, bonds have properties associated to them which, being often remarkably transferable, are extremely useful for rationalization. Predicting the *weakest* bond in a chemical structure is a very desirable ability in chemistry in order to rationalize, for example, potential chemical modifications to a scaffold molecule.

It is worth reflecting further on the association between BDEs and bonds. In chemistry, we usually associate BDEs to the *strength* of bonds quite acritically. Equating what we refer to as bond strength to BDE, however, may be far more nuanced. After all, the BDE is not a strictly vertical energy as the well-depth parameter in Equation 5.1. This is coherent at times, as we do not understand bond

breaking as an exclusively vertical process since it does include some effects that are not strictly related with the bond itself. BDEs contain mostly thermodynamic information that we can use to predict global energy changes in chemical reactions, but are ill-suited to understand dynamic chemical phenomena.

Limitations of Bond Dissociation Energies

BDEs have an innate dependency on the reference *non-bonded* state. For the same covalent bond (e.g. H_2), it is possible to calculate two different BDEs, with respect to two hydrogen atoms and with respect to H^+ and H^-. In the case of H_2 we expect that the dissociation into two atoms will be representative, but in other bonds both situations may coexist, and if the bond has marked ionic character, the dissociation into a pair of ions might be the most probable outcome. This issue becomes far more complex in multiply bonded species, where the number of possible non-bonded states increases exponentially.

The BDE is formally calculated as the difference in energy between two points in the spin-coordinate PES of a system. This requires assigning a bonded and an un-bonded state, which is done in terms of spin multiplicity and a single bond coordinate. However, all other coordinates are usually relaxed. Coupled with potential spin-state relaxation, this energy lowering is what we call the Reorganization Energy, RE.

If RE is large, it might be the major contribution to the BDE. The other term in the BDE is the *strictly* vertical energy of the bond, which we may call the Intrinsic Bond Energy (IBE) for now and we will develop later on.

At times, separating RE and IBE is reasonably feasible. For instance, the electronic IBE of ethene can be calculated as the electronic energy difference between $H_2C{=}CH_2$ in its closed-shell singlet state and the two H_2C fragments, with the same geometry, in their triplet $^3B_1$ state (cf. Scheme 5.8 A). The triplet multiplicity is formally suitable for the formation of the double bond in ethene. In a symmetric covalent bond, polarization effects can be assumed to be negligible, and thus we assume that this IBE is strictly vertical. Now, RE may be computed by calculating the energy lowering due to relaxation of the resulting H_2C fragments towards their optimal geometry and electronic state.

In this first case RE is small compared to the IBE, as the geometry and electronic state for the methylene fragments are close to the optimized minima. However, if we apply the same decomposition for the electronic IBE of ethyne, which should be computed with respect to the $^4\Sigma^-$ quartet state of the methylidine radical, we find that the resulting CH fragments differ in energy from the $^2\Pi$ doublet minima (Figure 5.8 B) by more than 40 kcal/mol.

In particularly strained systems, RE may be even dominating with respect to IBE. In turn, the BDEs may suggest that the bond in question is *weak* or *easy* to break, which is the type of information that we are usually after. This is not necessarily true: the bond breaking might be thermodinamically favored, but require a humongous amount of energy to break due to a very large IBE.

As we have discussed in depth (cf. Chapter 1.3 and thereafter), the chemical bond concept is notably fuzzy. Consequently, defining or probing this *intrinsic* property of chemical bonds is far from a solved problem. Different approaches have arisen in both Chapters 3 and 4 over different theories. For this reason, the strength associated with a chemical bond is hard to estimate, and the BDE reigns supreme as a quantity in spite of its limitations, and BDEs are far more used in benchmarking and testing efforts within quantum chemistry than other bond strength indicators.

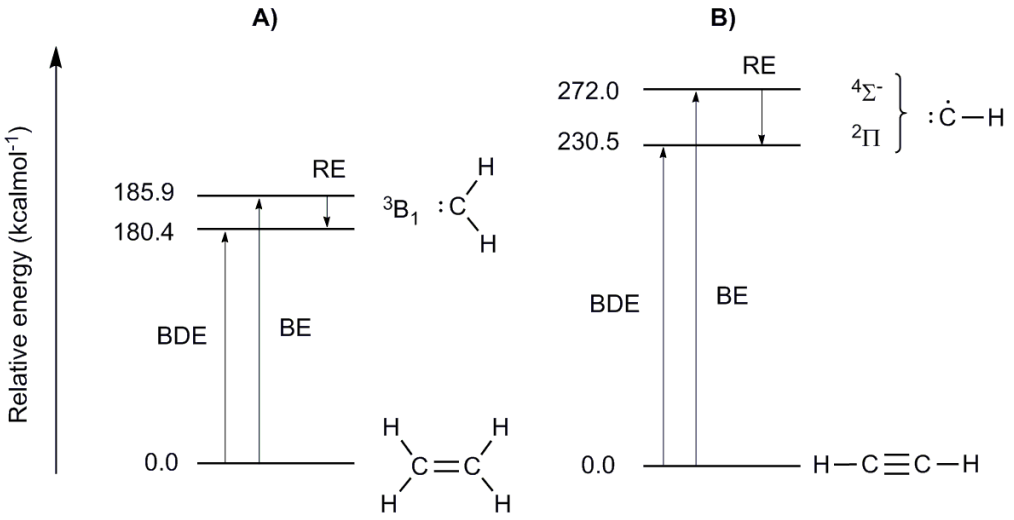

Figure 5.8: Energy levels for the homolitic bond breaking of **A)** ethene into 2 CH_2 fragments, with and without geometrical relaxation in the $^3B_1$ state and **B)** ethyne into 2 CH fragments in the $^4\Sigma^-$ state and relaxed to the $^2\Pi$ state.

Limitations of Bond Energies

Similar to the BDE, we find the concept of Bond Energy (BE) in the general chemistry literature. The IUPAC states that the BE is "the average value of the gas-phase bond dissociation energies (usually at a temperature of 298 K) for all bonds of the same type within the same chemical species." [3] Again, this definition is suitable from the point of view of thermodynamics and experimentation, but it clearly misses some desirable properties: it averages out the BDEs of bonds that should be very different at an individual level.

Let us discuss a simple example in this regard. The C–H BE in methane is, according to this definition, 1/4 of the atomization energy of methane, which can be calculated to be approximately 390 kcal/mol which suggests a BE of 97.5 kcal/mol for each individual C–H bond. Naturally, this does not mean that each bond breaking step leading to C+4 H is associated with this BDE, although it may suggest so for an unexperienced reader.

We reasonably expect that every subsequent C–H bond breaking requires a different amount of energy, and the C–H bonds at every step have significantly different properties – just like $^{\bullet}CH_3$ is quite different to CH_4. Indeed, thermodynamic models and calculations agree that the first C–H bond has a larger BDE of about 105 kcal/mol, and successive dissociations have subsequently smaller BDEs to a total of 390 kcal/mol. Hence, the concept of BE as recognized by the IUPAC is quite ineffective as a way to convey bond strength which is nevertheless based in the already limited BDE.

Intrinsic Bond Energies

IBEs can be deemed to be an equilibrium property, in the sense that the bond is properly described by the wavefunction of the system at the equilibrium geometry. The IBE is something hidden on the molecular wave function that characterizes the fuzzy entity we call a chemical bond. This becomes apparent using, for example, the VBT framework

(cf. Section 3.2), but should be generally true because the wavefunction contains all the relevant information.

Alternatively, we may use the IQA approach (cf. Subsection 4.2.3) to quantify interbasin energies between subsets of basins, which is an ultimately intrinsic energy. Such a calculation, however, depends strongly on the topological partitioning of the system. For the time being, we simply lack a general observable to extract this information from the wavefunction in a straightforward way.

Undoubtedly, both chemical bonds and IBEs are invaluably important for the rationalization of chemical phenomena.[58, 59, 60, 61] Relating IBEs and BDEs to geometric or electronic features is widespread in the chemical community,[62, 63] because IBEs are a far more representative measurement of the ease of breaking a given bond.

On the other hand, REs can be calculated formally by estimating the relaxation of the individual fragments, that is, RE is in principle independent of the features of the bond that was broken; no detailed information of the features of the bond is needed.

Consequently, it is reasonable to think that an equilibrium property, such as the IBE, could be predicted on the basis of other equilibrium properties. It is not necessary as clear that the BDE should be predictable on the basis of other equilibrium properties because the relative stability of fragments is not encoded in such descriptors. In other words, we do not expect that the stability of constituent fragments, which manifests in RE, is encoded in the wavefunction of a system. We do expect, however, that the characteristics of a chemical bond are (e.g. resistance to elongation, forces arising from electron unpairing).

For this reason, in the following Subsections, a BCM-type ansatz based on the electron density, the kinetic energy density and geometrical considerations will be presented – all of those are equilibrium properties. We will fit our model to a selected database in order to calculate proportionality constants, and use it to estimate IBEs for C–C bonds.

5.3.2 A simple Ansatz for Intrinsic Bond Energies

In the next Subsection we will fit a simple ELF-BCM model to the IBEs of some selected symmetric C–C bonds. After all, C–C bonds are the basis of organic chemistry and present a somewhat striking variation in length and formal bond order. They are also relevant in many other areas, such as materials science, where carbon allotropes are of interest.

In order to fit our model we only need to use bond charges, q (as given by the integration of ELF basins) and equilibrium bond lengths R_{eq}, which appear in Equation 5.17. Strictly speaking, we do not require any other information to reach our goal. While the goal of this Section is mostly exemplary, a model relating these two simple properties with the IBE would be a potentially useful tool for the interpretation of electronic structure calculations.

With this goal in mind, we will depart from a simple ELF-BCM conforming expression

$$W = D + C_{V2}^{BN}\frac{q}{R} + C_{V}^{NN}\frac{1}{R} + C_{T}^{B}\frac{q}{R^2} \tag{5.29}$$

which is a symmetric version of Equation 5.24 in which we assume all exchange-correlation terms are negligible and all dependencies with respect to R hold.

It must be noted that by fitting a given reference dataset to Equation 5.29 other properties (e.g. Equations 5.16 and 5.15) are not enforced. Additional constraints should be added if several properties were to be fitted at the same time. As a consequence, parameters derived from fitting to Equation 5.29 will produce biased

dissociation curves with respect to R. High fidelity dissociation curves could be obtained by enforcing the expressions above with a fixed bond charge q in a more sophisticate multi-purpose approach.

At this point, it must be noted that the working expression for the kinetic term is not well-founded regarding the scaling of q, just as we noted in Equation 5.26. This is critical here because q is one of our two sources of information. Hence, we will first revisit the crude approach of the previous Section.

Simple kinetic energy terms

The Morse potential in Equation 5.1 may be rewritten to present an attractive and repulsive term:

$$W = D_e(1 - e^{-\beta(R-R_{eq})})^2 = D_e(1 + e^{-2\beta(R-R_{eq})} - 2e^{-\beta(R-R_{eq})}) \tag{5.30}$$

It thus becomes apparent that the equilibrium well results from the difference in the slopes of two exponential terms.

The positive term, which dominates at small R, has a slope $\propto 2D_e e^{\beta(R_{eq}-R)}$, while the negative term has a slope $\propto -2D_e e^{-2\beta(R_{eq}-R)}$. These two slopes are exactly equal when $R = R_{eq}$. If $R < R_{eq}$ the negative term dominates, and at larger $R > R_{eq}$ the positive one does.

In the BCM ansatz, and given the physical interpretation of the different terms, stabilization arises from the Coulombic $C_V^{BN}\frac{q}{R}$ term, while destabilization comes from a combined $C_V^{NN}\frac{1}{R}+C_T^B\frac{q}{R^2}$ term, including kinetic and repulsive nuclei-nuclei electrostatic contributions. The ratio of the slopes of the repulsive and attractive terms in the BCM is thus $\propto (C_V^{NN}R + 2qC_T^B)/qC_V^{BN}R$.

The first term must fulfill $C_V^{NN}/qC_V^{BN} < 1$ for the attractive term to eventually dominate (i.e. for the bonded state to be stable). On the other hand, for most of R – specially in constrained bonds – the leading term is $2qC_T^B/C_V^{BN}R$, which highlights the critical importance of the kinetic term in the correct description of the bonded state.

Considering that the original kinetic energy term is not particularly well suited for a 3D system, we already introduced a slight modification in Equation 5.26, in which the original $1/R^2$ dependence is unaltered. This dependence was verified extensively in Section 5.2.

Naturally, this model kinetic energy still suffers from some of the deficiencies of the original term. In this sense, integrating a more sophisticated inhomogeneous kinetic energy density within the disynaptic bond basin $\Omega_{C,C}^V$ should lead to better results, mirroring DFT development. However, our goal is to be extremely simple.

We may argue that gradient expansions of the kinetic energy density of the homogeneous electron gas involve square gradients of the density. The integral of such quantities over a volume is related to the surface integral of the electron density gradient over the interbasin area. From this crude assumption, we may propose terms that contain a parameter-free damping of q, as long as it scales with R while preserving the limits of the original model at $R \to \infty$ and $R \to 0$. These terms stem from the assumption that, as the distance increases the interbasin surface of the bond must increase or decrease following an unknown dependency.

Two plausible terms that satisfy these requirements are

$$T_1 = C_{T1}^B \frac{q^{\frac{5}{3}acot(R_{eq})}}{R_{eq}^2}$$
$$T_2 = C_{T2}^B \frac{q^{\frac{5}{3}atan(R_{eq})}}{R_{eq}^2}$$

Similar damping expressions can be constructed using the Gauss error function and its complementary as far as $R > 0$ in all the parametric space, but trigonometric functions are easier to manipulate analytically. We consequently favour these expressions so far, keeping in mind the crudeness of our model.

Indeed, interpretation is straightforward so far. T_1 is meant to dissipate the charge as the bond expands. T_2 attains the opposite, dissipating the charge when the bond is contracted. After all, which beavior will be more representative is unknown.

Simple coulombic terms

As detailed in Section 5.1, C_V^{BN} and C_V^{NN} are related by $C_V^{NN} = (C_V^{BN})^2/16$ in the original model assuming the charge equalization condition.

Because charge equalization might not hold here, which was discussed in Section 5.2, we should have to explicitly calculate core charges for our model. Alternatively, an independent scaling factor for each term can be added. This is particularly well justified as a shielding effect: charges are not strictly punctual, particularly so in bonds. Therefore, the effective Coulomb term for the C_V^{BN} and C_V^{NN} terms should be different.

In principle, the weight of the bond-nuclei term is expected to be higher than the nuclei-nuclei term both because its an electrostatic interaction over a shorter distance and because, after all, bonding does take place. In any case, both approaches will be tested empirically.

Note that in the case of symmetric C–C bonds, both $\int_{\Omega_C^C} \rho(\mathbf{r}) d\mathbf{r}$ and the size of Ω_C^C remain constant, as the core of the carbon atoms does not participate in the bonding: both Z and ν may be considered constants. Thus, the effective bond path νR_{eq} does not represent bond strength or bond order, which in turn ought to be captured by q and its variation with R.

As a final remark, recall that the expression in Equation 5.29 is symmetry constrained. If the dependency of all electrostatic interaction terms is properly adjusted to $1/R$, then the resulting C_V^{BN} term will be an average as soon as symmetry is broken (see Subsection 5.1.2 for details and interpretation). However, we expect a good degree of atomistic transferability as per the results in the previous Section (cf. Subsection 5.2.3 in particular) and thus we deem this both acceptable and preferrable over introducing another distinct parameter. As far as possible, we will emphatize simplicity over accuracy, and thus disregard the inclusion of additional parameters.

Intrinsic Bond Energy ansatzs

According to the discussion before, and departing from Equation 5.29, five different working expressions are put forward:

$$IBE_1 = C_V^{BN} \frac{q}{R_{eq}} + (C_V^{BN})^2 \frac{1}{16 R_{eq}} + C_T^B \frac{q}{R_{eq}^2} \tag{5.31}$$

$$IBE_2 = C_V^{BN}\frac{q}{R_{eq}} + C_V^{NN}\frac{1}{R_{eq}} + C_T^B\frac{q}{R_{eq}^2} \tag{5.32}$$

$$IBE_3 = C_V^{BN}\frac{q}{R_{eq}} + C_V^{NN}\frac{1}{R_{eq}} + C_{T0}^B\frac{q^{5/3}}{R_{eq}^2} \tag{5.33}$$

$$IBE_4 = C_V^{BN}\frac{q}{R_{eq}} + C_V^{NN}\frac{1}{R_{eq}} + C_{T1}^B\frac{q^{\frac{5}{3}acot(R_{eq})}}{R_{eq}^2} \tag{5.34}$$

$$IBE_5 = C_V^{BN}\frac{q}{R_{eq}} + C_V^{NN}\frac{1}{R_{eq}} + C_{T2}^B\frac{q^{\frac{5}{3}atan(R_{eq})}}{R_{eq}^2} \tag{5.35}$$

Note that the sophistication increases from IBE_1 to IBE_4 and IBE_5, but also the degrees of freedom increase from 2 in Equation 5.31 to 3 in all other expressions.

5.3.3 Intrinsic Bond Energies of C-C bonds

As explained in the previous Subsection, our target is the IBE of C−C covalent bonds. For this, we definitely require a set of reference IBEs, which is not trivial considering the difficulties highlighted in Subsection 5.3.1.

With these issues in mind, a curated selection of C−C bonds was considered, covering different bond orders, relative strengths, geometrical constrains and keeping possible polarization or non-covalent effects to a minimum. Bond breaking should be accomplishable in a localized way, with negligible 1,4-interactions that bind both fragments. Secondly, symmetry is deemed desirable to minimize polarization effects that rightfully belong in RE. Finally, molecular complexity has to be limited in order to clearly select the appropriate electronic state, based in the C atoms involved in the bond under examination.

The complete list of molecules in the reference set is the following: C_3H_6 (**1**), $H_3C{-}CH_3$ (**2**), C_6H_6 (**3**), $H_3C_4{-}C_4H_3$ (**4**), $H_2C{=}CH_2$ (**5**), $HC{\equiv}C{-}C{\equiv}CH$ (**6**), $HC{\equiv}CH$ (**7**) and C_2 (**8**). A set of fluorinated analogues have been included for validation purposes, considering the interest some of these molecules arise.[64, 65, 66] It is the case for the *gauche-* and *trans-* conformations of 1,2-Difluoroethane (**9** and **10** respectively), the *cis-* and *trans-* isomers of 1,2-Difluoroethylene (**11** and **12**), and Tetrafluoroethylene (**13**). This makes a total of 13 different chemical environments for C−C bonds. Symmetry is respected in all cases. The composition of the set attempts to minimize RE and nonbonded interactions and hence provide IBEs that are both accurate and representative.

The calculated molecules are shown in Figure 5.9 with the relevant bonds highlighted in red. IBEs, internuclear equilibrium distances and $\Omega_{C,C}^V$ populations q were extracted accordingly for each bond under consideration. In cases where several disynaptic bond basins existed, the integration was performed over all of them. In the special case of C_2, the full valence density was considered to belong to the bond, due to the formal bond order of 4. This assumption will be revisited later.

The influence of Basis Set Superposition Errors (BSSE) and Spin Contamination (SC) in the IBE calculations was assessed with high level calculations at the CCSD level using a compound extrapolation scheme for Complete Basis Set (CBS) extrapolation, in which the HF self-consistent field energy is extrapolated using the cc-PVDZ, cc-PVTZ and cc-PVQZ basis sets and the correlation energy is extrapolated using the cc-PVDZ and cc-PVTZ basis sets.[67] Helgaker's two and three-point extrapolation formulas were

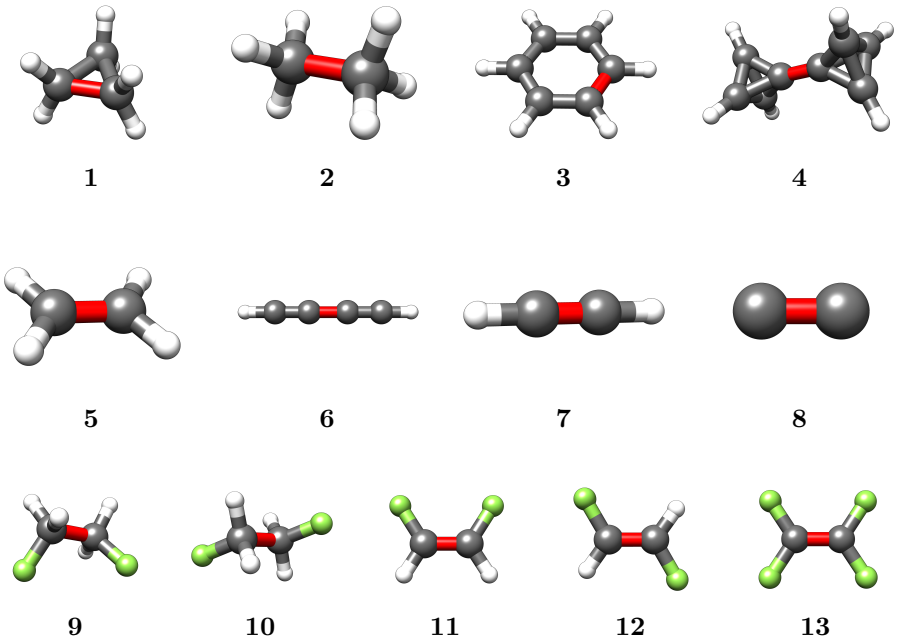

Figure 5.9: Calculated molecules in the parametrization set. H, C and F atoms are depicted as white, grey and light green balls-and-sticks, respectively. Relevant C−C bonds are colored in red.

used to approximate CBS results.[68] Results are expected to be very close to the CBS limit, and are in approximate agreement with the trends of most DFAs.

SC is not very large nor sensitive to basis set size, as reported by the S^2 values in the different basis set sizes (see Table 5.21), indicated by the dz, tz and qz subscripts. In particular, note that SC has more impact in HF calculations than in KS-DFT, which is the main domain of application of our model.

Molecule	$E_{molecule}$ (a.u.)	$E_{fragment}$ (a.u.)	IBE (kcal/mol)	S^2_{dz}	S^2_{tz}	S^2_{qz}
2	-79.7473	-39.7822	114.73	7.5840	7.5814	7.5838
5	-78.5034	-39.1060	182.84	2.0131	2.0128	2.0131
7	-77.2459	-38.4130	263.41	3.7543	3.7542	3.7543

Table 5.21: Reference data for some molecules in the molecule set at the CCSD/CBS level.

Test calculations can be performed using the full basis set of the molecule for the calculations on fragments at the CCSD/cc-PVTZ level. BSSE corrections do not alter our analysis significantly, as shown by the results in Table 5.22. Do note, however, that the usage of the full molecular basis set gives IBEs consistently lower than the previous benchmark due to the increase in basis set flexibility for the monomers.

Molecule	$E_{molecule}$ (a.u.)	$E_{fragment}$ (a.u.)	IBE (kcal/mol)	$S^2_{tz,molecule}$
2	-79.7040	-39.7642	110.15	7.5839
5	-78.4636	-39.0908	176.97	2.0131
7	-77.2087	-38.4020	253.98	3.7543

Table 5.22: Reference data for some molecules in the molecule set at the CCSD/cc-PVTZ level using the full molecular basis set.

This comes to show that the basis set choice in our work is appropriate and does not incur in significant error due to incompletion. The choice of DFA will be discussed thoroughly later in this Subsection (see the discussion in 5.3.3.0).

As a last necessary thought, we need to verify the consistency of our approach. As we discussed in the previous Subsection, our idea requires that information about bond order and geometrical strain must be contained by the combination of the only two parameters, q and R_{eq}. As shown in Figures 5.10 A and 5.10 B for the bonds in our dataset, both parameters are in fact known to be crude descriptors of bond strength that have been previously used in the context of C−C bonds.[69]

Historically, the success of these descriptors has been very limited because dependence of such metrics with respect to IBE or BDE is not linear. In this sense, they are quite similar to $\rho(\mathbf{r}_{BCP})$ in the sense that both the ELF population and the distance are unmistakingly related to the bond strength, but only among strictly analogous chemical environments. It is important to note that in this case q and R_{eq} do encode different information, since collinearity with each other is not very high (cf. 5.10 C). This signals that they do contain information about different aspects of the bond.

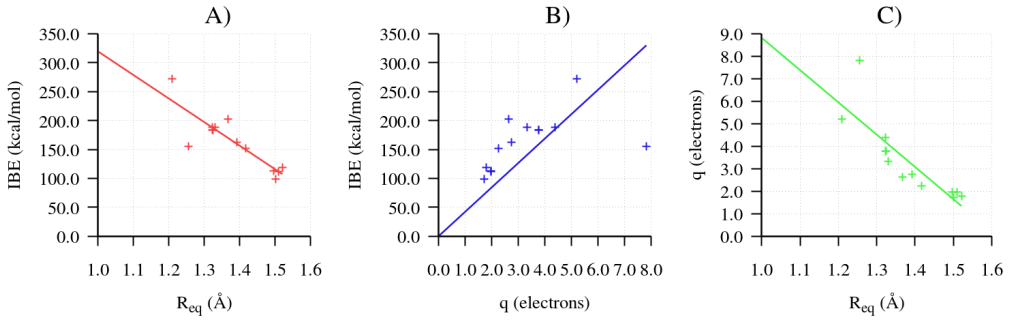

Figure 5.10: Linear correlations between R_{eq}, q and IBE for the C−C bonds in the molecule set. All calculations performed at the MP2-FC/def2-QZVP level.

Model selection

The proportionality coefficients were obtained by using the results of calculations of the dataset of C−C bonds at the ωB97XD/def2-QZVP level. The ωB97XD DFA is widely considered appropriate when dealing with covalent bonds in organic systems.[70] Correlation coefficients and parameters for the different models, IBE_1 to IBE_5 (see Equations 5.31 to 5.35) are collected in Table 5.23. The fit was performed using an ordinary least-squares algorithm in all cases.

Without imposing any additional restraints, only models IBE_3 and IBE_4 seem to accommodate the desired physical meaning, in which C_V^{BN} is the only positive (stabilizing) contribution to the IBE. They also present the best coefficients of determination and $F - statistic$ results, while the kurtosis result for IBE_4 is significantly closer to a normal distribution.

The inclusion of the electrostatic shielding degree of freedom from IBE_1 to IBE_2 is shown, on the basis of the adjusted r^2 value, to result in a meaningful improvement. Similarly, the kinetic energy term derived for IBE_3 is noticeably better than the original BCM one, although it does increase the kurtosis significantly. As hinted in the previous Section, such term is apt for non-strained covalent bonds, hence outliers are found among the database here considered. In particular, Cook's distance for the C_2 molecule in the IBE_3 model was found to be 12.861 while no other molecule has a value superior to 0.1. Thus, the inclusion of the damping term at short distances in the equation of IBE_4 successfully improves r^2 to a quantitative level by smoothing the anomalous C_2 molecule, while preserving the correct physical interpretation and limits.

The root mean square (RMS) error of IBE_4 is 4.2029 kcal/mol, which is in the same order of magnitude that can be assumed for the accuracy of DFT in many applications.

Concluding that IBE_4 is our best approximation, a robust linear model was used to fit the same data in order to check the influence of the fitting algorithm. The fitting was performed by iterative re-weighted least-squares using Huber weights. Relatively close parameters $C_V^{BN} = 229.7770$, $C_V^{NN} = -96.2613$ and $C_T^B = -90.2421$ were obtained, all within the standard errors of the coefficients of the ordinary least-squares model, which corroborates that outliers or high-leverage molecules are not substantially over-weighted in this model.

Similar conclusions may be drawn from calculations with a different level of theory. Consequently, we will use the expression of IBE_4 given in Equation 5.34 as our working model for the remaining of this Subsection. This has the implication that the charge is

Model	C_V^{BN}	C_V^{NN}	C_T^B	$F-statistic$	$Kurtosis$	r^2	Adjusted r^2
IBE_1	-51.1359	2614.8789	-52.6352	80.0	3.260	0.936	0.924
IBE_2	-236.1163	305.9522	278.2517	72.2	2.352	0.956	0.943
IBE_3	150.9831	-42.5211	-39.0838	146.7	6.626	0.978	0.971
IBE_4	247.6594	-120.5810	-96.6753	401.1	3.519	0.992	0.989
IBE_5	-26.6361	232.8136	25.2538	54.9	2.203	0.943	0.926

Table 5.23: Multivariate ordinary least-squares regression parameters C_V^{BN}, C_V^{NN} and C_T^B for models IBE_1 to IBE_5 (cf. Equations 5.31 to 5.35). The $F-statistic$ is calculated with respect to the trivial $C_V^{BN} = C_V^{NN} = C_T^B = 1$ model.

additionally dissipated as the bond expands with respect to the original BCM approach. For completeness, the fitting diagnostics to a selection of popular DFAs is given in Table 5.24.

Model	C_V^{BN}	C_V^{NN}	C_T^B	Kurtosis	r^2
$BE_4^{\omega B97XD}$	247.6594	-120.5810	-96.6753	3.519	0.992
IBE_4^{B3LYP}	248.5127	-128.7300	-95.8862	3.920	0.988
IBE_4^{HSE06}	236.4620	-111.8291	-91.5913	3.607	0.991
IBE_4^{PBEPBE}	225.7251	-100.8176	-85.1020	3.586	0.990
IBE_4^{BLYP}	237.1546	-120.5354	-89.5870	3.891	0.987
IBE_4^{TPSSh}	230.4442	-113.4220	-88.4728	3.442	0.990
IBE_4^{M062X}	246.4509	-114.5167	-96.2583	3.551	0.986
$IBE_4^{PW2PLYP}$	240.9731	-117.7614	-92.2118	3.774	0.990
IBE_4^{B2PLYP}	237.1362	-115.0569	-90.1315	3.744	0.990
IBE_4^{HF}	222.4675	-128.1798	-92.5961	3.196	0.991

Table 5.24: Multivariate ordinary least-squares regression parameters C_V^{BN}, C_V^{NN} and C_T^B for model IBE_4 for different levels of theory, where the method is indicated as a superscript and the basis set is def2-QZVP.

In this regard, it must be noted that the description that many DFAs give of the C_2 molecule, which has sometimes been called pathologically multiconfigurational, is not necessarily accurate.[71]

General trends of the model in Density Functional Theory

Previously, we have used just 13 datapoints calculated at the ωB97XD/def2-QZVP level. To study the effect of the DFA choice, as well as the transferability to other calculation levels, the same procedure was used to fit an extensive database (793 datapoints) including a set of 59 different DFAs in KS-DFT, HF and Frozen Core MP2 methods. The total array of 61 methods will be referred to as the DFA set with numbers *1* to *61*. All calculations were performed with the all electron quadruple-ζ

def2-QZVP basis set.[72] The complete list, as defined in the Gaussian 09 rev.D01 package[73], is given below including the numbering:

- *1* G96LYP
- *2* BVWN
- *3* M06L
- *4* M06
- *5* M062X
- *6* M06HF
- *7* M05
- *8* M052X
- *9* M11
- *10* N12SX
- *11* MN12SX
- *12* SOGGA11X
- *13* PW91VWN
- *14* TPSSh
- *15* BMK
- *16* BHandH
- *17* BHandHLYP
- *18* HSEH1PBE
- *19* wB97XD
- *20* LC-wPBE
- *21* CAM-B3LYP
- *22* APFD
- *23* B2PLYP-FC
- *24* mPW2PLYP-FC
- *25* HSEVWN
- *26* BRxVWN
- *27* BPBE
- *28* PW91PBE
- *29* PBEPBE
- *30* HSEPBE
- *31* mPW1PBE
- *32* mPW3PBE
- *33* BPW91
- *34* PW91PW91
- *35* PBEPW91
- *36* HSEPW91
- *37* B3PW91
- *38* mPW1PW91
- *39* MP2
- *40* BLYP
- *41* PW91LYP
- *42* PBELYP
- *43* HSELYP
- *44* B3LYP
- *45* mPW1LYP
- *46* HF
- *47* TPSSTPSS
- *48* XAlphaXa
- *49* BB95
- *50* PW91B95
- *51* PBEB95
- *52* HSEB95
- *53* SVWN
- *54* PKZBPKZB
- *55* B3P86
- *56* PKZBKCIS
- *57* BRxKCIS
- *58* OVWN
- *59* OPBE
- *60* OLYP
- *61* OB95

Results are shown in Figure 5.11 A with respect to the model terms, and in Figure 5.11 B with respect to the two parameters, q and R_{eq}.

The model derived from ordinary least-squares fitting to the complete database takes $C_V^{BN} = 232.2327$, $C_V^{NN} = -107.4466$ and $C_T^B = -88.9169$, which is quite close to previous results (see Table 5.23), with a coefficient of determination $r^2 = 0.985$. Various methods introduce additional variability, thus the kurtosis value increases to 7.036. The RMS error is slightly increased to 5.7890 kcal/mol, which then again is not too terrible for a semiquantitative model. In fact, it is remarkable considering its simplicity and the variability in the data set. In any case, it must be noted that the ensemble parameters reported above are not recommended for any in-depth analysis: method-specific parameters as the ones reported in Table 5.24 should be used instead, which lead to $R^2 > 0.99$ in most cases.

On the other hand, the high quality of the obtained fit reveals major similarities in the way different DFAs relate geometries, q and IBEs. Indeed, it can be said that all molecules suit the model irrespective of the calculation method.

Average absolute values of standardized residuals per method are presented in Figure 5.13. Residual values range from 0.5113 for Xα to 2.7600 for HF, which is to be expected. The kinetic term in IBE_4 is a crude correction on top of a homogeneous electron gas

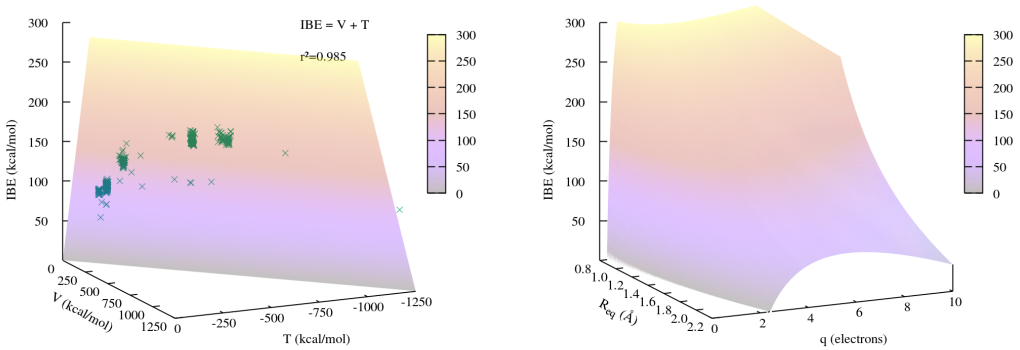

A) B)

Figure 5.11: Predicted IBEs with respect to **A)** T and V and **B)** q and R_{eq}. Reference data points in **A)** are shown in green. All energies in kcal/mol.

derivation, and therefore simple DFAs should provide good fits – that is, even if the predicted BEs are not accurate. On the other hand, HF is not based on the electron density and suffers from very inconsistent correlation treatment for different molecules. It is therefore coherent that it appears as an outlier here. Accordingly, most DFAs are evenly treated.

Regarding molecules instead, average absolute values of standardized residuals per molecule (recall the nomenclature introduced in Figure 5.9) are shown in 5.13. Average residual values per molecule range from 0.2084 for cyclopropane to 2.1310 for ethyne (**7**). No particular issues arise for any of the strained systems; the fact that ethyne is the upper limit is reasonable considering that it is the only triple bond in the parameter set and still the standardized residuals are not extremely odd. C_2 (**8**) has a large standard deviation in this average, pointing at the difficulties of capturing its correlated character in DFT that were discussed before. Different DFAs give largely different depictions of the molecule.

Having verified the approximate validity of our model irrespective of the DFA choice, we can analyze some of the features of our fitted model in some detail.

Assuming a fixed q, the model resembles a dissociation energy curve as seen in Figure 5.14. Note that for any given q, predicted energy minima correspond with extremely short R. In reality, q changes with R, therefore the energy quickly tends to 0 at long R as the bond charge is shifted to other regions of the molecule. Stronger bonds (as implied by higher values of q) are seen to be more sensitive to R, while smaller bond orders spawn a longer range of distances without changing IBE significantly. The model also gives an estimation for the maximum possible IBE for any given q.

If we fix R_{eq} instead, we find that there must be a number of shared electrons q that yields a maximal IBE, as shown in Figure 5.15. The curve, which has a global minimum, becomes steeper as bond length increases. This implies that very lengthy covalent bonds are constrained to an optimal number of shared electrons, while shorter bonds may exist

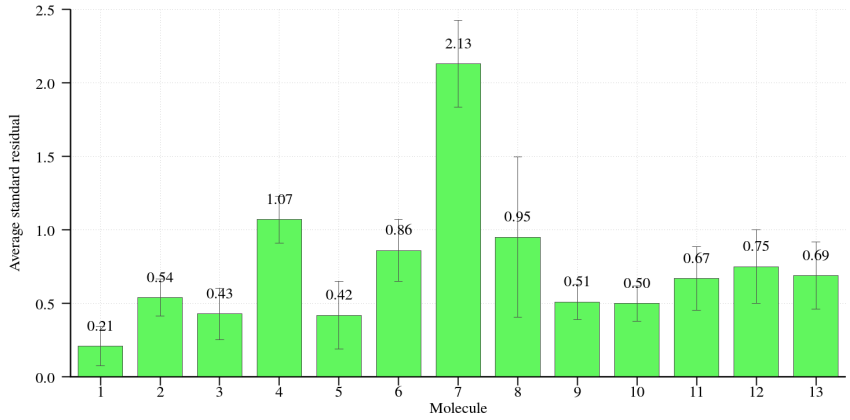

Figure 5.12: Averaged absolute value of standardized residuals per molecule in the test set. Molecule **7** corresponds to ethyne, molecule **8** corresponds to C_2. Error bars spawn one standard deviation for the given averages.

with different balances of terms. This is obviously coherent with what is found empirically: a huge variety of C−C bonds within reasonable single-bond and double-bond distances, but only very rare cases where the C−C distance is very large – as long as 1.8 Å for a formal single bond in some species.

Regarding C_2, it remains somewhat of an outlier but is reasonably well fitted by the model. This approves the usage of the whole valence density of the molecule as bond charge q, which corresponds to a formal quadruple bond ($q \approx 8.83$ electrons). However, the somewhat outlier nature of ethyne and dicarbon in our model is related to their particular nature but also influenced by the lack of other molecules with formal bond orders between 3 and 4 in the test set. This makes the statistical model inherently biased towards the lower bond orders, in spite of the use of robust regression techniques as evidenced in the analysis before.

As a final remark, note that all the fluorinated species are perfectly reproduced in the model even when isomers have extremely similar R_{eq} values. This signals that the electronic effects are perceived in the C−C bond through q and reflected in IBE. Hence, we may say that our model is sensitive to the chemical environment, and capable of modelling electronic features in a sophisticate way in spite of its extreme simplicity and limited number of parameters.

5.3.4 Applications of the model

In the previous Subsection it was shown that the proposed model is able to recover IBEs from equilibrium properties R_{eq} and q with a reasonable accuracy, in particular when using DFA-specific parameters. While extrapolating results towards high q and low R (formal bond orders ≥ 3) may not be accurate due to the construction of the dataset, interpolation within the single-to-double bond regime should provide highly accurate results.

Naturally, this may be changed by modifying (or expanding) the reference dataset, which is focused on single and double bonds. In any case, the model as it is suffices to demonstrate some simple applications.

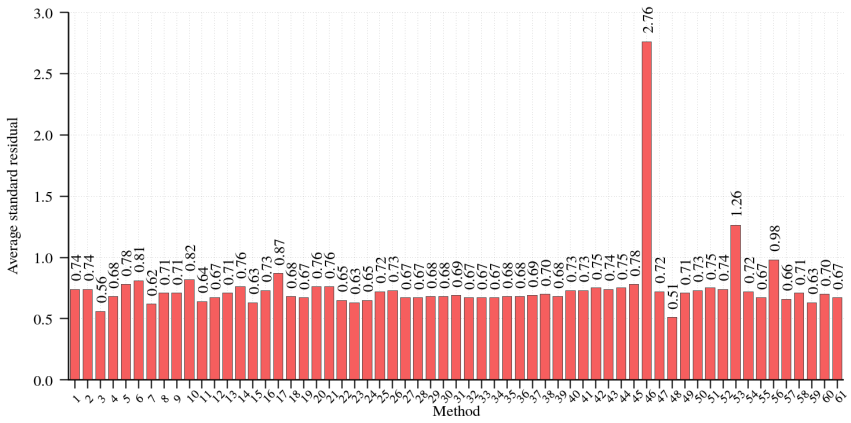

Figure 5.13: Averaged absolute value of standardized residuals per method in the test set. Method *46* corresponds to HF, method *48* corresponds to the Xα DFA.

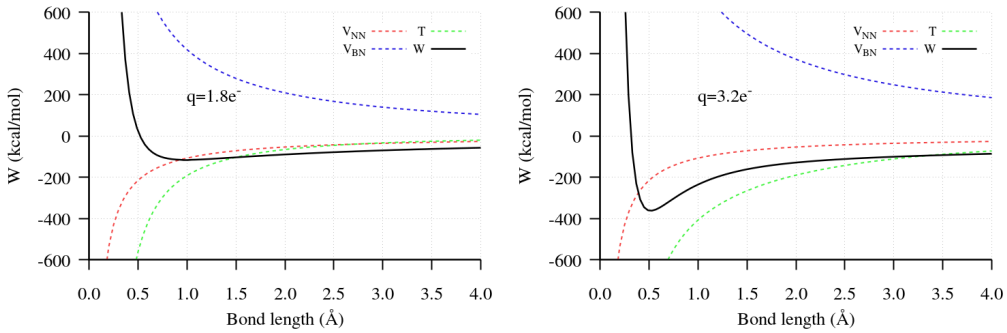

Figure 5.14: Evolution of V_{NN}, V_{BN} and T with R according to the fitted model parameters (IBE_4, Equation 5.34) for a fixed value of q.

C−C bonds in ferrocene

Ferrocene is somewhat of a misterious molecule due to its markedly non-Lewis character. Achieving a rational understanding of the electronic structure and bonding in ferrocene is quite hard from a FMT interpretative basis. With this in mind, a beautiful yet simple application of our model is comparing the IBE of C−C bonds of the cyclopentadienyl anion (Figure 5.16 A) on its own and in the ferrocene $Fe(C_5H_5)_2$ molecule (Figure 5.16 B) in order to evaluate the differences in strength of the carbon structure upon coordination.

The optimized geometries and wave functions for both systems, calculated at the ωB97XD/def2-QZVP level, give $q = 2.9002$ electrons and $R_{eq,\mathrm{C-C}} = 1.4067$ Å for the anion and $q = 2.5414$ electrons and $R_{eq,\mathrm{C-C}} = 1.4182$ Å for ferrocene. Coherently, a large amount of charge is transferred to the formally doubly charged iron atom upon complexation. In spite of this, IBEs of 159.88 and 146.12 kcal/mol are obtained respectively, which means that each C−C bond becomes 13.76 kcal/mol weaker in ferrocene.

At this theory level the IBE of C−C bonds in benzene is 159.62 kcal/mol, almost the same result obtained for the anion. Bond-nuclei attraction V_{BN} is increased in the

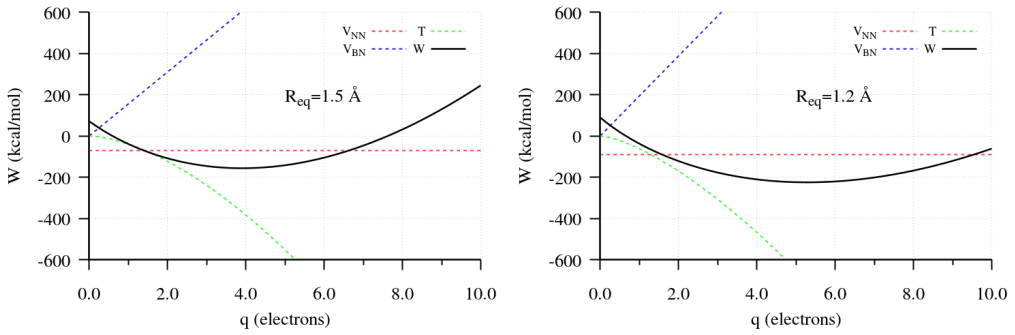

Figure 5.15: Evolution of V_{NN}, V_{BN} and T with q according to the fitted model parameters (IBE_4, Equation 5.34) for a fixed value of R_{eq}.

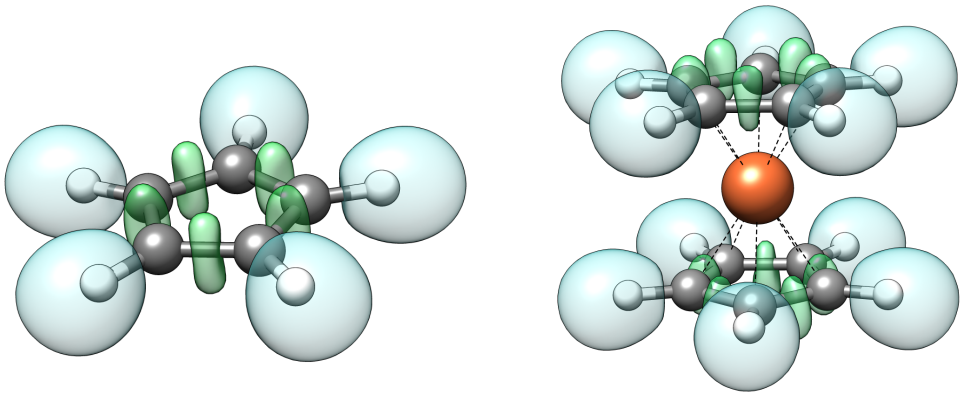

A) B)

Figure 5.16: Isosurfaces of $\eta_{ELF}(\mathbf{r}) = 0.85$ a.u. of **A)** the cyclopentadienyl anion, **B)** ferrocene $Fe(C_5H_5)_2$. C, H and Fe atoms shown as grey, white and orange balls-and-sticks respectively. C−C ELF basins are depicted in green, while C−H basins are colored light blue.

anion with respect to the neutral benzene, as given by the extra electron, but most of the stabilization is counteracted by an increase in T, rendering approximately the same IBE. When compared to ferrocene, the small loss in IBE per bond (mostly in form of V_{BN}, which decreases noticeably as q decreases) is globally justified by the formation of the haptic bond with the metallic center, and explains why the carbon structure remains similarly stable in the coordinated species.

From our analysis, we can say that no significant improvement in C−C cleavage is in principle expected in ferrocene when compared to the anion. The difference in bond strength, as estimated from the IBE, is in agreement with the changes in the stretching C−C frequency from ferrocene, around 1400 cm^{-1}, compared to benzene, around 1500 cm^{-1}.[74] Similar analysis may be performed on transition structures and molecular systems of interest in the context of computational organic and inorganic chemistry, all at a negligible cost.

C−C bonds in carbon allotropes

The presented model may be used to study solid state systems, among which carbon allotropes are highly important. Periodic systems may be studied computationally as well, and interpretation is often difficult due to the additional difficulties in orbital localization.

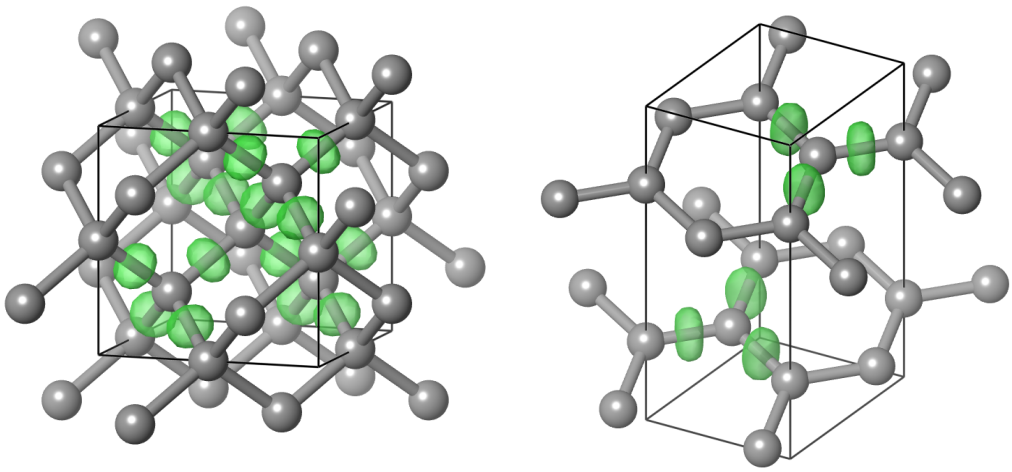

A) B)

Figure 5.17: Isosurfaces of $\eta_{ELF}(\mathbf{r}) = 0.85$ a.u. of **A)** diamond, **B)** graphite. C atoms are shown as grey spheres. C–C ELF basins are depicted in green.

As an example, we will examine two common allotropes of carbon, diamond and graphite. Optimizing the geometry of diamond using the HSE06 DFA (Figure 5.17 A) leads to a C–C equilibrium distance $R_{eq,\mathrm{C-C}} = 1.5359$ Å and the integration of the valence electron density in the ELF basins gives localized covalent bonds with $q = 2.0052$ electrons. With the HSE06 parameters, an IBE of 113.02 kcal/mol is obtained, which is analogous to the simple bond in ethane in the set (112.93 kcal/mol). This suggests that covalent bonds in diamond are very similar to simple C–C bonds elsewhere, with energetic differences arising purely from reorganization terms. Interestingly, the natural decomposition of the proposed ansatz shows that the alleviation of nuclear repulsion V_{NN} in diamond is able to counteract the loss of bond-nuclei stabilization.

Graphite (5.17 B), optimized and calculated at the same level of theory, presents an $R_{eq,\mathrm{C-C}} = 1.4154$ Å and $q = 2.6667$ electrons, which estimates a IBE of 148.42 kcal/mol, in the order of weaker aromatic bonds. In turn, this supports the notion that aromaticity in graphite is slightly different from smaller aromatic hydrocarbons, which has been suggested previously on different basis.[75] Coherently, we expect a graphite sheet to behave like an extended aromatic system in which bonds are somewhat weaker than the ones in benzene at the individual level.

This simply comes to show that a variety of systems can be tackled with our approach, including periodic materials, and coherent results are obtained.

Chapter 6

Density-Bond Energy Relationships

Contents

In Section 2.4 of Chapter 2, some of the main errors that plague DFT were introduced. In particular, we introduced the notion of density and functional errors in Subsection 2.5.3.

On the other hand, in Chapter 5 we have built an approach to the modelling of chemical bonds which, in spite of its simplicity, is semiquantitative within its domain of application. This was shown to be due to the strongly respected assumptions that the ELF-BCM approach uses as foundations. Several of the fundamental quantities that are used in this approach – and derivations thereafter – require accurate calculation of energetic and electronic features.

Thus, there is a feedback connection between both issues. Currently, DFT is not able to exactly connect the electron density $\rho(\mathbf{r})$ with the energy. We have built a semiquantitative model that achieves this at a local level using DFT data, but we do not know what the effect different DFAs have in the relationship between bonds and energies – we use DFT equilibrium properties to model DFT Intrinsic Bond Energies (IBEs).

In Section 5.3 it was shown for C−C bonds that, on average, DFAs seem to connect bonding densities, equilibrium geometries and IBEs similarly. In this Chapter, we will investigate further in this regard in the wider context of DFT. We will attempt to understand what the effect of different DFAs is on the local properties of chemical bonds, and most of all, the qualitative errors that may arise due to these discrepancies.

6.1 Density errors in modern Density Functional Approximations

As introduced in Section 2.4, DFAs to the exact exchange-correlation functional ($E_{xc}[\rho]$) are usually ordered along Jacob's ladder.[76] This classification uses the fact that higher rungs include more sources of information. An increase in sophistication, however, does not guarantee an increase in performance.

An increase in the number of sources of information does necessarily increase the flexibility of DFAs, allowing them to reproduce features that simpler models could not due to the additional degrees of freedom. Naturally, this is desirable. However, it also means that improvement can be "artificially" insufflated into DFAs through extensive parametrization and fitting. Indeed, this is a popular trend in DFA development, with many DFAs exceeding the 50 parameter mark. Recall, however, that even the simplest DFA is already parametrized to reproduce the HEG model.

Optimizing the parameters in a given DFA formulation always poses two troublesome questions: first one must determine which properties are the ones a fitted DFA should aim to reproduce; afterwards, a set of representative systems has to be chosen for those properties. In general, there are two viable approaches to this conundrum. One is to simply reduce the scope of a given DFA to a certain set of systems and properties, akin to what has been presented in the application of the ELF-BCM approach in Chapter 5, which will be representative for a small chemical space. The main alternative is the creation of vast datasets of chemical information, in an attempt to blindly cover as much chemical space as possible.

In the end, the amount of such parameters varies wildly among DFAs. Two general schools of thought with respect to parametrization coexist nowadays. Some authors try to avoid it at all costs, continuously searching for strict physical constraints that can be mathematically transferred to $E_{xc}[\rho]$.[77] Others embrace the inclusion of empirical

parameters as a necessary yet fruitful tool in the development of accurate DFAs, willing to counterbalance the increase in accuracy for the reference data with a somewhat limited scope.

Both approaches have in common that the energy of the system remains the most relevant observable in terms of parametrization, evaluation, and overall usage, be it in absolute or in relative terms. This is coherent with the fact that that the energy is the most important property, the prevalence of the Hamiltonian operator, and the connection of quantum mechanics and thermodynamics through energies. However, as it will be covered in the next Subsection, it might not always be the best criteria from the parametrization point of view – and finding alternative criteria might not be trivial either.

6.1.1 Quantification of Density Errors

Given the exact expression of $E_{xc}[\rho]$, the energy of a many-electron system is minimal for the exact density distribution (see Section 2.4). However, with DFAs, the relationship between energies and densities is not exactly known.

One practical consequence of this lack of an exact connection is that the self consistent density obtained through a SCF procedure using the KS scheme may not necessarily be the proper one. The only guaranteed fact is that the resulting density satisfies the KS equations for the corresponding exchange-correlation potential v_{xc}. As the SCF operates in terms of the energy, and understanding that the DFA of choice may or may not be close to $E_{xc}[\rho]$, the self-consistent density might not be accurate at all, quite independently from the accuracy of the energy. As previously stated, the energy – be it absolute or relative – is the most relevant property in DFA parametrization and benchmarking. In this context, it has been strongly suggested that excessive parametrization can lead to good thermochemical behavior precisely at the cost of a good description of $\rho(\mathbf{r})$ – and its derived scalar fields.

The electron density $\rho(\mathbf{r})$ can formally be expressed as the derivative of the total energy with respect to the external potential with a constant number of electrons N. From the point of view of simple interpolation theory it is easy to understand why a functional empirically fitted to reproduce the absolute energy may be inaccurate for the derivatives of the energy: just like any function may be fitted by a polynomial of arbitrary order, the energy can be fitted, but the derivatives may be completely wrong.

Summarizing: in KS-DFT uncontrolled effects (i.e. spurious error compensation) can lead to precise results in the energy, the density, both, or the improvement of one precisely at the cost of the other. As the number of empirical parameters increases, the energies may improve – as expected, due to the addition of degrees of freedom to the model – but $\rho(\mathbf{r})$ may worsen. Still, as we have seen in Chapter 4 and Chapter 5, $\rho(\mathbf{r})$-derived quantities contain accesible information related to the energy.

Indeed, attention has been drawn by different authors to the quality of the self-consistent electron density $\rho(\mathbf{r})$ in different DFAs, with a particular focus in recent DFAs that include a significant number of parameters.[78, 79, 80, 81, 82] However, density errors are far less trivial to evaluate than energy errors. In fact, $\rho(\mathbf{r})$ is well known for being rather robust with respect to the calculation level,[83] meaning that differences are generally small in relative terms.[84] In this Subsection we will try to cover some proposals and assess critically their potential issues.

$\rho(\mathbf{r})$	$E_{HF}[\rho]$	$E_{SVWN}[\rho]$	$E_{PBE}[\rho]$	$E_{B3LYP}[\rho]$
HF	-1.132514	-1.136549	-1.165341	-1.172321
SVWN	-1.131812	-1.137237	-1.165704	-1.172620
PBE	-1.131711	-1.136851	-1.166085	-1.173029
B3LYP	-1.131750	-1.136814	-1.166072	-1.173042
FCI	-1.082181	-1.103879	-1.133022	-1.136497

Table 6.1: Energies (a.u.) for the H_2 molecule at internuclear distance $R_{eq} = 0.76090$ using a cc-PVTZ basis set and different methods evaluated using different densities non-self-consistently.

Density error for a given Density Functional Approximation

In Subsection 2.5.3 (Equation 2.149) we defined the density error in terms of the energy, that is, the difference in energy for the exact density functional using the exact density – which is guaranteed to give the minimum energy – and an approximate density. Naturally, as the exact functional is not available, we can only use this definition in relative terms.

As an example, we may compare a few DFAs, namely SVWN, PBE and B3LYP, popular in many contexts, for the humble H_2 molecule once again, using an equilibrium distance $R_{eq} = 0.76090$ Å and a cc-PVTZ basis set. Some key results are summarized in Table 6.1, where the diagonal elements of the first block are the energy given by a DFA using its self-consistent density, and non-diagonal elements are the DFA evaluated on the self-consistent density of a different method. For reference, the FCI energy for this geometry and basis set is -1.172124 a.u. Note that Table 6.1 is not symmetric, which means that two DFAs may be connected following two different paths.

Using the reported data, and assuming that the one-particle density matrix from FCI is exact at this level of theory, we may calculate the density error ΔE^d terms of Equation 2.149 for the DFAs, and thus we obtain

$$\begin{aligned}
\Delta E^d_{SVWN} &= E_{SVWN}[\rho'] - E_{SVWN}[\rho] = -1.137237 + 1.103879 = -0.033358 \\
\Delta E^d_{PBE} &= E_{PBE}[\rho'] - E_{PBE}[\rho] = -1.166085 + 1.133022 = -0.033063 \\
\Delta E^d_{B3LYP} &= E_{B3LYP}[\rho'] - E_{B3LYP}[\rho] = -1.173042 + 1.136497 = -0.036545
\end{aligned}$$

where ρ' is the self-consistent density of the method and ρ is the FCI density. These results suggest that the density error is similar for all three DFAs, albeit a bit larger for B3LYP. As said before, the functional error ΔE^f (cf. Equation 2.150) cannot be calculated on an approximate density without the exact exchange-correlation functional, but we may decompose the total error ΔE (with respect to the FCI result) as $\Delta E = \Delta E^d + \Delta E^f$ to obtain the following functional errors:

$$\begin{aligned}
\Delta E^f_{SVWN} &= 0.034887 + 0.033358 = 0.068245 \\
\Delta E^f_{PBE} &= 0.006039 + 0.033063 = 0.039102 \\
\Delta E^f_{B3LYP} &= -0.000918 + 0.036545 = 0.035627
\end{aligned}$$

In this case, the evolution between rungs seems noticeable: B3LYP has a much smaller functional error than the LDA representative. Nevertheless, note that this analysis is highly biased due to the fact that we are not calculating ΔE^f explicitely. Hypothetically, we could have taken the alternative route, that is, calculating ΔE^f first and then deducing ΔE^d. As the total error is much smaller in B3LYP than in SVWN, the error we evaluate implicitely will probably be smaller.

Let us take HF as the exact exchange-correlation functional and density in order to demonstrate this point. Once again, we evaluate ΔE^d (in which the superscript 1 indicates calculated first) as

$$\begin{aligned} \Delta E^{d1}_{SVWN} &= -1.137237 + 1.136549 = -0.000688 \\ \Delta E^{d1}_{PBE} &= -1.166085 + 1.165341 = -0.000744 \\ \Delta E^{d1}_{B3LYP} &= -1.173042 + 1.172321 = -0.000721 \end{aligned}$$

Again, we get very even and small errors. We now evaluate the functional error ΔE^f in second place (hence the superscript 2) as before:

$$\begin{aligned} \Delta E^{f2}_{SVWN} &= 0.004723 + 0.000688 = 0.005411 \\ \Delta E^{f2}_{PBE} &= 0.033571 + 0.000744 = 0.034315 \\ \Delta E^{f2}_{B3LYP} &= 0.040528 + 0.000721 = 0.041249 \end{aligned}$$

According to which, B3LYP is has the largest functional error. Let us calculate the functional error first now as in Equation 2.150, using HF as the reference "exact" functional;

$$\begin{aligned} \Delta E^{f1}_{SVWN} &= -1.137237 + 1.131812 = -0.005425 \\ \Delta E^{f1}_{PBE} &= -1.166085 + 1.131711 = -0.034374 \\ \Delta E^{f1}_{B3LYP} &= -1.173042 + 1.131750 = -0.041292 \end{aligned}$$

The resulting ΔE^f is nearly opposite to the previous estimate in all cases. We now calculate the density error in second place as

$$\begin{aligned} \Delta E^{d2}_{SVWN} &= 0.004723 + 0.005425 = 0.010148 \\ \Delta E^{d2}_{PBE} &= 0.033571 + 0.034374 = 0.067945 \\ \Delta E^{d2}_{B3LYP} &= 0.040528 + 0.041292 = 0.081820 \end{aligned}$$

The resulting density errors are quite different and significantly larger. Let this example showcase the problems of this definition: the total error is a sort of state function, but only the total error is properly defined. Quite simply, $\Delta E^{f1} + \Delta E^{d2} = \Delta E^{d1} + \Delta E^{f2}$ but in general $\Delta E^{d1} \neq \Delta E^{d2}$. Consequently, this approach is not very pragmatic for the quantification of density errors in a global way, as it would be needed for parametrizing a given DFA ansatz. However, knowing its limitations it can be used critically at times in order to discuss DFT-related problems.

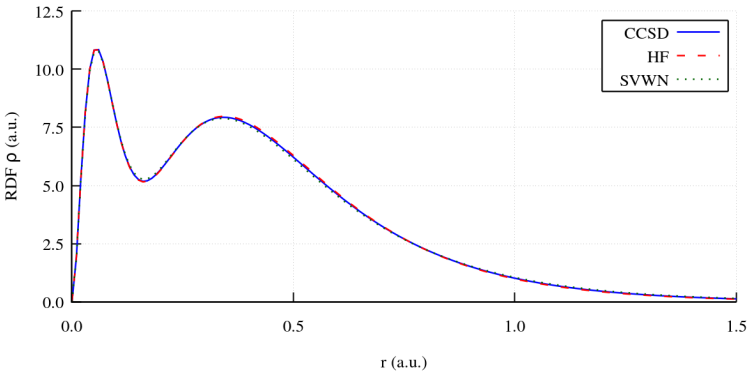

Figure 6.1: Radial Distribution Function (RDF) of the electron density of the Ne atom, calculated with different methods and the def2-QZVPP basis set.

Atomic radial distribution functions

As geometry independent systems, atoms are frequently used models. The radial distribution function of the electron density may be used to quantify density errors.[78] As suggested before, the electron density is quite robust, particularly so in atomic systems. This is due to the extremely strong nuclear potential. Considering the radial distribution function instead of the electron density itself somewhat alleviates the problem by downscaling the nuclear cusp, but still the resulting functions are close to a perfect overlap. This is exemplified on the Ne atom in Figure 6.1.

As a reference, for this system (consider that noble gas atoms are a typical reference dataset for DFA development) the error in the radial distribution function of $\rho(\mathbf{r})$ is always bound by 0.10 a.u. in absolute terms, while the function itself is, for the most part, well over an order of magnitude higher in value. Thus, it is quite hard to appreciate significant differences using this function as an indicator.

Instead of the density itself, we may examine the gradient of the electron density, $\vec{\nabla}\rho(\mathbf{r})$. Given the piece-wise pseudo-exponential shape of $\rho(\mathbf{r})$, we expect the gradient to be more sensitive than the density itself. However, the gradient is still quite robust for atomic systems, as showcased in Figure 6.3. In fact, it is so robust that basis set or algorithmic differences may be more significant than the exchange-correlation potential of choice – for atomic systems in particular.

The differences in gradient are highlighted in Figure 6.4, where it can be noted once more that the scale is extremely small compared to the function itself. In fact, the error is mellowed out in relative terms because the radial distribution function does not downscale the region with the largest values in this case (see Figure 4.3 for reference).

Arguably, the Laplacian of the electron density should be somewhat more sensitive. However, as argued for the gradient, higher order derivatives are far more sensitive to all other factors as well, such as integration grids or basis set choices. Hence, it does not seem that comparing the radial distribution functions of some arbitrary derivative of the density should be very informative.

Most of these issues stem from the fact that atoms are quite exceptional chemical systems. In fact, as suggested in Chapter 1, atoms as isolated quantum systems may be considered more of a model than a chemical species. The density distribution in atoms is very strongly governed by the nuclear potential and the role of the exchange-correlation

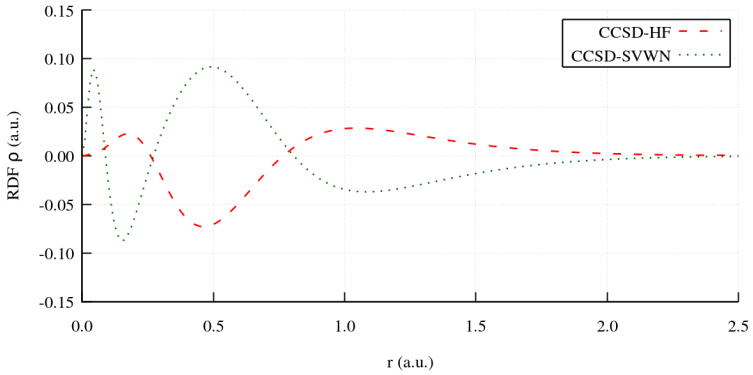

Figure 6.2: Electron density difference Radial Distribution Function (RDF) of the Ne atom with respect to the CCSD level, calculated with different methods and the def2-QZVPP basis set.

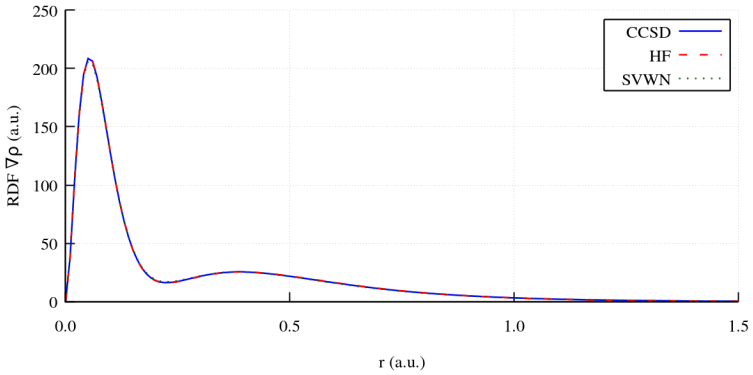

Figure 6.3: Radial Distribution Function (RDF) of the electron density gradient of the Ne atom, calculated with different methods and the def2-QZVPP basis set.

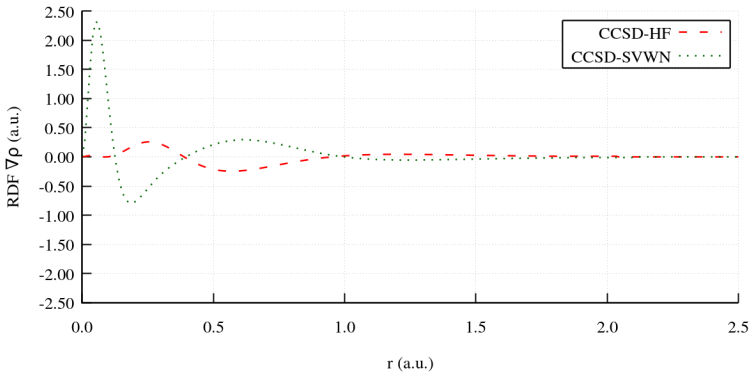

Figure 6.4: Electron density gradient difference Radial Distribution Function (RDF) of the Ne atom with respect to the CCSD level, calculated with different methods and the def2-QZVPP basis set.

potential of choice is very limited. In terms of the density error, we expect ΔE^d to be quite small for atoms. For instance, the Ne using a cc-PVDZ basis set leads to $E_{B3LYP}[\rho'] = -128.871112$ a.u.; if we use the HF density instead we obtain $E_{B3LYP}[\rho] = -128.870651$ a.u., that is, a negligible difference $\Delta E^{d1}_{B3LYP} = -0.000461$ a.u ≈ -0.29 kcal/mol. Similar results are obtained for other DFAs (e.g. $\Delta E^{d1}_{PBE} = -0.40$ kcal/mol) and for other atoms.

In this sense, and considering the values in Table 6.1, it must be noted that the ΔE^{d1} here is *much smaller* in relative terms, considering the much larger energy of Ne. This trend is actually preserved across a wide chemical space: atoms are very uninteresting systems because the features that matter most in chemistry (e.g. bonds, lone pairs) are actually missing. In DFT parlance, we may say that atoms are normal, meaning that the density error ΔE^{d1} is very small. We only expect ΔE^{d1} to be large in situations where a given DFA fails qualitatively in such a way that the self-consistent density is remarkably bad, and this is not the case for an atom where the density is controlled by the nuclear potential – and, to a lesser extent, the basis set choice.

On the other hand, because most of the density is accumulated in the nuclear cusps, atomic densities are very important in the total energy. DFAs relate local properties of $\rho(\mathbf{r})$ with the energy. Given that the value of $\rho(\mathbf{r})$ is higher in the proximity of the nuclei than in the rest of the molecule by several orders of magnitude, the energy of atoms may be a good indicator of the accuracy of a DFA.

Global density differences

Naturally, for a given molecular geometry we may calculate a density difference function in order to evaluate the quality of the density. As the FCI density is quite unaffordable, we may use for instance

$$\rho_{diff}(\mathbf{r}) = \rho_{CCSD(T)}(\mathbf{r}) - \rho(\mathbf{r}) \tag{6.1}$$

in which we assume that the CCSD(T) density matrix is a good reference. This is not a gratuitous assumption, but can be justified by the accuracy of the CCSD(T) method, which gives very good energies and also describes molecular dipole moments, which may be obtained experimentally. This signals that $\rho_{CCSD(T)}(\mathbf{r})$ is indeed a proper density distribution.

For convenience, we may also define a global descriptor Λ_{diff} by integrating over $\mathbf{r}$, as

$$\Lambda_{diff} = \int \mid \rho_{diff}(\mathbf{r}) \mid d\mathbf{r} \tag{6.2}$$

in which the absolute value is taken to avoid compensation from negative and positive regions. As the integration will usually be performed numerically, verifying the grid becomes straightforward. We simply need to assure that

$$\int \rho_{diff}(\mathbf{r}) d\mathbf{r} = 0 \tag{6.3}$$

because naturally the number of electrons N is the same. This is quite convenient. Λ_{diff} is also robust with respect to the integration grid. For example, taking the root mean square deviation – with respect to a reference density – over space, which is arguably a more representative statistical moment, is more sensitive to the grid construction (i.e. uneven sampling of high-error and low-error regions modifies the average significantly). In any case, both descriptors should be related to the distribution, and thus we will go

with the advantageous Λ_{diff} for simplicity. Do note that the grid sampling issue is quite critical, as showcased by the radial distribution function plot of Figure 6.2. There are several points in which the error is effectively 0, and thus there is a potential sampling scheme in which the error is zeroed out. We expect to avoid such issues with Λ_{diff}.

The robustness of $\rho(\mathbf{r})$, as well as its prevalence near nuclei, means that distributions do not change much qualitatively. This is shown for the CO molecule in Figure 6.5 using HF and the PBE DFA as examples at a fixed geometry ($R_{eq} = 1.1304$ Å). Empirically it is found that $\rho_{diff}(\mathbf{r})$ is maximal near nuclear positions, which is shown analogously in Figure 6.6. This is not very surprising, considering that most of the density is surrounding the nuclei. In this particular case, PBE seems to perform significantly worse in the vicinity of the nuclei.

However, in relative terms, the error is spread quite differently. Due to the fact that very small density values – over somewhat large regions of space – account for chemical bonds and lone pairs, the error in relative terms is usually significantly larger for bonding regions than for core regions. This is exemplified in Figure 6.7 using the same system as before. Note how, in relative terms, the error near the nuclei is less than 0.5%, while it can be up to 10% in some chemically meaningful regions. In fact, sampling a variety of chemical systems reveals that these relative errors can be even larger, up to a striking 25%.

Thus, at this point it seems coherent to think about density error localization, rather than quantification. If we attempt to quantify density errors in absolute terms we will mostly measure errors in core densities (i.e. surrounding the nuclei), which are not necessarily chemically relevant. Normalized metrics or arbitrary partitions can forfeit chemically relevant information, as it will be shown later using Λ_{diff} (Equation 6.2), and would naturally compromise any global measurement of ρ_{diff} as an indicator of quality.

As covered in Section 3.1 of Chapter 3 from the orbital point of view, and in Section 4.2 from the real space point of view, we expect chemistry to arise from deviations from atomic behavior. This much can be understood as the formation of molecular orbitals from the interaction of atomic orbitals (e.g. bonding orbitals), leading to larger probability densities, or as a reorganization of $\rho(\mathbf{r})$ itself (i.e. apparition of critical points). Core densities are disregarded as chemically meaningful in many contexts, including frozen core approximations (on which we have commented before), pseudopotentials in basis set expansions and even in the model developed in Chapter 5. Chemistry, at least for the most part, is quite disjointed from the feature of inner core electrons which do not interact, which is perhaps more easily understood considering the extremely low energies of core orbitals and the derivations in Section 3.1 and Subsection 3.1.1 in particular. For the most part, core orbitals remain unaltered upon chemical transformation and their contribution to the total energy is thus constant.

Due to the observations in this Subsection, and the aforementioned thoughts on the relevance of core densities, in the following Subsections we will try to use some tools from Chapter 4 to dissect the errors in $\rho(\mathbf{r})$ in space, instead of using global descriptors. We will, however, commence by understanding and demonstrating empirically how poorly global descriptors behave and how this ineffectivity is linked to the localization of density errors.

6.1.2 Delocalization Error

As we have seen in the previous Subsection, density errors are more significative (in relative terms) in bonding regions than in core regions. This observation can be

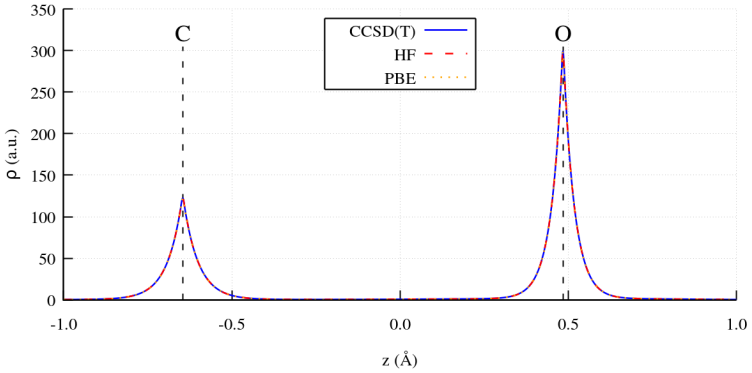

Figure 6.5: $\rho(z)$ along the internuclear axis of CO. Calculated with different methods and the cc-PVDZ basis set. Dashed lines indicate the position of each nuclei.

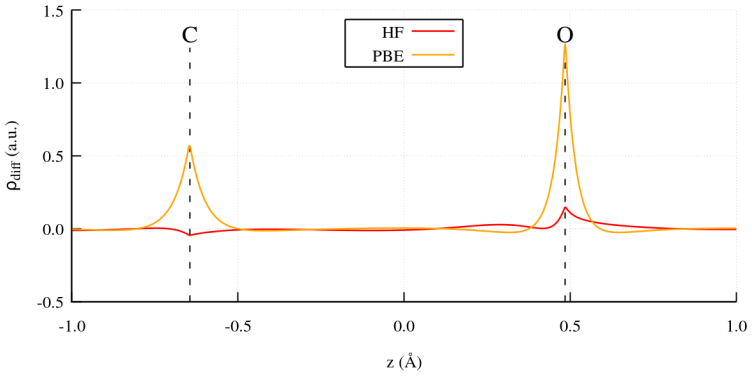

Figure 6.6: $\rho_{CCSD(T)}(z) - \rho(z)$ along the internuclear axis of CO. Calculated with different methods and the cc-PVDZ basis set. Dashed lines indicate the position of each nuclei.

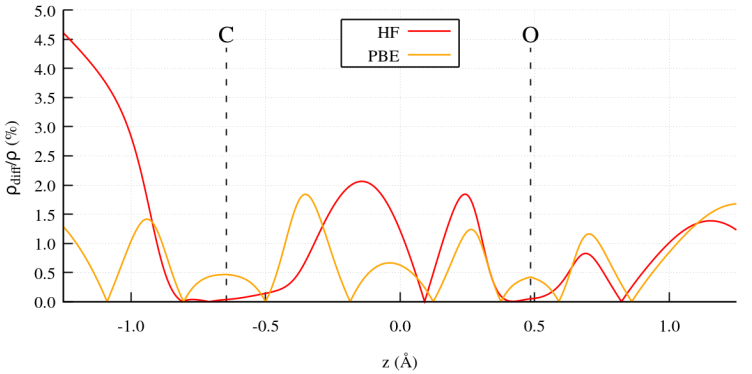

Figure 6.7: ρ_{diff} (Equation 6.1) as a percentage of $\rho_{CCSD(T)}(z)$ along the internuclear axis of CO. Calculated with different methods and the cc-PVDZ basis set. Dashed lines indicate the position of each nuclei.

understood in terms of the SIE (see Subsection 2.5.3), which is often interpreted in terms of delocalization. As we have discussed, local and semilocal DFAs suffer from dramatic SIEs which, specially at the low N limit, cause a qualitative breakdown. Recall that this is given by the fact that electrons interact with themselves because the exchange integral does not cancel out with the coulomb integral. In HFT, there is no SIE, but there is no instantaneous electron correlation whatsoever (see Section 2.3 for details): electrons do not interact with each other instantaneously.

Core electrons are tightly bound to the nuclear potential, which in most cases (as Z increases) is extremely strong in the vicinity. Hence, correlation effects are less relevant locally, as the one-electron electron-nuclei term is far larger. This does not mean that the correlation energy of core electrons is small, in fact it will almost always be very large (averaged per electron). However, we expect that it will almost always be the same in different chemical environments. Analogously, SIEs between core electrons will also be large due to the enormous values of $\rho(\mathbf{r})$ near nuclei, but constant and not qualitatively meaningful compared to the nuclear potential. Core-valence effects, however, may be relevant for an accurate description.

As far as covalent bonds are associated with localized electron densities which are far from the nuclei, it is reasonable to think about them as sensitive to both delocalization and correlation effects. In such a bond (e.g. covalent bond in H_2), there is a significant density accumulation, owing to the formation of a bonding orbital, in MO theory terms. The bonding orbital will be a linear combination of the hydrogen $1s$ AOs, which are exponentially decaying otherwise, and normalization will impose that it takes significant values in the internuclear region. Analogously, we expect the kinetic energy density to be quite reduced in the region belonging to the chemical bond. Now, in this covalent bond, the two electrons that belong to the bonding orbital have opposite spin and are consequently correlated through Pauli's principle. In HFT there is no more correlation to be seen: the two electrons will only interact electrostatically with an average, and the probability density of the MO will be maximal near nuclei (for illustrative purposes, the electron density in H_2 is presented in Figure 4.2). Therefore, other than the α and β spin restriction, the electrons in the bond barely interact with each other.

In a local DFA, however, the situation is quite different. Because the electrons formally interact with themselves, the coulombic repulsion they feel with respect to each other is significanlly increased. The two electrons can not be very localized due to this additional (unphysical) repulsion: they tend to spread more. This is not surprising, as LDA is based on the homogeneous electron gas, in which electrons are spread homogeneously.

Let us exemplify this. In a minimal basis set calculation of H_2 there is no optimization of the MO coefficients (recall Subsection 3.1.1), therefore the only density difference between HF and a given DFA is R_{eq}, which enters in the MO expression through the overlap integral, and the energy evaluation that determines the optimal bond length. Coherently, R_{eq} is (using a minimal STO-3G basis set) 0.7122 Å at the HF level, and increases to 0.7361 Å using the SVWN3 LDA. The FCI result is $R_{eq} = 0.7349$, which lays in between the two results but significantly closer to the DFT calculation. For reference, MP2 leads to $R_{eq} = 0.7237$ which is also in between them. In a sense, the DFA mimics correlation effects, albeit the effect is subtle in this case.

If we move to a more sensitive system, $H_2{}^+$, we now find $R_{eq} = 1.0606$ for HF/STO-3G and $R_{eq} = 1.1454$ for the LDA. The difference is almost a 10% of the internuclear distance because here SIE is not compensated by correlation effects missing in HF.

This fact systematically leads to DFT energetically favouring delocalized densities due to the energetic penalty SIE inflicts in localized densities. Hence, these errors are sometimes referred to as delocalization error.

Bond length alternation

A prototypical example of delocalization error in action is the description of conjugated systems. Conjugated double bond chains are sensitive to this error because HF tends to localize electrons, leading to stronger double bonds and weaker single bonds, and LDAs tends to make all distances similar to each other due to the artificial delocalization of the density. Thus, as in the previous example, the optimized geometries are significantly affected by the method.

Thus, we may collect the differences between two approximate methods in a single number known as Bond Length Alternation (BLA)[85]:

$$BLA = \frac{\sum_i l_{db,i} - l_{sb,i}}{i}$$

where $l_{db,i}$ and $l_{sb,i}$ are the lengths of adjacent double and single bonds for each ith $-$CH$=$CH$-$ unit. Small BLAs reveal that double and single bonds are very similar in length and vice-versa. Consequently, we may predict HF to lead to large BLAs, with strongly localized double and single bonds that are dissimilar in length, and LDAs to lead to smaller BLAs. A BLA near 0 means that all bonds are nearly equal. Note that BLAs can be calculated using bond orders or other descriptors for bonds.

The evolution of BLA with the number of $-$CH$=$CH$-$ units, calculated with different methods, is presented in Figure 6.8. As expected, HF provides the least delocalized and LDA the most delocalized conjugated system. The reference value at hand, calculated with the a simplified coupled cluster method (details on the CC2 method can be found in Reference [86]), as well as other calculation levels, all fall within the HF/LDA range. The difference between the HF and LDA value is quite large: at two $-$CH$=$CH$-$ units it represents 30% of the absolute value, and it increases with the length of the chain. This leads to a large overall difference between the two methods, and a qualitatively different description of the system. It also exemplifies a well-known caveat of delocalization error: it depends on the size of the system, which is a tremendous pitfall for the modelling of certain periodic systems.

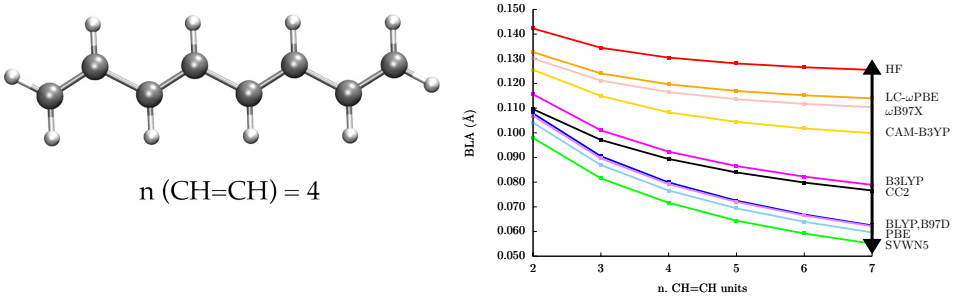

Figure 6.8: Bond Length Alternation (Å) in a chain of conjugated double bonds as the length of the chain increases. Calculations carried out with different DFAs, Hartree-Fock and CC2.

6.1.3 Localization of Density Errors

Different subspaces of $\rho(\mathbf{r})$ contribute differently to the energy in DFT.[87, 88] Analogously, different energy-based corrections of DFAs, such as those for self-interaction errors (cf. Subsection 2.5.3), have been shown to affect the density in a similar way in internuclear regions.[89, 90]

In Subsection 6.1.1 we have shown how, in relative terms, the description of bonding regions is far more method-dependant than those of core regions. As discussed in the previous Subsection, we expect the density on bonding regions to be particularly important for the correct description of chemical phenomena. Indeed many DFAs are parametrized with respect to relative energies (e.g. reaction energy barriers), where core effects are expected to remain quite constant. Thus, there is a possibility that energy-based parametrization strategies indirectly improve the density in some meaningful regions of space.

Potentially, this implies that a heavily parametrized DFA that draws on relative energies may be very accurate at describing bonding densities, even if the core densities (which are more relevant for absolute energies) are ill-described. As shown before, any global measurement of the quality of $\rho(\mathbf{r})$ would unfairly deem this DFA "unphysical" or "density-error prone", because core densities are prevalent in absolute terms. On the other hand, it could be argued that such a DFA is more chemical than one that accurately describes the absolute energy of, for instance, He, but underestimates reaction energy barriers.

The only way to clarify this question is evaluating the quality of $\rho(\mathbf{r})$ not as a global indicator, but rather focusing on a given localized region of space. As seen in Chapter 4, partitioning schemes based in the kinetic energy density are particularly well suited for this purpose. As an example, the electron density and two scalar fields that were discussed in Chapter 4 for the CO molecule are shown in Figure 6.9. Note how both ELF and LOL are able to separate the core region containing most of the density from the valence region.

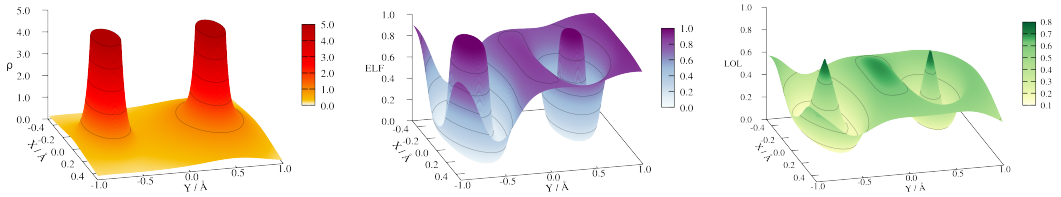

Figure 6.9: Functions calculated over the σ_v plane of the CO molecule at the CCSD/cc-PVDZ level: **A)** $\rho(\mathbf{r})$ **B)** $\eta_{ELF}(\mathbf{r})$ **C)** $\eta_{LOL}(\mathbf{r})$.

Let us bring back the LOL from Subsection 4.3.1 (see Equations 4.48 and 4.49 for details). Recall that $\eta_{LOL}(\mathbf{r}) = 1/2$ when the kinetic energy density of the system is equivalent to that of an HEG of the same density.

Figure 6.10 shows $\rho_{diff}(\mathbf{r})$ over the σ_v plane of the N_2 molecule coupled with $\eta_{LOL}(\mathbf{r}) = 1/2$ countours, as calculated at a fixed equilibrium geometry $R_{eq} = 1.0984$ Å and a very large aug-cc-pCVQZ basis set. Note how the bonding region, as contained by the LOL isosurface, matches a distinct excess or defect of electron density depending on the method. Recall that, given the definition in Equation 6.1, $\rho_{diff}(\mathbf{r}) < 0$ imply an excess of electron density given by the method with respect to CCSD(T).

It seems, therefore, that HF accumulates more density than it should in the bonding region, while local and semilocal DFAs have a deficit of electron density in the bond. The LDA, GGA and hybrid representatives (SVWN3, PBE and TPSSh) present increasing quality while belonging to a similar trend in which $\rho(\mathbf{r})$ is generally higher than the reference in the core region and spreads in a relatively smooth way compared to HF. The fact that hybrids seem to be somewhat in between HF and local DFAs, and thus provide a better density, is to be expected: if HF and GGAs manifest opposite trends, they should somehow compensate each other when HF-like exchange is combined with local correlation. M062X, on the other hand, exhibits a different error distribution over the plane, which resembles a linear combination of HF and GGA far less. In a way, this means that the parametric degrees of freedom in its formulation are able to introduce significant flexibility with respect to a simpler DFA; but it also means that the behavior is less predictable in this regard. Note that, so far, our observations agree with the analysis in Subsection 6.1.2 in terms of delocalization error.

More $\rho_{diff}(\mathbf{r})$ maps are given in Figures 6.11 to 6.13. It is clearly apparent that some error distributions are related with chemical entities, such as the one of HF or SVWN3, while others are quite bizarre (e.g. M06L). Given our observation, it can be suggested that *some* DFAs localize errors in an intuitive way, while others do not. This does not interfere with our previous analysis: the error in absolute terms is always maximal in the core regions, and only by removing those we can begin to appreciate valence errors which we expect to be more meaninhful. Indeed, these features do not seem to be related with the global performance of a given DFA, as measured by Λ_{diff}. This is in turn showcased in Figures 6.14 and 6.15, which are analogous calculations for the CO and C_2H_6 molecules at their respective CCSD(T)/aug-cc-pCVQZ equilibrium geometries: DFAs that lead to very similar Λ_{diff} values have significantly different error localization patterns (e.g. BHandH and M052X in the case of CO, with almost identical $\Lambda_{diff} = 0.1165$ a.u. and $\Lambda_{diff} = 0.1168$ a.u.).

Analogously, it may be noted that HF consistently has an excess of electron density in the bonds considered, which are in all cases covalent. Other than that, Λ_{diff} increases significantly on average when moving from CO or N_2 to C_2H_6, in spite of remaining within the same number of electrons, because more nuclei mean more cusps on which the error is maximal. Hence, global descriptors are not very transferable (on top of biased).

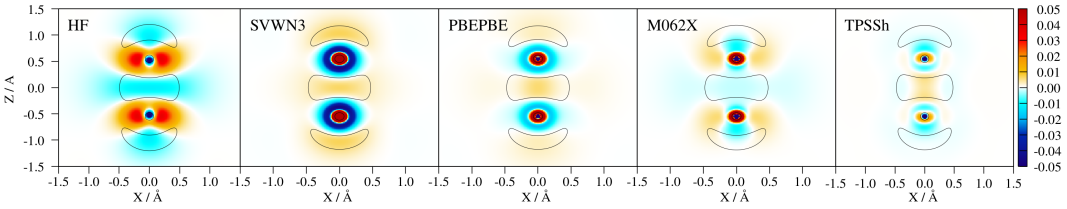

Figure 6.10: Electron density difference ($\rho_{diff}(\mathbf{r})$, Equation 6.1) maps on the σ_v planes of the N_2 molecule at R_{eq}. $\eta_{LOL}(\mathbf{r}) = 0.5$ isolines are shown in black. Methods are detailed in the top left corners, left to right: HF, SVWN3, PBEPBE, M062X and TPSSh. Basis set is aug-cc-pCVQZ in all cases.

There is a final, often overlooked, downfall to consider in global descriptors: wherever we are not purely focused on atoms (see the previous Subsection in that regard) the geometry comes into play. Λ_{diff} can only be computed with a static molecular geometry. However, as we have seen, the very subtle – but likely key – differences in bonding regions

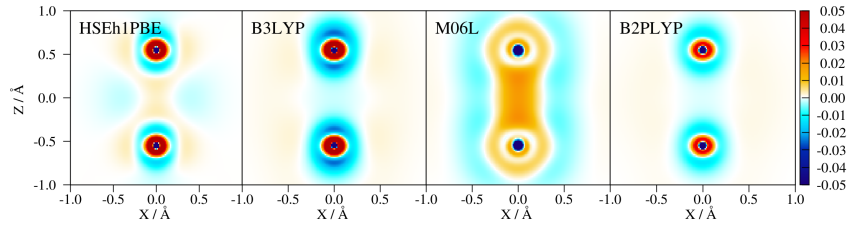

Figure 6.11: Electron density difference ($\rho_{diff}(\mathbf{r})$, Equation 6.1) maps on the σ_v planes of the N_2 molecule at R_{eq}. Methods are detailed in the top left corners, left to right: HSEh1PBE, B3LYP, M06L and B2PLYP-FC. Basis set is aug-cc-pCVQZ in all cases.

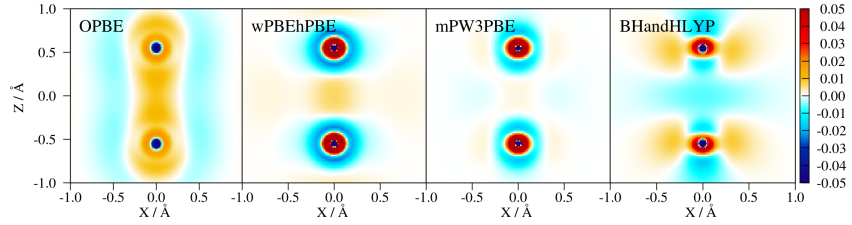

Figure 6.12: Electron density difference ($\rho_{diff}(\mathbf{r})$, Equation 6.1) maps on the σ_v planes of the N_2 molecule at R_{eq}. Methods are detailed in the top left corners, left to right: OPBE, wPBEhPBE, mPW3PBE and BHandHLYP. Basis set is aug-cc-pCVQZ in all cases.

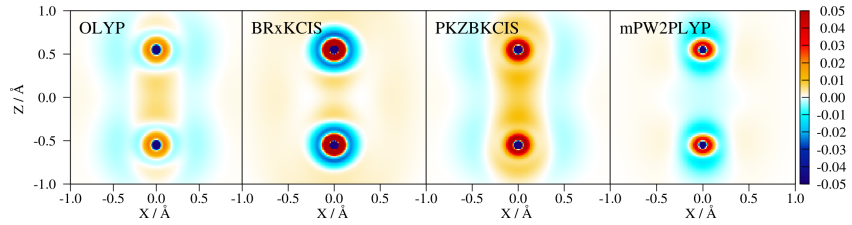

Figure 6.13: Electron density difference ($\rho_{diff}(\mathbf{r})$, Equation 6.1) maps on the σ_v planes of the N_2 molecule at R_{eq}. Methods are detailed in the top left corners, left to right: OLYP, BRxKCIS, PKZBKCIS and mPW2PLYP-FC. Basis set is aug-cc-pCVQZ in all cases.

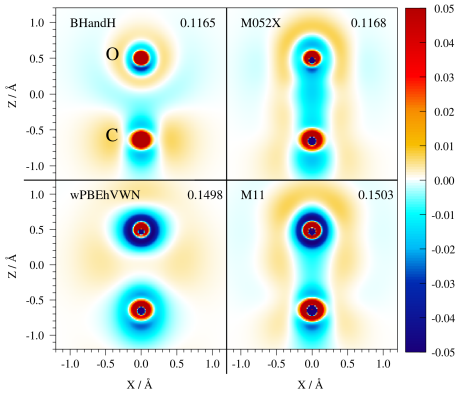

Figure 6.14: Electron density difference ($(\rho_{diff}(\mathbf{r})$, Equation 6.1) maps on the σ_v planes of the CO molecule at R_{eq}. Methods are detailed in the top left corners, left to right and top to bottom: BHandH, M052X, wPBEhVWN and M11. Their values of Λ_{diff} are: 0.1165, 0.1168, 0.1498 and 0.1503 a.u. respectively. Basis set is aug-cc-pCVQZ in all cases.

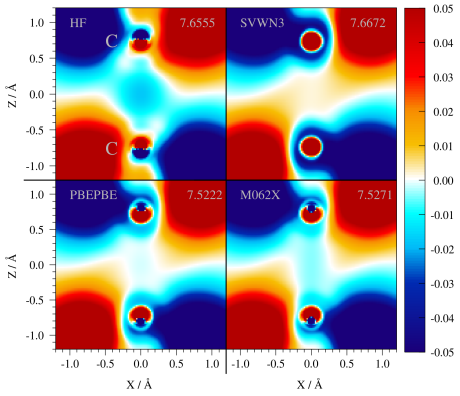

Figure 6.15: Electron density difference ($\rho_{diff}(\mathbf{r})$, Equation 6.1) maps on the σ_v planes of the ethane C_2H_6 molecule at R_{eq}. Methods are detailed in the top left corners, left to right and top to bottom: HF, SVWN3, PBEPBE and M062X. Their values of Λ_{diff} are: 7.6555, 7.6672, 7.5222 and 7.5271 a.u. respectively. Basis set is aug-cc-pCVQZ in all cases.

may quickly switch signs if geometries are reoptimized. Such is the scale of the density differences in bonding regions that a small geometric distortion may affect the difference significantly, even qualitatively.

For instance, let us assume that HF will always place an excess of electron density in covalent bond regions with respect to CCSD(T) – at the CCSD(T) equilibrium geometry. This accumulated density will naturally alleviate the internuclear repulsion, and hence should lead to a shorter bond if the geometry is reoptimized at the HF level of theory. The resulting contraction may as well end up dispersing density from the internuclear axis so that, if each of them is considered in their equilibrium geometries, $\rho(\mathbf{r})$ is the same. This means that, for the same density, HF alleviates the internuclear repulsion much better in terms of energy.

The opposite may be happening with local DFAs, which have been shown so far to place less electron density in bonding regions than CCSD(T). This comes to show the possible bias introduced by fixing the geometry. Arguably, most "normal" systems do not have very distinctly different geometries for different (well-established) methods. On the other hand, precisely the systems in which DFT desperately needs improvement may have vastly different equilibrium geometries in different levels of theory. For instance, the He_2 dimer that was showcased in Chapter 2 (Subsection 2.5.4) is such an example, in spite of its simplicity.

Global descriptors and properties

So far we have strongly argued Λ_{diff}, as well as other global descriptors of the quality of $\rho(\mathbf{r})$, should not be that effective due to the localization of density errors. As in Chapter 5, a diverse array of DFAs is required to test our assumptions empirically. In this Chapter,

we will use a set of 59 different DFAs in KS-DFT, plus HF and Frozen Core MP2 methods. The total array of 61 methods will be referred to as the DFA set with numbers *1* to *61*. The list of all DFAs and the numbering is available in the corresponding Subsection 5.3.3, as it is the same as before. A significantly larger aug-cc-pCVQZ quadruple-ζ basis set was used in this Chapter to ensure that basis set incompleteness is negligible; this basis set includes a set of core functions to improve the description of the nuclear cusps.

Let us start by looking at the CO molecule once more. Λ_{diff} was calculated for all the DFA set. In this particular case, the use of the CCSD(T) density as a reference is supported by the calculated dipole moment of 0.1169 D, within the uncertainty of the experimental value of 0.112 ± 0.005 D.[91] As shown in Figure 6.16, Λ_{diff}, for a set of functionals, is not correlated with the root mean square deviation of absolute or atomization energies (ΔE_{atom}) with respect to CCSD(T), nor with a better dipole moment, all calculated at the same geometry. This is particularly telling, because obviously we expect an appropiate distribution to give an appropiate dipole moment. As Λ_{diff} measures absolute deviations, we might have hoped that it would be correlated with worse dipole moments, because at a constant N it could potentially measure the "charge-transfer" between the two atoms. However, this is not the case, signaling that most of the reorganization is strictly intra-core. The two largest errors in the dipole moment do match the two largest values of Λ_{diff}, but all other DFAs are indistinguishable. At the same time, do note the scale of the errors in the dipole moment, which can be as large as a 350% – these are not small errors. All things considered, it appears that such reorganizations are, for the most part, chemically irrelevant; and therefore Λ_{diff} is not meant to correlate with the accuracy of any relevant property.

In order to check whether the Λ_{diff} was correlated with the error in localized regions of space, we computed the population of the ELF disynaptic basin Ω^V_{CO}, which for simplicity we shall denote Ω_b where the b subscript indicates simply "bond". Note that the population of such disynaptic basins was consistently called q in the context of the ELF-BCM approach (cf. Section 5.2). As shown in the last panel of Figure 6.16, there is no correlation between Λ_{diff} values and the accuracy of the electron population of the triple bond, Ω_b. This corroborates that Λ_{diff} is, for the most part, dominated by errors in core regions.

Summarizing, this example on the CO molecule proofs that the errors in the electron density cannot be related to the errors in properties on their own. As previously critisized, recall that Λ_{diff} and similar descriptors must be computed using frozen geometries and relatively strong electronic forces may be present for some DFAs. All our observations so far are replicated in N_2 (Figure 6.17), C_2H_6 (Figure 6.18) and other molecules. Consequently, the minimization of Λ_{diff} as a DFA parametrization criterion does not seem to be useful at all, nor it is useful for interpretative purposes because it is not able to grasp the localization patterns of density errors.

Localized descriptors

As we have thoroughly argued and shown that global descriptors, as introduced in Subsection 6.1.3, are a poor choice for most applications, we will switch to a different paradigm from now on.

By focusing only on the electronic population of a given covalent bond, given by the disynaptic ELF basin Ω_b, we may reveal explicitly the effect of different DFAs in the chemical bond. In principle, integrating $\rho(\mathbf{r})$ in Ω_b gives a number of electrons associated with the bond, at any given geometry, and thus constitutes a transferable index because,

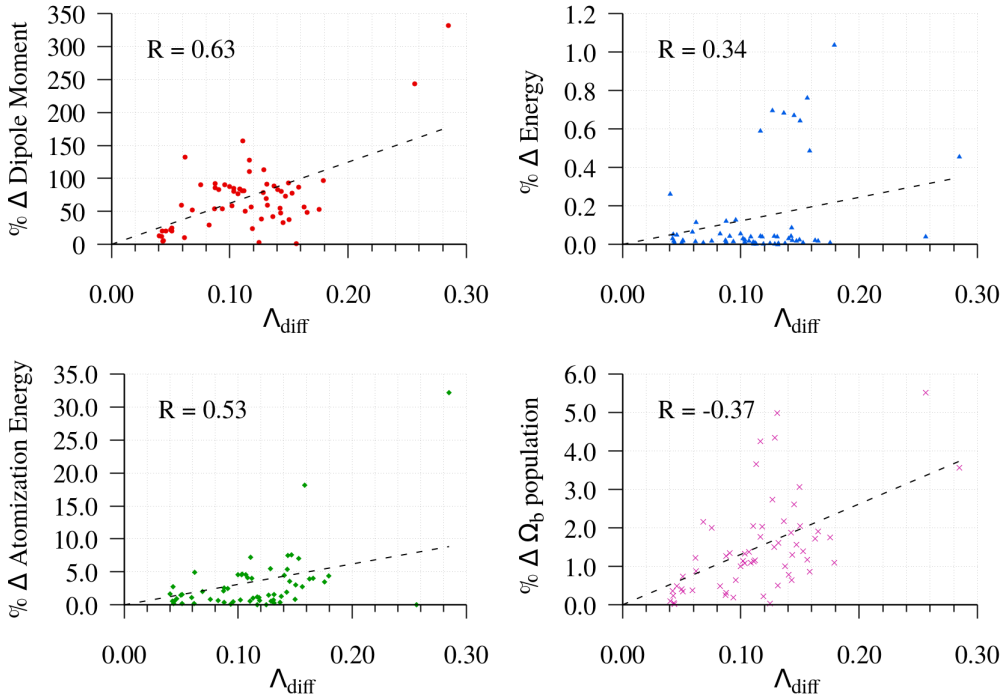

Figure 6.16: Correlation between Λ_{diff} and the relative error with respect to the CCSD(T) reference in several properties for the CO molecule at R_{eq} for the DFA set. Least-squares fits are drawn as dashed black lines with their Pearson correlation coefficients shown top left of each plot.

in this case, geometries can be optimized tightly for every method. This is coherent because, due to the robustness of $\rho(\mathbf{r})$, the change in geometry from a given reference to the minima of the potential energy surface for each DFA may switch a method from an "overpopulated" (i.e. more density than the reference in the bond region) basin to an "underpopulated" one, better reflecting the character of the DFA. Other integrated topological descriptors, such as AIM charges (see Section 4.2 of Chapter 4), are equally comparable at different geometries.

Following the previous example, for which we know that the CCSD(T) density is accurate, the bond populations for all the methods in the DFA set have been calculated. As in Chapter 5, attractors and basins have been merged accordingly in order to retrieve the full triple bond population whenever needed, as not all DFAs provide isotopological ELF profiles due to degeneracy issues (see Section 4.3 for details). Raw results are presented in the Appendix (Section A.2), but a small selection is collected in Table 6.2 for illustrative purposes. Once more, results match previous observations, with HF being clearly the most populated basin, and both PBE and SVWN3 less populated than the CCSD(T) reference, as per the delocalization error they suffer. Most higher rungs DFAs give bonding densities somewhat in between.

As noted before, from an electrostatic point of view higher charge concentrations in bonding domains should coherently lead to stronger bonds, and indeed HF seems to lead to bonds that are both shorter and have higher densitiy values. Figure 6.19 A shows that

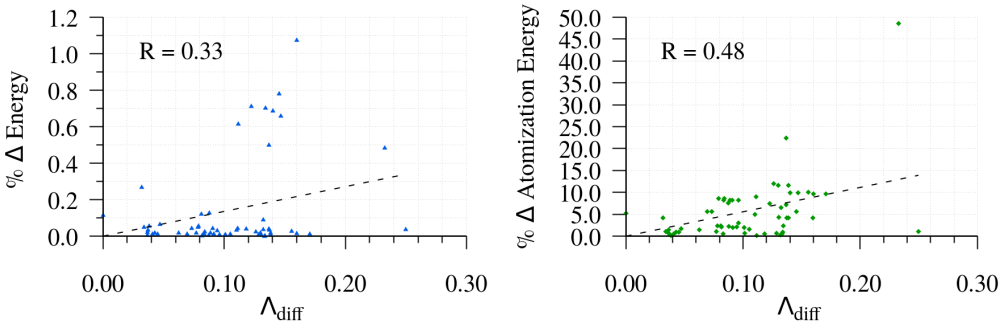

Figure 6.17: Correlation between Λ_{diff} and the relative error with respect to the CCSD(T) reference in several properties for the N_2 molecule at R_{eq} for the DFA set. Least-squares fits are drawn as dashed black lines with their Pearson correlation coefficients shown top left of each plot.

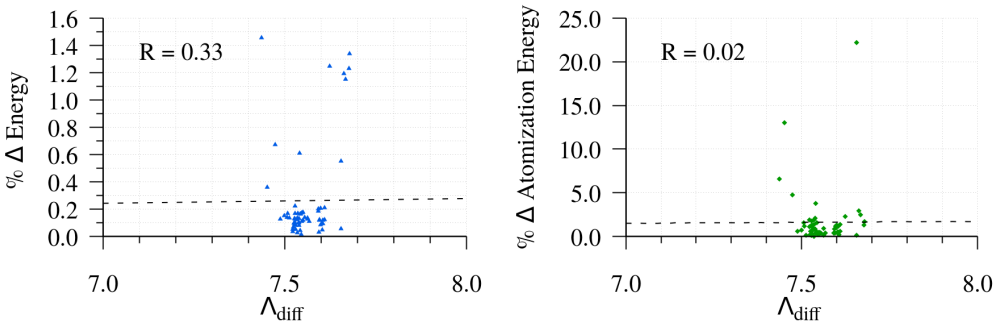

Figure 6.18: Correlation between Λ_{diff} and the relative error with respect to the CCSD(T) reference in several properties for the ethane C_2H_6 molecule at R_{eq} for the DFA set. Least-squares fits are drawn as dashed black lines with their Pearson correlation coefficients shown top left of each plot.

Method	Pop. Ω_b	Vol. Ω_b	R_{eq}	ω_h	ΔE_{atom}
PBEPBE	3.0110	59.09	1.1353	2162.47	269.16
BLYP	2.9835	54.84	1.1355	2161.34	262.21
B3LYP	3.0874	62.45	1.1237	2251.95	255.69
mPW1LYP	3.1014	63.45	1.1218	2266.82	251.96
HF	3.3040	74.56	1.1019	2426.46	175.70
SVWN3	3.0607	59.65	1.1255	2237.59	303.93
CCSD(T)	3.0741	71.51	1.1294	2168.92	257.25

Table 6.2: Descriptors for the respective equilibrium geometries of CO. Population of Ω_b in electrons, volume of Ω_b in a.u.$^{-3}$, equilibrium distances (R_{eq}) in Å, harmonic frequencies (ω_h) in cm^{-1} and atomization energies (ΔE_{atom}) in kcal/mol.

this is not necessarily the case at all times, as a linear dependency leads to a fitted line with $r^2 = 0.5184$. The same applies for N_2 and C_2H_6, in Figures 6.20 A and 6.21 A, respectively. Similar results are obtained for harmonic frequencies (Figures 6.19 C, 6.20 C, and 6.21 C). This is coherent because harmonic frequencies are usually collinear with bond lengths.

Regarding energetic features, the electronic population of Ω_b does not strongly correlate with the atomization energy ΔE_{atom} of the C≡O bond, as shown in Figure 6.19B. Neither it does with the atomization energy of N_2 (Figure 6.20 B), nor with the Bond Dissociation Energy (BDE) of the C−C bond in ethane (Figure 6.21 B). It should be noted that strong trends may be observed in certain handpicked subsets (e.g. DFA families with the same correlation term), but this does not justify in any way a rigorous connection between the bonding density and the atomization energy that can be used as a reference.

Finally, volume and population of Ω_b are not inter-correlated (Figures 6.19 D, 6.20 D and 6.21 D), which signals that the integrated electron density of the basin is related to the quality of both $\rho(r)$ and $\tau(r)$, as a larger volume does not imply a higher integrated charge. In these cases, bond basins usually are enclosed by larger valence basins (from lone pairs or hydrogenoid bonds) and thus a reasonable volume estimate can be obtained. Still, a numerical threshold based on the electron density is used to limit volumes whenever the function is asymptotically decaying ($\rho(\mathbf{r}) \leq 0.001$ a.u.).

Perhaps surprisingly, the CCSD(T) result lies within the cloud of DFA results for all three systems hereby presented (Figures 6.19–6.21) and, in many cases, roughly lies at separation between pure and hybrid DFAs. The pure-hybrid distinction is blurred in the case of ethane (Figure 6.21) because certain DFAs overlocalize C−C bonds, while others favor localizing C−H bonds instead. This circumstance exemplifies how increasingly polyatomic molecules may achieve, through error compensation, accurate results in DFT.

For harmonic frequencies, atomization energies and bond lengths, GGAs, meta-GGAs and low-exact exchange functionals fall close to the MP2-to-CCSD(T) level. The success of DFT in any of these features, and in bonding densities, is remarkable; moreso when compared to the HF results which are in principle similar in computational cost and in nature. CCSD(T), as expected, gives harmonic frequencies, distances and atomization energies within 1% of the experimental values in all cases.

While DFAs surrounding the CCSD(T) result are very accurate at a relatively low cost, it is also evident that some hybrid DFAs, specially those with a high percentage of exact exchange, tend to deviate towards the HF results. Given that HF is exchange-focused, it may be suggested that there is an underlying connection between exchange effects, correlation effects and bonding densities. This will be investigated in the following Subsection in detail.

6.1.4 The role of exact exchange in bonding densities

In Subsection 2.5.2 of Chapter 2 we introduced hybrid DFAs which incorporate exact exchange, which is justified along the adiabatic connection. In this sense, note that the success of hybrid DFAs can, a priori, be attributed to a variety of reasons. As we have discussed before, increased flexibility in the formulation, due to additional adiabatic parameters, should naturally result in better results in benchmark sets. The SIE correction, due to exchange cancelling self-interaction, is naturally key in many cases, as exemplified in H_2^+ in Subsection 2.5.4. A third potential reason that we want to highlight now is the fact that non-local behavior is incorporated through exchange into

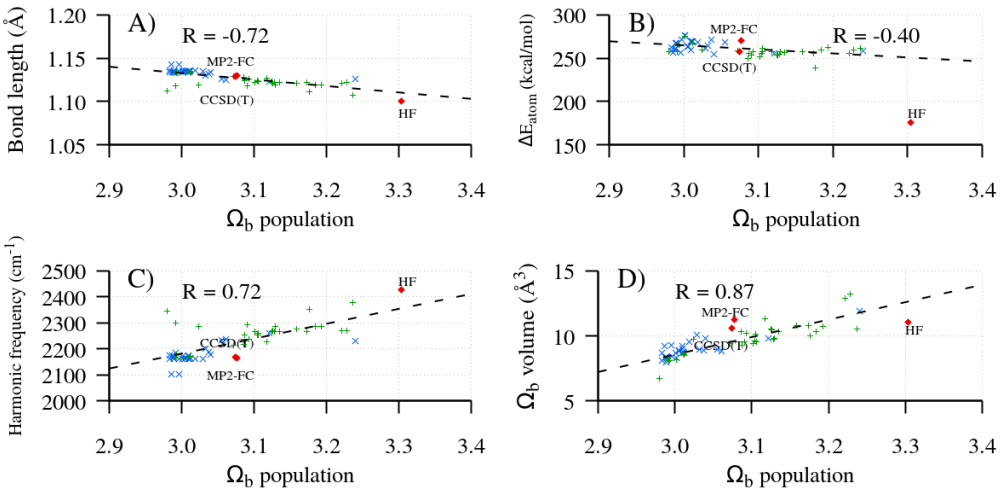

Figure 6.19: Correlation between the population of Ω_b and several descriptors for the CO molecule as calculated by the DFA set, HF, MP2 and CCSD(T). **A)** Bond length (Å) **B)** ΔE_{atom} (kcal/mol) **C)** Harmonic frequencies (cm^{-1}) **D)** Ω_b volumes (Å^3). Pure functionals are colored blue, hybrid and double hybrid functionals are colored green, and wavefunction methods are colored red. Least-squares fits to the DFA set data are drawn as dashed black lines with their Pearson correlation coefficients shown in each plot.

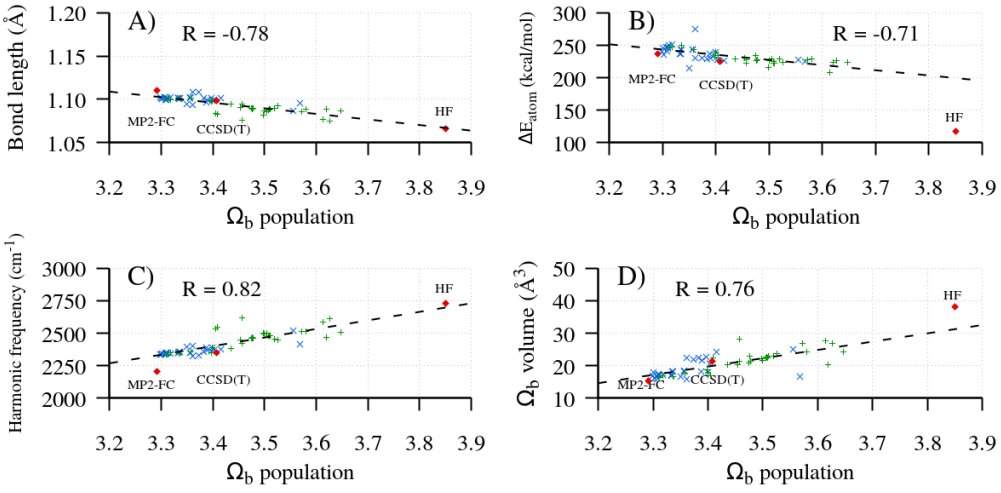

Figure 6.20: Correlation between the population of Ω_b and several descriptors for the N_2 molecule as calculated by the DFA set, HF, MP2 and CCSD(T). **A)** Bond length (Å) **B)** ΔE_{atom} (kcal/mol) **C)** Harmonic frequencies (cm^{-1}) **D)** Ω_b volumes (Å^3). Pure functionals are colored blue, hybrid and double hybrid functionals are colored green, and wavefunction methods are colored red. Least-squares fits to the DFA set data are drawn as dashed black lines with their Pearson correlation coefficients shown in each plot.

otherwise local DFAs. Exchange is non-local by default, while the exchange-correlation terms in LDAs and GGAs are all based in local properties of $\rho(\mathbf{r})$. Hence, the inclusion of exact exchange is, beyond question, a valuable asset of DFA development.

In the previous Subsection we have appreciated that the electron density in the ELF disynaptic basin Ω_b is apparently related to the amount of exact exchange in the DFA formulation. As HF, which is quite poor in energetic aspects but better founded than DFT in others (recall Subsection 2.5.4) tends to place an excess of electron density in bonding regions, leading to shorter covalent bonds and coherently wrong dipole moments, this trend in DFT deserves an investigation.

Consequently, a consistent series of DFAs with increasing HF-like exchange E_x^{HF} was created. A family of simple one parameter hybrid DFAs based on the well-known B3LYP DFA can be built, which we shall designate BX-LYP.

The BX-LYP single-parameter hybrid series of functionals were built using Gaussian09 rev.D01. Based on the three-parameter formulation of B3LYP, a simplified version was used in which the exchange-correlation energy takes the form:

$$E_{xc}^{BX-LYP} = aE_x^{HF} + (1-a)(E_x^{Slater} + \Delta E_x^{B88}) + E_C^{LDA} + (1-a)(E_c^{LYP} - E_c^{LDA}) \quad (6.4)$$

The BX-LYP series takes a values ranging from 0.10 to 0.90, with the systematic nomenclature of B10%LYP, B20%LYP etc. up to B90%LYP.

Analogously, we build a family of one parameter hybrid DFAs based on the simple SVWN3 LDA, which we shall call SX-VWN3. The SX-VWN3 series takes the form:

$$E_{xc}^{SX-VNW3} = aE_x^{HF} + (1-a)E_x^{Slater} + E_C^{LDA} \quad (6.5)$$

In which a takes values ranging from 0.10 to 0.90 with the systematic nomenclature of S10%VWN3 etc. Note that both series converge to the same result when $a \to 1$.

As a first example, let us calculate and reoptimize CO using the BX-LYP family. Results are collected in Table 6.3, where the increase in population in Ω_b as the E_x^{HF} contribution increases is evident, as well as the shortening of the internuclear equilibrium distance R_{eq} and the increase of the harmonic frequencies ω_h. In fact, the percentage of exact exchange is linearly correlated with these features with very high coefficients of determination: 0.034 more electrons in the bond basin per 10% more E_x^{HF} ($r^2 = 0.999$), while R_{eq} shrinks in 0.0043 Å ($r^2 = 0.995$) and the harmonic frequency increases in 34.85 cm^{-1} ($r^2 = 0.997$).

Surprisingly, the atomization energy also decreases linearly as E_x^{HF} increases: 4.393 kcal/mol less per 10% , with coefficient of determination $r^2 = 0.999$. In fact, this trend is completely off the mark for many reasons. First of all, because we would expect a shorter, tighter bond to be *stronger* as measured by ΔE_{atom}. In general, we associate larger bonding densities, shorter distances and larger frequencies with bond strength. However, as we discussed thoroughly in Subsection 5.3.1 of the previous Chapter, the atomization energy (which is simply the BDE for a diatomic) is not an intrinsic property. This point will be revisited later on. Secondly, note that the the CCSD(T) value for ΔE_{atom} in CO (as reported in Table 6.2) is 257.25 kcal/mol, with a bond population of 3.0741. The bond population is nailed at approximately 20% E_x^{HF} and the reference atomization energy is obtained at approximately 10%. This seems to justify a small percentage of exact exchange, between 10% and 20% , which is not far from the composition of the original B3LYP DFA and other general-purpose DFAs.

Again, this is not a unique feature of the CO molecule. Figure 6.22 shows analogous results for N_2. The analysis becomes blurred once more atoms are included due to the

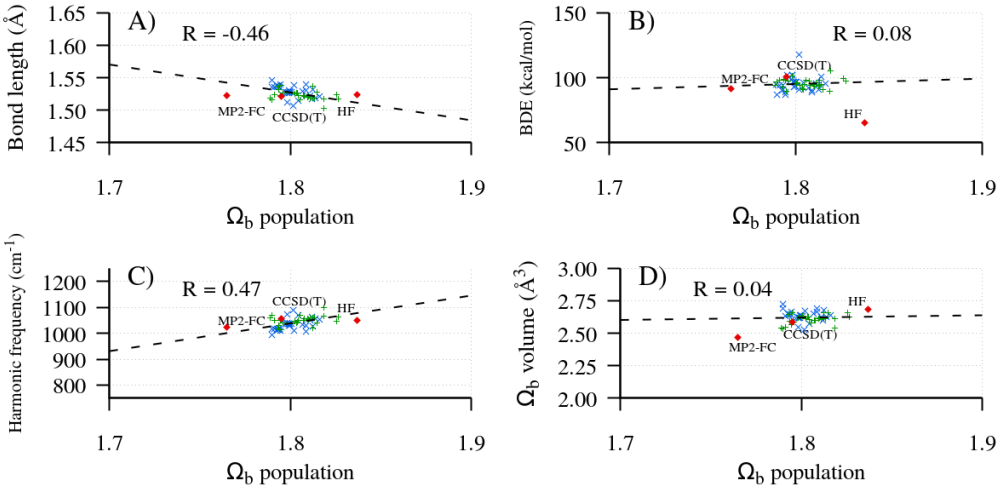

Figure 6.21: Correlation between the population of Ω_b and several descriptors for the ethane C_2H_6 molecule as calculated by the DFA set, HF, MP2 and CCSD(T). **A)** Bond length (Å) **B)** Bond Dissociation Energy (kcal/mol) **C)** Harmonic frequencies (cm^{-1}) **D)** Ω_b volumes ($Å^3$). Pure functionals are colored blue, hybrid and double hybrid functionals are colored green, and wavefunction methods are colored red. Least-squares fits to the DFA set data are drawn as dashed black lines with their Pearson correlation coefficients shown in each plot.

Method	Pop. Ω_b	Vol. Ω_b	R_{eq}	ω_h	ΔE_{atom}
B10%LYP	3.0354	58.68	1.1297	2156.56	257.13
B20%LYP	3.0789	61.91	1.1243	2198.18	252.21
B30%LYP	3.1014	62.19	1.1192	2237.55	247.46
B40%LYP	3.1373	64.53	1.1145	2274.88	242.86
B50%LYP	3.1764	68.85	1.1101	2310.33	238.41
B60%LYP	3.2126	67.45	1.1059	2344.07	234.10
B70%LYP	3.2465	71.05	1.1020	2376.21	229.92
B80%LYP	3.2778	753.21	1.0983	2406.88	225.87
B90%LYP	3.3090	76.44	1.0948	2436.16	221.95

Table 6.3: Descriptors for the respective equilibrium geometries of CO. Population of Ω_b in electrons, volume of Ω_b in a.u.$^{-3}$, equilibrium distances (R_{eq}) in Å, harmonic frequencies (ω_h) in cm^{-1} and atomization energies (ΔE_{atom}) in kcal/mol.

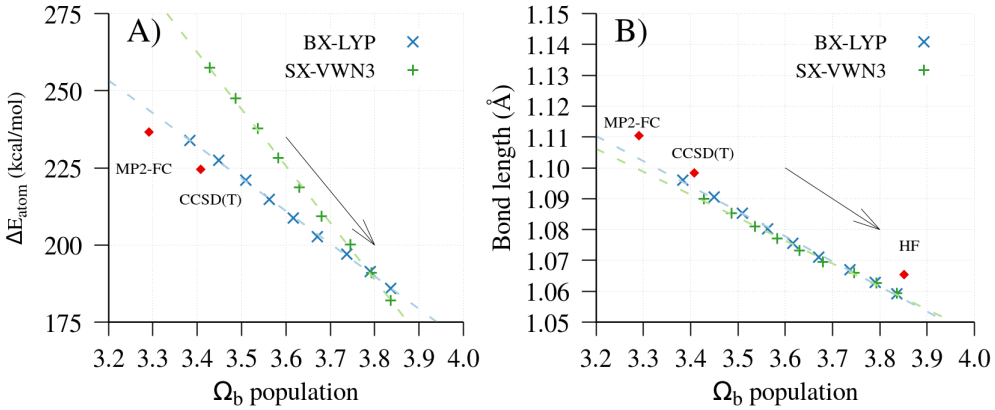

Figure 6.22: Correlation between the population of Ω_b (in electrons) of the N_2 molecule and its **A)** atomization energy (ΔE_{atom}) in kcal/mol, **B)** equilibrium bond length in Å. BX-LYP, in blue, consists on a B3LYP modification with increasing amounts of E_x^{HF} (10–90%). SX-VWN3, in green, is a SVWN3 modification with increasing amounts of HFX (10–90%). Arrows point in the direction of increasing E_x^{HF}. Least-squares fits to each series are drawn as dashed colored lines.

same type of error compensations that arose in the previous Subsection for ethane, but it is apparent in covalent diatomics that more E_x^{HF} linearly leads to a higher population on the bond, and generally displaces the results in geometries and frequencies towards the HF limit. Considering the blue crosses in Figure 6.22 A, corresponding to BX-LYP, it can be clearly seen how a E_x^{HF} contribution of 10-20% renders the correct population in Ω_b, as for CO. In this case, accurate atomization energies are obtained with approximately 20% E_x^{HF}, while optimal bond lengths (Figure 6.22 B) are obtained at approximately 10% E_x^{HF}. Higher percentages lead to a total breakdown. As per the strong collinearity of bond lengths and harmonic frequencies, the same behavior applies.

Note that in the SX-VWN3 family (green crosses in Figure 6.22) accurate atomization energies require much higher E_x^{HF} content, up to 40%, and are not in line with the optimization of the bond population. Thus, the correct energetic description can be artificially obtained by tuning the adiabatic connection, but a proper bonding density is not achievable within this parametric space. Different properties may indeed have different optimal spaces in terms of the parameters that have to be adjusted in a given DFA.[92]

The most immediate takeaway is that, in agreement with what has been covered in Subsection 5.3.1 in some detail, BDEs are not appropriate for discussing many of the notions that we associate to bond strength. In particular, note that atomic systems are quite particular with respect to chemistry as a whole (i.e. they represent a very limited chemical space). By virtue of their characteristics – high multiplicity and charge concentration –, atoms are subject to large self-interaction errors, which are alleviated by E_x^{HF}; an uneven treatment of this error in single atoms may lead to correct – or wrong – atomization energies for completely unphysical reasons.

However, so far we have used families of DFAs with varying percentages of exact exchange. In those calculations there will be an associated density error but also an associated functional error, using concepts from Subsection 6.1.1. We will try to study both effects independently next.

Calculations on non-self-consistent densities

As we have shown, higher amounts of E_x^{HF} seem to lead to lower atomization energies in spite of higher populations in Ω_b and shorter bonds. The effect of increasing the bonding density can be explicitly investigated using what has been called Density Corrected DFT (DC-DFT), which is quite simply analogous to the evaluation of density errors. That is, the electron density is obtained using a self-consistent field method at a given level of theory, but the final energy is evaluated using a different DFA. The use of inconsistent densities has been thoroughly justified both from a conceptual and a practical point of view recently.[93]

Using the extremely large aug-cc-pCVQZ quadruple-ζ basis set, self-consistent BLYP densities have been used in combination with the BX-LYP family of DFAs to assess the effect of E_x^{HF} in the DFA that can be associated with the "functional error". The resulting composite methods have been named BLYP//BX-LYP (density, then evaluation). On the other hand, self-consistent densities from the one-parameter hybrid BX-LYP DFA have been coupled to the BLYP and B3LYP DFAs. As shown before, in this family the bonding density in Ω_b scales linearly with the E_x^{HF} percentage. Analogously, the resulting methods have been termed BX-LYP//BLYP and BX-LYP//B3LYP respectively. This way, the "density error" can be evaluated. Thus, we isolate the effect of E_x^{HF} on the density from the effect on the DFA. Geometries have been conveniently optimized in all cases using tight numerical gradients.

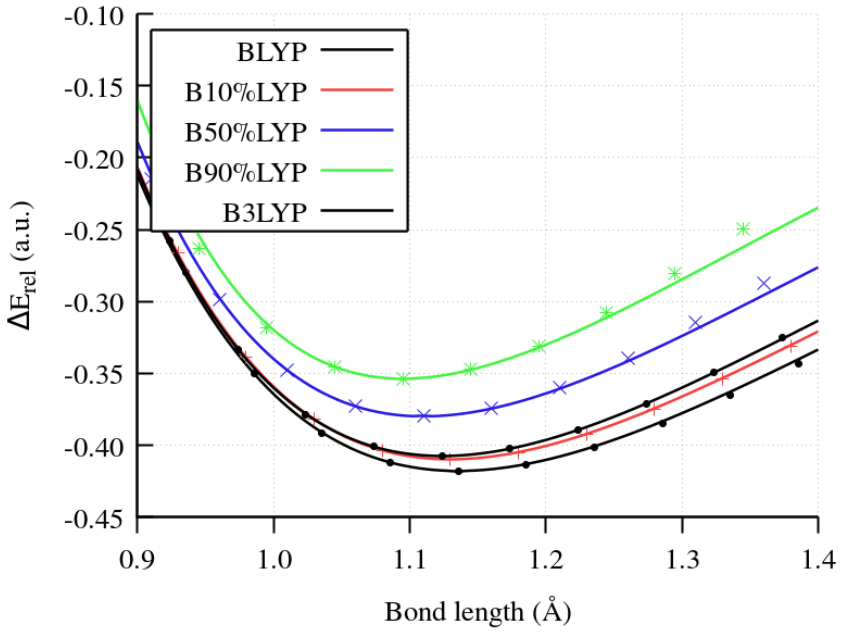

Figure 6.23: Dissociation curves for the CO molecule calculated with different methods. Data points have been fitted to a Morse potential. BLYP and B3LYP are shown in black solid and dashed lines respectively, and BX-LYP variants (B10%LYP, B50%LYP and B90%LYP) are shown in red, blue and green small lines respectively. ΔE_{rel} is the relative energy in atomic units with respect to the isolated atoms.

Let us see the combined density and functional-driven effects in the dissociation

Method	β N_2	β CO
BLYP	2.5742	2.2556
B3LYP	2.7966	2.3703
B10%LYP	2.7072	2.3192
B50%LYP	3.0946	2.5487
B90%LYP	3.4491	2.7466
B10%LYP//BLYP	2.5752	2.2662
B50%LYP//BLYP	2.5878	2.3222
B90%LYP//BLYP	2.6562	2.4001

Table 6.4: Well amplitude parameters β in the Morse potential fits for dissociation curves with different methods for both the N_2 and CO molecules. See Equation 5.1 for the Morse potential function.

curves for the CO molecule and N_2 molecules. These are shown in Figures 6.23 and 6.24 respectively, calculated with different methods. The aforementioned effects of increased E_x^{HF} DFAs are noticeable in both cases: equilibrium distances shrink and potential well amplitudes diminish. We may fit both curves to Morse potentials (recall Equation 5.1) and analyse the effect in β, the parameter that controls well amplitude. A selection is presented in Table 6.4. β increases as E_x^{HF} does, in agreement with our observation (albeit not quite as linearly as R_{eq}) which leads to steeper potential wells. Note that, as seen in Figures 6.23 and 6.24, the Morse fits are remarkably good near the equilibrium region in all cases. In fact, only the highest E_x^{HF} methods deviate noticeably from the Morse potential fit, having an even sharper descent into the well.

If the increase in E_x^{HF} affects only the density, as in the BX-LYP//BLYP family, the effect is the same (i.e. trends in the same direction) but significantly reduced. The same applies in the BLYP//BX-LYP family. In all cases, functional-driven errors are predominant and the use of the BLYP density barely perturbs the curves with respect to the BX-LYP self-consistent densities. However, this much is expected: the difference in the densities is relatively small, and thus the density error is larger than the density error.

Figure 6.25 shows, in a different scale, the effect of different bonding densities with the same DFA. Note that the effects are very subtle because, once more, N_2 is what has been termed as normal (i.e. it does not suffer from a significant density-driven error), and thus the description given by a DFA does not change significantly upon slightly varying $\rho(\mathbf{r})$. In any case, as stated before, the effect of increasing the bonding density non-selfconsistently is akin to increasing the E_x^{HF} contribution: it shortens bonds and reduces the well amplitude.

As a sidenote, the GGA BLYP exhibits significantly greater sensibility to the input density than the hybrid B3LYP. Thus, BLYP can be considered more "abnormal" than B3LYP for this specific system. B3LYP DFA is hardly different when evaluated on its own self-consistent density, the B10%LYP one, or in the B50%LYP one. In this sense, it is extremely "normal". In both BLYP and B3LYP the difference between 10% and 50% HFX is negligible (even more so in B3LYP), yet the difference between 50% and 90% is noticeable. Considering that the bonding population in Ω_b scales linearly with the E_x^{HF}

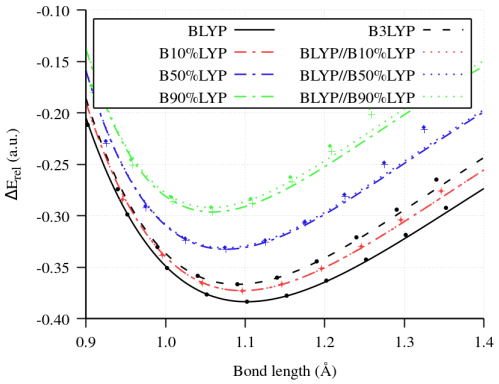

Figure 6.24: Dissociation curves for the N_2 molecule calculated with different methods. Data points have been fitted to a Morse potential. BLYP and B3LYP are shown in black solid and dashed lines respectively, and BX-LYP variants (B10%LYP, B50%LYP and B90%LYP) are shown in red, blue and green dashed-dotted lines, respectively. ΔE_{rel} is the relative energy in atomic units with respect to the isolated atoms.

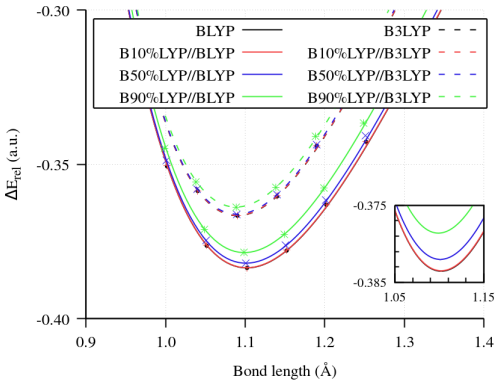

Figure 6.25: Dissociation curves for the N_2 molecule calculated with different methods. Data points have been fitted to a Morse potential. BLYP and B3LYP are shown in solid and dashed lines respectively. Methods evaluated on self-consistent densities are shown in black, while BX-LYP densities (B10%LYP, B50%LYP and B90%LYP) are shown in red, blue and green, respectively. Inset highlights the nearly perfect overlap between BLYP and B3LYP and their 10% variants. ΔE_{rel} is the relative energy in atomic units with respect to the isolated atoms.

content, this signals that the amplitude of the Morse well has power dependency on the bonding population – and thus E_x^{HF}. This suggests that, in order to correct density-driven errors, a qualitatively different density should be used, such as the HF one, as hinted in previous works.[94]

At this point, there is no doubt that the effect of E_x^{HF} in covalent bonds leads to bonds that are not only shorter but also more resilient to elongation, and that this effect has a density-driven contribution and a functional-driven contribution, both in the same direction. We expect the density-driven contribution to be small in most "normal" cases. However, density errors may be superior to those related strictly to the energy evaluation of the DFA for some abnormal systems. As we have seen, the relative depth of a given valley on a potential energy curve can change by tuning the density. The effect of density-based corrections may be even higher if vibrational energies are considered, as in the calculation of free energy profiles with anharmonicity corrections, and specially so in the calculation of precise kinetic constants where recrossing effects are considered implicitly or explicitly.[95] In other words: whenever chemistry is not reduced to differences between points of a PES.

Hence, at this point we may suggest that incorporating very large percentages of exact exchange E_x^{HF} in a given DFA formulation is not recommendable. This increase will linearly lead to incorrect bonding densities in covalent bonds, which will have a clear effect on, at least, calculated bond lengths and frequencies. A reasonable consensus between LDAs and HF seems to be found in hybrids with a 10–20% of E_x^{HF}.

A balanced treatment of errors in DFT is needed to guarantee that BDEs and atomization energies are representative of the description of chemical systems, and not inherently biased towards atoms.

6.2 Qualitative effects of density and functional errors

In the previous Section we have highlighted how delocalization errors affect the density of localized chemical bonds from both the density-driven and functional-driven points of view. We have also showcased some of the major effects in selected systems, notably the bond shortening that HF and DFAs with large amounts of E_x^{HF} produce with respect to a reference.

However, as already discussed, error compensation arises in polyatomic systems, which somewhat hampers analysis. As in the case of ethane, delocalization errors may stretch some covalent bonds at the cost of shortening less localized bonds. This mellows geometric differences, although it carries onto significant features, such as calculated infrarred spectra. In any case, it is not easy to map this interplay of effects, in which the scope is already quite limited (i.e. only covalent bonds, only delocalization errors) in the vast context of general purpose DFT.

In this sense, this Section will be devoted to a particular qualitative example of limit behavior due to delocalization errors in chemical bonds, which is the calculation of the optimized geometries of periodic systems. Accordingly, it will be quite succint and exemplary. The goal is to proof how, in a general way, the observations in the previous Section can be used to predict qualitative differences due to the different downsides in one-body Hamiltonian approaches in solid state systems.

6.2.1 Delocalization error in ionic bonds

In the previous Section (cf. Subsection 6.1.2) we have studied the effects of delocalization error in localized bonds, predominantly covalent. As discussed in some depth in Chapter 1, perfect covalency is defined, unlike perfect ionicity. We can, however, use a model system, as the Na – Cl dimer, to show how delocalization errors affect very ionic bonds, just as we did before with H_2.

Again, we optimize the Na – Cl internuclear distance with different methods. This time we will use a significantly larger triple-ζ basis set, def2-TZVP. Using HF, we obtain $R_{eq} = 2.3838$ Å, while a LDA representative (SVWN3) leads to $R_{eq} = 2.3235$ Å. Apparently, the ordering has been reversed: HF now leads to longer bonds, and LDA leads to shorter ones. For reference, at the CCSD level we obtain $R_{eq} = 2.3862$ Å, which is much closer to the HF result, unlike before.

Let us fix a consensus geometry at $R_{eq} = 2.38$ Å to investigate $\rho(\mathbf{r})$ in some detail. Results are shown in Figures 6.26 to 6.28, in which it is once again clear that errors are much larger in relative terms in the bonding region, and thus core densities are approximately constant. The most significant change is that HF now leads to a lack of electron density in the internuclear region. From a purely electrostatic criteria, and assuming core densities are nearly identical, this should lead to longer bonds. In other words, the relative behavior is inversed with respect to covalent bonds once the ionicity is increased significantly. From a different perspective, the ionic bond can be understood as electrostatic interactions between effective atomic charges. The Mulliken charges at the HF level are ± 0.730 a.u., which is quite close to the ideal one-electron transfer; LDA is far less ionic in this sense, ± 0.618 a.u. Again, for reference, CCSD natural orbitals lead

to Mulliken charges of ±0.703 a.u., which is approximately in between and closer to the HF result. If instead we look at the AIM charges, we obtain ±0.923 a.u., while the LDA result is ±0.876 a.u., which is once more less ionic.

What this comes to show is how different chemical bonds are affected differently by delocalization effects. In this particular case, HF leads to a localized situation in atomic terms: the density is effectively over-localized, but near the atoms instead of in the internuclear midpoint. On the contrary, LDA still delocalizes unphysically, which results in an increased density (with respect to the reference) along the internuclear axis, and a subsequently shortened equilibrium bond length. This reasoning will bear significance in the following Subsection.

6.2.2 Calculation of cell parameters

DFT is routinely used to model periodic systems. One of the simplest features of a periodic crystal is the dimension of the unit cell, or cell parameters. From the experimental point of view, a routine X-ray diffractometer measurement can determine cell parameters with an excellent precision. With a modern experimental setup, the uncertainty can be as low as some parts in 10^{-4} a.u., even for organic crystals, which can be lessened by a further order of magnitude by employing special techniques.[96]

Let us exemplify with a simple case: NaCl, face-centered cubic sodium chloride. In the first work by Bragg, dating back to 1913, the value of the cell parameter a_{expt} was set to 4.45 Å, only to be corrected in the same year to the value of 5.62 Å, which is remarkably close to the currently accepted value of 5.6401 Å.[97, 98] Owing to its simplicity, the geometry of the unit cell is often the first quantity that is used to test the adequacy of a computational model against experimental data.

Noting that the geometry optimization of a solid – which yields the cell parameters – does not have an associated random error, the calculated cell parameter a_{calc} value will be affected by systematic errors related to the one-body Hamiltonian approach, the basis set expansion and small numerical inaccuracies (e.g. integral truncation). We may thus split the error in a_{calc} with respect to a_{expt} into modelization errors, that have to do with the approximation of two-body effects, and discretization errors, which have to do with the finite treatment of infinite series (i.e. basis set, sampling and truncation).[99]

In the realm of model errors, a key difference between wavefunction and DFT methods must be noticed: the first ones can build systematic improvements adding correlation on top of a HF reference (cf. Section 2.3), while DFT is hard to improve systematically. Indeed, as we have discussed in the previous Section, climbing Jacob's ladder does not necessarily mean achieving a better description (i.e. a more expensive or sophisticated functional will not necessarily lead to a better result). In any case, DFT is by far the preferred approach to model periodic systems, and many DFAs remain extremely popular.

As discretization errors can be systematically improved, we may focus in model errors in cell parameters, and we will try to rationalize such errors. Calculations in this Section were performed using the `CRYSTAL` code [100] and triple-ζ basis sets (in general, the POB-TZVP familiy).[101] Details of calculations can be found in the Appendix. As our two extreme situations, we will use HF and the VBH LDA.[102] In principle, as long as we avoid non-covalent interactions and strongly correlated systems, the most prevalent problem should be delocalization error.[103, 104]

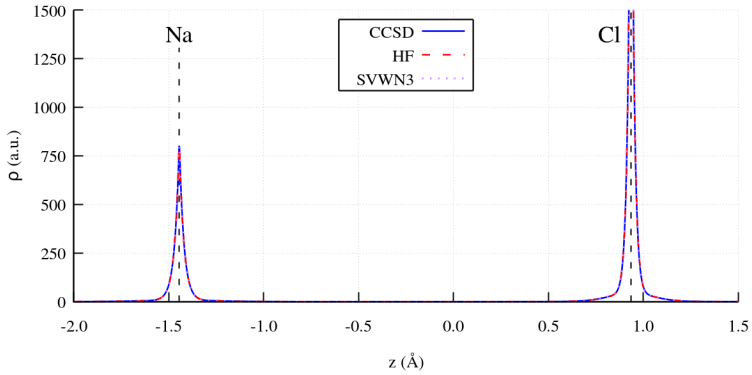

Figure 6.26: $\rho(z)$ along the internuclear axis of Na−Cl. Calculated with different methods and the def2-TZVP basis set. Dashed lines indicate the position of each nuclei.

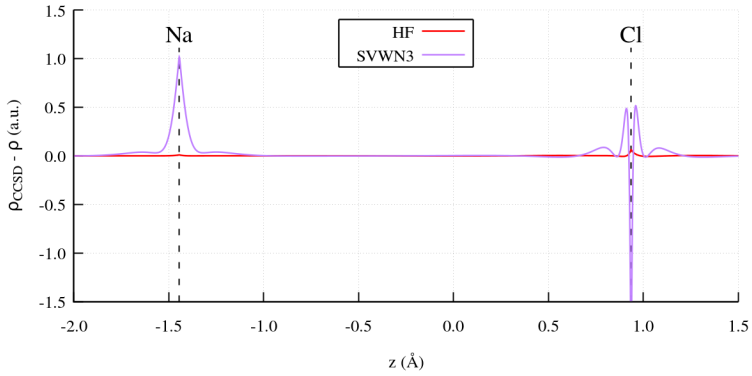

Figure 6.27: $\rho_{CCSD}(z) - \rho(z)$ along the internuclear axis of Na−Cl. Calculated with different methods and the def2-TZVP basis set. Dashed lines indicate the position of each nucleus.

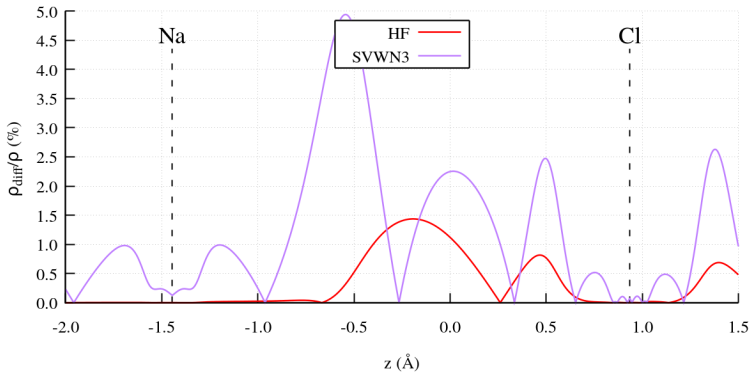

Figure 6.28: ρ_{diff} (Equation 6.1 using $\rho_{CCSD}(\mathbf{r})$ as reference) as a percentage of $\rho_{CCSD}(z)$ along the internuclear axis of Na−Cl. Calculated with different methods and the def2-TZVP basis set. Dashed lines indicate the position of each nucleus.

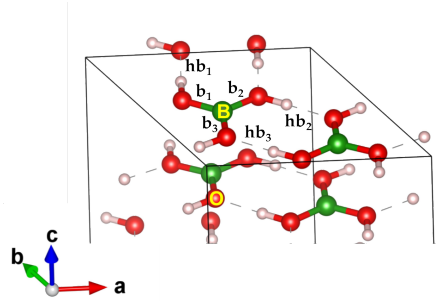

Figure 6.29: Structure of the $B(OH)_3$ crystal. Main distances have been labelled as in Table 6.5.

Distances	HF	VBH	expt.[105]
b_1	1.359	1.368	1.377
b_2	1.358	1.364	1.351
b_3	1.357	1.364	1.349
hb_1	1.874	1.398	1.822
hb_2	1.882	1.416	1.843
hb_3	1.880	1.411	1.911
B−O	3.697	2.758	3.187

Table 6.5: Geometrical parameters of the $B(OH)_3$ crystal. Bond labels refer to Figure 6.29. Distances are in Å. The structure was resolved at T=297 K.

Delocalization effects in boric acid crystals

In order to ascertain whether the error in cell parameters is effectively controlled by delocalization effects – in the absence of strong correlation and non-covalent interactions –, we will tackle a simple case first.

In the crystal structure of boric acid, belonging to space group $P\,3_2$ (the corresponding primitive cell is shown in Figure 6.29 for reference), $B(OH)_3$ molecules are organized in sheets which are parallel to the a,b plane and perpendicular to the c axis. Presumably, the sheets in the crystal are stabilized by a network of strong hydrogen bonds, while across-sheet contacts are regulated by weaker non-covalent interactions. Thus, we expect the results to be affected both by long-range and delocalization errors differently in different directions.

Table 6.5 collects the experimental, the HF and VBH LDA values of the relevant geometrical features: *(i)* intramolecular B−O bond distances (b_n), *(ii)* intermolecular O−H hydrogen bonds (hb_n) and *(iii)* and inter-sheet B−O distance (B−O). Results clearly show that, as expected, intramolecular distances are only slightly affected by the choice of method (b_1 to b_3). In fact, HF leads to shorter intramolecular (i.e. covalent) bonds than the LDA representative – due to the lack of electron correlation–, but the overall accuracy is good and not subject to important deviations. However, the description of the non-covalent interactions is terribly described due to the lack of long range effects (cf. Subsection 2.5.3). Due to the missing attractive potentials, very long intermolecular distances are obtained. The difference between the values is as large as 0.4 Å for the hydrogen bonds (hb_1 to hb_3) and is even more significant when looking at the B−O distance (along the c axis), which accounts for inter-sheet contacts: HF predicts a distance almost 1 Å larger than LDA. Summarizing: in this case, the wrong description of non-covalent interactions leads to wrong cell parameters and a qualitatively wrong description of the crystal.

Hence, as shown by this simple example, our assumptions with respect to delocalization effects in lattice parameters seems to hold within the aforementioned limits. However, as separating effects is not generally trivial, different simple systems will be tackled independently in order to ascertain trends and their relation with chemical families.

Covalent solids

Two a priori covalent solids are carbon allotropes, as appearing in Section 5.3 of Chapter 5: graphite and diamond present no electronegativity differences. However, we expect graphite layers to interact non-covalently. Such interactions are ill-described by DFT on their own accord, as shown before for the $B(OH)_3$ crystal, and consequently we will not study graphite here. Similarly, we will avoid molecular solids for the time being due to the interference of long range errors.

The structure of diamond (which was previously shown in Figure 5.17) does not present non-covalent interactions in principle. Cell parameters a calculated with different methods and basis sets are presented in Table 6.6. In this case, VBH leads to a smaller cell parameter than HF, while PBE and other higher rung DFAs all lead to larger values of a. There is a subtle increase in the lattice parameter of almost all methods as the basis set *shrinks* from a triple-ζ POB-TZVP to a more limited 6-31d1G, but trends remain mostly unaltered. The same observation carries on to compressibility curves, as presented in Figure 6.30, but does not seem to apply to the derivatives of the energy with respect to a: the three methods are fitted by nearly identical parabolas. Similar but somewhat accentuated results are obtained for the same $A4$ structure of Si, where HF lead sto $a = 5.4355$ Å but VBH gives $a = 5.3505$ Å, and the $A4$ structure of Ge, where HF and VBH give $a = 5.6700$ Å and $a = 5.5582$ Å respectively (all data are reported in the Appendix). Experimental results are in all cases much closer to the HF values.

These results seem incoherent as per our previous observations: we would naively expect HF to lead to far more localized C–C, Si–Si and Ge–Ge bonds and thus compress the unit cell, or perhaps to a unit cell that can be compressed somewhat easier. This does not seem to be the case. However, the large deviation between VBH and PBE is quite revealing: the LDA homogeneously smooths out the density, leading to en electronic structure which is far more conductive. In diamond, the predicted band gap is approximately 4.1124 eV using VBH, and over 12 eV using HF. For Si, VBH leads to a very small band gap of 1.0535 eV, while HF predicts 6.3702 eV. This situation is energetically favored in LDAs, and thus the unit cell is reduced.

On the contrary, HF privileges localized bonding schemes. As the symmetry imposed in the calculation forbids localization through bond alternation (recall the discussion in Subsection 6.1.2), the increased average repulsion is handled by expanding the unit cell and keeping the band structure clearly insulating. In any case, these highly symmetric structures are hard to interpret due to multiple errors overlapping, including discretization issues.

Basis set	HF	VBH	PBE	B3LYP	PW91	M06	M062X
POB-TZVP	3.5493	3.5268	3.5688	3.5675	3.5680	3.5438	3.5576
6-31d1G	3.5594	3.5395	3.5822	3.5802	3.5812	3.5561	3.5671

Table 6.6: Cell parameters a of diamond in Å calculated with different methods and basis sets.

Ionic solids

The chemical space of pure crystals is richer in ionic bonds than that of single molecules (e.g. N_2). Hence, in spite of our interest for localized bonds, we will test our assumptions

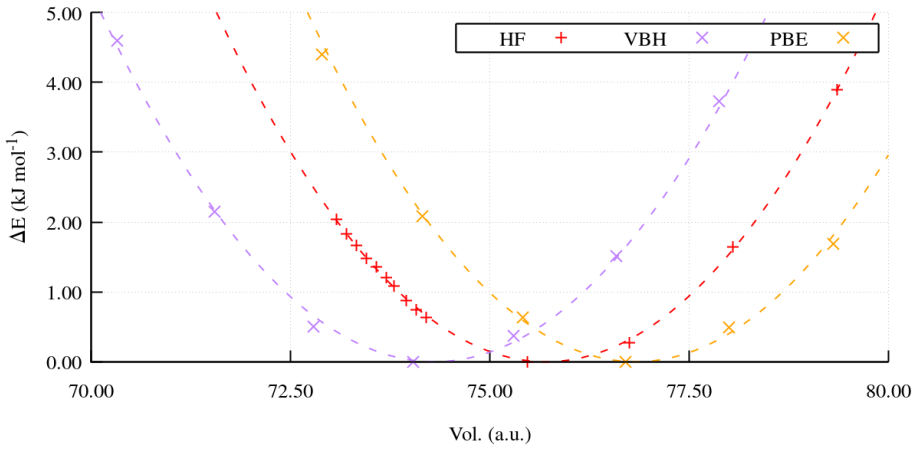

Figure 6.30: Relative energy per unit cell with respect to primitive cell volume for diamond as calculated using different methods and the POB-TZVP basis set. Dashed lines represent parabolic fits to the datapoints.

in typical ionic solids, in which we assume that non-covalent interactions are negligible and the most important error source is the delocalization error. Recall that the effects of delocalization error arise from the counterbalance between SIE and the lack of correlation effects, and may manifest differently for different chemical environments.

Again, we will focus in cell parameters as a representative geometrical property. The HF and LDA (in this case, championed by the VBH DFA) values of cell parameter a of a selection of systems are reported in Figure 6.31 (the complete dataset is available in the Appendix). Parameters calculated with HF and LDA are in all cases smaller and larger, respectively, than the experimental data. This may seem counterintuitive, but is quite coherent.

In a way, because HF and LDAs constitute limit cases of delocalization error, they provide an error bar of sorts that surrounds the experimental values. In Figure 6.31 the green and black bars represent the absolute and normalized amplitudes, respectively, of the hypothetical error bars associated to each structure.

Interestingly, some trends are noticeable among families. For instance, in the LiF-KI family of binary rocksalt structures the absolute error bar in increases with the size of the cell parameter but the normalized error bar remains fairly constant along the family (with the sole exception of the smallest structure, LiF). Analogous considerations can be drawn for other other families reported in Figure 6.31.

Accepting that delocalization errors are responsible for the size of the error bar, this suggests that chemically related systems present similar qualitative balances of correlation and self-interaction. On the one hand, this is to be expected, because we classify such compounds based on properties which ultimately arise from the atomic composition as well. On the other hand, it means that once that the effect of the delocalization error on one member of a given family is known, the corresponding incidence of delocalization errors for different members of the same family can be quickly estimated. The transferability of delocalization errors may be of interest to improve upon current DFAs.

Molecular solids

As anticipated, the discussion of molecular solids is significantly more complex. First and foremost, correctly describing non-covalent interactions, which we expect to be quite relevant, is very hard.[106] This issue was introduced in Subsection 2.5.3.

Secondly, thermal expansion, which is very small for other systems, is much more important in the geometry of the lattice. In fact, in small molecules whose intermolecular distances contribute to the cell size to a large extent, thermal expansion is significant and can involve volume expansion up to 8% moving from 0 K to room temperature.[107] The minimization of the potential energy of the crystal with respect to the lattice parameters does not account for these thermal effects.

Conveniently, non-covalent interactions are attractive, and therefore shrink the cell, while thermal effects enlargen it. As the two effects go in opposite directions, they partially cancel out. We may hope that the cancellation is sufficient to render delocalization effects the most important once more.

This happens to be the case, as suggested by Figure 6.32, which shows the experimental values and the HF and LDA limit values, calculated for a series of molecular solids without accounting for neither thermal nor long range non-covalent interactions. Some further validation is given in the Appendix A.4. The hypothetical error bars that the HF and LDA results delimitate is significantly increased for these systems (Figure 6.32) compared to the ionic ones (Figure 6.31). As discussed for Table 6.5, this is due to the dependence of intermolecular distances on the method employed. The neglect of thermal expansion and non-covalent interactions are of extreme importance in the simulation of molecular solids and generally cannot be neglected. In this case, it seems that the resulting net effect is, for the most part, some orders of magnitude inferior to the method-dependent error.

As it was the case for ionic solids, all experimental values of cell parameters fall within the error bars, with the only exception of acetylene crystals. Without further discussion, this suggests that our hypothesis regarding the effect of delocalization errors in bond lengths – and, thus, cell parameters – is quite valid. HF and LDAs give extreme behaviors due to delocalization errors.

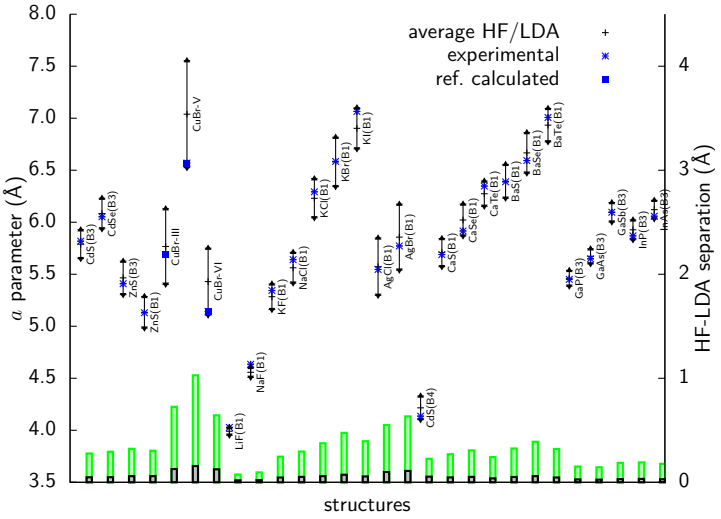

Figure 6.31: Calculated HF (top, triangle) and LDA (bottom, inverted triangle) cell parameters for 28 binary ionic solids with indication of the experimental reference value. Green bars represent the width of the error bar, black bars the same quantity normalized by the experimental cell parameter.

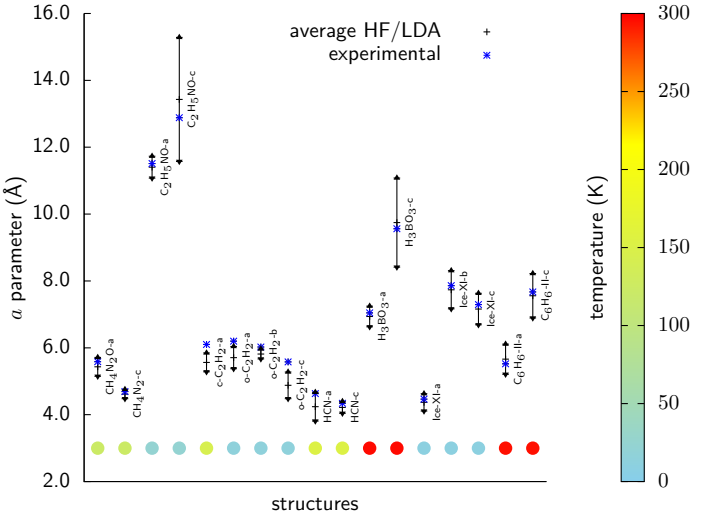

Figure 6.32: Calculated HF (top, triangle) and LDA (bottom, inverted triangle) cell parameters for 8 molecular solids with indication of the experimental reference value. The temperature corresponding to the experimental observation is reported.

Chapter 7

Conclusions and outlook

In this thesis we have developed a model that is able to reproduce the key features of localized chemical bonds with a simple physical interpretation. Examples of application have been presented and suggested, and the parametrization conundrum has been discussed in depth. Relevant to this last aspect and the foundations of the model itself, the effect of certain density functional approximations in relevant properties through the electron density have been examined.

This manuscript was conceived to be illustrative, dealing with several interplaying conceptual and methodological issues in modern quantum chemistry. Hence, numerous simple examples have been developed and presented in an attempt to guide the reader without placing too much of a mathematical burden. At the same time, priority has been given to argumentation over numerical results – the raw in silico results can be found in the Appendix for interested readers – while hoping to preserve rigour in our treatment of these complex issues. Having to oversimplify certain aspects, as many numerical ones, is unavoidable considering the width and breadth of the different branches of quantum chemistry that are involved in our interests.

The way we think about chemistry is determined, at least up to a certain point, by the models we deem representative and the conceptual frameworks they bear. For centuries, chemistry was – and in a way still is – the science of in vitro (i.e. in solution) matter. For this reason, much of our chemical intuition arises from very specific contexts and circumstances. This may turn to be very limiting as technical advances let us devise and operate increasingly sophisticate chemical dispositives. Advances in enzymatic catalysis and nanotechnology, for example, require atomistic control as of today. As we hardly can create what we can not imagine, perhaps going beyond the atomistic level requires intuition beyond that scale as well. Reflecting on this fact, it becomes easy to see how abundant subatomic concepts are in chemistry, chiefly in the form of electron pairs – owing much to Lewis. On the other hand, the interplay between such entities and atomic properties is quite hard to picture because they arise from very different models.

Quite recently, notions such as "frustrated Lewis pairs" or "resonance-assisted hydrogen bonds" have begun gaining traction, and have been used in order to design new applications. From the ontology of quantum mechanics, neither Lewis pairs nor (chemical) resonance amount to much. However, they are useful for the chemical sciences: there is a parallel ontology, which perhaps is not meant to be reduced to linear operators, that pursues science and achieves results within its own logic and episteme.

We have also highlighted how methods of quantum chemistry (i.e. electronic structure solvers) are approximate at many levels. Many of the qualitative approximations have

been discussed in some depth; others (e.g. the Born-Oppenheimer approximation, closed quantum systems) have been assumed quite plainly. Strictly quantitative discretization and numerical features have been neglected, as we deem those less relevant. Among those, we have focused on orbitals and their deficiencies from the conceptual point of view, both in molecular orbital theory (cf. Section 3.1) and valence bond theory (cf. Section 3.2). While succinct, the relevant points have been brought to the table for open discussion: orbitals do not exist in exact many-body theory, they become increasingly difficult to interpret as system size increases, and they – or concepts defined thereof – are often sensitive to basis set definitions. Naturally, this does not mean that orbitals can not or should not be used for chemical interpretation, as long as their limitations are highlighted as clearly as their strengths.

In Chapter 4, we have reviewed some of the key features of quantum chemical topology. The three most important advantages of topological techniques are their privileged connection to DFT, which is the de facto workhorse of quantum chemistry nowadays; the definition of its scalar fields in exact many-body theory; and the relative robustness of many of its techniques with respect to discretization errors. However, many deficiencies still exist, as clear univocous interpretations are still lacking and many useful scalar fields coexist in the literature. Quantitative approaches to quantum chemical topology are extremely powerful, but suffer harshly from these issues: partitioned energy terms can only be as good as the original partitioning is. Some attention has been devoted to the symmetry-related and isotopological problems of the ELF, for instance. Still, this is a promising area of development.

The topic of non-covalent interactions merits some discussion in this same direction: as they are usually hard to describe using DFT, which generally leads to significant quantitative and qualitative errors, how can we be sure that the scalar fields resulting from DFT can give a proper interpretation? This is particularly relevant given the prevalence that so-called dispersion corrections have in modern DFT.

After reflecting on the two main families of chemical interpretation from computation, we have brought forward a new approach to the modelling of chemical bonds. Our approach is based in three simple ideas:

i) Chemical bonds can be likened to an electron density accumulation, the bond charge q, between to effective positive potentials which can be likened to atomic cores.

ii) The bond particle should interact electrostatically with those atomic cores.

iii) The bond particle has a certain kinetic energy that depends on the allowed region of space for the bond.

These ideas are inherited from a semiclassical approach by Borkman, Parr and co-workers, which suffered from some undesirable issues that prevented wider usability.[52, 53, 54, 55] The interpretation of chemical bonds given by the original model has been merged with the depiction given by the ELF, resulting in a significant increase in available data and richer interpretation. In fact, thanks to the usage of the ELF, we have properly identified cores as inert and bonds as resulting from valence electrons, which more naturally matches chemical insight.

Coherently, we have shown that the main assumptions of this new model can be transferred to energy terms arising from a quantitative partitioning of the energy. Using this equivalence, the model has been validated: we have shown that it grasps proper physical trends, at least in a certain chemical space. Due to the very nature of the initial assumptions, which imply that the chemical bond is a local entity, the model fails

dramatically for metallic bonds. A way to judge the metallicity of a bond is also given that is able to predict such failures.

The utility of the ELF-BCM approach has been showcased, including the nuanced parametrization conundrum, by fitting intrinsic bond energies for C−C bonds along the bond order series. Similar applications can be developed for a variety of properties of diverse chemical spaces, and the resulting accuracies are expected to be, at least, semiquantitative.

During the construction and the application of the model, some interesting questions arose related to the impact of the underlying level of theory. As previously commented, the effect of the quality of the electron density in quantum chemical topology is an often overlooked issue. At the same time, the DFT community is immersed in a heated debate to discern the most sensible approach to new approximate functionals.

Thus, a critical examination on how to evaluate density-related errors in DFT was given, in which the importance of chemical intuition is highlighted. Core densities are, for the most part, inert. Errors are localized in such regions but very small in relative terms. On the other hand, errors in valence regions can often be understood qualitatively by reflecting on model assumptions and the framework of quantum chemical topology. While the relevance of the energy can not possibly be understated, it has been shown that parametrization focused in some specific energy differences may overlook relevant points, leading to unphysical features and subsequent errors. The brightest example of these may be given by the effect of localization and delocalization on geometries. A certain parametric space may require a large amount of exact exchange to fit a certain energy difference. However, the cost in unphysical localization may be dramatic and end up incurring in other troublesome failures. In a way, chemical insight should be usable to design proper approaches to DFA development as much as concepts arising from computational methods are useful for synthetic chemists.

Contributions

The most relevant contributions of this work can be summarized as:

- A critical overview of the main frameworks of chemical interpretation has been given, including folk molecular theory, approaches based in orbitals and quantum chemical topology. Attention was paid to the concept of atom, as subsequently involved in chemical structure theories and chemical bonding, and the impact that atomistic thinking has in chemistry.

- A new semiquantitative model, the Electron Localization Function – Bond Charge Model (ELF-BCM) has been constructed and applied. In its careful construction, utmost attention was paid to interpretation and validation: a consistent domain of applicability was found, its limitations clearly understood. Metallic bonds are not properly described by this model, nor any bond in which a local density accumulation is not representative of the bond.

- An example application of the ELF-BCM approach was given while involving aspects of interpretation of chemical bonds and their properties. Semiquantitative predictive qualities were inferred, in line with many current DFAs.

- An understandable way to study density errors in DFT has been proposed using the ELF, which matches well-established chemical insight and interpretation. In

particular, critical misconceptions that may arise from considerations of the electron density without any chemical consideration were highlighted: core densities can bias some metrics without bearing much chemical significance.

- It has been argued, in light of previous findings, that DFT development may need to include more properties than energies – and atomization or bond dissociation energies in particular – in parametrization sets in order to properly constrain the optimization of empirical parameters.

Setbacks

Perhaps the most frustrating setback in the developments hitherto covered is the impossibility of covering an ever expanding chemical space. Simply put, there are too many systems, ranging from atoms to incredibly exotic molecules. Apparently simple systems can hide utmost complexity – thinking about how and why C_2 is far more complex than N_2 may be a good example –, leading to dramatic failures in approximate methods. It is therefore extremely hard to establish any hard limit upon any consideration: we can only extrapolate from minimal samples, hoping that somewhat vague intuition will hold.

On the other hand, acritically calculating and studying thousands of molecules may not be particularly useful – in general –, and illustrative –in particular. In this work we have consistently chosen few familiar examples over larger – but perhaps shallower – coverage. As the calculations on ethane show, error compensation becomes a major factor once the molecular complexity stats increasing, which then requires statistical treatment of increasingly large databases. Ideally, one should always practice depth and breadth. But, as the reader will perhaps agree, in quantum chemistry circumstances are rarely ideal. In this sense, the elaboration of curated representative databases is probably a pragmatic compromise.

The same issues that arise in terms of chemical space apply when regarding the combinatorial explosion of levels of theory, given by the choice of basis set and method. In particular, the DFA gallery seems infinite at times. As far as possible, a representative selection has been used, and basis sets have been shown to be suitable for the goal at hand – from minimal for simple examples to extremely large at times. Again, we beg the reader for forgiveness if this or that DFA or approach has not been taken into account.

Other than this significantly frustrating issue, it is perhaps mandatory to emphasize how forgotten chemistry is in terms of philosophy and history, at least when compared to other scientific fields as physics and medicine. This is particularly remarkable given how uncertain the conceptual future of chemistry is. For instance, whether molecular orbital theory or Lewis structures will survive in undergraduate education in the next 50 years is quite an open question. The history of atoms and the VSEPR model are taught to students remarkably early in most curricula. Will this continue to be the case in the next 50 years? Should it be? One wonders...

Open issues

Finding a proper closure for this work is quite hard, considering how vast the possible applications of the ELF-BCM approach are. From the construction point of view, perhaps cementing a kinetic energy expression that explicitly takes into account more sophisticate

features of the density would be desirable. Other than that, the model is probably usable as it is, coupled to DFT, and able to offer significant insight.

For applications, an ambitious but possibly rewarding effort would be developing atom-based parameters for main group elements. Then, possibly, those potentials could be used either for subatomic force field development or for tight binding schemes. Both possibilities are extremely enticing. At a first glance, our approach, which can seamlessly treat lone pairs and bonds on equal footing, is naturally polarizable. This contrasts with atomistic force fields, which usually incorporate polarization effects in crude – or at least, less aesthetic – manner. Strain is equally incorporated in our model without any particular effort: bonds bend, lone pairs interact on their own and are displaced at will. The possibilities are doubtlessly interesting and manifold. A major requirement is verifying whether the partitioning given by the ELF, when condensed to point-wise entities, is good at describing electrostatic potentials. This more accessible task will surely be accomplished in the near future, while the complete force field will more than likely have to wait unless a larger community is involved.

In second place, albeit equally attractive, developing DFAs using alternative parametrization approaches seems interesting. Starting from a simple hybrid, perhaps re-optimizing parameters while considering dipole moments or multipole moments as well as energies would lead to something interesting. Most DFAs are terribly bad at describing dipole moments, and this can not be understated. Why should, for instance, a multilevel approach which uses DFT be accurate if the density distribution is terrible? Luckily, the DFT community is taking these issues quite seriously. We can only hope that the debate will be prolific and that concerted effort and competition will lead to better, more accurate DFAs than those available today.

As the work hereby developed has been in close contact with many different subfields of quantum chemistry, the list of open issues could be continued ad infinitum. However, any expansion has to be truncated to be useful, and the two major points have been covered so far. At this point, only the future will tell whether such ambitious tasks will be developed further, be it by me or by others with shared interests. What is clear is that quantum chemistry has, as a discipline, an ordeal of an undertaking before itself: it seems unlikely that we will run out of things to do anytime soon.

List of publications

Articles related to this thesis

[1] R. Laplaza, V. Polo, and J. Contreras-García, "A bond charge model ansatz for intrinsic bond energies: Application to c–c bonds," *The Journal of Physical Chemistry A*, vol. 124, no. 1, pp. 176–184, 2020

[2] R. Laplaza, V. Polo, and J. Contreras-García, "Localizing electron density errors in density functional theory," *Phys. Chem. Chem. Phys.*, vol. 21, pp. 20927–20938, 2019

[3] F. Peccati, R. Laplaza, and J. Contreras-García, "Overcoming distrust in solid state simulations: Adding error bars to computational data," *The Journal of Physical Chemistry C*, vol. 123, no. 8, pp. 4767–4772, 2019

[4] J. Munárriz, R. Laplaza, A. Martín Pendás, and J. Contreras-García, "A first step towards quantum energy potentials of electron pairs," *Phys. Chem. Chem. Phys.*, vol. 21, pp. 4215–4223, 2019

Other articles

[5] R. A. Boto, F. Peccati, R. Laplaza, C. Quan, A. Carbone, J.-P. Piquemal, Y. Maday, and J. Contreras-Garcıa, "Nciplot4: Fast, robust, and quantitative analysis of noncovalent interactions," *Journal of Chemical Theory and Computation, In Press*, 2020

[6] R. Laplaza, J. Contreras-Garcia, F. Fuster, F. Volatron, and P. Chaquin, "The "inverted bonds" revisited: Analysis of "in silico" models and of [1.1.1]propellane by using orbital forces," *Chemistry – A European Journal*, vol. 26, no. 30, pp. 6839–6845, 2020

[7] J. Munárriz, R. Laplaza, and V. Polo, "A bonding evolution theory study on the catalytic noyori hydrogenation reaction," *Molecular Physics*, vol. 117, no. 9-12, pp. 1315–1324, 2019

[8] R. Villanueva, S. Romero-Tamayo, R. Laplaza, J. Martínez-Olivan, A. Velázquez-Campoy, J. Sancho, P. Ferreira, and M. Medina, "Redox- and ligand binding-dependent conformational ensembles in the human apoptosis-inducing factor regulate its pro-life and cell death functions," *Antioxidants & Redox Signaling*, vol. 30, no. 18, pp. 2013–2029, 2019

[9] J. Quero, S. Cabello, T. Fuertes, I. Mármol, R. Laplaza, V. Polo, M. C. Gimeno, M. J. Rodriguez-Yoldi, and E. Cerrada, "Proteasome versus thioredoxin reductase competition as possible biological targets in antitumor mixed thiolate-dithiocarbamate gold(iii) complexes," *Inorganic Chemistry*, vol. 57, no. 17, pp. 10832–10845, 2018

[10] M. Martínez-Júlvez, G. Goñi, D. Pérez-Amigot, R. Laplaza, I. Ionescu, S. Petrocelli, M. Tondo, J. Sancho, E. O. Orellano, and M. Medina, "Identification of inhibitors targeting ferredoxin-NADP+ reductase from the xanthomonas citri subsp. citri phytopathogenic bacteria," *Molecules*, vol. 23, no. 1, p. 29, 2017

Appendix A

Compendium of in silico results

Contents

A.1 Reference data for the fitting of the ELF-BCM ansatz in C-C bonds

The complete curated dataset is available in an accesible format in R. Laplaza, V. Polo, and J. Contreras-García, "A bond charge model ansatz for intrinsic bond energies: Application to c–c bonds," *The Journal of Physical Chemistry A*, vol. 124, no. 1, pp. 176–184, 2020.

Molecule	R_{eq} (Å)	q (e^-)	IBE (kcal/mol)	q/R_{eq}
1	1.4996	1.74	97.54	1.16
2	1.5227	1.80	115.40	1.19
3	1.3868	2.75	159.63	1.99
4	1.4234	2.23	142.25	1.57
5	1.3211	3.35	186.06	2.54
6	1.3720	2.61	169.00	1.90
7	1.1932	5.21	265.40	4.36
8	1.2447	7.83	113.03	6.29
9	1.5021	1.98	107.46	1.32
10	1.5151	1.96	106.07	1.29
11	1.3181	3.78	177.08	2.87
12	1.3169	3.79	176.43	2.88
13	1.3181	4.41	182.46	3.35

Table A.1: Reference data for the molecule set at the ωB97XD/def2-QZVP level.

Molecule	R_{eq} (Å)	q (e^-)	IBE (kcal/mol)	q/R_{eq}
1	1.5011	1.73	99.19	1.15
2	1.5211	1.79	118.11	1.18
3	1.3915	2.75	162.36	1.98
4	1.4167	2.24	151.42	1.58
5	1.3298	3.33	188.87	2.51
6	1.3668	2.64	202.47	1.93
7	1.2087	5.20	272.25	4.30
8	1.2558	7.82	154.86	6.23
9	1.4969	1.98	113.04	1.32
10	1.5089	1.96	111.83	1.30
11	1.3242	3.77	183.91	2.84
12	1.3233	3.78	183.12	2.85
13	1.3230	4.37	188.25	3.30

Table A.2: Reference data for the molecule set at the MP2-FC/def2-QZVP level.

Molecule	R_{eq} (Å)	q (e^-)	IBE (kcal/mol)	q/R_{eq}
1	1.5005	1.74	96.58	1.16
2	1.5225	1.80	113.04	1.18
3	1.3889	2.75	163.52	1.98
4	1.4199	2.25	142.00	1.58
5	1.3245	3.34	186.50	2.52
6	1.3650	2.65	171.43	1.94
7	1.1982	5.19	275.82	4.33
8	1.2510	7.83	130.00	6.26
9	1.4980	1.98	106.81	1.32
10	1.5104	1.96	105.58	1.30
11	1.3191	3.77	178.41	2.86
12	1.3180	3.78	177.74	2.87
13	1.3178	4.39	182.56	3.33

Table A.3: Reference data for the molecule set at the RmPW2PLYP-FC/def2-QZVP level.

A.2 Calculated equilibrium descriptors of simple molecules

Molecule	N_2		CO			C_2H_6	
Method	ΔE_{atom}	Λ_{diff}	ΔE_{atom}	Λ_{diff}	$\mathcal{D}$	ΔE_{atom}	Λ_{diff}
G96LYP	235.89	0.1102	260.13	0.1180	0.184	700.42	7.6048
BVWN	241.23	0.1226	260.99	0.1268	0.162	718.13	7.6766
M06L	225.16	0.1322	259.04	0.1307	0.198	711.76	7.5917
M06	222.97	0.1012	259.79	0.1132	0.058	711.80	7.5671
M062X	227.11	0.0771	259.45	0.0755	0.011	710.00	7.5271
M06HF	227.13	0.2497	257.12	0.2564	-0.168	717.17	7.5081
M05	223.50	0.1332	257.97	0.1316	0.048	713.35	7.5257
M052X	225.87	0.1184	257.22	0.1168	-0.012	711.32	7.5280
M11	233.91	0.1386	259.31	0.1498	0.008	713.39	7.4877
N12SX	214.97	0.1303	253.81	0.1376	0.014	707.97	7.5622
MN12SX	223.09	0.1285	255.87	0.1288	-0.016	703.75	7.5386
SOGGA11X	228.23	0.1051	255.88	0.1104	0.022	710.95	7.5500
PW91VWN	247.00	0.1402	266.39	0.1449	0.155	729.86	7.6629
TPSSh	222.18	0.0340	250.23	0.0428	0.141	718.51	7.5994
BMK	229.41	0.0817	262.49	0.0684	0.056	712.29	7.5473
BHandH	224.83	0.1117	260.35	0.1165	-0.032	742.80	7.4739
BHandHLYP	207.72	0.0874	238.64	0.1108	-0.067	700.74	7.5958
HSEH1PBE	225.03	0.0383	254.83	0.0461	0.093	710.35	7.5245
wB97XD	225.88	0.0408	256.83	0.0508	0.093	712.00	7.5442
LC-wPBE	227.94	0.0626	257.79	0.0616	0.105	710.08	7.5132
CAM-B3LYP	229.09	0.0913	256.98	0.0936	0.054	715.35	7.5625
APFD	225.81	0.0370	255.80	0.0425	0.103	713.35	7.5281
B2PLYP-FC	231.34	0.0961	258.83	0.1189	0.145	710.31	7.6055
mPW2PLYP-FC	228.92	0.1011	257.09	0.1247	0.113	711.61	7.6026
HSEVWN	247.00	0.1468	265.08	0.1503	0.160	726.43	7.6672
BRxVWN	237.29	0.1455	264.27	0.1563	0.118	721.07	7.6783
BPBE	237.36	0.0693	263.81	0.0877	0.217	706.06	7.5397
PW91PBE	243.14	0.0835	269.24	0.1034	0.211	717.78	7.5266
PBEPBE	243.91	0.0791	269.11	0.0999	0.220	716.73	7.5223
HSEPBE	243.06	0.0906	267.90	0.1083	0.216	714.28	7.5299
mPW1PBE	222.63	0.0452	253.49	0.0500	0.091	708.11	7.5279
mPW3PBE	227.93	0.0366	257.82	0.0432	0.111	715.71	7.5332

Table A.4: Atomization energies (ΔE_{atom}) in kcal/mol, Λ_{diff} values in atomic units, and dipole moments ($\mathcal{D}$) in Debyes for the N_2, CO and C_2H_6 molecules in their respective CCSD(T) equilibrium geometries. (Part 1)

Molecule	N_2		CO			C_2H_6	
Method	ΔE_{atom}	Λ_{diff}	ΔE_{atom}	Λ_{diff}	$\mathcal{D}$	ΔE_{atom}	Λ_{diff}
BPW91	237.34	0.0733	263.61	0.0908	0.214	706.99	7.5476
PW91PW91	243.12	0.0887	269.03	0.1068	0.207	718.72	7.5346
PBEPW91	243.89	0.0841	268.90	0.1032	0.216	717.67	7.5301
HSEPW91	243.05	0.0962	267.70	0.1120	0.212	715.23	7.5380
B3PW91	226.00	0.0366	255.89	0.0439	0.111	712.59	7.5432
mPW1PW91	222.58	0.0429	253.26	0.0509	0.088	708.99	7.5356
MP2-FC	236.31	0.0002	270.00	0.0621	0.271	707.84	7.6555
BLYP	240.67	0.1370	262.16	0.1426	0.181	704.62	7.6095
PW91LYP	246.42	0.1600	267.54	0.1654	0.174	716.22	7.5986
PBELYP	247.16	0.1559	267.37	0.1626	0.183	715.08	7.5936
HSELYP	246.39	0.1707	266.21	0.1758	0.179	712.71	7.6027
B3LYP	229.95	0.0783	255.65	0.0827	0.083	711.98	7.5923
mPW1LYP	225.84	0.0832	251.88	0.0872	0.054	706.40	7.5953
HF	115.40	0.2325	174.48	0.2848	-0.271	551.63	7.6555
TPSSTPSS	228.35	0.0470	254.36	0.0593	0.187	718.89	7.6091
XAlphaXa	215.13	0.1597	268.58	0.1792	0.230	662.39	7.4367
BB95	244.89	0.1113	271.30	0.1284	0.209	712.17	7.5509
PW91B95	250.63	0.1302	276.65	0.1470	0.202	723.71	7.5390
PBEB95	251.43	0.1263	276.53	0.1435	0.211	722.67	7.5344
HSEB95	250.60	0.1386	275.33	0.1528	0.207	720.25	7.5424
SVWN	274.82	0.1368	303.91	0.1584	0.218	801.31	7.4515
PKZBPKZB	229.91	0.0812	256.36	0.0875	0.225	710.32	7.5459
B3P86	234.08	0.0318	261.59	0.0404	0.102	735.93	7.5405
PKZBKCIS	229.55	0.0878	256.15	0.0957	0.222	695.76	7.5227
BRxKCIS	239.15	0.1323	271.06	0.1428	0.172	721.54	7.5281
OVWN	229.95	0.1343	258.14	0.1366	0.166	725.17	7.6243
OPBE	226.60	0.1337	261.19	0.1314	0.224	714.21	7.4992
OLYP	229.47	0.0946	259.25	0.1019	0.185	711.74	7.5550
OB95	233.96	0.1375	268.67	0.1404	0.214	720.12	7.5067
CCSD(T)	224.61	0.0000	257.25	0.0000	0.117	709.01	0.0000

Table A.5: Atomization energies (ΔE_{atom}) in kcal/mol, Λ_{diff} values in atomic units, and dipole moments ($\mathcal{D}$) in Debyes for the N_2, CO and C_2H_6 molecules in their respective CCSD(T) equilibrium geometries. (Part 2)

Method	Pop. Ω_b	Vol. Ω_b	R_{eq}	ω_h	ΔE_{atom}
G96LYP	3.3020	108.25	1.1008	2340.92	235.90
BVWN	3.3077	108.69	1.0999	2343.26	241.23
M06L	3.5682	112.80	1.0951	2413.85	225.18
M06	3.6198	137.33	1.0884	2465.60	223.15
M062X	3.5724	180.76	1.0854	2512.34	227.42
M06HF	3.4571	190.74	1.0759	2615.55	228.11
M05	3.5265	159.81	1.0928	2447.22	223.56
M052X	3.4090	151.71	1.0829	2543.64	226.32
M11	3.4050	113.21	1.0835	2534.05	234.31
N12SX	3.4979	149.83	1.082	2501.05	215.45
MN12SX	3.6475	164.06	1.0869	2504.36	223.33
SOGGA11X	3.5808	163.80	1.0881	2516.18	228.43
PW91VWN	3.3099	116.77	1.099	2348.34	247.00
TPSSh	3.4568	144.80	1.0943	2418.89	222.21
BMK	3.5194	154.03	1.0894	2456.13	229.55
BhandH	3.6265	181.73	1.0746	2608.60	225.91
BhandHLYP	3.6139	187.06	1.0767	2585.54	208.61
HSEH1PBE	3.5089	151.68	1.0884	2480.19	225.20
wB97XD	3.4996	146.07	1.0871	2491.17	226.11
LC-wPBE	3.5550	168.10	1.0863	2520.45	228.21
CAM-B3LYP	3.5051	150.36	1.0855	2498.70	229.39
APFD	3.4987	150.91	1.0893	2471.40	225.95
B2PLYP-FC	3.3980	127.16	1.0977	2346.33	231.35
mPW2PLYP-FC	3.4361	136.91	1.0942	2383.69	228.95
HSEVWN	3.3178	113.13	1.0995	2347.16	247.00
BrxVWN	3.3877	121.91	1.0964	2386.26	237.30
BPBE	3.3339	114.79	1.1018	2350.17	237.38
PW91PBE	3.3361	123.31	1.101	2354.45	243.15
PBEPBE	3.3562	124.60	1.1022	2350.65	243.93
HSEPBE	3.3582	119.95	1.1015	2353.42	243.07
mPW1PBE	3.5105	154.42	1.0882	2481.43	222.82
mPW3PBE	3.4774	144.21	1.09	2459.18	228.05

Table A.6: Descriptors for the respective equilibrium geometries of N_2. Population of Ω_b in electrons, volume of Ω_b in a.u.$^{-3}$, equilibrium distances (R_{eq}) in Å, harmonic frequencies (ω_h) in cm^{-1} and atomization energies (ΔE_{atom}) in kcal/mol. (Part 1)

Method	Pop. Ω_b	Vol. Ω_b	R_{eq}	ω_h	ΔE_{atom}
BPW91	3.3332	113.55	1.1014	2350.98	237.36
PW91PW91	3.3345	121.92	1.1006	2355.69	243.13
PBEPW91	3.3559	123.15	1.1018	2351.45	243.91
HSEPW91	3.3575	118.77	1.1011	2354.22	243.06
B3PW9	3.4770	143.37	1.09	2458.78	226.12
mPW1PW91	3.5079	153.23	1.0878	2482.51	222.78
MP2-FC	3.2911	103.13	1.1105	2201.86	236.53
BLYP	3.2994	113.55	1.1021	2333.24	240.69
PW91LYP	3.3009	121.40	1.1013	2337.51	246.43
PBELYP	3.3068	114.61	1.1025	2333.58	247.18
HSELYP	3.3102	111.06	1.1018	2336.38	246.41
B3LYP	3.4537	137.62	1.0901	2448.19	230.07
mPW1LYP	3.4769	154.70	1.0881	2468.18	226.03
HF	3.8509	258.21	1.0655	2729.25	117.62
TPSSTPSS	3.4027	139.29	1.0995	2367.54	228.35
XalphaXa	3.3504	111.54	1.0941	2392.73	215.16
BB95	3.3103	114.83	1.1018	2341.84	244.91
PW91B95	3.3120	115.41	1.101	2346.14	250.65
PBEB95	3.3176	115.96	1.1022	2342.36	251.46
HSEB95	3.3356	112.73	1.1015	2345.15	250.62
SVWN	3.3610	106.74	1.0937	2405.14	274.85
PKZBPKZB	3.3734	147.23	1.1087	2326.48	230.09
B3P86	3.4743	141.12	1.0893	2463.13	234.22
PKZBKCIS	3.3618	150.51	1.1088	2323.00	229.73
BrxKCIS	3.3993	121.52	1.0988	2385.94	239.15
OVWN	3.3896	144.95	1.0994	2368.13	229.95
OPBE	3.4163	163.17	1.1017	2372.51	226.62
OLYP	3.3832	150.89	1.1016	2357.41	229.49
OB95	3.3968	153.47	1.1016	2365.27	233.97
CCSD(T)	3.4074	143.46	1.0984	2346.79	224.61

Table A.7: Descriptors for the respective equilibrium geometries of N_2. Population of Ω_b in electrons, volume of Ω_b in a.u.$^{-3}$, equilibrium distances (R_{eq}) in Å, harmonic frequencies (ω_h) in cm^{-1} and atomization energies (ΔE_{atom}) in kcal/mol. (Part 2)

Method	Pop. Ω_b	Vol. Ω_b	R_{eq}	ω_h	ΔE_{atom}
G96LYP	2.9885	53.69	1.1344	2169.64	260.17
BVWN	2.9875	56.52	1.1337	2174.92	261.01
M06L	3.2405	80.34	1.1264	2231.17	259.05
M06	3.2279	89.13	1.1216	2268.34	259.88
M062X	3.1841	69.94	1.1193	2286.62	259.60
M06HF	2.9797	45.33	1.1119	2345.17	257.59
M05	3.1173	76.23	1.1267	2228.43	257.98
M052X	2.9914	54.66	1.1178	2297.91	257.42
M11	3.0239	65.90	1.1193	2286.33	259.45
N12SX	3.0901	64.41	1.1183	2294.32	253.98
MN12SX	3.2214	86.93	1.1214	2269.71	255.96
SOGGA11X	3.1734	72.88	1.1220	2264.93	255.96
PW91VWN	2.9912	55.58	1.1326	2183.06	266.41
TPSSh	3.0863	69.73	1.1283	2216.43	250.23
BMK	3.1930	72.24	1.1192	2287.44	262.64
BhandH	3.2369	71.16	1.1077	2379.06	261.07
BhandHLYP	3.1761	67.65	1.1110	2352.76	239.15
HSEH1PBE	3.1281	65.92	1.1219	2266.02	254.91
wB97XD	3.1353	69.73	1.1217	2267.40	256.92
LC-wPBE	3.1585	72.92	1.1207	2275.14	257.90
CAM-B3LYP	3.1289	66.14	1.1193	2286.71	257.12
APFD	3.1217	65.99	1.1228	2259.14	255.86
B2PLYP-FC	3.0717	63.66	1.1286	2213.65	258.83
mPW2PLYP-FC	3.0934	68.70	1.1256	2237.53	257.11
HSEVWN	2.9929	54.75	1.1332	2178.53	265.10
BrxVWN	3.0323	60.55	1.1303	2201.01	264.27
BPBE	3.0050	60.10	1.1352	2163.14	263.86
PW91PBE	3.0092	62.03	1.1342	2171.40	269.27
PBEPBE	3.0110	59.09	1.1353	2162.47	269.16
HSEPBE	3.0112	58.17	1.1347	2166.98	267.94
mPW1PBE	3.1249	71.11	1.1218	2266.82	253.57
mPW3PBE	3.1052	68.24	1.1235	2253.35	257.87

Table A.8: Descriptors for the respective equilibrium geometries of CO. Population of Ω_b in electrons, volume of Ω_b in a.u.$^{-3}$, equilibrium distances (R_{eq}) in Å, harmonic frequencies (ω_h) in cm^{-1} and atomization energies (ΔE_{atom}) in kcal/mol. (Part 1)

Method	Pop. Ω_b	Vol. Ω_b	R_{eq}	ω_h	ΔE_{atom}
BPW91	3.0056	59.73	1.1349	2166.08	263.65
PW91PW91	3.0094	58.63	1.1338	2174.32	269.06
PBEPW91	3.0121	58.73	1.1350	2165.38	268.94
HSEPW91	3.0119	57.72	1.1344	2169.90	267.73
B3PW9	3.1043	64.86	1.1236	2252.97	255.94
mPW1PW91	3.1255	70.68	1.1214	2269.92	253.35
MP2-FC	3.0767	75.92	1.1348	2166.23	270.04
BLYP	2.9835	54.84	1.1355	2161.34	262.21
PW91LY	2.9891	56.54	1.1344	2169.46	267.57
PBELYP	2.9897	56.09	1.1356	2160.45	267.42
HSELYP	2.9913	55.63	1.1350	2164.92	266.25
B3LYP	3.0874	62.45	1.1237	2251.95	255.69
mPW1LYP	3.1014	63.45	1.1218	2266.82	251.96
HF	3.3040	74.56	1.1019	2426.46	175.70
TPSSTPSS	3.0401	66.20	1.1335	2176.55	254.38
XalphaXa	3.0548	60.50	1.1261	2233.34	268.59
BB95	2.9964	56.94	1.1354	2162.07	271.35
PW91B95	3.0012	58.73	1.1343	2170.37	276.68
PBEB95	3.0016	55.92	1.1355	2161.32	276.58
HSEB95	3.0019	55.03	1.1349	2165.77	275.37
SVWN	3.0607	59.65	1.1255	2237.59	303.93
PKZBPKZB	2.9957	62.78	1.1432	2103.75	256.61
B3P86	3.1057	64.30	1.1228	2258.76	261.65
PKZBKCIS	2.9859	62.01	1.1432	2103.71	256.40
BrxKCIS	3.0370	60.05	1.1322	2186.67	271.07
OVWN	2.9834	58.65	1.1336	2175.45	258.16
OPBE	3.0287	67.92	1.1354	2161.96	261.24
OLYP	3.0093	60.98	1.1354	2162.23	259.30
OB95	3.0188	64.59	1.1355	2161.04	268.72
CCSD(T)	3.0741	71.51	1.1294	2168.92	257.25

Table A.9: Descriptors for the respective equilibrium geometries of CO. Population of Ω_b in electrons, volume of Ω_b in a.u.$^{-3}$, equilibrium distances (R_{eq}) in Å, harmonic frequencies (ω_h) in cm^{-1} and atomization energies (ΔE_{atom}) in kcal/mol. (Part 2)

Method	Pop. Ω_b	Vol. Ω_b	R_{eq}^{CC}	R_{eq}^{CH}	ω_h	ΔE_{atom}
G96LYP	1.7943	17.87	1.5362	1.0962	1015.80	89.18
BVWN	1.7944	17.99	1.5397	1.0910	1008.62	87.06
M06L	1.8043	17.38	1.5149	1.0881	1068.41	96.40
M06	1.7897	17.11	1.5154	1.0895	1067.58	96.46
M062X	1.7946	17.32	1.5230	1.0886	1049.91	97.94
M06HF	1.8126	17.94	1.5369	1.0854	1018.91	98.17
M05	1.7889	17.13	1.5184	1.0895	1060.42	94.10
M052X	1.7913	17.17	1.5239	1.0861	1048.89	97.77
M11	1.7958	17.46	1.5263	1.0923	1041.02	97.36
N12SX	1.8054	17.41	1.5153	1.0859	1068.74	97.93
MN12SX	1.8267	17.70	1.5167	1.0919	1063.79	97.41
SOGGA11X	1.8258	17.93	1.5237	1.0911	1047.39	99.18
PW91VWN	1.7933	17.86	1.5369	1.0907	1015.31	90.82
TPSSh	1.8148	17.95	1.5276	1.0919	1038.15	90.57
BMK	1.7937	17.48	1.5319	1.0905	1028.29	98.48
BhandH	1.8186	17.16	1.5031	1.0873	1098.29	105.14
BhandHLYP	1.8184	17.61	1.5172	1.0831	1064.96	89.52
HSEH1PBE	1.8136	17.63	1.5186	1.0912	1059.44	94.58
wB97XD	1.8072	17.55	1.5226	1.0899	1050.48	97.41
LC-wPBE	1.8120	17.52	1.5173	1.0899	1063.18	94.27
CAM-B3LYP	1.8078	17.53	1.5210	1.0892	1054.39	93.85
APFD	1.8111	17.72	1.5224	1.0918	1049.76	95.44
B2PLYP-FC	1.8024	17.64	1.5246	1.0886	1045.97	94.29
mPW2PLYP-FC	1.8044	17.60	1.5226	1.0874	1051.09	94.61
HSEVWN	1.7948	17.92	1.5378	1.0914	1012.95	89.67
BrxVWN	1.7897	18.40	1.5461	1.0879	993.98	86.79
BPBE	1.7996	17.81	1.5296	1.0980	1031.28	93.24
PW91PBE	1.7993	17.68	1.5269	1.0977	1037.79	97.10
PBEPBE	1.8006	17.75	1.5279	1.0988	1035.14	96.87
HSEPBE	1.8008	17.76	1.5278	1.0984	1035.55	95.94
mPW1PBE	1.8126	17.62	1.5190	1.0907	1058.63	93.87
mPW3PBE	1.8097	17.62	1.5205	1.0917	1054.72	94.78

Table A.10: Descriptors for the respective equilibrium geometries of C_2H_6. Population of Ω_b in electrons, volume of Ω_b in a.u.$^{-3}$, C–C equilibrium distances (R_{eq}^{CC}) and C–H equilibrium distances (R_{eq}^{CH}) in Å, harmonic frequencies (ω_h) in cm^{-1} and atomization energies (ΔE_{atom}) in kcal/mol. (Part 1)

Method	Pop. Ω_b	Vol. Ω_b	R_{eq}^{CC}	R_{eq}^{CH}	ω_h	ΔE_{atom}
BPW91	1.7991	17.80	1.5297	1.0973	1031.04	92.93
PW91PW91	1.7987	17.68	1.5271	1.0970	1037.56	96.79
PBEPW91	1.7998	17.74	1.5281	1.0982	1034.90	96.55
HSEPW91	1.8005	17.75	1.5279	1.0977	1035.31	95.63
B3PW9	1.8101	17.66	1.5214	1.0913	1052.72	93.28
mPW1PW91	1.8122	17.62	1.5191	1.0900	1058.63	93.55
MP2-FC	1.7951	17.47	1.5213	1.0875	1054.42	100.50
BLYP	1.7925	17.90	1.5382	1.0969	1011.02	90.47
PW91LY	1.7912	17.77	1.5355	1.0966	1017.47	94.21
PBELYP	1.7932	17.84	1.5366	1.0978	1014.72	93.95
HSELYP	1.7932	17.85	1.5364	1.0973	1015.08	93.05
B3LYP	1.8034	17.72	1.5268	1.0905	1039.79	91.71
mPW1LYP	1.8042	17.70	1.5262	1.0894	1041.47	91.11
HF	1.8369	18.10	1.5239	1.0835	1048.91	65.51
TPSSTPSS	1.8122	18.05	1.5319	1.0944	1027.17	90.57
XalphaXa	1.7981	17.19	1.5124	1.1039	1071.29	101.81
BB95	1.7979	17.72	1.5280	1.0961	1035.46	98.54
PW91B95	1.7952	17.60	1.5254	1.0958	1041.88	102.28
PBEB95	1.7983	17.67	1.5264	1.0970	1039.28	102.04
HSEB95	1.7983	17.67	1.5263	1.0965	1039.67	101.13
SVWN	1.8016	17.03	1.5062	1.0986	1087.43	117.93
PKZBPKZB	1.8088	18.15	1.5398	1.1040	1006.27	90.42
B3P86	1.8108	17.57	1.5190	1.0903	1058.62	95.98
PKZBKCIS	1.8019	18.02	1.5382	1.1032	1009.81	90.79
BrxKCIS	1.7896	18.16	1.5357	1.0943	1016.94	94.59
OVWN	1.8088	17.97	1.5303	1.0900	1031.22	88.71
OPBE	1.8161	17.82	1.5209	1.0970	1052.32	95.26
OLYP	1.8067	17.90	1.5288	1.0957	1033.67	92.15
OB95	1.8138	17.73	1.5189	1.0950	1057.58	100.81
CCSD(T)	1.7651	16.63	1.5231	1.0883	1024.52	91.51

Table A.11: Descriptors for the respective equilibrium geometries of C_2H_6. Population of Ω_b in electrons, volume of Ω_b in a.u.$^{-3}$, C–C equilibrium distances (R_{eq}^{CC}) and C–H equilibrium distances (R_{eq}^{CH}) in Å, harmonic frequencies (ω_h) in cm^{-1} and atomization energies (ΔE_{atom}) in kcal/mol. (Part 2)

A.3 Calculated cell parameters of periodic systems

The complete set of experimental references for the different cell parameters can be found in F. Peccati, R. Laplaza, and J. Contreras-García, "Overcoming distrust in solid state simulations: Adding error bars to computational data," *The Journal of Physical Chemistry C*, vol. 123, no. 8, pp. 4767–4772, 2019 and references thereof.

Structure	HF	LDA	PBE	Experimental
Acetamide a	11.7302	11.0741	11.4534	11.513
Acetamide c	15.2858	11.5760	13.6922	12.883
AgBr B1	6.1736	5.5398	5.7650	5.7721
AgCl B1	5.8483	5.2972	5.4924	5.5463
AgI B4 a	4.8344	4.3752	4.5310	4.592
AgI B4 c	7.7939	7.1767	7.4257	7.510
AlAs B3	5.6684	5.5689	5.6507	5.661
AlN B4 a	3.1080	3.0906	3.1350	3.111
AlN B4 c	4.9734	4.9411	5.0138	4.981
AlP B3	5.4519	5.3381	5.4142	5.463
AlSb B3	6.1263	6.0018	6.1068	6.136
BaSe B1	6.8619	6.4723	6.6351	6.593
BaS B1	6.5567	6.2311	6.3846	6.389
BaTe B1	7.0939	6.7734	6.9443	7.007
BN B3	3.6050	3.5818	3.6302	3.616
BP B3	4.5894	4.4923	4.5584	4.358
BAs B3	4.8490	4.7776	4.8429	4.777
Benzene a	6.1104	5.2112	5.7515	5.5220
Benzene b	5.1952	5.1327	5.7747	5.4396
Benzene c	8.2223	6.8928	6.9076	7.6726
Boric acid a	7.2444	6.6285	6.9198	7.0453
Boric acid c	11.0798	8.4123	10.1364	9.5608
C A4	3.5493	3.5268	3.5688	3.56679
CaO B1	4.8592	4.7319	4.8458	4.805
Carbonate apatite a	9.6957	9.2769	9.5475	9.521
Carbonate apatite b	9.7777	9.4495	9.7386	9.521
Carbonate apatite c	6.9122	6.7382	6.8929	6.872
CaSe B1	6.1750	5.8685	6.0315	5.916
CaS B1	5.8433	5.5730	5.7239	5.689
CaTe B1	6.3956	6.1531	6.2949	6.348
CaTiO3	3.8546	3.8095	3.8895	3.8240
CdSe B4 a	4.4248	4.20618	4.3299	4.2322
CdSe B4 c	7.1376	6.8052	6.9917	6.9088
CdSe B3	6.2312	5.9368	6.1079	6.052
CdSe B1	5.8075	5.5091	5.6686	5.5445
CdS B4 a	4.3288	4.1027	4.2325	4.1365
CdS B4 c	6.9438	6.6138	6.8112	6.7160
CdS B3	5.9277	5.6507	5.8056	5.818
CdS B1	5.5261	5.2611	5.4028	5.30

Table A.12: Cell parameters in Å.

Structure	HF	LDA	PBE	Experimental
Cubic acetylene	5.8457	5.2827	5.6688	6.1020
CuBr III⋆	6.1298	5.4040	5.6093	5.689
CuBr V⋆	7.5535	6.5245	6.7548	6.570
CuBr VI⋆	5.7510	5.1072	5.2918	5.1425
GaAs B3	5.7444	5.6003	5.7215	5.648
GaP B3	5.5367	5.3854	5.4946	5.451
GaSb B3	6.1889	6.0022	6.1660	6.096
Ge A4	5.6700	5.5582	5.6859	5.658
HCN a	4.6689	3.8088	4.4553	4.63
HCN c	4.3952	4.0419	4.2331	4.34
Ice XI a	4.6282	4.1105	4.3508	4.465
Ice XI b	8.3080	7.1658	7.5757	7.859
Ice XI c	7.6290	6.6885	7.0967	7.292
InN B4 a	3.5997	3.5530	3.6226	3.537
InN B4 c	5.7436	5.6875	5.8042	5.704
InAs B3	6.2102	6.0326	6.1959	6.058
InP B3	6.0228	5.8317	5.9859	5.869
InSb B3	6.6198	6.4257	6.6133	6.479
KBr B2	4.1238	3.8123	3.9949	3.74
KBr B1	6.8174	6.3423	6.6475	6.585
KCl B2	3.8523	3.6123	3.7829	3.634
KCl B1	6.4180	6.0430	6.3135	6.29294
KF B2	3.2460	3.0911	3.2526	3.06
KF B1	5.4070	5.1606	5.4049	5.3437
KI B2	4.3053	4.0347	4.2127	3.94
KI B1	7.1000	6.7058	7.0119	7.0655
LaAlO3	3.8152	3.7710	3.8420	3.7913
LiF B1	4.0280	3.9532	4.1099	4.028
MgAl2O4	8.0628	8.0510	8.1980	8.0832
Na_2He (ext. pressure 300 GPa)	3.9250	3.8951	3.9305	3.9500
NaCl B1	5.7116	5.4080	5.6420	5.6401
NaF B1	4.6047	4.5096	4.6877	4.6354
Orthorombic acetylene a	6.0403	5.3737	5.7973	6.198
Orthorombic acetylene b	5.9638	5.6665	5.8662	6.023
Orthorombic acetylene c	5.2771	4.4776	5.0035	5.578

Table A.13: Cell parameters in Å. ⋆ The reference value is calculated and not experimentally determined.

Structure	HF	LDA	PBE	Experimental
RbBr B1	7.1152	6.6279	6.9420	6.82
RbCl B1	6.6810	6.3022	6.5583	6.53
RbF B1	5.7240	5.5046	5.7441	5.59
RbI B1	7.3409	6.9400	7.2476	7.26
Si A4	5.4355	5.3505	5.4234	5.430
Sodalite frame	9.1110	9.0146	9.1982	8.86343
SrSe B1	6.5568	6.2610	6.4334	6.234
SrS B1	6.2220	6.0130	6.1487	5.990
SrTe B1	6.5975	6.3786	6.5250	6.640
ZnS B1	5.2860	4.9825	5.1282	5.13
ZnS B4 a	3.8227	3.7487	3.8596	3.8227
ZnS B4 c	6.4882	6.1340	6.2930	6.2607
ZnS B3	5.6259	5.3040	5.4539	5.4093
ZnSe B3	5.8400	5.5276	5.6688	5.668
ZnTe B3	6.3063	5.9498	6.1381	6.089

Table A.14: Cell parameters in Å.

A.4 Thermal expansion and noncovalent interactions in molecular solids

A derivation of Grimme's two-parameters dispersion correction (cf. Subsection 2.5.3) adapted for periodic solid state calculations is implemented in the `CRYSTAL` code for the functional B3LYP.[118, 119] The method, that takes the name of B3LYP-D*, has been tested on molecular crystals extensively.[119]

The optimized geometries for a set of molecular solids using both B3LYP and B3LYP-D* are presented below in Table A.15. Assuming that B3LYP does not account for dispersion at all, the percent shrinking of the cell deriving from dispersion can be calculated comparing to B3LYP-D* and afterwards compared with the cell shrinking observed when moving from HF to the LDA. Results indicate that the contribution of dispersion is always inferior to the HF-LDA volume change, showing that dispersion only has a secondary effect compared to the delocalization error in this regard.

	HF	LDA	PBE	EXPT	B3LYP	B3LYP-D*	D Shr. (%)	HF-LDA Shr. (%)
acetamide	1821.51	1229.45	1555.51	1478.85	1626.11	1388.15	15	33
cubic acetylene	199.76	147.42	182.17	226.31	185.74	171.92	7	26
orthorombic acetylene	190.10	136.34	170.16	208.20	175.19	161.24	8	28
HCN	95.81	58.63	84.02	93.04	87.39	75.09	14	39
boric acid	503.57	320.10	420.33	410.98	444.44	369.80	17	36
Ice XI	293.34	197.01	233.91	255.32	248.28	241.35	3	33

Table A.15: Volumes of crystallographic cells ($Å^3$) and cell volume shrinking owing to dispersion effects (D Shr.) and to the change from HF to LDA (HF-LDA Shr.).

The effect of thermal expansion can be modelled using the quasi-harmonic approximation. Results for hydrogen cyanide and cubic acetlyene, representatives of dipole-dipole weak interactions and van der Waals effects respectively, are collected in Figures A.1 and A.2 using the implementation in the `CRYSTAL17` code.[120, 100] with a step amplitude of 3.5% in volume, 100 temperature points from 10 K to 300 K and the Grüneisen formalism.

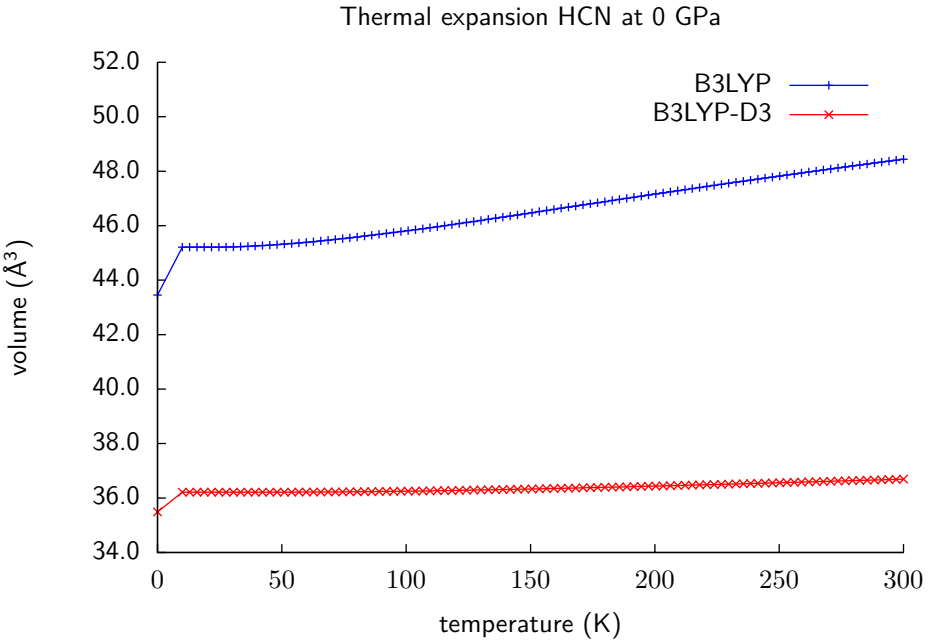

Figure A.1: Cell volume dependence on temperature (K) of HCN calculated with the B3LYP functional with and without Grimme's D3 dispersion.

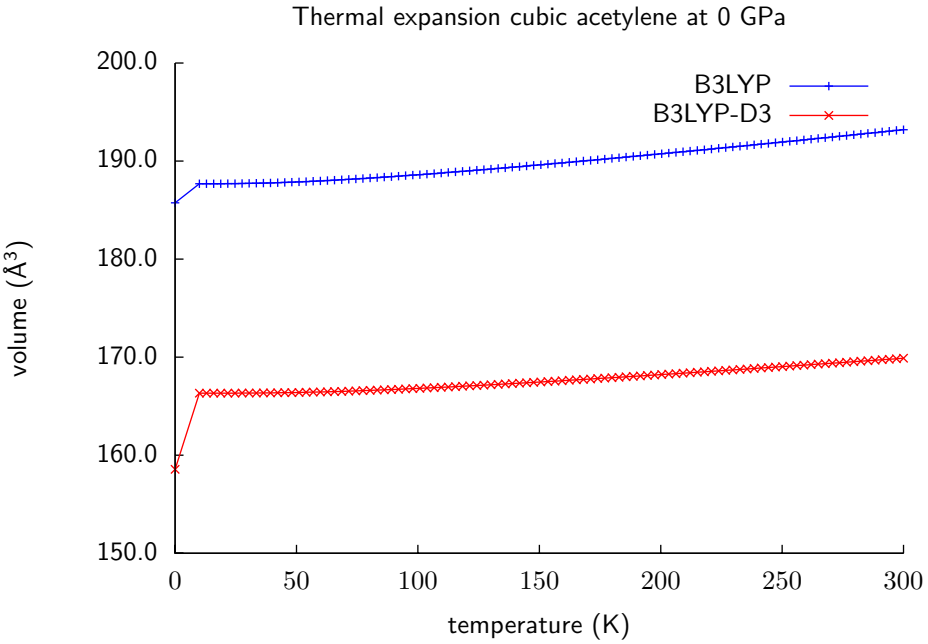

Figure A.2: Cell volume dependence on temperature (K) of cubic aceylene calculated with the B3LYP functional with and without Grimme's D3 dispersion.

The most important variation of the cell volume of both systems is given by the introduction of the zero-point vibrational energy. From that point on, the volume dependence on the temperature is smooth until 300 K. With respect to the initial cell parameter, inclusion thermal effects leads to approximately 11 % volume increase, which is significantly inferior to the variability associated to the choice of functional for these systems.

Bibliography

[1] J. L. Ramsey, "Molecular shape, reduction, explanation and approximate concepts," *Synthese*, vol. 111, no. 3, pp. 233–251, 1997.

[2] P. J. S. Gómez and F. Martín, "Quantum vs. classical chemistry in university chemistry education: A case study of the role of history in thinking the curriculum," *Chem. Educ. Res. Pract.*, vol. 4, pp. 131–148, 2003.

[3] M. Nič, J. Jirát, B. Košata, A. Jenkins, and A. McNaught, eds., *IUPAC Compendium of Chemical Terminology*. IUPAC, 2009.

[4] A. Szabo and N. S. Ostlund, *Modern quantum chemistry: introduction to advanced electronic structure theory*. Courier Corporation, 1989.

[5] J. C. Slater, "The theory of complex spectra," *Phys. Rev.*, vol. 34, pp. 1293–1322, 1929.

[6] P. Pulay, "Improved scf convergence acceleration," *Journal of Computational Chemistry*, vol. 3, no. 4, pp. 556–560, 1982.

[7] Y. A. Wang, C. Y. Yam, Y. K. Chen, and G. Chen, "Communication: Linear-expansion shooting techniques for accelerating self-consistent field convergence," *The Journal of Chemical Physics*, vol. 134, no. 24, p. 241103, 2011.

[8] J. Harris, "Simplified method for calculating the energy of weakly interacting fragments," *Phys. Rev. B*, vol. 31, pp. 1770–1779, 1985.

[9] R. McWeeny and B. Sutcliffe, "Methods of molecular quantum mechanics," *Vol. XV*, 1959.

[10] R. G. Parr, *Density functional theory of atoms and molecules*. Springer, 1980.

[11] P. Hohenberg and W. Kohn, "Inhomogeneous electron gas," *Physical review*, vol. 136, no. 3B, p. B864, 1964.

[12] M. Levy, "Universal variational functionals of electron densities, first-order density matrices, and natural spin-orbitals and solution of the v-representability problem," *Proceedings of the National Academy of Sciences*, vol. 76, no. 12, pp. 6062–6065, 1979.

[13] M. Levy, "Electron densities in search of hamiltonians," *Physical Review A*, vol. 26, no. 3, p. 1200, 1982.

[14] V. Sahni and J. Gruenebaum, "Remarks on local and nonlocal exchange and correlation-energy calculations of surface energies and work functions," *Phys. Rev. B*, vol. 25, pp. 6275–6280, 1982.

[15] W. Kohn and L. J. Sham, "Self-consistent equations including exchange and correlation effects," *Physical review*, vol. 140, no. 4A, p. A1133, 1965.

[16] S. Vosko, L. Wilk, and M. Nusair, "Accurate spin-dependent electron liquid correlation energies for local spin density calculations: a critical analysis," *Canadian Journal of physics*, vol. 58, no. 8, pp. 1200–1211, 1980.

[17] A. D. Becke, "Density-functional exchange-energy approximation with correct asymptotic behavior," *Physical review A*, vol. 38, no. 6, p. 3098, 1988.

[18] J. P. Perdew, K. Burke, and Y. Wang, "Generalized gradient approximation for the exchange-correlation hole of a many-electron system," *Phys. Rev. B*, vol. 54, pp. 16533–16539, 1996.

[19] C. Lee, W. Yang, and R. G. Parr, "Development of the colle-salvetti correlation-energy formula into a functional of the electron density," *Physical review B*, vol. 37, no. 2, p. 785, 1988.

[20] J. P. Perdew, K. Burke, and M. Ernzerhof, "Generalized gradient approximation made simple," *Physical review letters*, vol. 77, no. 18, p. 3865, 1996.

[21] J. P. Perdew, S. Kurth, A. Zupan, and P. Blaha, "Accurate density functional with correct formal properties: A step beyond the generalized gradient approximation," *Physical review letters*, vol. 82, no. 12, p. 2544, 1999.

[22] J. Tao, J. P. Perdew, V. N. Staroverov, and G. E. Scuseria, "Climbing the density functional ladder: Nonempirical meta–generalized gradient approximation designed for molecules and solids," *Physical Review Letters*, vol. 91, no. 14, p. 146401, 2003.

[23] Y. Zhao and D. G. Truhlar, "A new local density functional for main-group thermochemistry, transition metal bonding, thermochemical kinetics, and noncovalent interactions," *The Journal of Chemical Physics*, vol. 125, no. 19, p. 194101, 2006.

[24] A. D. Becke, "A new mixing of hartree–fock and local density-functional theories," *The Journal of Chemical Physics*, vol. 98, no. 2, pp. 1372–1377, 1993.

[25] C. Adamo and V. Barone, "Toward reliable density functional methods without adjustable parameters: The pbe0 model," *The Journal of chemical physics*, vol. 110, no. 13, pp. 6158–6170, 1999.

[26] Y. Zhao and D. G. Truhlar, "The m06 suite of density functionals for main group thermochemistry, thermochemical kinetics, noncovalent interactions, excited states, and transition elements: two new functionals and systematic testing of four m06-class functionals and 12 other functionals," *Theoretical Chemistry Accounts*, vol. 120, no. 1-3, pp. 215–241, 2007.

[27] T. Yanai, D. P. Tew, and N. C. Handy, "A new hybrid exchange–correlation functional using the coulomb-attenuating method (CAM-b3lyp)," *Chemical Physics Letters*, vol. 393, no. 1-3, pp. 51–57, 2004.

[28] J.-D. Chai and M. Head-Gordon, "Long-range corrected hybrid density functionals with damped atom–atom dispersion corrections," *Physical Chemistry Chemical Physics*, vol. 10, no. 44, p. 6615, 2008.

[29] E. Brémond and C. Adamo, "Seeking for parameter-free double-hybrid functionals: The PBE0-DH model," *The Journal of Chemical Physics*, vol. 135, no. 2, p. 024106, 2011.

[30] S. Grimme, "Semiempirical hybrid density functional with perturbative second-order correlation," *The Journal of Chemical Physics*, vol. 124, no. 3, p. 034108, 2006.

[31] S. Grimme, J. Antony, S. Ehrlich, and H. Krieg, "A consistent and accurate ab initio parametrization of density functional dispersion correction (dft-d) for the 94 elements h-pu," *The Journal of Chemical Physics*, vol. 132, no. 15, p. 154104, 2010.

[32] A. D. Becke and E. R. Johnson, "A unified density-functional treatment of dynamical, nondynamical, and dispersion correlations," *The Journal of Chemical Physics*, vol. 127, no. 12, p. 124108, 2007.

[33] L. A. Burns, V. Mayagoitia, B. G. Sumpter, and C. D. Sherrill, "Density-functional approaches to noncovalent interactions: A comparison of dispersion corrections (dft-d), exchange-hole dipole moment (xdm) theory, and specialized functionals," *The Journal of Chemical Physics*, vol. 134, no. 8, p. 084107, 2011.

[34] S. Shaik and P. C. Hiberty, *A chemist's guide to valence bond theory.* Hoboken, N.J: Wiley-Interscience, 2008.

[35] P. C. Hiberty and S. Shaik, "Breathing-orbital valence bond method - a modern valence bond method that includes dynamic correlation," *Theoretical Chemistry Accounts: Theory, Computation, and Modeling (Theoretica Chimica Acta)*, vol. 108, pp. 255–272, Nov. 2002.

[36] P. L. Popelier and F. M. Aicken, "Atomic properties of amino acids: Computed atom types as a guide for future force-field design," *ChemPhysChem*, vol. 4, no. 8, pp. 824–829, 2003.

[37] C. F. Matta and R. J. Boyd, *The Quantum Theory of Atoms in Molecules.* New York: Wiley-VCH, 2007.

[38] R. F. W. Bader, *Atoms in Molecules: A Quantum Theory.* Oxford, UK: Oxford Science Publications, 1990.

[39] R. F. Bader, "A bond path: a universal indicator of bonded interactions," *The Journal of Physical Chemistry A*, vol. 102, no. 37, pp. 7314–7323, 1998.

[40] M. A. Blanco, A. Martín Pendás, and E. Francisco, "Interacting quantum atoms: a correlated energy decomposition scheme based on the quantum theory of atoms in molecules," *Journal of Chemical Theory and Computation*, vol. 1, no. 6, pp. 1096–1109, 2005.

[41] A. D. Becke and K. E. Edgecombe, "A simple measure of electron localization in atomic and molecular systems," *The Journal of chemical physics*, vol. 92, p. 5397, 1990.

[42] A. Savin, "The electron localization function (elf) and its relatives: interpretations and difficulties," *Journal of Molecular Structure: THEOCHEM*, vol. 727, no. 1, p. 127, 2005.

[43] K. Ruedenberg and M. W. Schmidt, "Why does electron sharing lead to covalent bonding? a variational analysis," *Journal of computational chemistry*, vol. 28, no. 1, pp. 391–410, 2007.

[44] H. L. Schmider and A. D. Becke, "Two functions of the density matrix and their relation to the chemical bond," *The Journal of chemical physics*, vol. 116, no. 8, p. 3184, 2002.

[45] H. Jacobsen, "Chemical bonding in view of electron charge density and kinetic energy density descriptors," *Journal of computational chemistry*, vol. 30, no. 7, p. 1093, 2009.

[46] H. Jacobsen, "Kinetic energy density and covalent bonding–a complementary analysis at the border of bond and no bond," *Dalton Transactions*, vol. 39, no. 23, p. 5426, 2010.

[47] K. Finzel, "Elf and its relatives a detailed study about the robustness of the atomic shell structure in real space," *International Journal of Quantum Chemistry*, vol. 114, no. 22, p. 1546, 2014.

[48] E. R. Johnson, S. Keinan, P. Mori-Sanchez, J. Contreras-Garcia, A. J. Cohen, and W. Yang, "Revealing noncovalent interactions," *Journal of the American Chemical Society*, vol. 132, no. 18, p. 6498, 2010.

[49] R. A. Boto, J. Contreras-García, J. Tierny, and J.-P. Piquemal, "Interpretation of the reduced density gradient," *Molecular Physics*, pp. 1–9, 2015.

[50] B. Silvi, "The synaptic order: a key concept to understand multicenter bonding," *Journal of molecular structure*, vol. 614, no. 1, pp. 3–10, 2002.

[51] B. Silvi, A. Savin, *et al.*, "Classification of chemical bonds based on topological analysis of electron localization functions," *Nature*, vol. 371, no. 6499, pp. 683–686, 1994.

[52] R. G. Parr and R. F. Borkman, "Chemical binding and potentialenergy functions for molecules," *The Journal of Chemical Physics*, vol. 46, no. 9, pp. 3683–3685, 1967.

[53] R. F. Borkman and R. G. Parr, "Toward an understanding of potentialenergy functions for diatomic molecules," *The Journal of Chemical Physics*, vol. 48, no. 3, pp. 1116–1126, 1968.

[54] R. G. Parr and R. F. Borkman, "Simple bondcharge model for potentialenergy curves of homonuclear diatomic molecules," *The Journal of Chemical Physics*, vol. 49, no. 3, pp. 1055–1058, 1968.

[55] R. F. Borkman, G. Simons, and R. G. Parr, "Simple bondcharge model for potentialenergy curves of heteronuclear diatomic molecules," *The Journal of Chemical Physics*, vol. 50, no. 1, pp. 58–65, 1969.

[56] A. Pasternak, "Electronegativity based on the simple bond charge model," *Chemical Physics*, vol. 26, no. 1, pp. 101 – 112, 1977.

[57] P. W. Ayers and S. Jenkins, "Bond metallicity measures," *Computational and Theoretical Chemistry*, vol. 1053, pp. 112–122, Feb. 2015.

[58] S. Grimme, "Theoretical bond and strain energies of molecules derived from properties of the charge density at bond critical points," *Journal of the American Chemical Society*, vol. 118, no. 6, pp. 1529–1534, 1996.

[59] S. T. Howard, M. K. Cyranski, and L. Z. Stolarczyk, "On the calculation of bond energies from atomization energies," *Chem. Commun.*, pp. 197–198, 2001.

[60] K. Exner and P. v. R. Schleyer, "Theoretical bond energies: A critical evaluation," *The Journal of Physical Chemistry A*, vol. 105, no. 13, pp. 3407–3416, 2001.

[61] D. W. Brenner, O. A. Shenderova, J. A. Harrison, S. J. Stuart, B. Ni, and S. B. Sinnott, "A second-generation reactive empirical bond order (REBO) potential energy expression for hydrocarbons," *Journal of Physics: Condensed Matter*, vol. 14, no. 4, pp. 783–802, 2002.

[62] A. A. Zavitsas, "Quantitative relationship between bond dissociation energies, infrared stretching frequencies, and force constants in polyatomic molecules," *The Journal of Physical Chemistry*, vol. 91, no. 22, pp. 5573–5577, 1987.

[63] A. Martín Pendás and E. Francisco, "Real space bond orders are energetic descriptors," *Phys. Chem. Chem. Phys.*, vol. 20, pp. 16231–16237, 2018.

[64] L. Goodman, H. Gu, and V. Pophristic, "Gauche effect in 1,2-difluoroethane. hyperconjugation, bent bonds, steric repulsion," *The Journal of Physical Chemistry A*, vol. 109, no. 6, pp. 1223–1229, 2005.

[65] D. Banerjee, A. Ghosh, S. Chattopadhyay, P. Ghosh, and R. K. Chaudhuri, "Revisiting the 'cis-effect' in 1,2-difluoro derivatives of ethylene and diazene using ab initio multireference methods," *Molecular Physics*, vol. 112, no. 24, pp. 3206–3224, 2014.

[66] D. M. Andrada, J. L. Casals-Sainz, A. Martín-Pendás, and G. Frenking, "Dative and electron-sharing bonding in c2f4," *Chemistry – A European Journal*, vol. 24, no. 36, pp. 9083–9089, 2018.

[67] T. H. Dunning, "Gaussian basis sets for use in correlated molecular calculations. i. the atoms boron through neon and hydrogen," *J. Chem. Phys.*, vol. 90, no. 2, pp. 1007–1023, 1989.

[68] T. Helgaker, W. Klopper, H. Koch, and J. Noga, "Basis-set convergence of correlated calculations on water," *J. Chem. Phys.*, vol. 106, no. 23, pp. 9639–9646, 1997.

[69] D. Chesnut, "The use of parameter ratios to characterize the formal order of chemical bonds," *Chem. Phys.*, vol. 271, no. 1, pp. 9 – 16, 2001.

[70] J.-D. Chai and M. Head-Gordon, "Long-range corrected hybrid density functionals with damped atom–atom dispersion corrections," *Phys. Chem. Chem. Phys.*, vol. 10, pp. 6615–6620, 2008.

[71] S. Shaik, D. Danovich, W. Wu, P. Su, H. S. Rzepa, and P. C. Hiberty, "Quadruple bonding in c2 and analogous eight-valence electron species," *Nature Chemistry*, vol. 4, no. 3, pp. 195–200, 2012.

[72] F. Weigend and R. Ahlrichs, "Balanced basis sets of split valence, triple zeta valence and quadruple zeta valence quality for h to rn: Design and assessment of accuracy," *Phys. Chem. Chem. Phys.*, vol. 7, pp. 3297–3305, 2005.

[73] M. J. Frisch, G. W. Trucks, H. B. Schlegel, G. E. Scuseria, M. A. Robb, J. R. Cheeseman, G. Scalmani, V. Barone, B. Mennucci, G. A. Petersson, H. Nakatsuji, M. Caricato, X. Li, H. P. Hratchian, A. F. Izmaylov, J. Bloino, G. Zheng, J. L. Sonnenberg, M. Hada, M. Ehara, K. Toyota, R. Fukuda, J. Hasegawa, M. Ishida, T. Nakajima, Y. Honda, O. Kitao, H. Nakai, T. Vreven, J. A. Montgomery, Jr., J. E. Peralta, F. Ogliaro, M. Bearpark, J. J. Heyd, E. Brothers, K. N. Kudin, V. N. Staroverov, R. Kobayashi, J. Normand, K. Raghavachari, A. Rendell, J. C. Burant, S. S. Iyengar, J. Tomasi, M. Cossi, N. Rega, J. M. Millam, M. Klene, J. E. Knox, J. B. Cross, V. Bakken, C. Adamo, J. Jaramillo, R. Gomperts, R. E. Stratmann, O. Yazyev, A. J. Austin, R. Cammi, C. Pomelli, J. W. Ochterski, R. L. Martin, K. Morokuma, V. G. Zakrzewski, G. A. Voth, P. Salvador, J. J. Dannenberg, S. Dapprich, A. D. Daniels, Farkas, J. B. Foresman, J. V. Ortiz, J. Cioslowski, and D. J. Fox, "Gaussian 09, Revision D.01." Gaussian Inc. Wallingford CT 2009.

[74] C. Latouche, F. Palazzetti, D. Skouteris, and V. Barone, "High-accuracy vibrational computations for transition-metal complexes including anharmonic corrections: Ferrocene, ruthenocene, and osmocene as test cases," *Journal of Chemical Theory and Computation*, vol. 10, no. 10, pp. 4565–4573, 2014.

[75] I. A. Popov, K. V. Bozhenko, and A. I. Boldyrev, "Is graphene aromatic?," *Nano Research*, vol. 5, no. 2, pp. 117–123, 2012.

[76] J. P. Perdew and K. Schmidt, "Jacob's ladder of density functional approximations for the exchange-correlation energy," *AIP Conference Proceedings*, vol. 577, no. 1, pp. 1–20, 2001.

[77] J. Sun, A. Ruzsinszky, and J. P. Perdew, "Strongly constrained and appropriately normed semilocal density functional," *Phys. Rev. Lett.*, vol. 115, p. 036402, 2015.

[78] M. G. Medvedev, I. S. Bushmarinov, J. Sun, J. P. Perdew, and K. A. Lyssenko, "Density functional theory is straying from the path toward the exact functional," *Science*, vol. 355, no. 6320, pp. 49–52, 2017.

[79] P. Verma and D. G. Truhlar, "Can Kohn–Sham density functional theory predict accurate charge distributions for both single-reference and multi-reference molecules?," *Physical Chemistry Chemical Physics*, vol. 19, no. 20, pp. 12898–12912, 2017.

[80] D. S. Ranasinghe, A. Perera, and R. J. Bartlett, "A note on the accuracy of KS-DFT densities," *The Journal of Chemical Physics*, vol. 147, no. 20, p. 204103, 2017.

[81] P. D. Mezei, G. I. Csonka, and M. Kállay, "Electron Density Errors and Density-Driven Exchange-Correlation Energy Errors in Approximate Density Functional Calculations," *Journal of Chemical Theory and Computation*, vol. 13, no. 10, pp. 4753–4764, 2017.

[82] K. R. Brorsen, Y. Yang, M. V. Pak, and S. Hammes-Schiffer, "Is the Accuracy of Density Functional Theory for Atomization Energies and Densities in Bonding Regions Correlated?," *The Journal of Physical Chemistry Letters*, vol. 8, no. 9, pp. 2076–2081, 2017.

[83] J. A. Dobado, H. Martínez-García, Molina, and M. R. Sundberg, "Chemical bonding in hypervalent molecules revised. application of the atoms in molecules theory to y3 x and y3 xz (y = h or ch3; x = n, p or as; z = o or s) compounds," *Journal of the American Chemical Society*, vol. 120, no. 33, pp. 8461–8471, 1998.

[84] M.-C. Kim, E. Sim, and K. Burke, "Understanding and reducing errors in density functional calculations," *Phys. Rev. Lett.*, vol. 111, p. 073003, 2013.

[85] D. Jacquemin and C. Adamo, "Bond Length Alternation of Conjugated Oligomers: Wave Function and DFT Benchmarks," *J. Chem. Theory Comput.*, vol. 7, no. 2, pp. 369–376, 2011.

[86] O. Christiansen, H. Koch, and P. Jørgensen, "The second-order approximate coupled cluster singles and doubles model cc2," *Chemical Physics Letters*, vol. 243, no. 5, pp. 409 – 418, 1995.

[87] A. K. Theophilou, "A novel density functional theory for atoms, molecules, and solids," *The Journal of Chemical Physics*, vol. 149, no. 7, p. 074104, 2018.

[88] A. Nagy, "Density functional theory from spherically symmetric densities," *The Journal of Chemical Physics*, vol. 149, no. 20, p. 204112, 2018.

[89] V. Polo, E. Kraka, and D. Cremer, "Electron correlation and the self-interaction error of density functional theory," *Molecular Physics*, vol. 100, no. 11, pp. 1771–1790, 2002.

[90] Q. Zhao and H. J. Kulik, "Where does the density localize in the solid state? divergent behavior for hybrids and dft+u," *Journal of Chemical Theory and Computation*, vol. 14, no. 2, pp. 670–683, 2018.

[91] J. S. Muenter, "Electric dipole moment of carbon monoxide," *Journal of Molecular Spectroscopy*, vol. 55, pp. 490–491, 1975.

[92] P. Pernot, B. Civalleri, D. Presti, and A. Savin, "Prediction uncertainty of density functional approximations for properties of crystals with cubic symmetry," *The Journal of Physical Chemistry A*, vol. 119, no. 21, pp. 5288–5304, 2015.

[93] A. Wasserman, J. Nafziger, K. Jiang, M.-C. Kim, E. Sim, and K. Burke, "The importance of being inconsistent," *Annual Review of Physical Chemistry*, vol. 68, no. 1, pp. 555–581, 2017.

[94] Y. Kim, S. Song, E. Sim, and K. Burke, "Halogen and chalcogen binding dominated by density-driven errors," *The Journal of Physical Chemistry Letters*, vol. 10, no. 2, pp. 295–301, 2019.

[95] H. O. Pritchard, "Recrossings and transition-state theory," *The Journal of Physical Chemistry A*, vol. 109, no. 7, pp. 1400–1404, 2005.

[96] F. H. Herbstein, "How Precise are Measurements of Unit-Cell Dimensions From Single Crystals?," *Acta Crystallogr. A*, vol. 56, no. 4, pp. 547–557, 2000.

[97] A. Authier, *Early Days of X-ray Crystallography*. OUP Oxford, 2013.

[98] W. H. Bragg and W. L. Bragg, "The Reflection of X-Rays by Crystals," *Proc. Royal Soc. Lond. A Math. Phys. Eng. Sci.*, vol. 88, no. 605, pp. 428–438, 1913.

[99] E. Cancès and G. Dusson, "Discretization Error Cancellation in Electronic Structure Calculation: Toward a Quantitative Study," *ESAIM: M2AN*, vol. 51, no. 5, pp. 1617–1636, 2017.

[100] R. Dovesi, A. Erba, R. Orlando, C. M. Zicovich-Wilson, B. Civalleri, L. Maschio, M. Rérat, S. Casassa, J. Baima, S. Salustro, and B. Kirtman, "Quantum-mechanical condensed matter simulations with crystal," *WIREs Computational Molecular Science*, vol. 8, no. 4, p. e1360, 2018.

[101] M. F. Peintinger, D. V. Oliveira, and T. Bredow, "Consistent gaussian basis sets of triple-zeta valence with polarization quality for solid-state calculations," *Journal of Computational Chemistry*, vol. 34, no. 6, pp. 451–459, 2012.

[102] U. von Barth and L. Hedin, "A local exchange-correlation potential for the spin polarized case. i," *Journal of Physics C: Solid State Physics*, vol. 5, no. 13, pp. 1629–1642, 1972.

[103] A. J. Cohen, P. Mori-Sánchez, and W. Yang, "Insights into Current Limitations of Density Functional Theory," *Science*, vol. 321, no. 5890, pp. 792–794, 2008.

[104] J. Autschbach and M. Srebro, "Delocalization Error and Functional Tuning in Kohn-Sham Calculations of Molecular Properties," *Acc. Chem. Res.*, vol. 47, no. 8, pp. 2592–2602, 2014.

[105] R. R. Shuvalov and P. C. Burns, "A New Polytype of Orthoboric Acid, H_3BO_3 3T," *Acta Cryst. C*, vol. 59, no. 6, pp. i47–i49, 2014.

[106] N. Marom, A. Tkatchenko, M. Rossi, V. V. Gobre, O. Hod, M. Scheffler, and L. Kronik, "Dispersion interactions with density-functional theory: Benchmarking semiempirical and interatomic pairwise corrected density functionals," *J. Chem. Theory Comput.*, vol. 7, no. 12, pp. 3944–3951, 2011.

[107] M. Cutini, B. Civalleri, M. Corno, R. Orlando, J. G. Brandenburg, L. Maschio, and P. Ugliengo, "Assessment of different quantum mechanical methods for the prediction of structure and cohesive energy of molecular crystals," *J. Chem. Theory Comput.*, vol. 12, no. 7, pp. 3340–3352, 2016.

[108] R. Laplaza, V. Polo, and J. Contreras-García, "A bond charge model ansatz for intrinsic bond energies: Application to c–c bonds," *The Journal of Physical Chemistry A*, vol. 124, no. 1, pp. 176–184, 2020.

[109] R. Laplaza, V. Polo, and J. Contreras-García, "Localizing electron density errors in density functional theory," *Phys. Chem. Chem. Phys.*, vol. 21, pp. 20927–20938, 2019.

[110] F. Peccati, R. Laplaza, and J. Contreras-García, "Overcoming distrust in solid state simulations: Adding error bars to computational data," *The Journal of Physical Chemistry C*, vol. 123, no. 8, pp. 4767–4772, 2019.

[111] J. Munárriz, R. Laplaza, A. Martín Pendás, and J. Contreras-García, "A first step towards quantum energy potentials of electron pairs," *Phys. Chem. Chem. Phys.*, vol. 21, pp. 4215–4223, 2019.

[112] R. A. Boto, F. Peccati, R. Laplaza, C. Quan, A. Carbone, J.-P. Piquemal, Y. Maday, and J. Contreras-Garcıa, "Nciplot4: Fast, robust, and quantitative analysis of noncovalent interactions," *Journal of Chemical Theory and Computation, In Press*, 2020.

[113] R. Laplaza, J. Contreras-Garcia, F. Fuster, F. Volatron, and P. Chaquin, "The "inverted bonds" revisited: Analysis of "in silico" models and of [1.1.1]propellane by using orbital forces," *Chemistry – A European Journal*, vol. 26, no. 30, pp. 6839–6845, 2020.

[114] J. Munárriz, R. Laplaza, and V. Polo, "A bonding evolution theory study on the catalytic noyori hydrogenation reaction," *Molecular Physics*, vol. 117, no. 9-12, pp. 1315–1324, 2019.

[115] R. Villanueva, S. Romero-Tamayo, R. Laplaza, J. Martínez-Olivan, A. Velázquez-Campoy, J. Sancho, P. Ferreira, and M. Medina, "Redox- and ligand binding-dependent conformational ensembles in the human apoptosis-inducing factor regulate its pro-life and cell death functions," *Antioxidants & Redox Signaling*, vol. 30, no. 18, pp. 2013–2029, 2019.

[116] J. Quero, S. Cabello, T. Fuertes, I. Mármol, R. Laplaza, V. Polo, M. C. Gimeno, M. J. Rodriguez-Yoldi, and E. Cerrada, "Proteasome versus thioredoxin reductase competition as possible biological targets in antitumor mixed thiolate-dithiocarbamate gold(iii) complexes," *Inorganic Chemistry*, vol. 57, no. 17, pp. 10832–10845, 2018.

[117] M. Martínez-Júlvez, G. Goñi, D. Pérez-Amigot, R. Laplaza, I. Ionescu, S. Petrocelli, M. Tondo, J. Sancho, E. O. Orellano, and M. Medina, "Identification of inhibitors targeting ferredoxin-NADP+ reductase from the xanthomonas citri subsp. citri phytopathogenic bacteria," *Molecules*, vol. 23, no. 1, p. 29, 2017.

[118] S. Grimme, "Semiempirical GGAtype Density Functional Constructed with a LongRange Dispersion Correction," *J. Comput. Chem.*, vol. 27, no. 15, pp. 1787–1799, 2006.

[119] B. Civalleri, C. M. Zicovich-Wilson, L. Valenzano, and P. Ugliengo, "B3LYP Augmented with an Empirical Dispersion Term (B3LYP-D*) as Applied to Molecular Crystals," *Cryst. Eng. Comm.*, vol. 10, pp. 405–410, 2008.

[120] A. Erba, M. Shahrokhi, R. Moradian, and R. Dovesi, "On how differently the quasi-harmonic approximation works for two isostructural crystals: Thermal properties of periclase and lime," *J. Chem. Phys.*, vol. 142, no. 4, p. 044114, 2015.